SKB

Evaluation and modelling report of Task 9A based on comparisons and analyses of predictive modelling results for the REPRO WPDE experiments

Task 9 of SKB Task Force GWFTS – Increasing the realism in solute transport modelling based on the field experiments REPRO and LTDE-SD

J M Soler, I Neretnieks, L Moreno, L Liu,

S Meng, U Svensson, P Trinchero, A Iraola,

H Ebrahimi, J Molinero, P Vidstrand,

G Deissmann, J Říha, M Hokr, A Vetešník,

D Vopálka, L Gvoždík, M Polák, D Trpkošová,

V Havlová, D-K Park, S-H Ji, Y Tachi, T Ito

SVENSK KÄRNBRÄNSLEHANTERING

Evaluation and modelling report of Task 9A based on comparisons and analyses of predictive modelling results for the REPRO WPDE experiments

Task 9 of SKB Task Force GWFTS – Increasing the realism in solute transport modelling based on the field experiments REPRO and LTDE-SD

J M Soler[1], I Neretnieks[2], L Moreno[2], L Liu[2], S Meng[2],

U Svensson[3], P Trinchero[4], A Iraola[4], H Ebrahimi[4], J Molinero[4],

P Vidstrand[5], G Deissmann[6], J Říha[7], M Hokr[7], A Vetešník[8],

D Vopálka[8], L Gvoždík[9], M Polák[9], D Trpkošová[10], V Havlová[10],

D-K Park[11], S-H Ji[11], Y Tachi[12], T Ito[12]

1 Institute of Environmental Assessment and Water Research, IDAEA-CSIC
2 Royal Institute of Technology, KTH
3 Computer-aided Fluid Engineering AB
4 Amphos 21
5 Svensk Kärnbränslehantering AB
6 Forschungszentrum Jülich
7 Technical University of Liberec
8 Czech Technical University in Prague
9 PROGEO
10 ÚJV Řež AS
11 Korea Atomic Energy Research Institute (KAERI)
12 Japan Atomic Energy Agency (JAEA)

Abstract

The GWFTS Task Force (www.skb.se/taskforce) is an international forum in the area of conceptual and numerical modelling of groundwater flow and solute transport in fractured rock. The REPRO Water Phase Diffusion Experiments WPDE-1 and WPDE-2 were two matrix diffusion experiments in gneiss performed at POSIVA's ONKALO underground facility in Finland. Synthetic groundwater containing several conservative and sorbing radiotracers (tracer pulses) was injected along a borehole interval. Flow rates were 20.1 µL/min (WPDE-1) and 10.0 µL/min (WPDE-2). The objective of Task 9A was the predictive modelling of the tracer breakthrough curves using "conventional" modelling approaches (constant diffusion and sorption in the rock, no or minimum rock heterogeneity). Several teams, using different modelling approaches, participated in this exercise.

An important conclusion from the exercise is that even if the objective of Task 9A was to look at matrix diffusion, the modeling results were finally very sensitive to the magnitude of dispersion in the borehole opening, which is related to the flow of water and not to transport and retention in the rock. Focusing on the tails of the breakthrough curves, which are more directly related to matrix diffusion and less influenced by advection and dispersion in the borehole opening, the results from the different teams were more comparable. However, the results still showed differences related to the rock matrix. The thickness of the matrix considered in the model is an important factor for non-sorbing tracers (HTO, ^{36}Cl). The assumption or not of reduced porosities and diffusion coefficients for ^{36}Cl (anion exclusion) affects the tails of the breakthrough curves, since the level of the tails should be proportional to the square root of the product of the effective diffusion coefficient and the rock capacity factor.

Very significant differences have been observed between the models in the results for the most strongly sorbing tracer (^{133}Ba). Spatial discretisation may play an important role here. These results only include the main peak of the breakthrough curve, due to the large retardation. Additionally, one of the DFN models always shows very high tails for all tracers, and late peak arrival times for sorbing tracers. These differences may be related to the implementation of rock capacity (porosity plus sorption) in the numerical model. Other differences in the models (slightly different positions of the peaks, small differences in first arrival times) are probably due to numerical/discretisation effects. Regarding the sensitivity analyses (upper and lower breakthrough curves, additional results), they confirmed the large sensitivity of the results to dispersion. And within the ranges of values of the reported supporting experimental data (porosities, diffusion coefficients, distribution coefficients), results for all tracers showed very little sensitivity with respect to porosity. Non-sorbing tracers (HTO, ^{36}Cl) were only significantly affected by the magnitude of dispersion in the borehole opening, while sorbing tracers were also affected by the values of diffusion and sorption parameters.

Even if Task 9A was designed to be a blind modeling exercise, the models have also been finally compared to the measured experimental breakthroughs. Experimental results in both experiments tend to show relatively small activities, wide breakthroughs and early first arrivals, which are similar to model results using large dispersivity values. However, breakthroughs are always very sharp and show at least 2 well defined peaks, which suggest the existence of multiple flow paths or channels, with very small dispersivities in each channel. Also, ^{22}Na and ^{85}Sr seem to sorb less than expected from the reported laboratory K_d values, or to diffuse more slowly than expected in the rock matrix. Experimental results for the non-sorbing tracers (HTO, ^{36}Cl) show relatively small activities in the tails of the breakthrough curves. Values of diffusion coefficients and/or porosities slightly smaller than those reported from the laboratory studies may apply to these experimental conditions.

Sammanfattning

Task Force GWFTS (www.skb.se/taskforce) utgör ett internationellt forum inom konceptuell och numerisk modellering av grundvattenflöde och transport av lösta ämnen i sprickigt berg. Vattenfas-diffusionsexperimenten REPRO WPDE-1 och WPDE-2 var två experiment som fokuserade på matrisdiffusion i gneiss och utfördes i Posivas underjordiska anläggning ONKALO i Finland. Syntetiskt grundvatten innehållande flera icke-sorberande och sorberande radionuklider injicerades (i spårpulser) längs ett borrhålsintervall. Flödeshastigheterna var 20,1 µl/min (WPDE-1) och 10,0 µl/min (WPDE-2). Syftet med Task 9A var att utföra prediktiv modellering för framtagande av genombrottskurvor för spårämnena med hjälp av "konventionella" modelleringsmetoder (konstant diffusion och sorption i berget, ingen eller minsta möjliga heterogenitet i berget). Flera modellerings-grupper, med olika modelleringsmetoder, deltog i denna övning.

En viktig slutsats från övningen är, att även om syftet med Task 9A var att studera matrisdiffusion, var modelleringsresultaten till slut mycket känsliga för den hydrodynamiska dispersionen i den cylindriska borrhålsöppningen. Dispersionen är mer relaterad till flödet av vatten och inte retention i berg. Om man fokuserar på svansarna i genombrottskurvorna, vilka är mer direkt relaterade till matrisdiffusion och mindre påverkad av advektion och dispersion i borrhålet, så är resultaten från de olika grupperna mer jämförbara. Resultaten påvisade dock fortfarande skillnader relaterade till bergmatrisen. Matrisens tjocklek som beaktas i modellerna är en viktig faktor för icke-sorberande spårämnen (HTO, ^{36}Cl). I de fall då reducerade porositeter och diffusionskoefficienter för ^{36}Cl antogs (pga anjonuteslutning), påverkades svansarna i genombrottskurvorna, eftersom nivån på svansarna bör vara proportionella mot kvadratroten ur produkten av den effektiva diffusionskoefficienten och kapacitetsfaktorn.

Mycket stora skillnader har observerats i resultaten från modellerna för det, i detta experiment, starkast sorberande spårämnet (^{133}Ba). Spatiell diskretisering kan spela en viktig roll här. Dessa resultat omfattar endast huvuddelen av genombrottskurvan, på grund av den stora retardationen. En av de DFN-baserade modellerna påvisar mycket höga nivåer på svansarna för samtliga spårämnen, samt långa transporttider för sorberande spårämnen. Dessa skillnader kan relateras till implementeringen av bergskapaciteten (porositet plus sorption) i den numeriska modellen. Andra skillnader i modellerna (något olika posi-tioner för topparna på kurvorna, små skillnader i första genombrottstid) beror förmodligen på numeriska – eller diskretiseringseffekter.

När det gäller känslighetsanalyserna (ytterligare resultat med övre och undre genombrottskurvor), bekräftade de den stora känsligheten i resultaten för dispersion. Inom ramen för de rapporterade stöd-jande experimentella värdena (porositeter, diffusionskoefficienter, fördelningskoefficienter), påvisar resultaten för alla spårämnen mycket liten känslighet med avseende på porositet. Icke-sorberande spårämnen (HTO, ^{36}Cl) påverkades endast och signifikant av dispersionsnivån i borrhålet, emedan sorberande spårämnen påverkades även av värdena på diffusions- och sorptionsparametrar.

Även om Task 9A utformades för att vara en blind samt prediktiv modellövning, har modellresultaten även slutligen jämförts med de uppmätta experimentella genombrottskurvorna. Experimentella resultat, från bägge experiment, tenderar att påvisa relativt låga aktiviteter, breda genombrottskurvor samt tidiga genombrott, det vill säga resultat liknande de som erhålls vid simulering med stora dispersionsvärden. De experimentella genombrottskurvorna är dock mycket skarpa och påvisar minst två väldefinierade toppar, vilket indikerar förekomsten av flera flödesvägar eller kanaler med mycket liten dispersivitet i varje kanal. Dessutom sorberar ^{22}Na och ^{85}Sr mindre än förväntat, med tanke på de rapporterade laboratorie-Kd-värdena, eller så diffunderar nukliderna långsammare än förväntat i bergmatrisen. De experimentella resultaten för de icke-sorberande spårämnena (HTO, ^{36}Cl) uppvisar relativt små akti-viteter i svansarna på genombrottskurvorna. Värdena på diffusionskoefficienter och/eller porositeter är möjligen något mindre, än de som har rapporterats från laboratorieundersökningarna, för dessa experimentella förhållanden.

Contents

1   Introduction

Task 9A, which was intended as a relatively simple "warm-up" case for Task 9, was designed for the modelling teams to make predictive calculations of tracer breakthrough curves in the ONKALO REPRO experiments (WPDE-1 and WPDE-2). In the experiments, synthetic groundwater containing several conservative and sorbing radiotracers (tracer pulses) had been injected along a borehole interval (Figure 1-1). Flow rates were 20.1 μL/min (WPDE-1) and 10.0 μL/min (WPDE-2). The objective of Task 9A was the predictive modeling of the tracer breakthrough curves using "conventional" modelling approaches (constant diffusion and sorption in the rock, no or minimum rock heterogeneity).

The experimental setup, flow rates, injected tracer activities and rock mineralogies were provided in the Task Description (Löfgren and Nilsson 2019), together with available experimental data (porosities, effective diffusion coefficients, capacity factors, batch sorption distribution coefficients). The modelling teams were asked to consider relatively simple conventional models (traditional advection-dispersion in the experimental borehole, Fickian diffusion and constant sorption distribution coefficients in the rock matrix, homogeneous rock properties), although more complex models could be used when providing alternative results. In addition to a central prediction, the modelling teams were also asked to provide upper and lower breakthrough curves, based mainly on parameter uncertainty.

In this evaluation report the results from the different modelling teams are compared and analysed. At the end, the experimental results (measured breakthrough curves) are also reported and compared with the predictions. It should be noted that the modelling teams were asked to ignore any possible previous knowledge of the experimental results and to provide pure blind predictions.
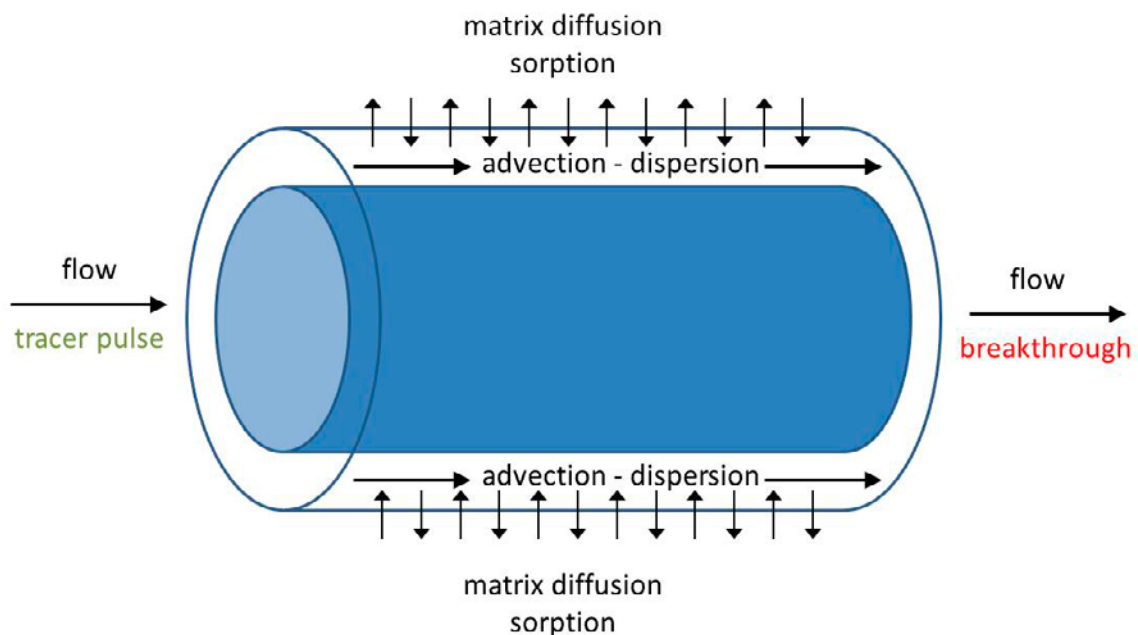

Figure 1-1. *Concept of the experiments. Water (continuous) and tracers (pulse) were injected at one end of the borehole interval. Water flowed along a cylindrical ring around an inner PEEK dummy and was sampled at the other end of the interval. The length and outer diameter of the interval were 1.905 m and 56.5 mm, respectively. The open cylindrical ring had an aperture of 1.25 mm.*

2 Models and parameters

Nine different modelling teams participated in Task 9A. Table 2-1 below gives a summary of the types of models they used. Details of the models can be found in the individual reports from the teams.

Table 2-1. The modelling teams participating in Task 9A, their concepts, and modelling codes or tools.

Team	Concept	Code or tool
Royal Institute of Technology (KTH)	2D linear	Analytical solution
Japan Atomic Energy Agency (JAEA)	Continuum model (2D radial), including a Borehole Disturbed Zone (1 mm)	GoldSim
Computer-Aided Fluid Engineering AB (CFE)	3D Discrete Fracture Network based (45° sector from the centre of the borehole) transformed into an equivalent porous medium, with solute transport by particle tracking	DarcyTools
Technical University of Liberec (TUL)	Mixed continuum-fracture model: 2D fracture + 3D rock (360° sector)	Flow123d
PROGEO	Continuum model (2D radial)	MT3DMS
Amphos 21 (A21)	Continuum model (2D radial)	PFLOTRAN
	3D (45° sector) Discrete Fracture Network based model	iDP (interface DarcyTools and PFLOTRAN)
ÚJV Řež A.S. (UJV)	Continuum model (2D radial)	GoldSim
Czech Technical University in Prague (CTU)	Continuum model (2D radial)	GoldSim
Korea Atomic Energy Research Institute (KAERI)	Continuum model (3D, 22.5° sector)	COMSOL Multiphysics

Table 2-2 below shows a compilation of parameters used in the different modelling exercises (central cases). In principle the Czech teams (UJV, TUL, CTU, PROGEO) had agreed to use the same parameter values, except for the thickness of the matrix. However, due to issues during the implementation of those values in the code, UJV ended up using smaller porosities. These teams also considered the 2 different lithologies (veined gneiss VGN, 92.1 % of the length, and pegmatitic granite PGR, 7.9 % of the length) surrounding the borehole. JAEA assumed the presence of a Borehole Disturbed Zone (BDZ) with a thickness of 1 mm and increased diffusion coefficients, porosities and distribution coefficients (corresponding to laboratory measured values in their concept). In addition, A21 and JAEA did not consider the time spent by the tracers in the inlet and outlet tubing of the experiment. Mean residence times of water in the experimental slot (1.905 m in length), defined as volume of the slot divided by volumetric flow rate, were 343 h (WPDE-1) and 689 h (WPDE-2). The additional times in the tubing, from the tracer vials to the sampling point, were 35.5 h (WPDE-1) and 71.3 h (WPDE-2).

Overall, the porosities, diffusion coefficients and distribution coefficients used by the different teams are rather similar (aside from the smaller porosities finally implemented by UJV). Notice that the VGN lithology dominates the composition of the rock matrix in the models used by the Czech groups. Other exceptions are the large ^{36}Cl porosities used by JAEA, CFE and KAERI (they used the same values as for HTO) and the large ^{36}Cl diffusion coefficients used by JAEA and CFE (CFE assumed that the calculations for HTO and ^{22}Na were applicable to ^{36}Cl and ^{85}Sr, respectively). The ^{36}Cl diffusion coefficients for PGR (7.9 % of the borehole length) used by the Czech groups were also very large, based on a reported value for that lithology ($D_e = 5 \times 10^{-13}$ m^2/s, Task Description). They also used large accessible porosities for ^{36}Cl in PGR.

Table 2-2. Parameters used by the different modelling teams (central cases).

Team	Matrix thickness (cm)	ρ_d (kg/m³)	D_e(HTO) (×10⁻¹³ m²/s)	ε(HTO)	D_e(Cl) (×10⁻¹⁵ m²/s)	ε(Cl)	D_e(Na) (×10⁻¹³ m²/s)	ε(Na)	K_d(Na) (×10⁻³ m³/kg)	D_e(Sr) (×10⁻¹³ m²/s)	ε(Sr)	K_d(Sr) (×10⁻³ m³/kg)	D_e(Ba) (×10⁻¹³ m²/s)	ε(Ba)	K_d(Ba) (×10⁻² m³/kg)	Dispersion D_d (m²/s) or α_L (m)
KTH	Infinite	2650	2.00	0.01	5.0	0.000175	2.00	0.01	1.0	2.0	0.01	1.1	2.00	0.01	7.0	2×10^{-9} m²/s
TUL (VGN)	10	2700	1.83	0.0082	5.0	0.000175	4.65	0.0082	1.3	3.3	0.0082	1.1	1.47	0.0082	6.0	0.19 m
TUL (PGR)	10	2700	5.70	0.005	500	0.013	4.65	0.005	0.8	3.3	0.005	1.1	1.47	0.005	8.0	0.19 m
JAEA (matrix)	20	2740	1.80	0.0063	150	0.0063	2.10	0.0063	1.1	2.5	0.0063	0.59	2.50	0.0063	2.5	0.045 m
JAEA (BDZ)	20	2740	4.30	0.0097	350	0.0097	5.20	0.0097	1.3	6.0	0.0097	1.1	6.00	0.0097	6.0	0.045 m
UJV (VGN)	100	2700	1.83	0.0004	5.0	4.4×10^{-5}	4.65	0.0017	1.3	3.3	0.0021	1.1	1.47	0.0014	6.0	0.19 m
UJV (PGR)	100	2700	5.70	0.0014	500	0.0010	4.65	0.0020	0.8	3.3	0.0024	1.1	1.47	0.0016	8.0	0.19 m
CTU (VGN)	28 (2 for ¹³³Ba)	2700	1.83	0.0082	5.0	0.000175	4.65	0.0082	1.3	3.3	0.0082	1.1	1.47	0.0082	6.0	0.19 m
CTU (PGR)	28 (2 for ¹³³Ba)	2700	5.70	0.005	500	0.013	4.65	0.005	0.8	3.3	0.005	1.1	1.47	0.005	8.0	0.19 m
CFE	2.8	2700	2.00	0.009	200	0.009	2.00	0.009	1.0	2.0	0.009	1.0	2.00	0.009	7.0	0
A21	1.8	2750	2.50	0.01	5.0	0.0002	2.50	0.01	1.3	2.5	0.01	1.1	2.50	0.01	6.0	0.001 m
PROGEO (VGN)	20	2700	1.83	0.0082	5.0	0.000175	4.65	0.0082	1.3	3.3	0.0082	1.1	1.47	0.0082	6.0	0.20 m
PROGEO (PGR)	20	2700	5.70	0.005	500	0.013	4.65	0.005	0.8	3.3	0.005	1.1	1.47	0.005	8.0	0.20 m
KAERI	7	2700	2.50	0.0063	5.0	0.0063	4.65	0.0063	1.26	3.3	0.0063	1.1	1.47	0.0063	6.16	0.19 m

ρ_d: Bulk dry density.
D_e: Effective diffusion coefficient.
ε: Porosity.
K_d: Distribution coefficient.
D_d: Dispersion coefficient.
α_L: Longitudinal dispersivity.

The dispersion coefficient used by KTH is equivalent to dispersivities of 2.6×10^{-3} m WPDE-1, and 5.3×10^{-3} m WPDE-2.

3 Results and discussion

3.1 WPDE-1 (central cases)

3.1.1 HTO

Figure 3-1 shows the calculated breakthrough curves (normalised decay-corrected activity flow NDCAF vs. time) for HTO. The most striking feature is the difference between the results from the teams assuming very small dispersivities (KTH, A21, CFE) and the results from the rest of the teams, who considered larger dispersivities (ranging from 0.045 m to 0.20 m). Small dispersivities result in tall and narrow breakthrough curves with very sharp arrivals, while larger dispersivities result in much shorter and wider curves with very early first arrivals (much earlier than the mean residence time of water in the borehole slot). JAEA assumed a smaller dispersivity in the slot (0.045 m), compared to the values of 0.19–0.20 m used by other teams. The effect of this inter-mediate value of dispersivity can also be readily seen from the results.

When looking at the results in a log-log scale (Figure 3-1b), the main peak is dominated by advection-dispersion in the slot, while the tail is controlled by out-diffusion from the rock matrix to the water flowing in the slot. The typical slope of the tail in a log-log plot, when matrix diffusion is not limited by the thickness of the rock matrix, and for linear diffusion orthogonal to the direction of flow, is −1.5 (Painter et al. 1998). The different values of dispersivity affect solute transport in the slot, where water flow takes place. These very different results are not due to differences in matrix diffusion, which was in principle the focus of the experiment. However, differences due to matrix diffusion can also be observed.

From analytical solutions for planar fracture geometries (Tang et al. 1981, Sudicky and Frind 1982), matrix thickness should only affect the slope of the tail of the breakthrough curve and not its level. Figure 3-2 show results of calculations performed with the CrunchFlow code (Steefel et al. 2015a, Steefel and Molins 2016). The parameters of the calculations are the same as those used by the Czech TUL, PROGEO and CTU groups, but considering only veined gneiss (VGN) as the rock type around the borehole. The different breakthrough curves are for different matrix thicknesses (100, 10, 1.75 cm).
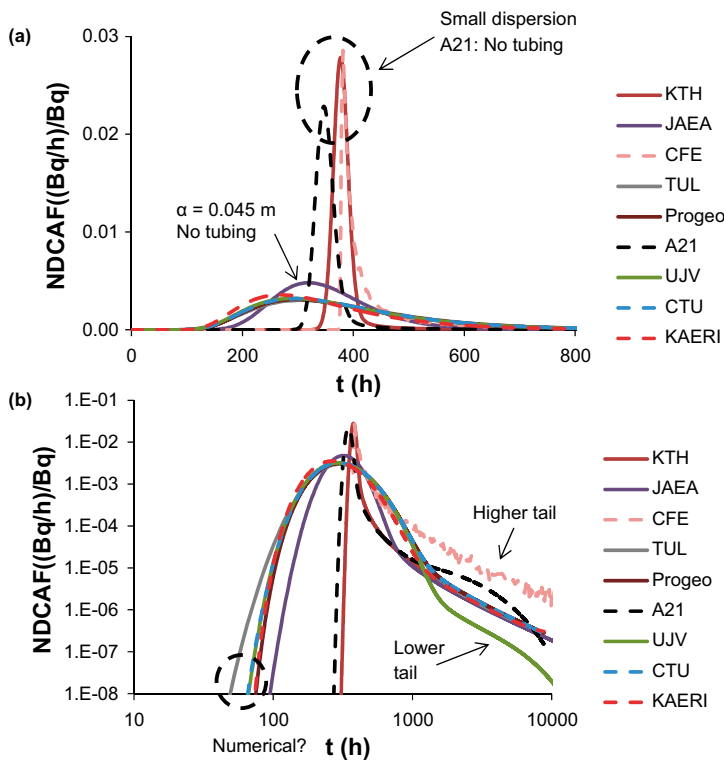

Figure 3-1. WPDE-1 model results for HTO (NDCAF vs. time). (a) linear – linear scale, (b) log – log scale.
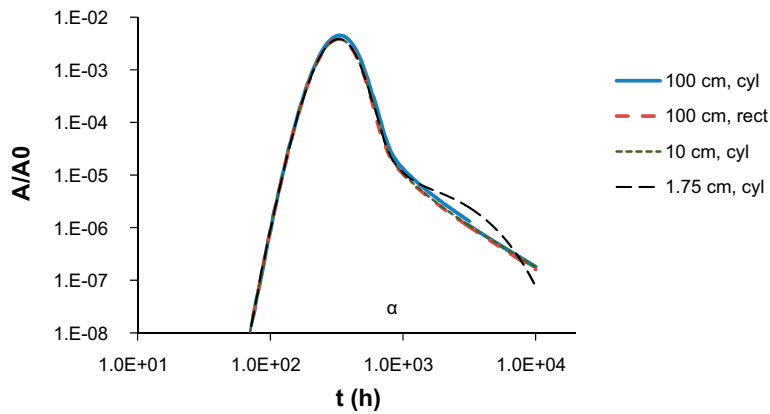
Figure 3-2. *WPDE-1 model results for HTO (relative activities A/A0 vs. time) using CrunchFlow. Tubing (inlet and outlet) is not included in the calculation. Results are for different matrix thicknesses (100, 10, 1.75 cm) and geometries (cylindrical – 2D radial, and rectangular – 2D linear).*

Different geometries (cylindrical –2D radial– and rectangular –2D linear–) are also compared for the largest matrix thickness. The results show that matrix thickness only has an effect if a very thin matrix is considered. The effect of the different geometries should be more evident for the case of a very thick matrix. However, the results show no effect, due to the thin (< 10 cm) diffusion profiles in the rock matrix during the calculations.

Concerning the differences in the tails of the breakthrough curves, the level of tail from CFE is much higher than that from KTH or A21. The level of the tail is proportional to the square root of $D_e\varepsilon$(conservative tracers) or $D_e\alpha$ (sorbing tracers), where $\alpha$is the rock capacity factor (Painter et al. 1998, Neretnieks and Moreno 2003; see also Appendix A by KTH in this report; $\alpha = \varepsilon + \rho_d K_d$). The values of D_e and ε used by CFE are basically the same as those from KTH, and they should result in a very similar tail. Also, the level of the tail from UJV is much lower than those from TUL, PREOGEO or CTU. This difference is due to the smaller porosities that were implemented by UJV compared to those used by the other Czech teams (Table 3-1).

The tail of the breakthrough curve from A21 shows clearly an effect from the very limited matrix thickness considered (1.8 cm). The very thin matrix results in an initial flattening of the slope shortly after the peak and a pronounced drop in activity starting at about t = 4 000 h (Figure 3-1b). The reason for the higher tail in the results from CFE is not clear at the moment.

The results from KAERI are very similar to those from the Czech TUL, PROGEO and CTU teams. The small difference in the first arrival times between the different Czech teams and also KAERI (Figure 3-1b) is probably due to numerical reasons, e.g. differences in the numerical grids implemented in the models.

3.1.2 ^{36}Cl

Figure 3-3 shows the calculated breakthrough curves (NDCAF vs. time) for ^{36}Cl. As in the case of HTO, the most striking feature is the difference between the results from the teams assuming very small dispersivities (KTH, A21, CFE) and the results from the rest of the teams. JAEA used a large intermediate value of dispersivity (0.045 m).

Also, the results (Figure 3-3b) show the relatively high activities in the tail of the curve from CFE (compare KTH or A21 vs. CFE) and low activities in the tail from UJV (compare UJV vs. TUL-PROGEO-CTU). UJV implemented smaller porosities compared to the rest to of the Czech teams (Table 3-1), which explains the lower tail. CFE used the same breakthrough curve for HTO as applicable to ^{36}Cl, which explains the higher level of the tail (larger D_e and ε values). JAEA used D_e and ε values very similar to those for HTO, explaining also the high level of its corresponding tail.
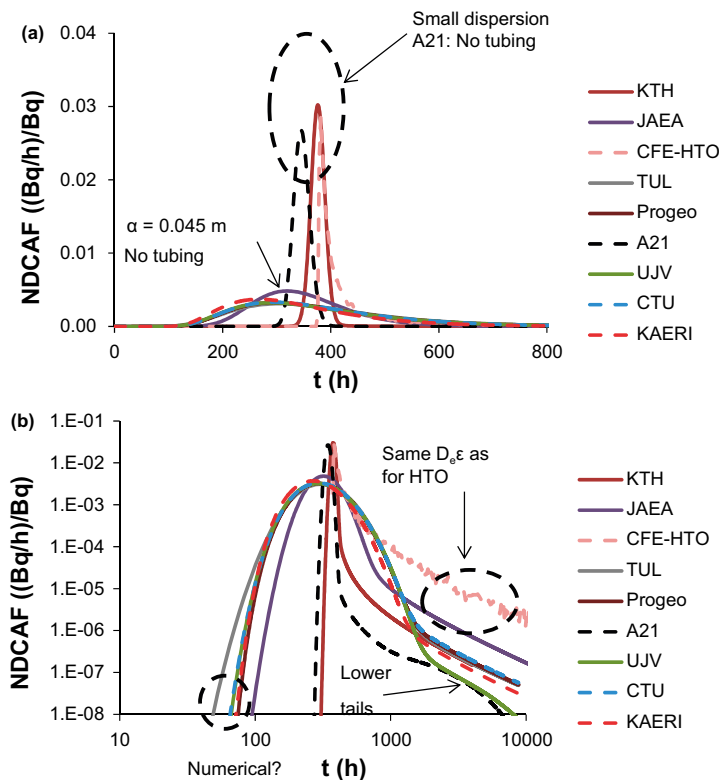
Figure 3-3. *WPDE-1 model results for ^{36}Cl (NDCAF vs. time). (a) linear – linear scale, (b) log – log scale.*

The tails of the curves from KTH and A21 should be practically the same (practically equal D_e and ε values), but the levels are clearly different. The reason for this difference is not clear at the moment. Also, the level of the tails should be lower than that from KAERI, which used the same value of D_e but a larger porosity. The breakthrough curve from A21 shows a drop in activity starting at about 2 000 h due to the thin matrix considered (1.8 cm).

The small difference in the first arrival times between the different Czech teams and also KAERI (Figure 3-3b) is probably due to numerical reasons, e.g. differences in the numerical grids implemented in the models.

3.1.3 ^{22}Na

Quick inspection of the results already shows that there is more variability in the main peak than in the case of the non-sorbing tracers (Figure 3-4). Variability in the tails is less. Comparing the results of KTH and A21 (small dispersivities), the lower peak and slightly higher tail from A21 are consistent with the slightly higher D_e and K_d values (Table 3-1).

Also, the results from PROGEO show a tall and early peak (taller and earlier than those from TUL, CTU or UJV). The reason for this taller and earlier peak lies in the implementation of transversal dispersivity. PROGEO implemented a zero transversal dispersivity in the slot, while the othe Czech teams implemented values ranging from 0.019 m to 0.19 m. This implemented transversal dispersivity resulted in an increased net diffusion/dispersion coefficient at the slot-rock interface (due to averaging between the properties of the different domains at the interface), with a corresponding net increase in solute fluxes through the interface, explaining the extra retardation (lower and later peaks) in the results from TUL, CTU and UJV. The initial flatter slope of the tail of the PROGEO results is due to the same effect. This effect was negligible for the non-sorbing tracers.

Notice also that the lower tail observed in the HTO and ^{36}Cl results from UJV cannot be observed here. This is due to the fact that the rock capacity factor is dominated here by sorption, and there is no noticeable effect from the smaller porosities implemented by UJV.
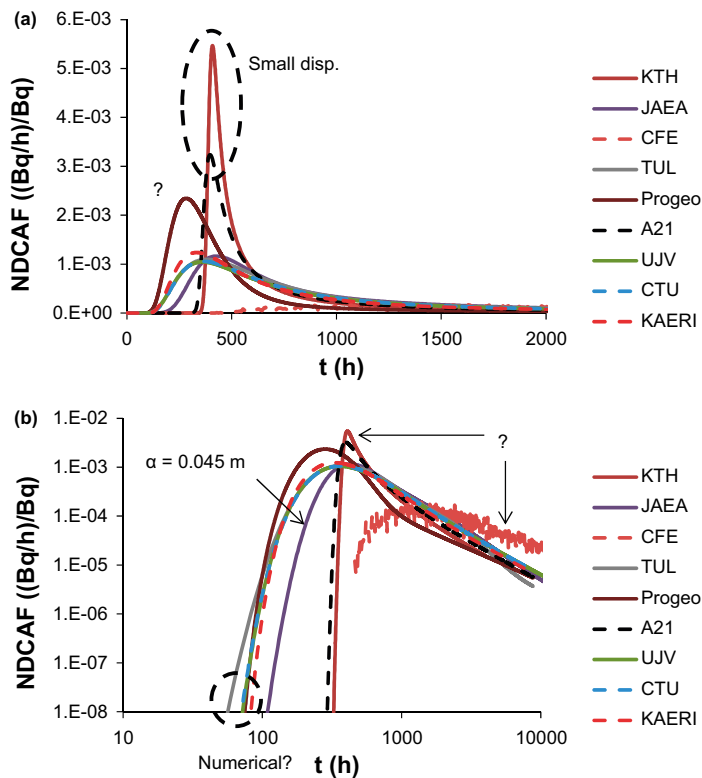
Figure 3-4. WPDE-1 model results for ^{22}Na (NDCAF vs. time). (a) linear – linear scale, (b) log – log scale.

Results from CFE, which should in principle be comparable to those from KTH or A21 (small dispersivities), show a very highly retarded breakthrough.

The results from KAERI are very similar to those from UJV and CTU, with only very slightly taller and earlier peaks (Figure 3-4a). KAERI also implemented transversal dispersion in their calculations ($\alpha_L = \alpha_T$). The difference in the first arrival times between the different Czech teams and also KAERI is probably due to numerical reasons (Figure 3-4b).

The results from JAEA are intermediate between those of TUL-UJV-CTU and those from KTH and A21, consistent with the intermediate value of dispersivity used by JAEA. The tails of the different curves, except those from PROGEO and CFE, are all rather similar (Figure 3-4b), pointing to a similar response of the models to matrix diffusion and sorption, compared to the large differences in the main peak caused by the different dispersivity values. The tails of the curves should indeed be proportional to the square root of $D_e\alpha$.

3.2 WPDE-2 (central cases)

3.2.1 HTO

The results (Figure 3-5) show the same trends already seen in WPDE-1 (Figure 3-1). The most striking feature is the difference between the results from the teams assuming very small dispersivities (KTH, A21, CFE) and the results from the rest of the teams, who considered larger dispersivities (ranging from 0.045 m to 0.20 m). JAEA used a large intermediate value of dispersivity (0.045 m).

Regarding the differences due to matrix diffusion, the level of tail of the breakthrough curve from CFE is higher than that from KTH or A21. The values of D_e and ε used by CFE are basically the same as those from KTH, and they should result in a very similar tail. Also, the level of the tail from UJV is much lower than those from TUL, PREOGEO or CTU. As discussed above (Section 3.1.1), the reason for this inconsistency is due to the smaller porosities implemented by UJV (Table 3-1).
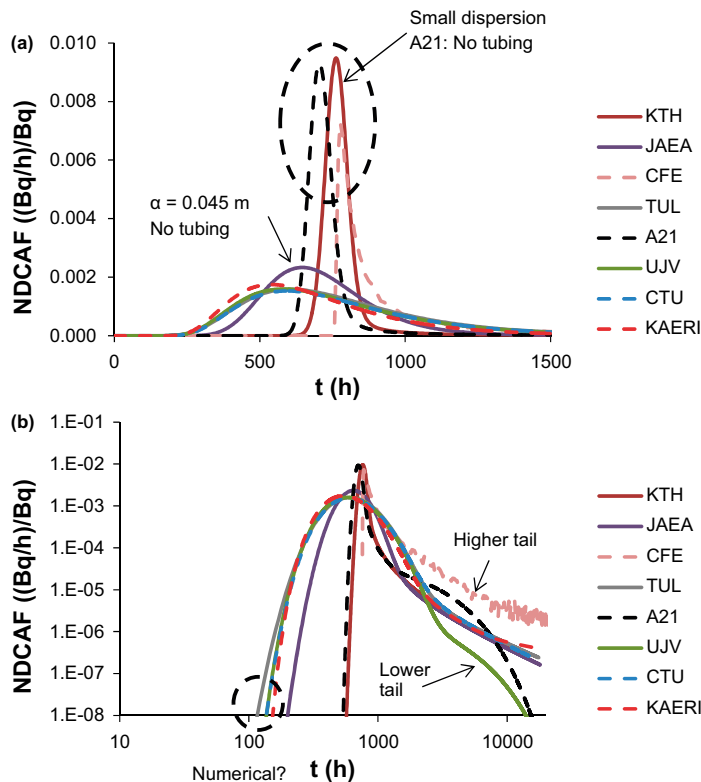
Figure 3-5. *WPDE-2 model results for HTO (NDCAF vs. time). (a) linear – linear scale, (b) log – log scale.*

The very thin matrix considered by A21 results in a pronounced drop in activity starting at about t = 5 000 h (Figure 3-5b).

The results from KAERI are very similar to those from TUL, UJV and CTU, with only very slightly taller and earlier peaks (Figure 3-5a). The small difference in the first arrival times between the different Czech teams and also KAERI (Figure 3-5b) is probably due to numerical reasons, e.g. differences in the numerical grids implemented in the models.

3.2.2 ^{36}Cl

The results (Figure 3-6) show the same trends already seen in WPDE-1 (Figure 3-3). As in the case of HTO, the most striking feature is the difference between the results from the teams assuming very small dispersivities (KTH, A21, CFE) and the results from the rest of the teams. JAEA used a large intermediate value of dispersivity (0.045 m).

Also, the results (Figure 3-6b) show the relatively high activities in the tail of the curve from CFE (compare KTH or A21 vs. CFE) and low activities in the tail from UJV (compare UJV vs. TUL-CTU). CFE used the same breakthrough curve for HTO as applicable to ^{36}Cl, which explains the higher level of the tail (larger D_e and ε values). The lower level of the tail in the results from UJV is explained by the small porosities that were implemented (Table 3-1). JAEA used D_e and ε values very similar to those for HTO, explaining also the high level of its corresponding tail.

The tails of the curves from KTH and A21 should be practically the same (practically equal D_e and ε values), but the levels are clearly different. The reason for this difference is not clear at the moment. Also, the level of the tails should be lower than that from KAERI, which used the same value of D_e but a larger porosity. The breakthrough curve from A21 shows a drop in activity starting at about 3 000 h due to the thin matrix considered (1.8 cm).

The results from KAERI are very similar to those from TUL, UJV and CTU, with only very slightly taller and earlier peaks (Figure 3-6a). The difference in the first arrival times between the different Czech teams and also KAERI is probably due to numerical reasons (Figure 3-6b).
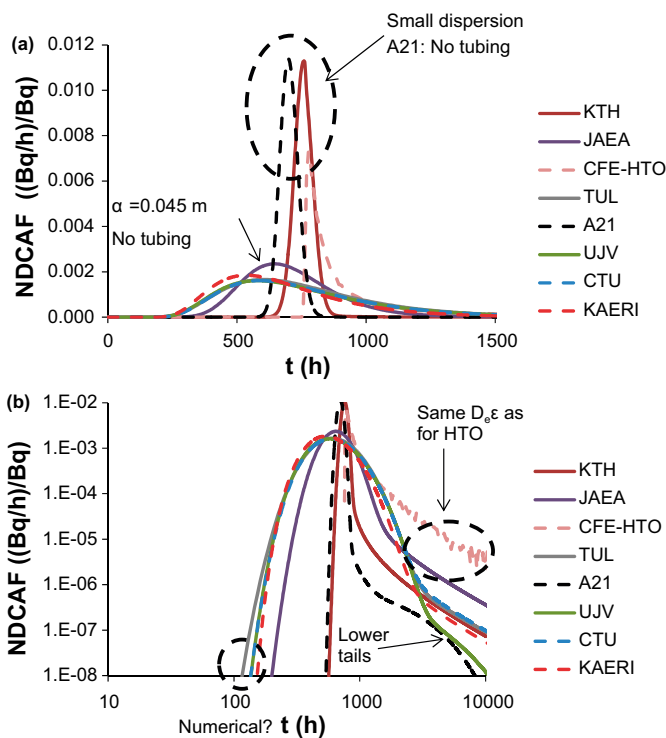
Figure 3-6. *WPDE-2 model results for ^{36}Cl (NDCAF vs. time). (a) linear – linear scale, (b) log – log scale.*

3.2.3 ^{22}Na

Quick inspection of the results shows that the peak from A21 is shorter than the one from KTH (both teams using small dispersivities; Figure 3-7a), which is consistent with the slightly higher D_e and ε values used by A21 (Table 3-1). The peak from TUL is also slightly taller than those from UJV and CTU. The results from KAERI are very similar to those from TUL, with only slightly earlier peak arrival times (Figure 3-7a). Results from CFE, which should in principle be comparable to those from KTH or A21 (small dispersivities), show a very highly retarded breakthrough (Figure 3-7b).
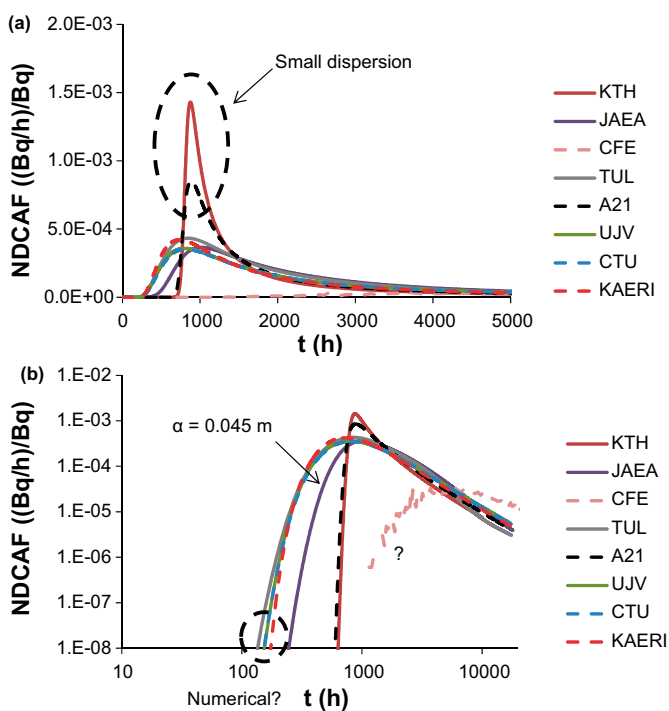
Figure 3-7. *WPDE-2 model results for ^{22}Na (NDCAF vs. time). (a) linear – linear scale, (b) log – log scale.*

The results from JAEA are intermediate between those of TUL-UJV-CTU-KAERI and those from KTH and A21, consistent with the intermediate value of dispersivity used by JAEA. The tails of the different curves, except the one from CFE, are all rather similar, pointing to a similar response of the models to matrix diffusion and sorption, compared to the large differences in the main peak caused by the different dispersivity values. The difference in the first arrival times between the different Czech teams and also KAERI is probably due to numerical reasons (Figure 3-7b).

3.2.4 ^{85}Sr

The results from ^{85}Sr (Figure 3-8) show trends which are very similar to those of ^{22}Na (Figure 3-7). The peak from A21 is shorter than the one from KTH (both teams using small dispersivities; Figure 3-8a), which is consistent with the slightly higher D_e value used by A21 (Table 3-1). The peak from TUL is also slightly taller than those from UJV and CTU. The results from KAERI are very similar to those from TUL, with only slightly earlier peak arrival times (Figure 3-8a). Results from CFE, which should in principle be comparable to those from KTH or A21 (small dispersivities), show a very highly retarded breakthrough (Figure 3-8b).

The results from JAEA are intermediate between those of TUL-UJV-CTU-KAERI and those from KTH and A21, consistent with the intermediate value of dispersivity used by JAEA. The tails of the different curves, except the one from CFE, are all rather similar, pointing to a similar response of the models to matrix diffusion and sorption, compared to the large differences in the main peak caused by the different dispersivity values. The difference in the first arrival times between the different Czech teams and also KAERI is probably due to numerical reasons (Figure 3-8b).
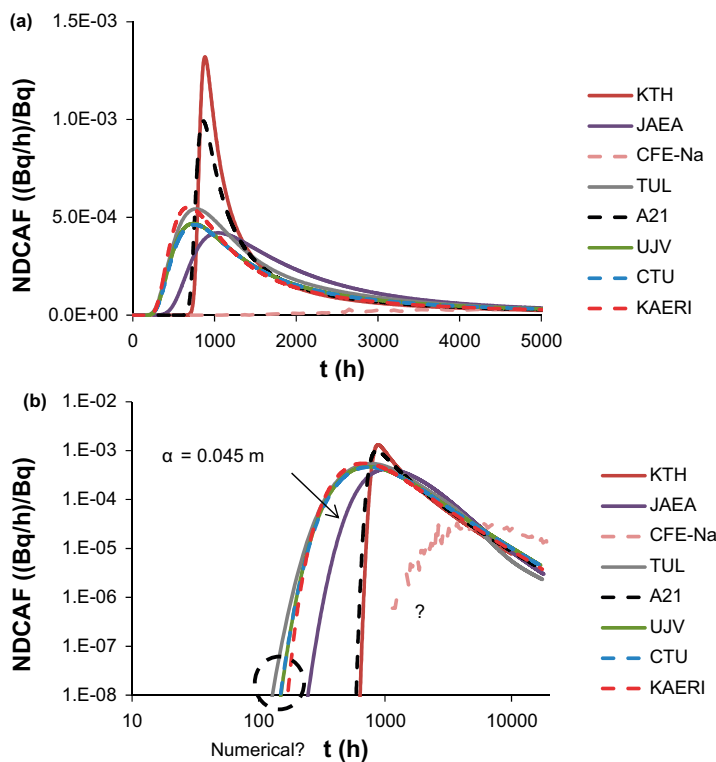
Figure 3-8. *WPDE-2 model results for ^{85}Sr (NDCAF vs. time). (a) linear – linear scale, (b) log – log scale.*

3.2.5 ^{133}Ba

This set of the results (Figure 3-9), corresponding to the most strongly sorbing tracer, shows the highest variability between the different teams. The results from CFE show a very highly retarded breakthrough.

The results from UJV and CTU are practically identical, but those from TUL show a very tall and late peak and a very flat tail. The 3 teams used the same parameters (except for the smaller porosities implemented by UJV, which have no effect here). A spatial discretisation effect (discretisation normal to the slot-rock interface), which can be very important for strongly sorbing tracers, may play a significant role here.

The results from KAERI are similar to those from UJV-CTU, but they show a taller peak. The results from JAEA show a lower and later peak. And those from CFE show an even lower and later peak.

The strongly-sorbing nature of the tracer causes very late breakthrough tails. Those very late times were not considered in the calculations (Figure 3-9b). Therefore, detailed comparison of the tails is not possible.
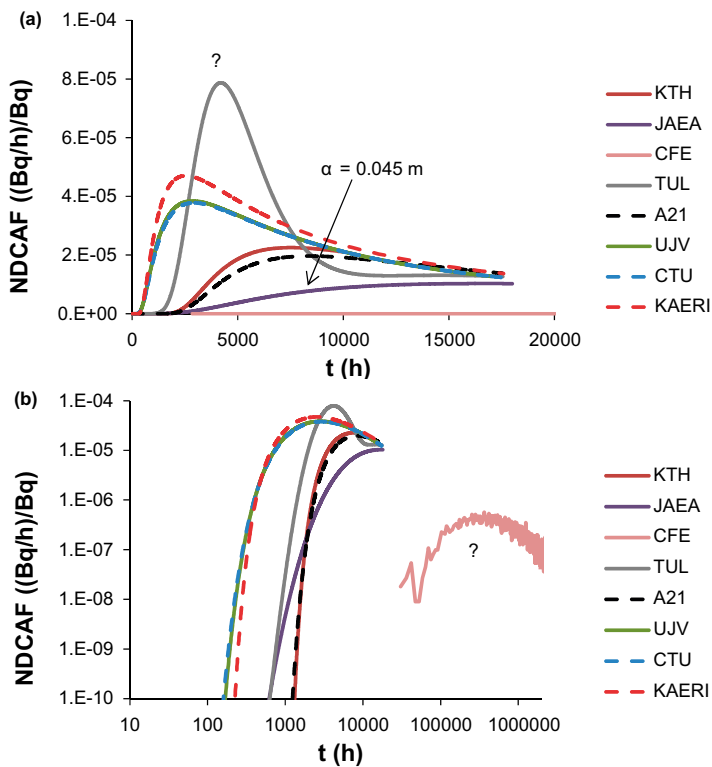

Figure 3-9. *WPDE-2 model results for ^{133}Ba (NDCAF vs. time). (a) linear – linear scale, (b) log – log scale.*

3.3   Sensitivity analyses: upper and lower predictions, additional results

In addition to a central prediction, modelling teams were asked to present upper and lower break-through curves for the different tracers. Additional results, from additional sensitivity studies or alternative model concepts could also be presented. A summary of the presented results and conclusions is reported here. Further details can be found in the individual reports from the modelling teams.

KTH provided upper and lower curves for the different tracers based on variations in the value of the Materials Property Group (MPG = $\varepsilon(D_pR)^{0.5} = (D_e\alpha)^{0.5}$), where R is the retardation factor and α is the rock capacity factor. The value of MPG was multiplied and divided by 3.15 to obtain upper and lower curves for each tracer. Additional results were provided by using different values of the dispersion coefficient in the slot for HTO (WPDE-1).

JAEA presented upper and lower curves for each tracer based on the uncertainties (ranges of values) in the supporting experimental data (sorption and diffusion parameters). Single upper and lower curves were those resulting from the changes in the parameter having the largest effect in the results. Additional results considered the effect of dispersion in the slot ($\alpha = 0$, 0.045 m, 0.1 m) and also an alternative model with 2 different flow channels (10 % of the slot with 3 times the average velocity and 90 % of the slot with 0.78 times the average flow velocity).

CFE presented an alternative model with 2 different flow channels (20 % of the slot with 2 times the average velocity and 80 % of the slot with 0.75 times the average flow velocity).

TUL reported upper and lower curves for each tracer and for each parameter examined, based on the uncertainties (ranges of values) in the supporting experimental data. The parameters examined were α (0.1, 0.19, 0.28 m), ε, K_d and D_e for the 2 rock types included in the models (VGN and PGR). In addition, the effect of discretisation (normal to flow) on the results for sorbing tracers was studied.

UJV reported upper and lower curves for each tracer and for each parameter examined, based on the uncertainties (ranges of values) in the supporting experimental data. The parameters examined were α (0.1, 0.19, 0.28 m), ε, K_d and D_e for the 2 rock types included in the models (VGN and PGR).

CTU provided single upper and lower curves based on the uncertainties (ranges of values) in the supporting experimental data. The upper/lower predictions report the maximum/minimum of all calculated breakthrough curves at a given time.

PROGEO reported additional results (WPDE-1) for (a) $\alpha = 0$, 0.1 m, 0.2 m, 0.28 m, (b) coarse vs. fine discretisation, and (c) a model with zero dispersivity but variable fracture aperture.

A21 provided upper and lower curves for each tracer by considering large and small values of both D_e and ε, keeping their ratio ($D_e/\varepsilon = D_p$) constant. Additional results for WPDE-2 (HTO, [22]Na) were reported for $\alpha = 0.001$ m and 0.02 m. An alternative model, using a 3D DFN, was also used to calculate results for WPDE-1 (HTO, [22]Na).

KAERI presented upper and lower curves for each tracer based on the uncertainties (ranges of values) in the supporting experimental data (D_e, K_d). Single upper and lower curves were those resulting from the changes in the parameter having the largest effect in the results. Additional results considered different values of dispersivity ($\alpha = 0.01\alpha_{ref}$, $0.1\alpha_{ref}$, $0.5\alpha_{ref}$, α_{ref}, $1.5\alpha_{ref}$). The effect of discretisation (normal to flow) was also studied.

An overall conclusion from the different sensitivity studies is that the magnitude of dispersion (including the assumption of different flow channels or a variable fracture aperture) has a strong effect on all tracers. Small dispersivities result in tall and narrow breakthrough curves with very sharp arrivals, while larger dispersivities result in much shorter and wider curves with very early first arrivals (much earlier than the mean residence time of water in the borehole slot). The presence of multiple flow channels (or variable fracture aperture) leads to a similar effect. Eventually, if the different flow paths have very different flow velocities, multiple tracer peaks appear in the breakthrough curves.

Numerical discretisation in the rock next to the surface of the slot affects mainly the more strongly sorbing tracers. A discretisation effect may for instance be behind the relatively tall and late peak for [133]Ba in WPDE-2 from TUL (Figure 3-10). In their sensitivity study (in the Appendix D), they show that a finer discretisation leads to earlier first arrival and peak times and shorter peaks (smaller peak activities). It is therefore important to check that results for sorbing tracers converge with respect to discretisation.

Several teams used the ranges of values of the supporting experimental data (porosities, diffusion coefficients, distribution coefficients) for their sensitivity studies. The conclusions are that results for all tracers show very little sensitivity with respect to porosity. Non-sorbing tracers (HTO, [36]Cl) are only significantly affected by the magnitude of dispersion in the slot, while sorbing tracers are also affected by the values of diffusion and sorption parameters.

3.4   Experimental results

Figures 3-10 to 3-17 show the calculated breakthrough curves together with the measured experimental data (all in terms of NDCAF vs. time). Measured decay-corrected activities at the outlet (Bq/g) were multiplied by the flow rate and divided by the injected activity to obtain NDCAF. Activities were measured in water samples for all tracers. For some of the tracers on-line activities were also measured.

Experimental results tend to show relatively small activities, wide breakthroughs and early first arrivals, which are similar to model results using large dispersivity values. However, breakthroughs are always very sharp (very rapid increases in activity) and show at least 2 well defined peaks, which suggest the existence of multiple flow paths or channels in the slot, with very small dispersivities in each channel (causing the very sharp breakthroughs). Also, experimental results for the non-sorbing tracers (HTO, [36]Cl) show tails with relatively low activities compared with modelling results. Slightly smaller diffusion coefficients and/or porosities may apply to these experimental conditions.

Experimental results for [22]Na (WPDE-1 and WPDE-2) and [85]Sr (WPDE-2) show tall and early tracer peaks together with rapid activity drops in the tails of the curves. These features seem to indicate that these tracers sorb less strongly than expected from the reported supporting experimental data (distribution coefficients), or that they diffuse more slowly than expected in the rock matrix. Experimental results for [133]Ba (WPDE-2) also show early peaks, although more consistent with some of the modelling results.

An additional feature of the measured breakthrough curves is that the first main tracer peak is taller in WPDE-1, while the second main peak is taller in WPDE-2. This feature could indicate heterogeneity with respect to diffusion/retention properties or channel geometries. Different flow geometries in WPDE-1 and WPDE-2 are also a possibility.
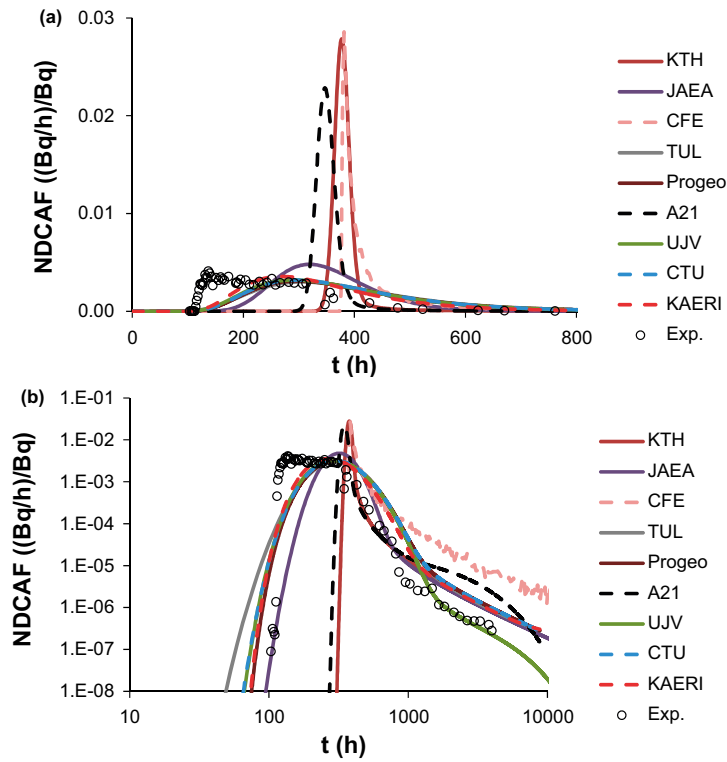
Figure 3-10. *WPDE-1 model and experimental results for HTO (NDCAF vs. time). (a) linear – linear scale, (b) log – log scale.*
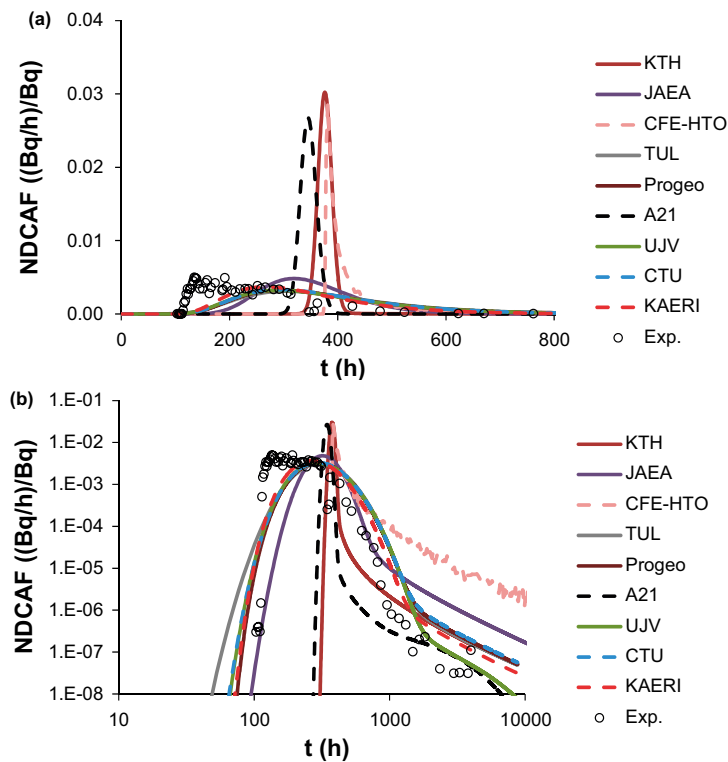

Figure 3-11. *WPDE-1 model and experimental results for ^{36}Cl (NDCAF vs. time). (a) linear – linear scale, (b) log – log scale.*
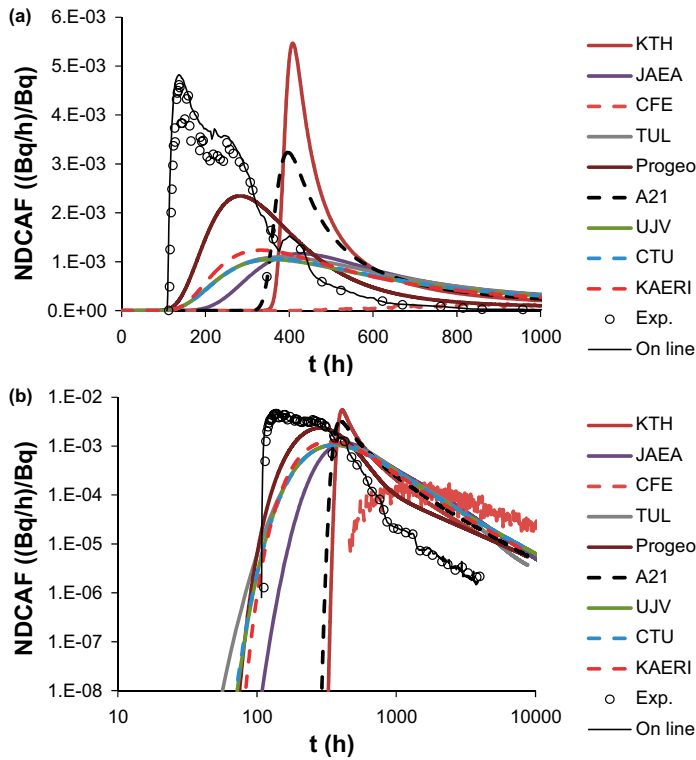
Figure 3-12. *WPDE-1 model and experimental results for ^{22}Na (NDCAF vs. time). (a) linear – linear scale, (b) log – log scale.*
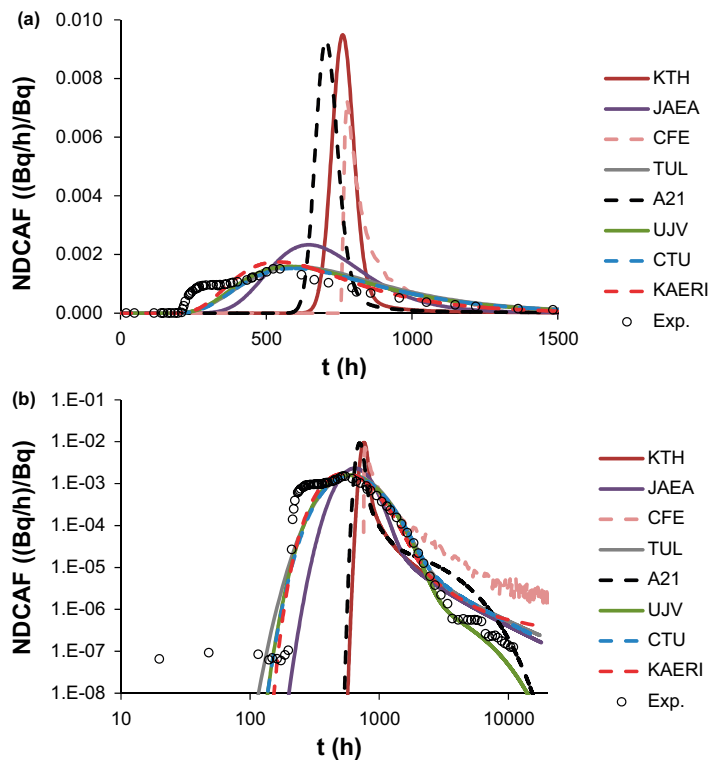

Figure 3-13. *WPDE-2 model and experimental results for HTO (NDCAF vs. time). (a) linear – linear scale, (b) log – log scale.*
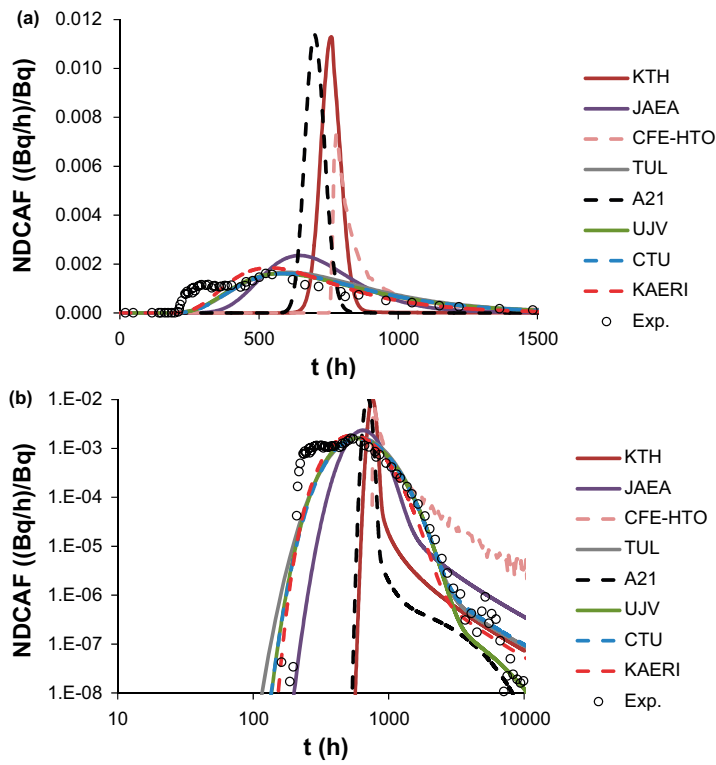
Figure 3-14. *WPDE-2 model and experimental results for ^{36}Cl (NDCAF vs. time). (a) linear – linear scale, (b) log – log scale.*
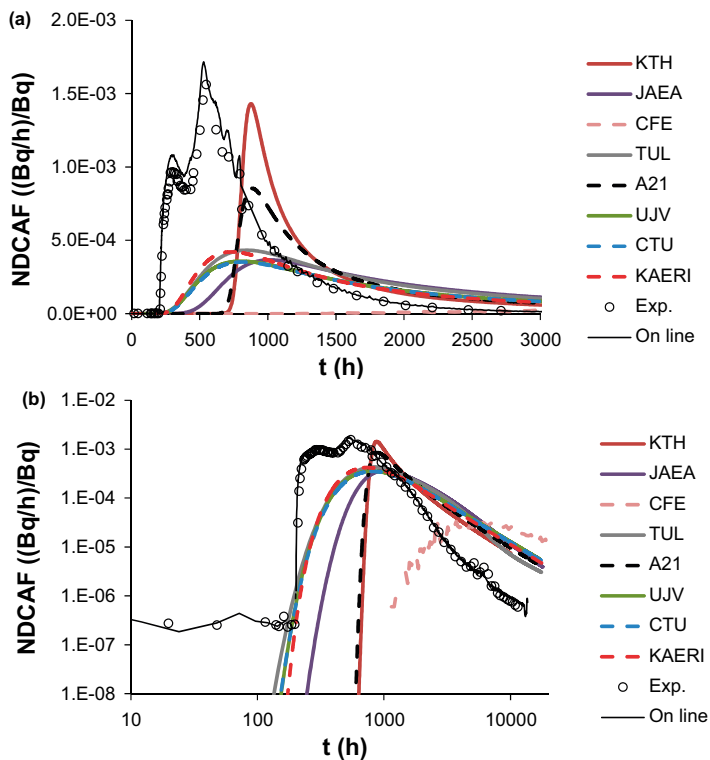

Figure 3-15. *WPDE-2 model and experimental results for ^{22}Na (NDCAF vs. time). (a) linear – linear scale, (b) log – log scale.*
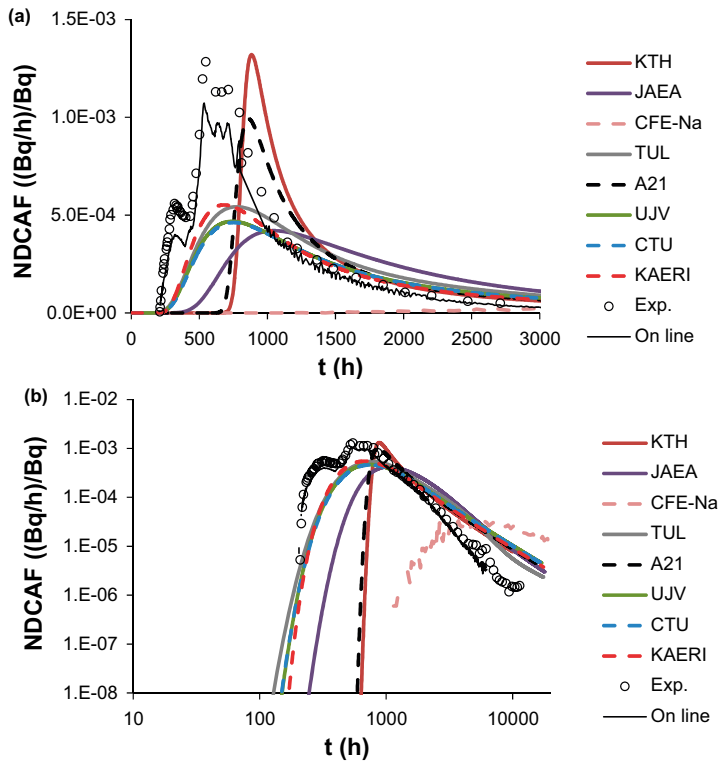
Figure 3-16. *WPDE-2 model and experimental results for ^{85}Sr (NDCAF vs. time). (a) linear – linear scale, (b) log – log scale.*
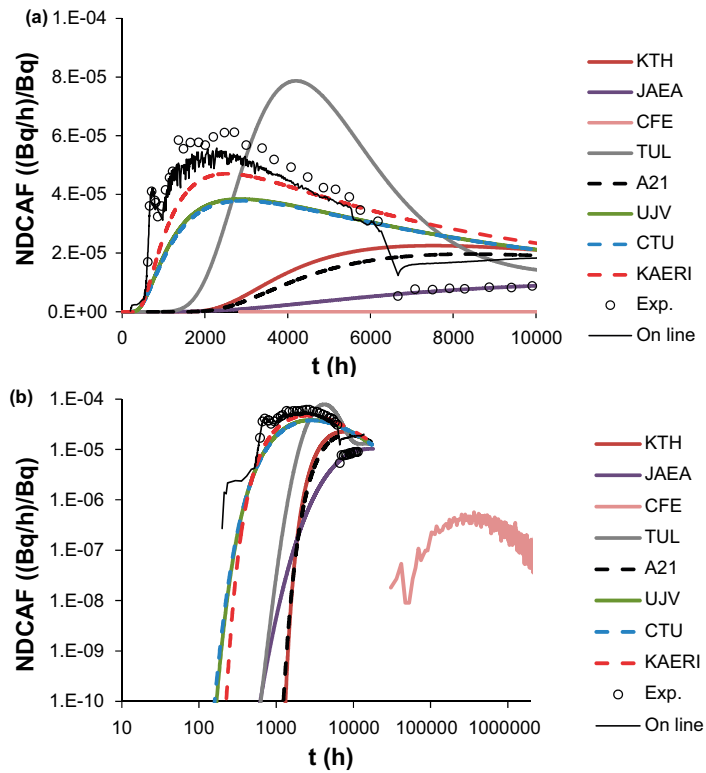

Figure 3-17. *WPDE-2 model and experimental results for ^{133}Ba (NDCAF vs. time). (a) linear – linear scale, (b) log – log scale.*

4   Summary and conclusions

An important conclusion from this exercise is that even if the objective of Task 9A was to look at matrix diffusion under in situ conditions, i.e. transport and retention in the rock matrix, the modelling results were finally very sensitive to the magnitude of dispersion in the slot, which is related to the flow of water and not to transport and retention in the rock. Additionally, a numerical effect arising form the implementation of transversal dispersivity in the slot seems to translate into additional retardation for sorbing tracers.

The fact that some teams did not consider the time spent by the tracers in the tubings at the inlet and outlet of the borehole interval induced some differences in the peak arrival times of the breakthrough curves. Other differences in the models (slightly different positions of the peaks, small differences in first arrival times) are probably due to numerical/discretisation effects.

The experimental setup was designed to favour mixing in the slot, but a channeling effect was still observed in the results. Unexpected effects such as this should be borne in mind in future tasks. Focusing on the tails of the breakthrough curves, which are more directly related to matrix diffusion and less influenced by advection and dispersion in the slot, the results from the different teams were more comparable. As shown by Poteri et al. (2018a, b) and Cvetkovic and Poteri (2019)[1], who used the residence time distribution approach to analyse the experimental results in terms of transport and retention of the tracers in the rock matrix, the effect of advection and dispersion in the slot can be separated from matrix diffusion. They concluded that the behaviour of HTO, ^{36}Cl and ^{22}Na in the rock matrix was similar in WPDE-1 and WPDE-2. However, the results from the modelling teams still showed differences related to the rock matrix. The thickness of the matrix considered in the model is an important factor for non-sorbing tracers (HTO, ^{36}Cl), and the assumption or not of reduced porosities and diffusion coefficients for ^{36}Cl (anion exclusion) also affects the tails of the breakthrough curves. Indeed, the tails of the curves should be proportional to the square root of $D_e\varepsilon$ ($D_e\alpha$ for sorbing tracers).

Very significant differences have been observed between the models in the results for the most strongly sorbing tracer (^{133}Ba). Spatial discretisation may play an important role here. These results only include the main peak of the breakthrough curve, due to the large retardation. Additionally, one of the DFN models always shows very high tails for all tracers, and late peak arrival times for sorbing tracers. These differences may be related to the implementation of rock capacity (porosity plus sorption) in the numerical model.

Regarding the sensitivity analyses (upper and lower breakthrough curves, additional results), they confirmed the large sensitivity of the results to dispersion. And within the ranges of values of the reported supporting experimental data (porosities, diffusion coefficients, distribution coefficients), results for all tracers showed very little sensitivity with respect to porosity. Non-sorbing tracers (HTO, ^{36}Cl) were only significantly affected by the magnitude of dispersion in the slot, while sorbing tracers were also affected by the values of diffusion and sorption parameters.

Even if Task 9A was designed to be a blind modelling exercise, the models have also been finally compared to the measured experimental breakthroughs. Experimental results tend to show relatively small activities, wide breakthroughs and early first arrivals, which are similar to model results using large dispersivity values. However, breakthroughs are always very sharp and show at least 2 well defined peaks, which suggest the existence of multiple flow paths or channels in the slot, with very small dispersivities in each channel. Also, ^{22}Na and ^{85}Sr seem to sorb less than expected from the reported laboratory K_d values, or to diffuse more slowly than expected in the rock matrix. ^{133}Ba also shows early breakthrough, but measurements are somewhat more consistent with some of the modelling calculations. Experimental results for the non-sorbing tracers (HTO, ^{36}Cl) show relatively small activities in the tails of the breakthrough curves. Slightly smaller values of diffusion coefficients and/or porosities may apply to these experimental conditions.

---

[1] A novel method for inferring basic transport parameters from tracer tests in rocks: Theory and two case studies in granite. Water Resources Research (in review).

4.1 Acknowledgements

References

SKB's (Svensk Kärnbränslehantering AB) publications can be found at www.skb.com/publications.

André M, Malmström M E, Neretnieks I, 2009a. Determination of sorption properties of intact rock samples: new methods based on electromigration. Journal of Contaminant Hydrology 103, 71–81.

André M, Malmström M E, Neretnieks I, 2009b. Specific surface area measurements on intact drillcores and evaluation of extrapolation methods for rock matrix surfaces. Journal of Contaminant Hydrology 110, 1–8.

Archie G E, 1942. The electrical resistivity log as an aid in determining some reservoir characteristics. Petroleum Transactions of the AIME 146, 54–62.

Autio J, Siitari-Kauppi M, Timonen J, Hartikainen K, Hartikainen J, 1998. Determination of the porosity, permeability and diffusivity of rock in the excavation-disturbed zone around full scale deposition holes using the ^{14}C-PMMA and He-gas methods. Journal of Contaminant Hydrology 35, 19–29.

Autio J, Hjerpe T, Siitari-Kauppi M, 2003. Porosity, diffusivity and permeability of EDZ in crystalline rock and effect on migration in a KBS-3 type repository. In Impact of the excavation disturbed or damaged zone (EDZ) on the performance of radioactive waste geological repositories. In Proceedings of a European Commission Cluster conference and workshop, Luxembourg, 3–5 November 2003, 149–155.

Barten W, 1996. Linear response concept combining advection and limited rock matrix diffusion in a fracture network transport model. Water Resources Research 32, 3285–3296.

Blunt M J, Bijeljic B, Dong H, Gharbi O, Iglauer S, Mostaghimi P, Paluszny A, Pentland C, 2013. Pore-scale imaging and modelling. Advances in Water Resources 51, 197–216.

Boving T B, Grathwohl P, 2001. Tracer diffusion coefficients in sedimentary rocks: correlation to porosity and hydraulic conductivity. Journal of Contaminant Hydrology 53, 85–100.

Byegård J, Johansson H, Skålberg M, Tullborg E-L, 1998. The interaction of sorbing and non-sorbing tracers with different Äspö rock types. Sorption and diffusion experiments in the laboratory scale. SKB TR-98-18, Svensk Kärnbränslehantering AB.

Crawford J, 2010. Bedrock K_d data and uncertainty assessment for application in SR-Site geosphere transport calculations. SKB R-10-48, Svensk Kärnbränslehantering AB.

Crawford J, 2013. Quantification of rock matrix K_d data and uncertainties for SR-PSU. SKB R-13-38, Svensk Kärnbränslehantering AB.

Crawford J, Neretnieks I, Malmström M E, 2006. Data and uncertainty assessment for radionuclide K_d partitioning coefficients in granitic rock for use in SR-Can calculations. SKB R-06-75, Svensk Kärnbränslehantering AB.

Cvetkovic V, 2016. Evaluation of WPDE1 and WPDE2 tests using the retention time distribution. In Minutes of Task Force GWFTS Workshop in Helsinki, Finland, October 26–27, 2016.

Cvetkovic V, Cheng H, 2008. Sorbing tracer experiments in a crystalline rock fracture at Äspö (Sweden): 3. Effect of microscale heterogeneity. Water Resources Research 44, W12447. doi:10.1029/2007WR006797

Dowd P A, Martin J A, Xu C, Fowell R J, Mardia K V, 2009. A three-dimensional fracture network data set for a block of granite. International Journal of Rock Mechanics and Mining Sciences 46, 811–818.

Eriksen T E, Jansson M, 1996. Diffusion of I$^-$, Cs$^+$ and Sr^{2+} in compacted bentonite. Anion exclusion and surface diffusion. SKB TR 96-16, Svensk Kärnbränslehantering AB.

EUR, 2005. Treatment of radionuclide transport in geosphere within safety assessments (RETROCK). Final report. Contract No. FIKW-CT-2001-20201. EUR 21230 EN, European Commission.

Gelhar L W, Welty C, Rehfeldt K R, 1992. A critical review of data on field-scale dispersion in aquifers. Water Resources Research 28, 1955–1974.

Glaus M A, Baeyens B, Bradbury M H, Jakob A, Van Loon L R, Yaroshchuk A, 2007. Diffusion of ^{22}Na and ^{85}Sr in montmorillonite: evidence of interlayer diffusion being the dominant pathway at high compaction. Environmental Science & Technology 41, 478–485.

GoldSim, 2010. GoldSim Version 10.1. GoldSim Technology Group.

GoldSim, 2014. GoldSim contaminant transport module user's guide, version 6.4. GoldSim Technology Group.

Hadermann J, Heer W, 1996. The Grimsel (Switzerland) migration experiment: integrating field experiments, laboratory investigations and modelling. Journal of Contaminant Hydrology 21, 87–100.

Haggerty R, Gorelick S M, 1995. Multiple-rate mass transfer for modelling diffusion and surface reactions in media with pore-scale heterogeneity. Water Resources Research 31, 2383–2400.

Haggerty R, McKenna S A, Meigs L C, 2000. On the late-time behavior of tracer test breakthrough curves. Water Resources Research 36, 3467–3479.

Hakanen M, Ervanne H, Puukko E, 2014. Safety case for the disposal of spent nuclear fuel at Olkiluoto. Radionuclide migration parameters for the geosphere. Posiva 2012-41, Posiva Oy, Finland.

Hammond G, Lichtner P, Mills R, 2014. Evaluating the performance of parallel subsurface simulators: an illustrative example with PFLOTRAN. Water Resources Research 50, 208–228.

Harbaugh A W, Banta E R, Hill M C, McDonald M G, 2000. MODFLOW-2000, the U.S. Geological Survey modular ground-water model – User guide to modularization concepts and the ground-water flow process. Open-File Report 00-92, U.S. Geological Survey.

Heer W, 1997. Modelling the Grimsel migration field experiments at PSI. In Paul Scherrer Institut Annual report 1996: annex IV: PSI nuclear energy and safety research, 65–72.

Hollenbeck K J, 1998. INVLAP. M: A matlab function for numerical inversion of Laplace transforms by the de Hoog algorithm. Available at: https://www.mathworks.com/matlabcentral/answers/uploaded_files/1034/invlap.m

Itälä A, Laitinen M, Tanhua-Tyrkkö M, Pulkkanen V-M, Olin M, 2010. COMSOL Multiphysics, TOUGHREACT and Numerrin comparison in some modelling tasks of spent nuclear fuel disposal. In Proceedings of the COMSOL Conference 2010 Paris.

JAEA, 2015. Preliminary assessment of geological disposal system for spent fuel in Japan – First progress report on direct disposal. JAEA-Research 2015-016, Japan Atomic Energy Agency.

JNC, 1999. H12: Project to establish technical basis for HLW disposal in Japan. Supporting report 3: Safety assessment of the geological disposal system. JNC TN1410 2000-04, Japan Nuclear Cycle Development Institute.

Jokelainen L, Meski T, Lindberg A, Soler J M, Siitari-Kauppi M, Martin A J, Eikenberg J, 2013. The determination of ^{134}Cs and ^{22}Na diffusion profiles in granodiorite using gamma spectroscopy. Journal of Radioanalytical and Nuclear Chemistry 295, 2153–2191.

Kajanto K, 2013. The effect of geometry on radionuclide transport in a bedrock fracture. Espoo: VTT Technical Research Centre of Finland. (VTT Technology 128)

Kato H, Muroi M, Yamada N, Ishida H, Sato H, 1995. Estimation of effective diffusivity in compacted bentonite. In Murakami T, Ewing R C (eds). Scientific basis for nuclear waste management XVIII: symposium held in Kyoto, Japan, 23–27 October 1994. Pittsburgh, PA: Materials Research Society. (Materials Research Society Symposium Proceedings 353), 277–284.

Kaukonen V, Hakanen M, Lindberg A, 1997. Diffusion and sorption of HTO, Np, Na and Cl in rocks and minerals of Kivetty and Olkiluoto. Posiva-97-07, Posiva Oy, Finland.

Lee J O, Birch K, Choi H-J, 2014. Coupled thermal-hydro analysis of unsaturated buffer and backfill in a high-level waste repository. Annals of Nuclear Energy 72, 63–75.

Li Q, Ito K, Wu Z, Lowry C S, Loheide I I S P, 2009. COMSOL Multiphysics: a novel approach to ground water modelling. Ground Water 47, 480–487.

Lichtner P C, Hammond G E, Lu C, Karra S, Bisht G, Andre B, Mills R T, Kumar J, 2013. PFLOTRAN User Manual. Available at: http://www.pflotran.org

Löfgren M, Nilsson K, 2019. Task description of Task 9A - modelling of REPRO experiments WPDE-1 and WPDE-2. Task 9 of SKB Task Force GWFTS – Increasing the realism in solute transport modelling based on the field experiments REPRO and LTDE-SD. SKB Report P-17-18, Svensk Kärnbränslehantering AB.

Malmström M E, Destouni G, Banwart S A, Strömberg B H E, 2000. Resolving the scale-dependence of mineral weathering rates. Environmental Science & Technology 34, 1375–1378.

Missana T, García-Gutiérrez M, Alonso U, Mingarro M, 2006. On radionuclide retention mechanisms in fractured geologic media. Journal of Iberian Geology 32, 55–77.

Molinero J, Trinchero P, de Vries L M, Ebrahimi H, Svensson U, 2016. The BRIDGE Project. Development, testing and application of a high performance computing framework for reactive transport modelling in crystalline roks (iDP). SKB R-15-17, Svensk Kärnbränslehantering AB.

Molins S, Trebotich D, Yang L, Ajo-Franklin J B, Ligocki T J, Shen C, Steefel C I, 2014. Pore-scale controls on calcite dissolution rates from flow-through laboratory and numerical experiments. Environmental Science & Technology 48, 7453–7460.

Molz F, 2015. Advection, dispersion, and confusion. Groundwater 53, 348–353.

Montoto M, Mateos F, 2006. Characterization of water pathways in low permeable rocks at the rock matrix scale: Methodological review. Journal of Iberian Geology 32, 197–213.

Muurinen A, 1994. Diffusion of anions and cations in compacted sodium bentonite. VTT Publications 168, Espoo, Finland.

NEA, 2012. Thermodynamic sorption modeling in support of radioactive waste disposal safety cases. NEA Sorption Project Phase III. Paris: OECD/NEA.

Neretnieks I, 1980. Diffusion in the rock matrix: an important factor in radionuclide retardation? Journal of Geophysical Research 85, 4379–4397.

Neretnieks I, 1983. A note on fracture flow dispersion mechanisms in the ground. Water Resources Research 19, 364–370.

Neretnieks I, Moreno L, 2003. Prediction of some in situ tracer tests with sorbing tracers using independent data. Journal of Contaminant Hydrology 61, 351– 360.

Neuman S P, 1995. On advective transport in fractal permeability and velocity fields. Water Resources Research 31, 1455–1460.

NUMO, 2013. Safety of the geological disposal project 2010. Safe geological disposal based on reliable technologies. English summary. NUMO-TR-13-05, Nuclear Waste Management Organization of Japan.

Ogata A, 1970. Theory of dispersion in a granular medium. Washington: U.S. Governemnt Printing Office. (Geological Survey Professional Paper 411-I). Available at: https://pubs.usgs.gov/pp/0411i/report.pdf

Ohlsson Y, 2000. Studies of ionic diffusion in crystalline rock. PhD thesis. Royal Institute of Technology, Sweden.

Ohlsson Y, Neretnieks I, 1998. Some evidence for surface ion mobility in rock. Journal of Contaminant Hydrology 35, 91–100.

Olin M, Tanhua-Tyrkkö M, Pulkkanen V-M, Itälä A, Rasilainen K, Seppälä A, Liukkonen M, 2008. Thermo-hydro-mechanical-chemical (THMC) modelling of the bentonite barriers in final disposal of high level nuclear waste. In Proceedings of the COMSOL Conference 2008 Hannover.

Ota K, Möri A, Alexander W R, Frieg B, Schild M, 2003. Influence of the mode of matrix porosity determination on matrix diffusion calculations. Journal of Contaminant Hydrology 61, 131–145.

Painter S, Cvetkovic V, Selroos J-O, 1998. Transport and retention in fractured rock: Consequences of a power-law distribution for fracture lengths. Physical Review E 57, 6917–6922.

Painter S, Cvetkovic V, Mancillas J, Pensado O, 2008. Time domain particle tracking methods for simulating transport with retention and first-order transformation. Water Resources Research 44. doi:10.1029/2007WR005944

Perko J, Seetharam S C, Mallants D, 2009. Simulation tools used in long-term radiological safety assessments: Project near surface disposal of category A waste at Dessel. NIROND-TR 2008-11 E, NIRAS-MP5-01 QUAL-LT Version 1, ONDRAF/NIRAS, Belgium.

Perko J, Seetharam S C, Mallants D, 2011. Verification and validation of flow and transport in cracked saturated porous media. In Proceedings of the COMSOL Conference 2011 Stuttgart.

Piqué A, Grandia F, Sena C, Arcos D, Molinero J, Duro L, Bruno J, 2010. Conceptual and numerical modelling of radionuclide transport in near-surface systems at Forsmark. SR-Site Biosphere. SKB R-10-30, Svensk Kärnbränslehantering AB.

Piqué A, Arcos D, Grandia F, Molinero J, Duro L, Berglund S, 2013a. Conceptual and numerical modeling of radionuclide transport and retention in near-surface systems. Ambio 42, 476–487.

Piqué A, Pękala M, Molinero J, Duro L, Trinchero P, de Vries L M, 2013b. Updated model for radionuclide transport in the near-surface till at Forsmark. Implementation of decay chains and sensitivity analyses. SKB R-13-02, Svensk Kärnbränslehantering AB.

Poteri A, Andersson P, Nilsson K, Byegård J, Skålberg M, Siitari-Kauppi M, Helariutta K, Voutilainen M, Kekäläinen P, Ikonen J, Sammaljärvi J, Lindberg A, Timonen J, Kuva J, Koskinen L, 2018a. The First Matrix Diffusion Experiment in the Water Phase of the REPRO Project: WPDE 1. Posiva Working Report 2017-23, Eurajoki, Finland.

Poteri A, Andersson P, Nilsson K, Byegård J, Skålberg M, Siitari-Kauppi M, Helariutta K, Voutilainen M, Kekäläinen P, 2018b. The Second Matrix Diffusion Experiment in the Water Phase of the REPRO Project: WPDE 2. Posiva Working Report 2017-24, Eurajoki, Finland.

Press W H, Teukolsky S A, Vetterling W T, Flannery B P, 2007. Numerical recipes: the art of scientific computing. 3rd ed. New York: Cambridge University Press.

Pulkkanen V-M, 2009. Radionuclide transport through different routes near a deposition hole for spent nuclear fuel. In Proceedings of the COMSOL Conference 2009 Milan.

Pulkkanen V-M, Nordman H, 2011. Effects of bedrock fractures on radionuclide transport near a vertical deposition hole for spent nuclear fuel. Posiva 2011-03, Posiva Oy, Finland.

Sardini P, Siitari-Kauppi M, Beaufort D, Hellmuth K H, 2006. On the connected porosity of mineral aggregates in crystalline rocks. American Mineralogist 91, 1069–1080.

Sardini P, Robinet J C, Siitari-Kauppi M, Delay F, Hellmuth K H, 2007. Direct simulation of heterogeneous diffusion and inversion procedure applied to an out-diffusion experiment. Test case of Palmottu granite. Journal of Contaminant Hydrology 93, 21–37.

Seetharam S C, Perko J, Jacques D, Mallants D, 2014. Influence of fracture networks on radionuclide transport from solidified waste forms. Nuclear Engineering and Design 270, 162–175.

Sentís M L, Altorfer F, Herfort M, Jakob A, Kosakowski G, Friedel S, 2009. Benchmark calculations with COMSOL of the transport of radionuclides through clay and bentonite barriers in a geological repository. In Proceedings of the COMSOL Conference 2009 Milan.

Skagius K, 1986. Diffusion of dissolved species in matrix of some Swedish crystalline rocks. PhD thesis. Royal Institute of Technology, Sweden.

Skagius K, Neretnieks I, 1986. Porosities and diffusivities of some nonsorbing species in crystalline rocks. Water Resources Research 22, 389–398.

Skagius K, Pettersson M, Wiborgh M, Albinsson Y, Holgersson S, 1999. Compilation of data for the analysis of radionuclide migration from SFL 3-5. SKB R-99-13, Svensk Kärnbränslehantering AB.

SKB, 2004. RETROCK Project. Treatment of geosphere retention phenomena in safety assessments. Scientific basis of retention processes and their implementation in safety assessment model (WP2). SKB R-04-48, Svensk Kärnbränslehantering AB.

Soler J M, Landa J, Havlova V, Tachi Y, Ebina T, Sardini P, Siitari-Kauppi M, Eikenberg J, Martin A J, 2015. Comparative modeling of an in situ diffusion experiment in granite at the Grimsel Test Site. Journal of Contaminant Hydrology 179, 89–101.

Steefel C I, Molins S, 2016. CrunchFlow. Software for modeling multicomponent reactive flow and transport. User's manual. Lawrence Berkeley National Laboratory, California.

Steefel C I, Appelo C A J, Arora B, Jacques D, Kalbacher T, Kolditz O, Lagneau V, Lichtner P C, Mayer K U, Meeussen J C L, Molins S, Moulton D, Shao H, Šimůnek J, Spycher N, Yabusaki S B, Yeh G T, 2015a. Reactive transport codes for subsurface environmental simulation. Computational Geosciences 19, 445–478.

Steefel C I, Beckingham L E, Landrot G, 2015b. Micro-continuum approaches for modeling pore-scale geochemical processes. Reviews in Mineralogy and Geochemistry 80, 217–246.

Stephan M, Docter J, 2015. JUQUEEN: IBM Blue Gene/Q® Supercomputer System at the Jülich Supercomputing Centre. Journal of Large-Scale Research Facilities 1. doi:10.17815/jlsrf-1-18

Sudicky E A, Frind E, 1982. Contaminant transport in fractured porous media: analytical solution for a system of parallel fractures. Water Resources Research 18, 1634–1642.

Svensson U, 2001a. A continuum representation of fracture networks. Part I: Method and basic test cases. Journal of Hydrology 250, 170–186.

Svensson U, 2001b. A continuum representation of fracture networks. Part II: Application to the Äspö Hard Rock laboratory. Journal of Hydrology 250, 187–205.

Svensson U, Ferry M, 2014. DarcyTools: a computer code for hydrogeological analysis of nuclear waste repositories in fractured rock. Journal of Applied Mathematics and Physics. doi:10.4236/jamp

Tachi Y, Yotsuji K, 2014. Diffusion and sorption of Cs^+, Na^+, I^- and HTO in compacted montmorillonite as a function of porewater salinity: Integrated sorption and diffusion model. Geochimica et Cosmochimica Acta 132, 75–93.

Tachi Y, Yotsuji K, Seida Y, Yui M, 2011. Diffusion and sorption of Cs^+, I^- and HTO in samples of the argillaceous Wakkanai Formation from the Horonobe URL, Japan: Clay-based modeling approach. Geochimica et Cosmochimica Acta 75, 6742–6759.

Tachi Y, Yotsuji K, Suyama T, Ochs M, 2014. Integrated sorption and diffusion model for bentonite. Part 2: porewater chemistry, sorption and diffusion modeling in compacted systems. Journal of Nuclear Science and Technology 51, 1191–1204.

Tachi Y, Ebina T, Takeda C, Saito T, Takahashi H, Ohuchi Y, Martin A J, 2015. Matrix diffusion and sorption of Cs^+, Na^+, I^- and HTO in granodiorite: laboratory-scale results and their extrapolation to the in situ condition. Journal of Contaminant Hydrology 179, 10–24.

Tang D, Frind E, Sudicky E A, 1981. Contaminant transport in fractured porous media: analytical solution for a single fracture. Water Resources Research 17, 555–564.

Trinchero P, Molinero J, Román-Ross G, 2014a. FASTREACT – A streamline-based approach for the solution of multicomponent reactive transport problems. SKB R-10-45, Svensk Kärnbränslehantering AB.

Trinchero P, Molinero J, Román-Ross G, Berglund S, Selroos J-O, 2014b. FASTREACT – An efficient numerical framework for the solution of reactive transport problems. Applied Geochemistry 49, 159–167.

Trinchero P, Painter S, Ebrahimi H, Koskinen L, Molinero J, Selroos J-O, 2016. Modelling radionuclide transport in fractured media with a dynamic update of K_d values. Computers & Geosciences 86, 55–63.

Trinchero P, Molinero J, Deissmann G, Svensson U, Gylling B, Ebrahimi H, Hammond G E, Bosbach D, Puigdomenech I, 2017. Implications of grain-scale mineralogical heterogeneity for radionuclide transport in fractured media. Transport in Porous Media 116, 73–90.

TUL, 2015. FLOW123D version 1.8.2, Documentation of file formats and brief user manual. Technical University of Liberec. Available at: http://flow123d.github.io/

Tullborg E-L, Larson S Å, 2006. Porosity in crystalline rocks – A matter of scale. Engineering Geology 84, 75–83.

Van Loon L R, Soler J M, Müller W, Bradbury M H, 2004. Anisotropic diffusion in layered argillaceous rocks: a case study with Opalinus clay. Environmental Science & Technology 38, 5721–5728.

Van Loon L R, Glaus M A, Müller W, 2007. Anion exclusion effects in compacted bentonites: towards a better understanding of anion diffusion. Applied Geochemistry 22, 2536–2552.

Vanýsek P, 2009. Ionic conductivity and diffusion at infinite dilution. 90th ed. In Lide D R (ed). CRC handbook of chemistry and physics: a ready-reference book of chemical and physical data. Boca Raton, FL: CRC Press.

Vetešník A, Landa J, Vokál A, Vopálka D, 2015. A sensitivity and probability analysis of the safety of deep geological repositories situated in crystalline rock. Journal of Radioanalytical and Nuclear Chemistry 304, 409–415.

Vopálka D, Filipská H, Vokál A, 2006. Some methodological modifications of determination of diffusion coefficients in compacted bentonite. In Van Iseghem P (ed). Scientific basis for nuclear waste management XXIX: proceedings of a meeting held in Ghent, Belgium, 12–16 September 2005. Warrendale, PA: Materials Research Society. (Materials Research Society Symposium Proceedings 932), 983–990.

Voutilainen M, Sardini P, Siitari-Kauppi M, Kekäläinen P, Aho V, Myllys M, Timonen J, 2013. Diffusion of tracer in altered tonalite: experiments and simulations with heterogeneous distribution of porosity. Transport in Porous Media 96, 319–336.

Widestrand H, Byegård J, Cvetkovic V, Tullborg E-L, Winberg A, Andersson P, Siitari-Kauppi M, 2007. Sorbing tracer experiments in a crystalline rock fracture at Aspo (Sweden): 1. Experimental setup and microscale characterization of retention properties. Water Resources Research 43, W10413. doi:10.1029/2006WR005277

Willmann M, Carrera J, Sánchez-Vila X, 2008. Transport upscaling in heterogeneous aquifers: what physical parameters control memory functions? Water Resources Research 44, W12437. doi:10.1029/2007WR006531

Witthüser K, Arnepalli D, Singh D N, 2006. Investigations on diffusion characteristics of granite and chalk rock mass. Geotechnical & Geological Engineering 24, 325–334.

Zheng, 2010. MT3D MS v5.3 supplemental user's guide. Technical Report to the U.S. Army Engineer Research and Development Center, Department of Geological Sciences, University of Alabama.

Appendices – Reports from the modelling teams

Content

Department of Chemical Engineering and Technology, Royal Institute of Technology, KTH, Stockholm, Sweden

Ivars Neretnieks, Luis Moreno, Longcheng Liu, Shuo Meng

A1 Introduction

We have modelled the REPRO experiments WPDE-1 and WPDE-2 as is found in the Task 9A Description.

A1.1 Background

We have worked with flow and transport in fractured crystalline rocks with porous matrices over a long time. Our interest is primarily aimed at applications to nuclear waste repositories. We have over the years developed analytical and numerical computation tools suitable for such applications and have performed numerous field and laboratory experiments related to this problem.

A1.2 Objectives

One immediate objective is to familiarise ourselves with the repro experiments and to do some scoping calculations.

Our main objective is to further validate our models using well designed experiments.

A1.3 Scope and limitations

Our modelling is based on the conventional advection-dispersion model coupled to matrix diffusion. For dispersion in this specific case we use Taylor dispersion in slot and in tubing. This dispersion is modelled as velocity dispersion in the slot. Radial and linear matrix diffusion is modelled accounting for retardation by linear sorption. No surface sorption is invoked for transport in the slot. The water residence time and dispersion in slot and tubes is accounted for. Ion exclusion effects for chloride are modelled. The rock is modelled as a homogeneous porous medium with regard to porosity and sorption properties. Likewise the slot is modelled as having constant aperture and fluid velocity although effects of velocity variations are discussed and explored by modelling of velocity dispersion.

We use primarily analytical solutions with linear diffusion to simulate the residence time distribution (RTD) and breakthrough curves (BTC) but assess errors when neglecting the effect of radial diffusion. Sensitivity analyses are used to assess how errors or variations in velocity, rock matrix porosity, diffusivity and distribution coefficients influence the results.

A2 Methodology and model

See Section A3 for details.

We have used a model that describes advection and dispersion (AD) in a narrow slot coupled to matrix diffusion (MD). Dispersion is accounted for as Taylor dispersion in the slot as well as in the inlet and outlet tubes. Matrix diffusion is modelled as being linear instead of radial for reasons explained in Section A3.

As Taylor dispersion in the slot marginally increases dispersion above that caused by molecular diffusion in the flowing water, this leads to a very sharp concentration front travelling with the velocity of the flowing water. This in turn induces numerical difficulties for numerical codes to solve the AD+MD equation as well as for an analytical solution (Tang et al. 1981). To avoid this we solve the AD equation setting dispersion equal to zero. Then a very simple analytical solution for A+MD is available for linear MD. In order to account for the neglected Taylor dispersion in the slot in the AD model the dispersion is modelled as velocity dispersion (VD) to give the same additional variance in residence times of the solutes. The VD in principle describes a bundle of streamlines, mixed at

the outlet, in which the RTD is modelled with A+MD model with a distribution of water residence times (t_w). The t_w distribution is chosen such that the same dispersion, Peclet number (Pec), results as that due to Taylor dispersion. This approach has the additional advantage besides being numerically accurate and stable that it can be used to also model dispersion in the slot caused by actual variations of velocity caused by variations in slot apertures.

The main uncertainties we deem to be those in pore diffusivity and matrix porosity for the non-sorbing tracers and in distribution coefficients for the sorbing tracers. For the upper and lower BTC predictions we lump these uncertainties in the materials property group (MPG), with the same variation for all tracers. The impact of uncertainties due to VD is illustrated in an example.

The presented BTC's in this report and in the Excel tables thus include the effects of advection in the slot with linear matrix diffusion and dispersion modelled as VD. Dispersion in the in- and outlet tubes is shown to have negligible impact on the residence time distribution (RTD).

A3 Model

A3.1 Introduction

The REPRO experiment is described in "SKB Task Force on Modelling of Groundwater Flow and Transport of Solutes".

In the experiments a solute tracer pulse is injected in water flowing through a circular slot in a borehole with a concentric dummy. Solute in the water in the slot diffuses in and out of the porous rock matrix. This causes the solute pulse to spread and to be retarded compared to the water residence time. Non-sorbing as well as sorbing tracers were used. Two experiments with partly different tracers and water flowrates were performed. The diameter of the borehole is 56.5 mm and the slot has an aperture of 1.25 mm. Detailed data on the experiment are summarised in the data section below.

The task is to predict the residence time distribution RTD, in the form of breakthrough curves, BTC's, of the different tracers as they pass the slot and arrive at the detector. The RTD's in inlet and outlet tubes are accounted for. We use a model that describes the advective flow in the slot coupled to a model that describes the diffusion in the pores of the rock matrix and sorption on the crystal surfaces in the matrix. In addition we explore the impact of Taylor dispersion and velocity dispersion on the RTD. The mathematical model is described in the section below.

A3.2 Model details

Advection and dispersion in the slot with diffusion in the rock matrix

The concentration evolution in time and along the slot length is described by the advection-dispersion equation coupled with the interaction with matrix diffusion. We call it the AD+MD equation

For the slot at any location x the concentration c varies with time as

$$R_a \frac{\partial c}{\partial t} = -u \frac{\partial c}{\partial x} + D_{Disp} \frac{\partial^2 c}{\partial x^2} + \frac{1}{b} D_p \varepsilon_p \frac{\partial c_p}{\partial r}\bigg|_{r=r_i} - \lambda R_a c \qquad \text{(Eq A-1)}$$

R_a is the surface retardation coefficient, D_{Disp} a diffusion-dispersion coefficient, u is the velocity in the slot, b is the slot aperture, r_i is the radius of the borehole. $R_a = 1$ in this report. The term 1/b can be seen as the flow wetted surface of the rock to the channel volume $\frac{1}{b} = \frac{2\pi r_i x_o}{b 2\pi r_i x_o}$ and this entity must be the same for the channel for both radial and cylindrical diffusion, discussed below, because we need to maintain the same flow velocity and water residence time in the channel. D_p is the pore diffusion coefficient in the pores of the rock matrix, ε_p the porosity and $\frac{\partial c_p}{\partial r}\big|_{r=r_i}$ the concentration gradient in the pore water at the interface between flowing water and rock matrix. The third term on the r.h.s. of Equation (A-1) describes the rate of solute exchange between flowing water and rock matrix. λ is the decay constant of the nuclide.

The initial and boundary conditions for Equation (A-1) are

$$c(t = 0, x) = 0 \qquad \text{(Eq A-2)}$$

$$c(t, 0) = c_{in}(t) = c_o e^{-\lambda t} \tag{Eq A-3}$$

where $c_{in}(t)$ denotes how the concentration to the inlet of the slot changes over time.

$$c(t, x \to \infty) = 0 \tag{Eq A-4}$$

Equation (A-3) and Equation (A-4) will be discussed in the section on Taylor dispersion in inlet and outlet tubes and in the slot.

Rock matrix diffusion

The concentration evolution in time and space in the pore water in the rock matrix is described by

$$\frac{\partial c_p}{\partial t} = \frac{D_a}{r} \frac{\partial}{\partial r}\left(r \frac{\partial c_p}{\partial r}\right) - \lambda c_p = D_a\left(\frac{\partial^2 c_p}{\partial r^2} + \frac{1}{r}\frac{\partial c_p}{\partial r}\right) - \lambda c_p \tag{Eq A-5}$$

Note that in this formulation we inherently assume that the diffusion and distribution coefficients are constant throughout the rock matrix and that they can be combined in a constant D_a. Variations of these entities will be addressed in later subtasks of Task 9. It is also assumed that diffusion in the x-direction is neglected. This is permissible because the transport rate in the x-direction by matrix diffusion is negligible compared to the rate of transport by advection in the slot under the conditions of the experiments.

$D_a = \frac{D_p}{R}$ is the apparent diffusion coefficient, R is the retardation factor due to linear reversible sorption, $R = 1 + \frac{K_d \rho_s}{\varepsilon_p}$, K_d is the mass distribution coefficient and ρ_s is here the bulk dry density of the rock matrix. The initial and boundary conditions for Equation (A-5) are

$$c_p(t = 0, r > r_i, x) = 0 \tag{Eq A-6}$$

$$c_p(t, r = r_i, x) = c(t, x) \tag{Eq A-7}$$

$$c_p(t, r \to \infty, x) = 0 \tag{Eq A-8}$$

It will be shown later that if one approximates the matrix diffusion to be linear instead of radial, this leads to some error for the non-sorbing tritium and chloride but the error is negligible for the sorbing nuclides. We will use linear diffusion omitting the term $\frac{1}{r}\frac{\partial c_p}{\partial r}$ because the solution is considerably simpler and the solution for the radial case causes numerical difficulties when the interaction with the rock matrix is very small, which is the case for the tritium and chloride in experiments.

Dispersion

Hydrodynamic dispersion modelled as Taylor dispersion

When water flows in a narrow tube or slot the velocity profile perpendicular to the flow direction becomes parabolic after a short distance. A solute will be more rapidly carried in the centre of the conduit than near the walls where the velocity is zero. However, molecular diffusion will tend to even out the concentration in the radial direction. The dispersion coefficient D_{Disp} in Equation (A-1) can be obtained by the following expression

$$D_{Disp} = D_{Taylor} = D_w(1 + \text{Const Pec}_w^2) \tag{Eq A-9}$$

D_w is the molecular diffusion coefficient in water and

$$\text{Pec}_w = \frac{u\,b}{D_w} \tag{Eq A-10}$$

b is the flow path aperture and Const = 1/192 and 1/210 for a circular tube and an infinitely wide slot respectively. This Peclet number describes the spread in residence times in relation to the mean travel time by molecular diffusion only.

Another Peclet number is now defined that describes the spread in residence times caused by dispersion based on the flowpath length L.

$$Pec_{Disp} = \frac{u\,L}{D_{Disp}} \qquad\qquad \text{(Eq A-11)}$$

This Peclet number also can be interpreted as twice the mean water residence time squared divided by the variance in residence times σ_{tv}^2. σ_{tv} is the standard deviation of the residence time.

$$Pec = 2\left(\frac{t_{w,mean}}{\sigma_{tv}}\right)^2 \qquad\qquad \text{(Eq A-12)}$$

The impact of Taylor dispersion in inlet and outlet tubes and in the slot will also be assessed as it may cause spreading of the inlet pulse as well as the BTC of the slot when measured downstream in the tube.

Velocity dispersion

The slot aperture varies slightly, which causes some variation in residence times along different streamlines in the slot and causes "velocity dispersion" (Neretnieks 1983).

This can be described by another Peclet number based on the mean water velocity and the standard deviation σ_{tv} of the mean water residence times along different streamlines or streamtubes (channels).

$$Pec_{vd} = 2\left(\frac{t_{w,mean}}{\sigma_{tv}}\right)^2 \qquad\qquad \text{(Eq A-13)}$$

When there is information of the spread in residence times along the flowpaths caused e.g. by variations in the slot aperture Pec_{vd} can be determined from Equation (A-13). It may be noted that this way of describing the velocity dispersion is based on the assumption that diffusion between streamlines is negligible. Velocity dispersion will be shown to be potentially larger than Taylor dispersion in the slot. Velocity dispersion can be described by Equation (A-13) and can also be expressed as a dispersion coefficient $D_{Disp,vd}$ if one wishes. However, we do not wish to do this for use in Equation (A-1) because the underlying mechanism is not comparable to Fickian diffusion, which is the basis for formulation of Equation (A-1) with the dispersion term. Instead the effect of velocity dispersion is model by Equation (A-21).

Combined dispersion effects

When there are different mechanisms in the same flowpath giving rise to dispersion the joint effect can be determined by adding the variances

$$Pec_{tot} = \frac{1}{\sum \dfrac{1}{Pec_i}} \qquad\qquad \text{(Eq A-14)}$$

For illustration and comparisons the combined effect of dispersion from different causes can be obtained from

$$D_{Disp} = \frac{u\,L}{Pec_{tot}} \qquad\qquad \text{(Eq A-15)}$$

However, we do not want to include velocity dispersion in such a combined entity because it leads to strange consequences. In Equation (A-1) D_{Disp} is a constant for a given velocity and the equation is solved based on that. A velocity dispersion coefficient always increases proportionally to travel distance. When velocity dispersion dominates dispersion it is therefore not correct to use Equation (A-1) with a constant D_{Disp} (Neretnieks 1983). However, when Pec_{vd} is large, more than several hundred, the use of Equation (A-1) gives similar BTC's to those obtained by Equation (A-21) below describing VD.

Some further simplifying assumptions

We already noted that diffusion in the rock matrix in the x-direction can be neglected resulting in a simplified Equation (A-5). Neglecting dispersion caused by Taylor dispersion and molecular diffusion, 3rd term in Equation (A-1), Equation (A-1) simplifies to

$$\frac{\partial c}{\partial t} = -u\frac{\partial c}{\partial x} + \frac{1}{b}D_p\varepsilon_p\frac{\partial c_p}{\partial r}\bigg|_{r=r_i} - \lambda c \tag{Eq A-16}$$

This also implies that only one boundary condition is needed for Equation (A-16), namely Equation (A-3); Equation (A-4) is not needed.

Dispersion giving rise to the same increase in the variance in the RTD as Taylor dispersion, will instead be modelled by VD.

It may be further noted that for short times, meaning, when the diffusion penetration distance into the matrix is less than on the order of the diameter of the borehole the impact of radial diffusion in Equation (A-5) given by the term $\frac{1}{r}\frac{\partial c_p}{\partial r}$ can be neglected and Equation (A-5) can be simplified to describe linear diffusion

$$\frac{\partial c_p}{\partial t} = D_a\frac{\partial^2 c_p}{\partial r^2} - \lambda c_p \tag{Eq A-17}$$

Further, assuming that the inlet boundary condition Equation (A-3) can approximated by a rectangular pulse (Decaying Top-Hat function)

$$c_{in}(t) = c_o e^{-\lambda t} \text{ for } 0 < t < \Delta t \tag{Eq A-18}$$

the solution to Equation (A-16) neglecting dispersion and Equation (A-17), neglecting the radial diffusion term with the initial conditions Equation (A-2) and Equation (A-6) and boundary conditions Equation (A-3), Equation (A-7) (using a top hat function during time Δt) and Equation (A-8) is (Neretnieks 1980)

$$c(t,x,t_w) = c_o e^{-\lambda t}\left[Erfc\left(\frac{FWS}{q}\frac{MPG}{2\sqrt{t-t_w}}\right) - Erfc\left(\frac{FWS}{q}\frac{MPG}{2\sqrt{t-t_w-\Delta t}}\right)\right] \tag{Eq A-19}$$

Erfc is the complementary error function, FWS is the flow wetted surface of the rock in the slot. q is the flowrate and MPG the materials property group, t_w is the water residence time in the slot. The two Erfc functions are 0 for $t < t_w$ and $t < t_w + \Delta t$ respectively.

$$MPG = \varepsilon_p\sqrt{D_p R} \tag{Eq A-20}$$

Sensitivity to variations in water residence time

When there are velocity variations that cause velocity dispersion in the slot this can be accounted for if the residence time distribution from inlet to outlet can be described by a probability density function, PDF, of t_w; $f(t_{w,mean}, \sigma_{tv})$. This PDF describes the spread of water residence times t_w around $t_{w,mean}$ in the slot.

The effluent concentration from the slot when accounting for the water residence time distribution then is

$$c_v(t,x) = \int_0^\infty f(t_{w,mean}, \sigma_{tv})\, c(t,x,t_w)dt_w \tag{Eq A-21}$$

For the probability density function for the residence time distribution we use the Gauss Normal Distribution. $t_{w,mean}$ is the mean and σ_{tv} its standard deviation of water residence times along the different streamlines.

$$f(t_{w,mean}, \sigma_{tv}) = \frac{1}{\sigma_{tv}\sqrt{2\pi}}e^{\frac{-(t_{w,mean}-t_w)^2}{2\sigma_{tv}^2}} \tag{Eq A-22}$$

Sensitivity to the materials property group, MPG

There are uncertainties in several parameters that influence MD. We have reasons to believe that the three most uncertain parameters, which at the same time have a strong impact on the BTC's are matrix porosity, distribution coefficient and pore diffusion coefficient. For the simplified formulation of the A+MD Equation (A-19) they influence the BTC through the materials property group MPG.

$$\text{MPG} = \varepsilon_p \sqrt{D_p R} = \varepsilon_p \sqrt{D_p \left(1 + \frac{K_d \rho_s}{\varepsilon_p}\right)} = \sqrt{D_p(\varepsilon_p{}^2 + \varepsilon_p K_d \rho_s)} \cong \sqrt{\varepsilon_p D_p K_d \rho_s} \quad \text{(Eq A-23)}$$

The last term in (23) is a good approximation for strongly sorbing tracers. For sorbing tracers ε_p, K_d and in D_p has the same impact on MPG. A factor of ten change in ε_p, K_d and in D_p results in a factor of 3.15 change in MPG. We deem the uncertainties in especially K_d to potentially be a factor of 10 up or down. This is because the measurements were based on crushed material of < 0.3 mm and details of the experiment are not available yet (Section 2.4.5 in Task Description). It has been found that for different particle sizes give different Kd's. They differ considerably from what large samples (> cm) give even when careful extrapolation with particle size is used to compensate for size effects (André et al. 2009a). See also discussions on uncertainty of K_d data by (Crawford 2013). We deem this to be the by far largest uncertainty for sorbing species. In the simulations of largest and smallest effects on the BTC's we use a factor of 3.15 larger and smaller values of MPG than the central value.

A3.3   Summary of data used

Geometry and flow data

Table A-1. Basic and derived data. Blue indicates derived values.

LSlot	1.905 m	Length of slot
di	0.0565 m	Diameter of borehole
δ	1.25 mm	Aperture of slot
Wy	0.1775 m	Width of slot in contact with rock π · di
VSlot	4.13×10^{-4} m³	Volume πδ (di−δ)L
LTubeIn	24.2 m	Length of inlet tube
LTubeOutDetect	25.7 m	Length of outlet tube to detector
LTubeOutCollect	30.3 m	Length of outlet tube to collector
dTube	1 mm	Inner diameter of tubes
Q1 WDPE-1	20.1×10^{-9} m³/min	Flowrate
D_w	2×10^{-9} m²/s	Diffusion coefficient in bulk water, same for all species
tw WDPE-1	342.72 h	Mean water residence time in slot
Δt	0.83 h	Injection pulse length
D_{Disp}	2.009×10^{-9} m²/s	Taylor dispersion coefficient WDPE-1
PecDisp	1464	Peclet number in slot
$\dfrac{\sigma_{tv}}{t_{w,mean}}$	0.0370	Relative standard deviation of RT due to Taylor dispersion, Equation (A-13)
Q2 WDPE-2	10.0×10^{-9} m³/min	Flowrate
tw WDPE-2	688.87 h	Mean water residence time in slot
Δt	4.94 h	Injection pulse length
D_{Disp}	2.002×10^{-9} m²/s	Taylor dispersion coefficient WDPE-2
PecDisp	731	Peclet number in slot
$\dfrac{\sigma_{tv}}{t_{w,mean}}$	0.052	Relative standard deviation of RT due to Taylor dispersion, Equation (A-12)

Rock properties

Table A-2. Data used in the modelling, Table numbers refer to Task Description 2015-05-12 (base case selected values).

ε	0.0019–0.027 (0.01)	In experimental section
α HTO	0.007–0.011 (0.01)	Rock matrix capacity factor (Table 2-9)
α Cl-	0.00015–0.0002 (0.000175)	Rock matrix capacity factor (Table 2-9)
ϱ_s	2 650 kg/m^3	Rock matrix density
D_e HTO	1.5–2.6 × 10^{-13} m^2/s (2 × 10^{-13} m^2/s)	Rock matrix effective diffusivity HTO
D_e Cl-	(0.05 × 10^{-13} m^2/s)	Rock matrix effective diffusivity Cl$^-$
D_p HTO and all other species except Cl-	(2 × 10^{-11} m^2/s)	Rock matrix pore diffusivity HTO, $D_p = D_e/ε$, derived value mean, ε = 0.01, D_e = 2 × 10^{-13}
K_d – Na	0.0008–0.0013 m^3/kg (0.001 m^3/kg)	Distribution coefficient Na (Table 2-11)
K_d – Sr	0.0011 m^3/kg	Distribution coefficient Sr
K_d – Ba	0.06–0.08 m^3/kg (0.07 m^3/kg)	Distribution coefficient Ba

Tracer data

Table A-3. Tracer data.

	WPDE-1 Injected activity Bq	WPDE-2 Injected activity Bq
HTO	17.1 × 10^6	31.1 × 10^6
Na-22	1.38 × 10^6	2.04 × 10^6
Cl-36	1.25 × 10^6	5.09 × 10^6
Sr-85	–	4.12 × 10^6
Ba-133	–	2.46 × 10^6
Injection volume in loop	0.999 mL	3 mL

A3.4   Some results

The BTC's as well as data for early arrival and tailing are supplied separately in the Excel tables given according to the template formats.

Recovery of tracers

Table A-4 shows the predicted recovery of the tracers in the two different experiments during the experimental time. The data do not consider that there has been decay.

Table A-4. Recovery of tracers.

WPDE-1	HTO	Na-22	Cl-36		
Central	0.986	0.771	0.986		
Upper	0.992	0.867	0.992		
Lower	0.953	0.595	0.953		
WPDE-2	**HTO**	**Na-22**	**Cl-36**	**Sr-85**	**Ba-133**
Central	0.987	0.783	0.987	0.772	0.021
Upper	0.994	0.874	0.995	0.868	0.186
Lower	0.955	0.518	0.956	0.598	0.000028

It is seen that for the sorbing tracers Na, Sr and Ba the predicted recovery is very sensitive to the value of the MPG.

Predicted tracer BTC's

The figures show the relative tracer flowrate, log(Bq/hr per Injected Bq)

Tritium WPDE-1

Figure A-1, shows the tritium BTC for the central case, middle curve, and for two cases where the materials property group MPG is 3.15 larger, lowest peak and 3.15 times smaller, highest peak. The right hand figure enlarges part of the left hand figure.

The BTC's for tritium for WPDE-2 are very similar in shape but start about a factor two later caused by the differences in water residence times.

Chloride WPDE-1

In Figure A-2 we have used the surprisingly low rock capacity factor $\alpha = 0.000175$ to obtain the highest peak. The mid curve is for $\alpha = 0.01$, which implies that no ion exclusion is assumed. $\alpha = 0.0315$ for the lowest peak. Similar curves are obtained for WPDE-2.

Sodium WPDE-1

Figure A-3, shows the Na-22 BTC for the central case, middle curve and for two cases where the materials property group MPG is 3.15 larger, lowest peak and 3.15 times smaller, highest peak.
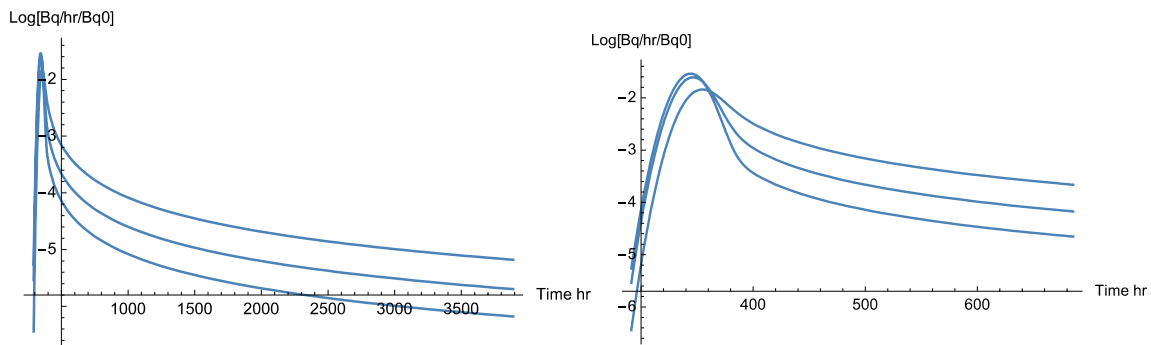
**Figure A-1.** *Tritium BTC for WPDE-1. Right figure detail of left figure.*
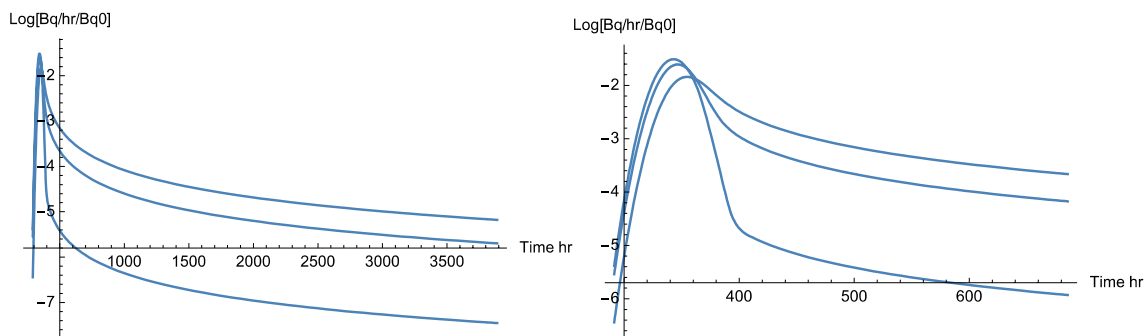
Figure A-2. *Chloride BTC for WPDE-1. Right figure detail of left figure.*
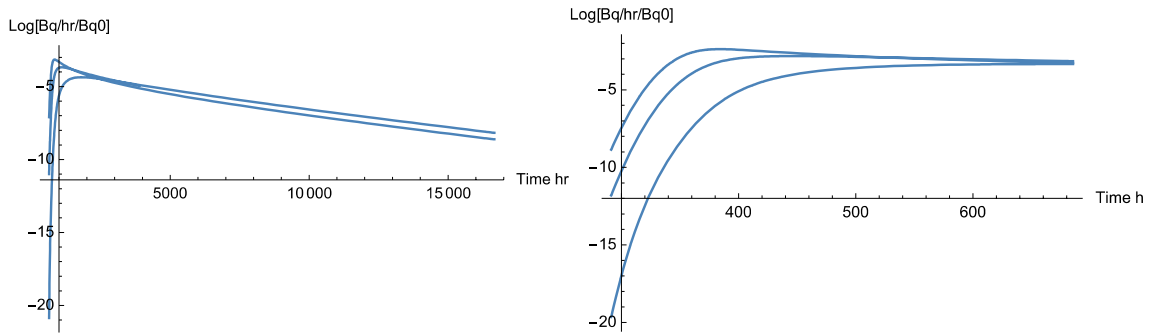
Figure A-3. Sodium BTC for WPDE-1. Right figure detail of left figure.

Strontium WPDE-2

Figure A-4, shows the strontium BTC for the central case, middle curve and for two cases where the materials property group MPG is 3.15 larger, lowest peak and 3.15 times smaller, highest peak

Barium WPDE-2

Figure A-5, shows the barium BTC, for the central case, middle curve and for two cases where the materials property group MPG is 3.15 larger, lowest curve and 3.15 times smaller, highest curve.
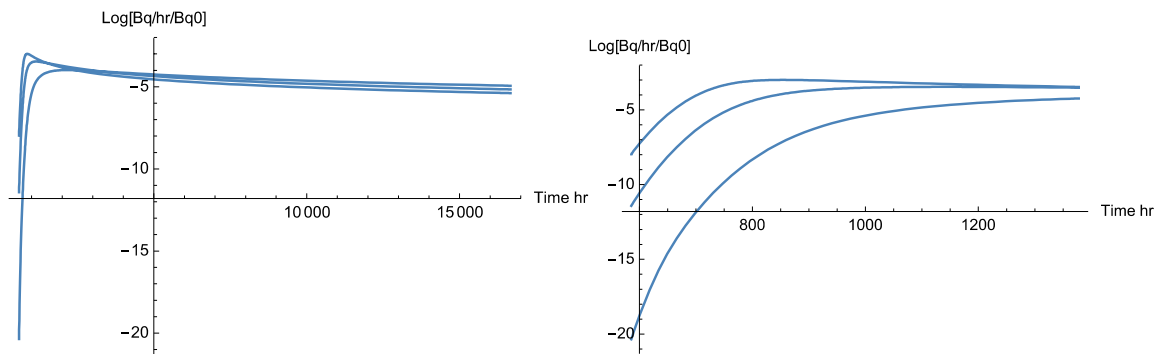
Figure A-4. Strontium BTC for WPDE-2. Right figure detail of left figure.
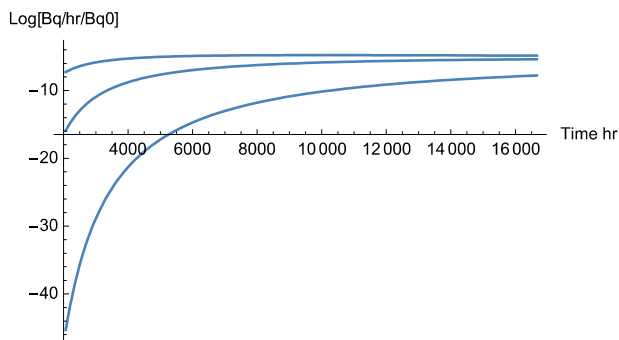
Figure A-5. Barium BTC for WPDE-2.

Further uncertainties

Impact of dispersion in the slot

We do not want to solve the AD+MD Equations (A-1) through (A-5) numerically nor use the Tang et al. (1981) analytical solution because both methods give rise to increasingly larger errors, the larger the Peclet number is, i.e. when the BTC is very sharp. The analytical solution even breaks down for large Peclet numbers. Instead the solution is obtained with very good approximation by using the model Equations (A-19), (A-20) and (A-22) with velocity dispersion with the same Peclet number. This has been found to give very accurate results with comparisons with the Tang et al. solution for Peclet numbers larger than thousand, which is about as high as the Tang et al. solution still gives reliable results. For Pec = 1000 the BTC by the Tang et al. solution and A+MD plus velocity dispersion curves differ less than 10 % in the peak.

The Taylor dispersion in the slot gives an effective diffusion/dispersion coefficient of $D_{Disp} = 2.009 \times 10^{-9}$ m^2/s, which gives a $Pec_{Disp} = \frac{u\,L}{D_{Disp}} = 1\,464$ for WPDE-1 and 731 for WPDE-2 respectively. These Peclet numbers imply that the equivalent standard deviation in residence times caused by Taylor dispersion are $\sigma_{tTaylor} = 0.037\ t_{w,mean}$ and $\sigma_{tTaylor} = 0.052\ t_{w,mean}$ for WPDE-1 and WPDE-2 respectively.

The potential impact of velocity dispersion is illustrated in Figure A-6. The uncertainties in slot aperture are given as 1.25 ± 0.1, which is 8 %. Assuming that $\frac{\sigma_{tv}}{t_{w,mean}}$ can be approximated by this value the joint value of $\sigma_{tv,joint}$ from the sum of variances is approximated by $\sigma_{tv,joint} = \sqrt{\sigma_{tv}{}^2 + \sigma_{tTaylor}{}^2} = 0.088\ t_{w,mean}$. Figure A-6 shows the BTC for Tritium for WPDE-1 with the peaked curve with $\sigma_{tv,joint} = 0.037\ t_{w,mean}$ and the other curve with $\sigma_{tv,joint} = 0.088\ t_{w,mean}$.

The BTC's in Figure A-6 suggest that if there in addition to Taylor dispersion in the slot are differences in velocities in the slot of the magnitude of 8 % of $t_{w,mean}$ this could considerably impact the BTC.

Impact of dispersion in the in- and outlet tubes

The Taylor dispersion in the inlet tube will spread the injected "top-hat" pulse during its travel through the 24.2 m long tube before the pulse enters the slot. The variance of the RTD for tritium BTC for WPDE-1 from the slot when the dispersion is only due to matrix diffusion is 2.04×10^9 s^2. The variance of the RTD for a pulse in the inlet tube is 2.97×10^5 s^2 due to Taylor dispersion. The additional spreading of the BTC at the outlet of the slot caused by the spreading of the pulse at the slot entrance is thus negligible because the variances are additive. The variance in the outlet tube is similar to that from the inlet tube and this can also be neglected.
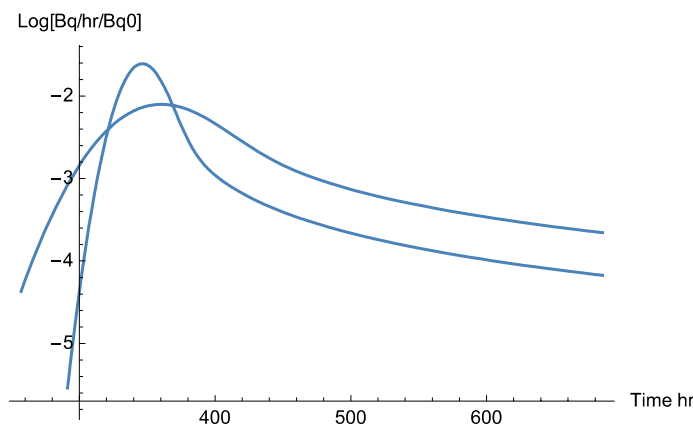

Figure A-6. *Tritium BTC for WPDE-1 with different dispersion values. Peaked curve $\frac{\sigma_{tv}}{t_{w,mean}} = 0.037$, other curve $\frac{\sigma_{tv}}{t_{w,mean}} = 0.088$.*

A4 Discussion and conclusions

A4.1 Radial vs linear diffusion

In our simulation we find that only 0.5–4.7 percent of the injected tritium (and chloride) is not recovered during the entire experimental time. This implies that matrix diffusion has had a very small impact on the residence time distribution. Our presently used computational tools for solving the radial diffusion case are not well adapted for cases where matrix diffusion has a very small impact if we at the same time wish to accurately describe the tail of the BTC. We explore how radial diffusion would deviate from the linear diffusion case we model.

The mass flux due to radial diffusion over the same surface area becomes increasingly larger with increasing contact time. For short times the fluxes are equal to those for linear diffusion. The increasing flux is because the cross section area for radial diffusion increases with distance from the borehole. Figure A-7 shows a comparison of fluxes for radial and linear diffusion with increasing time for sorbing and nonsorbing species. The ratio of fluxes is determined from the solution of the matrix diffusion Equations (A-5) and (A-17) respectively for a case where the concentration at the slot is constant. This condition exaggerates the difference compared to when there is flow and when there is a concentration profile along the slot. The figure also indicates the ratios for the two HTO experiments for the residence times of the two experiments. For sorbing tracers the time scales inversely proportional to the retardation factor R. With this scaling the figure also shows that the BTC for sorbing tracers are essentially not impacted by the radial geometry. This is because the penetration depth for them is a small fraction of the borehole radius. The errors in the BTC's are small in comparison to those caused by the uncertainties in MPG and t_w. Admittedly this is a crude comparison but should give some information on how the pulse travelling through the paths is influence by the difference in radial and linear diffusion during its transit.

Our tools (programs) used in these scoping calculations are well suited for radial diffusion cases when matrix diffusion has more that scant impact on the RTD of the solute. We have more sophisticated tools to be used later.

A4.2 On uncertainties of processes and mechanisms

The slot aperture variations could generate velocity dispersion. However, if the correlation lengths between channels are small, transverse diffusion will tend to even out the residence time differences between different streamtubes (flowpaths) and decrease the impact of aperture variations. There is no detailed information of aperture statistics and we will not address this effect more at present. It is expected that the solute transport in real fractures that have considerable aperture variability will be very important and generate considerable velocity dispersion. It is outside the scope of the present subtask.
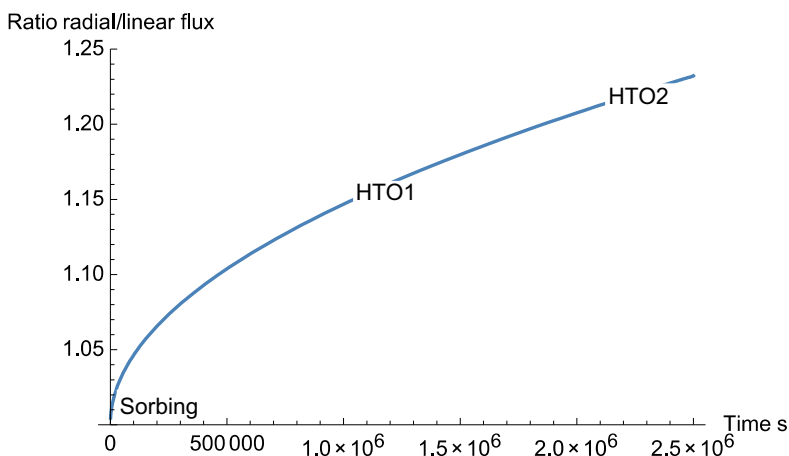

Figure A-7. *Ratio of flux for radial diffusion and linear diffusion vs. retardation scaled water residence time scaled with retardation factor t_w/R.*

Surface sorption can readily be incorporated in the modelling but there are no data available for the present experiment and we estimate the impact to be negligible.

Spatial variations of rock matrix porosity, distribution coefficients and pore diffusivity are not available and are also not expected to be readily available for real fractures in situ. Nevertheless such variations exist and must be addressed. This may be an important subtask to explore, both to gather information on the stochastic properties of such variations and to elucidate what this does to the RTD's. This would be a challenge to experimentalist as well as modellers.

The authors of the present report think that the largest uncertainties at present in predicting solute transport in fractured rock masses lie in

- Distribution coefficients variations in undisturbed (large) rock volumes adjacent to fractures

- Channelling or preferential flowpath geometries, including the magnitude of flow wetted surface, FWS, over which the solutes migrate in and out of the rock matrix

Computer-aided Fluid Engineering AB, Lyckeby, Sweden

Urban Svensson

B.1   Introduction

B1.1   Background

Radionuclide migration in a fractured granitic rock is controlled by a combination of processes, both macroscopic and microscopic. On the repository scale, say 1 km, numerical models have been developed and applied over the last few decades. However, it has been argued that it is the conditions in near field of the deposition hole that are the most critical; a few metres away from the deposition hole it is difficult to evaluate if a fast connection to a major fracture or fault is present. The recognition of the importance of the near field has led to studies of the rock matrix. These studies are mostly experimental and mathematical/numerical models seem to be less applied on the matrix scale.

During the last few years a development of matrix models has been initiated. The basic idea is to resolve the intergranular high porosity regions in detail. The code DarcyTools (Svensson and Ferry 2014) is used as the "computational engine".

B1.2   Objectives

Present a conceptual/mathematical/numerical model of a granitic rock, on the sub meter scale. Use this model to produce the requested predictions.

B1.3   Scope and limitations

The model to be presented is a three-dimensional high resolution model, using particle tracking to solve the transport problem. It is realized that this model may be unnecessarily complex for the task at hand. However, it is believed that the approach is motivated by coming work within Task 9, where "non-Fickian" diffusion is found from experimental data.

Regarding limitations one may state that the model to be used is under development and hence uncertain in many respects. Further, sorbing tracers have not been considered at all so far and the predicted break-through-curves (BTC) are for this reason very preliminary. Hopefully Task 9 will give a lot of useful experience to model sorbing tracers.

B2   Methodology and model

B2.1   Conceptual description of features, events and processes of the experiments

The REPRO experiment is described in the Task Description (TD, Löfgren and Nilsson 2019) for Task 9A and there is no need to repeat the information here. Briefly one can describe the experiment as: "a 1.9 m long slot with an aperture of 1.25 mm carries a tracer injected at the upstream end. The tracer diffuses in and out of the rock matrix, causing a spread and retardation of the pulse, which is recorded at the downstream end". One may also add that the slot is a circular slot in a borehole with a concentric dummy. Some comments:

*   The slot aperture is 1.25 ± 0.1 mm. The flow in the slot is a so called creeping flow (Re <<1) meaning that inertia forces can be neglected. The force balance is therefore due to the pressure gradient and viscous forces. It is not likely that channelling should be found for these conditions. A velocity profile will develop across the aperture. Taylor dispersion may then be needed to consider. However, for the conditions present it can be shown that the effect is negligible.

*   The matrix should be considered to be homogeneous in Task 9A, although a variation of properties along the slot is described in the TD and could be implemented in the model. This variation is however not expected to influence the BTC significantly. A variation of properties with distance from the slot will however influence the BTC. If such a variation exists is however not known.

B2.2 Description of features, events and processes in the conceptual model

A first task is to define the term matrix. A quick look through some books and papers did not result in a commonly accepted definition. This is perhaps not surprising as a continuous range of fractures and fissures builds up the fracture network. A useful (for the present work) separation of scales is given by Montoto and Mateos (2006): the rock mass scale (with fractures from a few metres up to several km long) and the intact rock scale (with fissures and cracks to the order of μm to dm). The present study will be concerned with the intact rock scale.

An illustration of the fracture system on the mm scale is given by Figure B-1. It will here be assumed that the fracture system seen in Figure B-1 is due to "the high porosity region between grains". Migration due to advection and diffusion is hence assumed to be due to this system. The length scale of the grains, say 2–3 mm, defines the length scale of the system. Above this length scale one can expect a fracture network with a continuous range of length scales. Here we will assume that a power law applies for these length scales.

A conceptual view of the fracture-matrix system is given in Figure B-2. It is clear that the large fracture may have branches and that the matrix is built up of a fracture network.
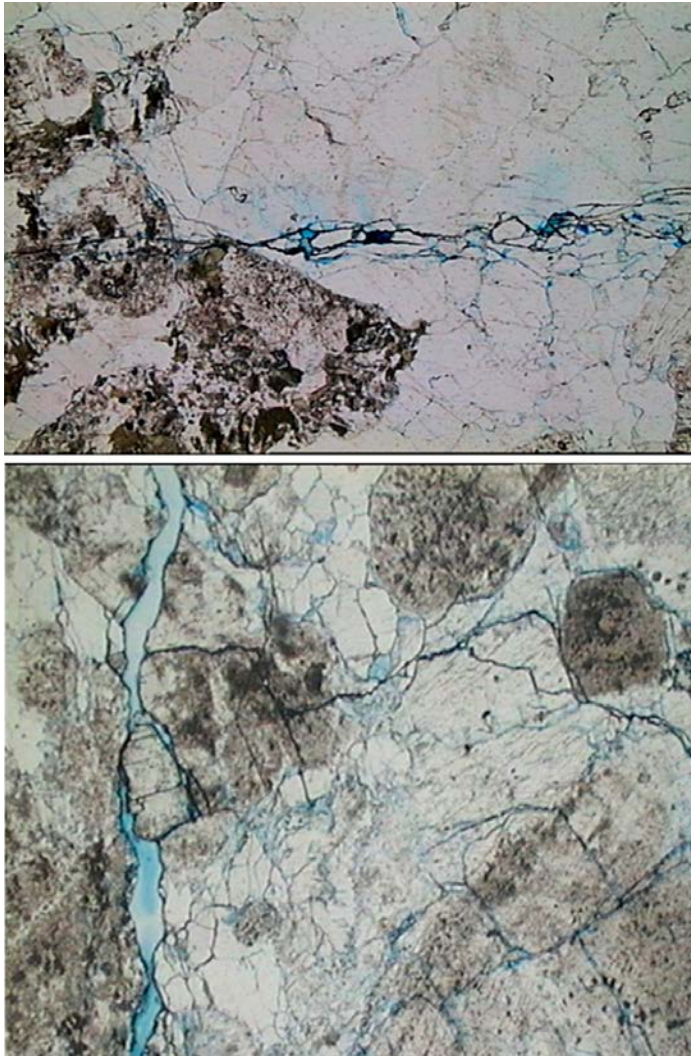
Figure B-1. *Grain size fractures. The photos cover an area of 2.5 × 2.5 mm (SKB, ITD-01-03).*
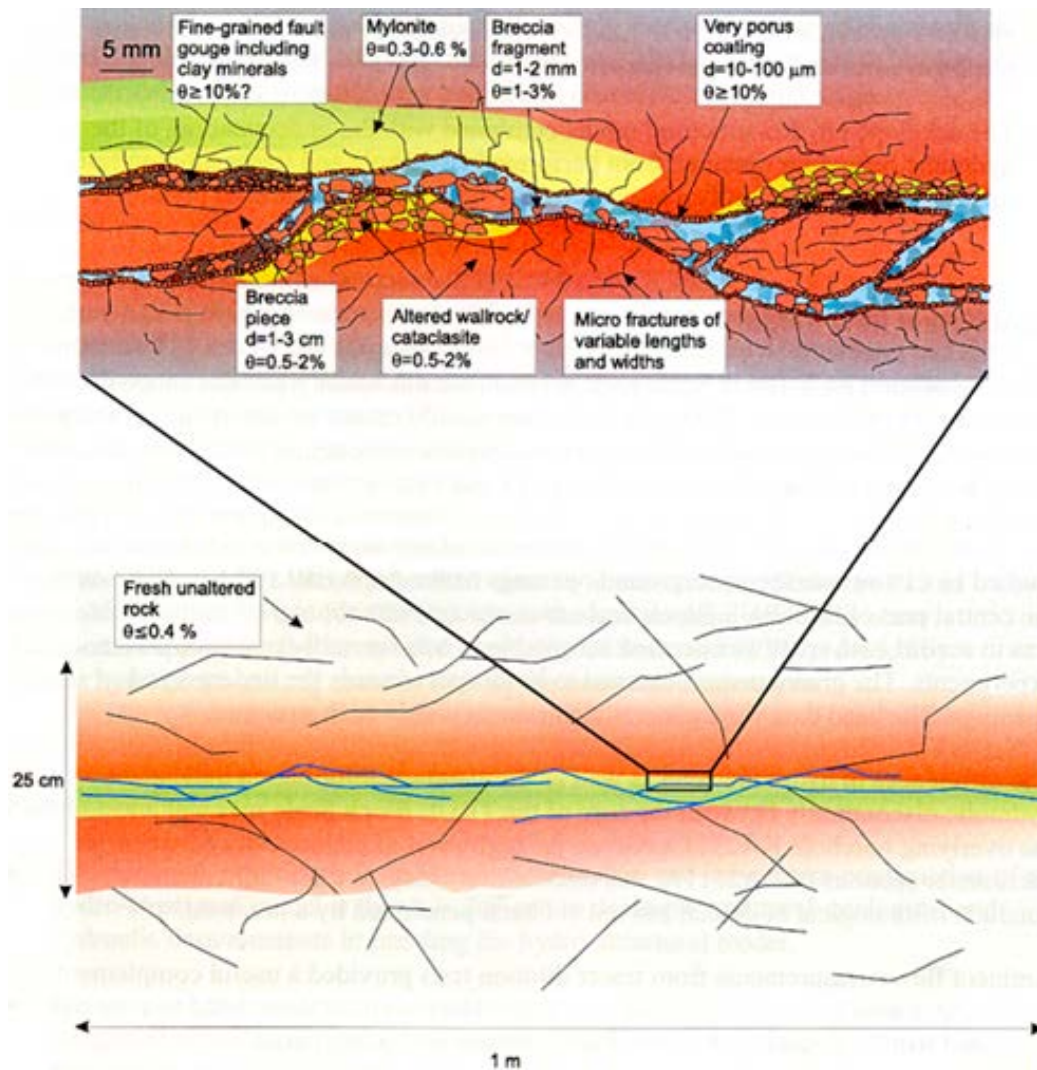
Figure B-2. *Illustration of the present conceptual model of the fracture-matrix system.*

The key points in the conceptual fracture model are illustrated in Figure B-3 and summarized by the following points:

• A "traditional" Discrete Fracture Network (DFN) model is assumed for fractures down to a length scale of 5 mm. The largest fracture in the DFN will be smaller than the computational domain.

• A grain size DFN (DFNgs), with the length scale interval 4–5 mm, will represent the high porosity regions between grains.

• Fractures smaller than 4 mm are represented as immobile volumes (only accessible by diffusion). It is expected that this system contains most of the porosity and flow wetted surface (FWS). The multi rate diffusion model (Haggerty and Gorelick 1995) will be used for this part of the network.

Regarding porosity, it will be assumed that only the connected porosity needs to be considered. The connected porosity is the part of the total porosity that can be reached by diffusion. Part of the connected porosity is available for flow.
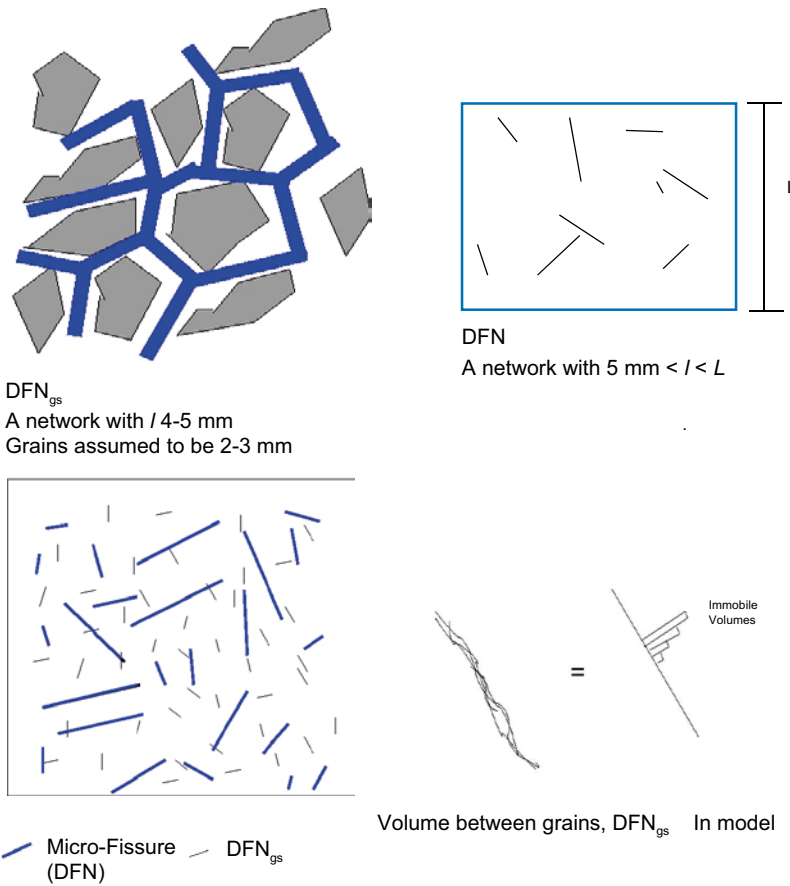
Figure B-3. *Conceptual model. The high porosity regions between grains form a fracture network (DFN$_{gs}$) with length scale 4–5 mm (top left). A traditional network (DFN) for l > 5 mm (top right) is added to the DFN$_{gs}$ to from the total network (bottom left). The high porosity regions (bottom right) are modelled as a constant aperture fracture with a set of immobile volumes (the multi rate model).*

B2.3 Model Setup

As mentioned, the code DarcyTools is used. An overview of the code can be found in Svensson and Ferry (2014) in addition to the available code documentation (a series of SKB reports). Here some features central for Task 9A will be in focus.

The computational domain and the grid are shown in Figure B-4. We follow the outline for the REPRO experiment, but only a 45° sector is considered to be needed to model as we assume that no channelling is present. The cell size is 0.125 mm in the channel and some distance into the matrix. Further into the matrix the cell size is 0.25 mm and even further out it is 0.5 mm. This results in a total number of cells of about 102 million cells.

The generation of fractures in the length interval l to $l + dl$ is governed by the following relation:

$$n = \mathrm{I} * \left[\left(\frac{l+dl}{l_{ref}} \right)^a - \left(\frac{l}{l_{ref}} \right)^a \right] / a$$

where n is the number of fractures per unit volume, I the intensity, l_{ref} a reference length (= 1 m) and a, the power law exponent.

The formulation of the matrix model requires that a number of parameters are set. In particular, the intensity of the 4–5 mm fractures and the ratio between immobile to mobile volumes, see Figure B-3. These parameters need to be tuned, considering data at the site. From the TD it is found that the matrix can be characterized as having a porosity around 0.01 and an effective diffusivity of 2×10^{-13} m^2/s; these will be our target values when tuning the model.
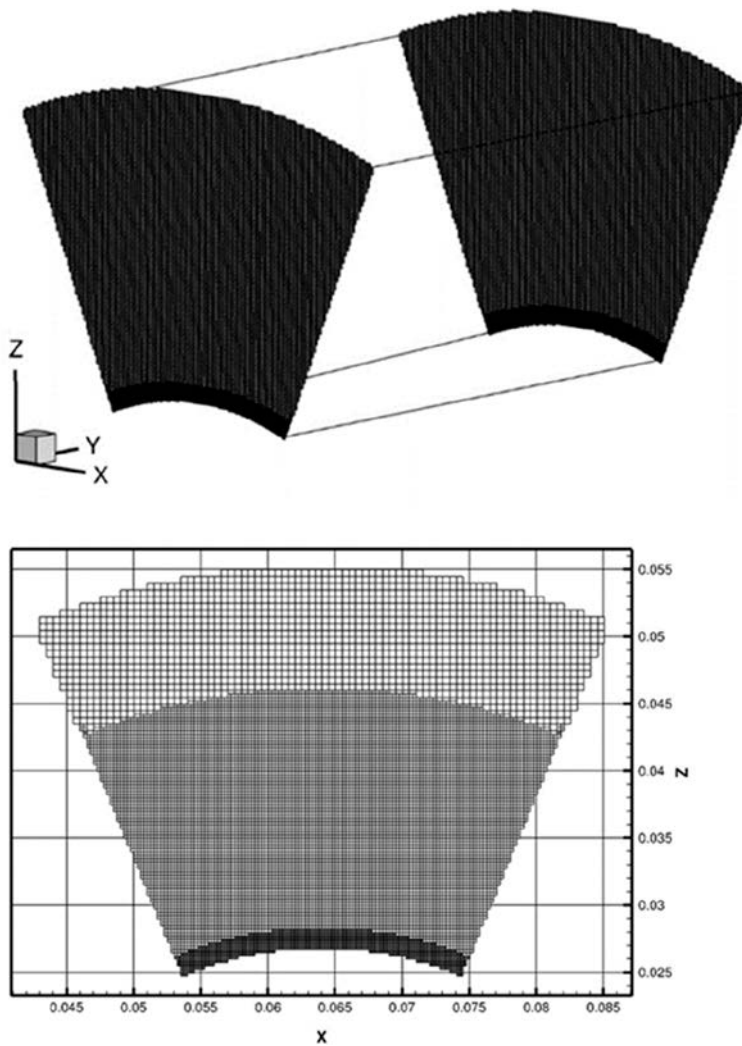
Figure B-4. Computational grid.

B2.4   Input data

The following points summarize the input data used:

- Geometry. The length of the slot is 1.905 m and the aperture 1.25 mm. The diameter of the borehole is 0.0565 m. Inlet and outlet tubes were not considered.

- Flow. Two flow rates were used; 20.1 µl/min for WPDE-1 and 10.0 µL/min for WPDE-2.

- Matrix. A porosity of 0.01 and an effective diffusivity of 2×10^{-13} m^2/s were used as target values when tuning the model.

- Sorption. For Na-22 and Sr-85 a K_d of 10^{-3} m^3/kg is used, while a K_d of 0.07 was used for Ba-133. HTO and Cl-36 are considered to be non-sorbing.

B2.5   Alternative models and sensitivity cases

In earlier work, the matrix model has been tuned to data relevant for the Forsmark site (a porosity around 0.002 and an effective diffusivity of 2×10^{-14} m^2/s). It is hence clear that the model needed to be adopted to the Task 9A site. A number of sensitivity tests were performed and a set of parameters were found:

- The DFN ($l > 5$ mm) needs an intensity factor. In Dowd et al. (2009) the fracture network in a 1 m^3 block of granite is analysed. It was found that the block had 76 fractures larger than 0.1 m. This gives an intensity factor of 0.6 and a power law coefficient of 3.6.

- The transmissivity relation, $T(l)$, was chosen with respect to a data compilation by the Äspö Task Force (Task 8). According to these data a relation $T = 10^{-10} l^2$ represents data well.

- The network has a Poiassonion space distribution and random orientation.

- The apertures were first calculated from the cubic law and the $T(l)$ relation above. This will however result in apertures of the magnitude 0.1 μm which seems unrealistically small (see for example Montoto and Mateos 2006). The apertures were for this reason set to 1μm.

- The intensity of the DFN_{gs} could not be based on data. The chosen value was found from test simulations, trying to fit data as good as possible.

- Immobile volumes were assumed to represent a volume two times greater than the volume generated by fractures with $l > 4$ mm.

As seen, some of the parameters are based on earlier experience, while some are specific for Task 9A.

The analytical solution for a homogeneous matrix was used in the tuning process. The adopted parameters were found to produce a BTC that matches the analytical solution, based on $D_{eff} = 2 \times 10^{-13}$ m²/s, see Figure B-5.
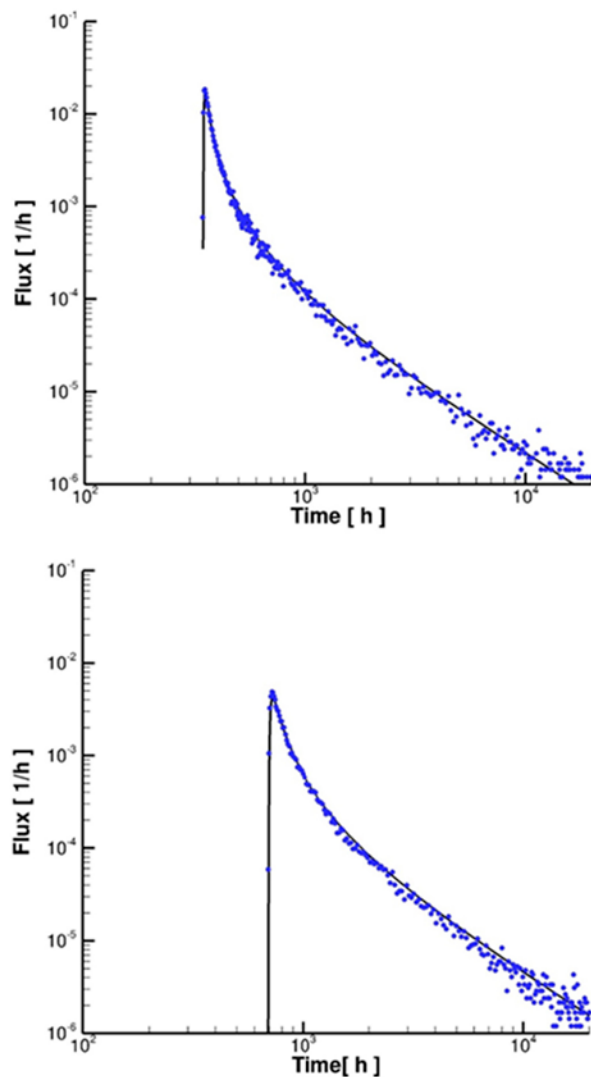
Figure B-5. *BTCs. Tuning of the matrix model. The analytical solution for $D_{eff} = 2 \times 10^{-13}$ m²/s (solid line) is compared to numerical solutions (dots).*

B3 Results and discussion

B3.1 The central prediction

Before these BTCs are presented some minor adjustments to the model will be listed:

- The porosity (see TD) is best estimated to 0.009. This value is achieved by a small change to the immobile volume.

- The injection pulse length was set to the correct time for WPDE-1 (50 min) and WPDE-2 (300 min).

- Time should be measured from the injection in the inlet tubes till the recording in the outlet tubes. The times spent in the tubes are added to the BTC:s.

In Figure B-6, the BTC:s are given for WPDE-1 and WPDE-2. A sharp peak is found for the conservative tracer, while a flatter peak is predicted for Na-22 and Sr-85. No recovery for Ba-133 was predicted for WPDE-2, during the experimental time.

Figure B-7 gives the corresponding cumulative BTC:s and numbers on the recovery are given in Table B-1.
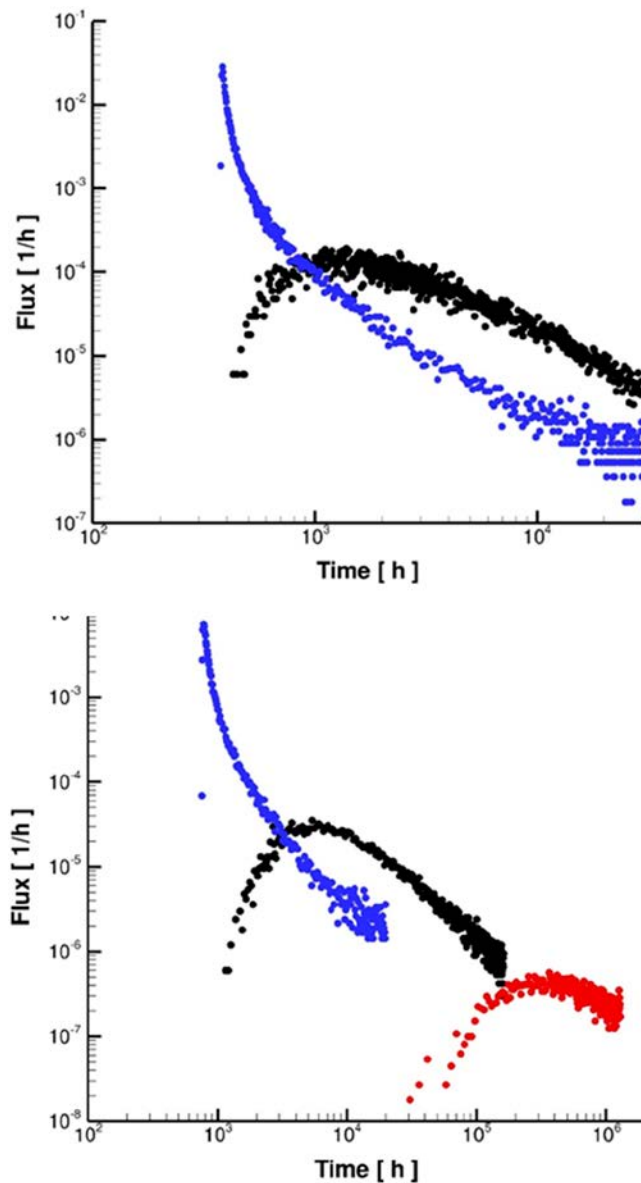
Figure B-6. BTCs for the central prediction. Blue dots represent HTO and Cl-36, black Na-22 and Sr-85 and red dots Ba-133.
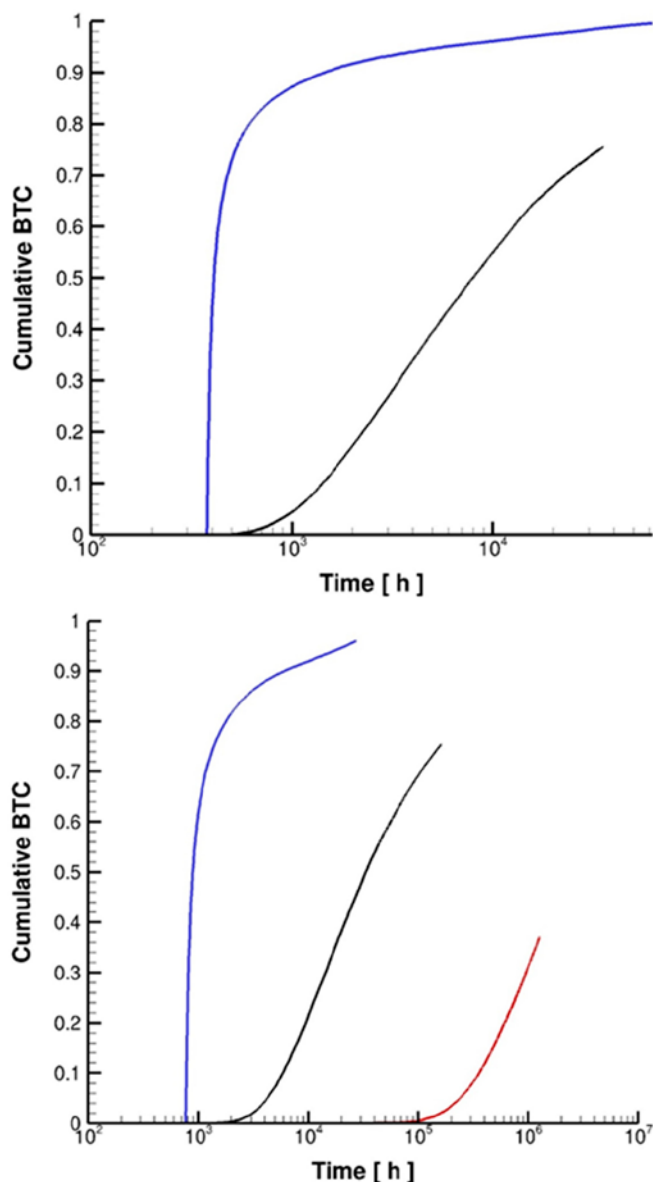
Figure B-7. *Cumulative BTCs for the central prediction. Blue lines represent HTO and Cl-36, black Na-22 and Sr-85 and red line Ba-133.*

Table B-1. Recovery of tracers after one year (WPDE-1) and two years (WPDE-2).

Case	HTO, Cl-36	Na-22, Sr-85	Ba-133
WPDE-1	0,96	0,52	na
WPDE-2	0,94	0,35	na

B3.2   Alternative models, sensitivity cases and results

It has not been discussed so far, but part of the simulation is the calculation of the flow field. Both the flow channel and the matrix are part of this simulation, even if the transport in the matrix is expected to be dominated by diffusion. The importance of advection in the matrix can hence be evaluated by the model, if so requested.

The most important parameters are however porosity and diffusion coefficients. The fields generated are shown in Figure B-8.

On the request of the technical committee of Task 9, an investigation of the shape of the BTC was carried out. The result is given in the next section.
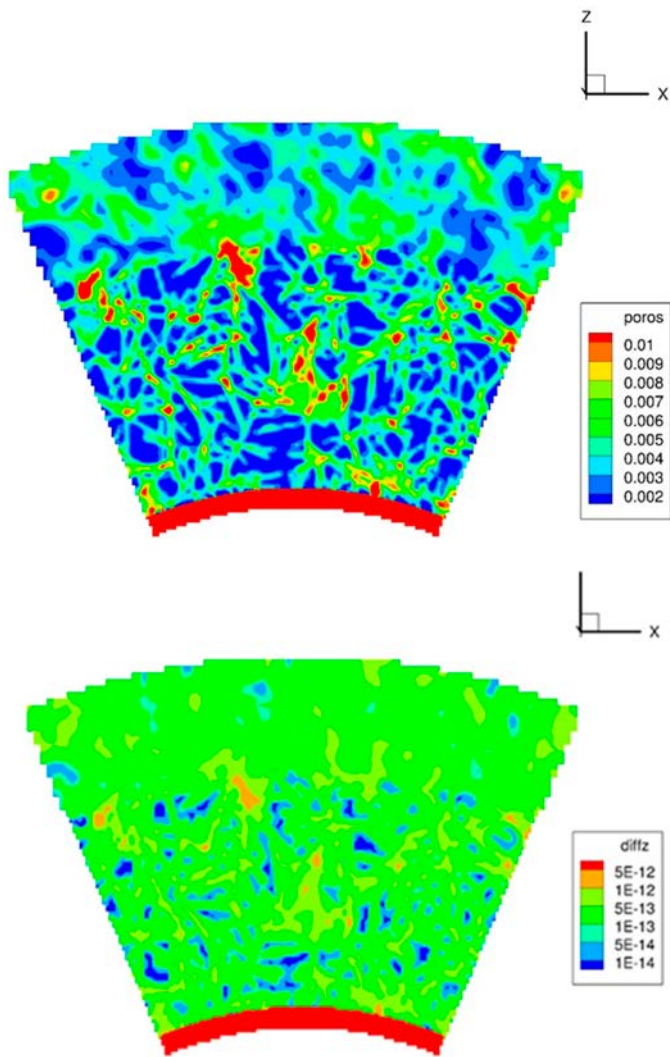
Figure B-8. *Generated porosity and diffusion coefficient fields.*

B3.3 Effect of a non-uniform flow field

Background

First results for Task 9A were presented at TF#34 in Kalmar, Sweden. It was obvious that the results for conservative tracers showed two different groups of results. One gave narrow tracer peaks, while the other group showed much wider peaks, with very early first arrival times. The results in the present report belong to the first group.

The technical committee for Task 9 then suggested that some additional simulations should be carried out; a large dispersion coefficient should be specified for the flowing fracture. It is however difficult to motivate a large dispersion coefficient, provided the experimental set-up agreed with the information given in the Task Description. However, the team that carried out the experiment has pointed out possible deviations from ideal conditions. In particular, two differences are significant: "possible variations in the shape of the drill hole cross-section" and "accuracy in centering of the drill hole dummy into the drill hole". Both will cause a variation in aperture which will lead to some form of channelling and thus violating the assumption of a uniform flow in the artificial fracture.

Objective

In this appendix a brief study of the effects of a non-uniform flow in the artificial fracture will be carried out.

Results

The assumed deviation from ideal conditions is illustrated in Figure B-9. As the flow velocity is proportional to the aperture squared, it is clear that even minor deviations are of importance.

The simplest possible non-uniform flow distribution is the top-hat profile, see Figure B-10. As we are only solving for a 45° sector, we cannot simulate the situation shown in Figure B-9. The results shown in this appendix are hence principal in nature and cannot be compared with experimental data.

The profile was generated by modifying the permeability (a Darcian flow is assumed) in the flowing fracture. It was of course ensured that the mean permeability, and hence the flow rate, was unchanged. It was further found that the lateral diffusivity needed to be reduced by an order of magnitude due to the shorter lateral distances (as compared to the situation shown in Figure B-9). Without this reduction lateral diffusion will even out the effect of the velocity profile.

The result is found in Figure B-11. As seen, the peak is lowered and less sharp, and the first arrival is changed significantly.

We have thus succeeded in our ambition to "generate a BTC with earlier first arrival and with a less sharp peak". It is argued that the introduction of a non-uniform velocity at least provides a physical argument for the unexpected behaviour, even if the net result is similar to using a large dispersion coefficient.

Discussion

The effects on the BTC just discussed can be further illuminated by some simulations using the analytical solution introduced in the main report (Figure B-5). The case is shown in Figure B-12 and the following points describe the procedure:

First the BTC for the uniform flow, U_0, is calculated and displayed (blue dots).

Next a top hat profile for velocity is assumed; $2U_0$ for a length of 20 % and $0.75U_0$ for 80 % of the width. Mean velocity is still U_0.

Two BTCs (green and blue lines) are calculated, using $2U_0$ and $0.75U_0$.

The two BTCs are added with weights 0.2 and 0.8. The result is the BTC given by the black dots.

The important thing to note is that we have produced a BTC with early first arrival and a wide peak. The early arrival is due to the part with $2U_0$ and the wide peak is due to the combination of the two BTCs. The irregular peak should in reality be smeared by transverse diffusion; a process that is not included in this case.

Concluding remarks

The following points emerge:

From the Task Description there is no obvious circumstance that should cause very early arrivals.

If a variation in aperture was present, this will certainly modify the BTC.

Here an idealized situation with a simple velocity profile has been evaluated. It has been shown that the noted effects (early arrivals and a flat peak) results. The same set-up as in the main report was used, i.e. a 45° sector constitutes the domain.

The analytical solution for a straight channel was used to further illuminate the effect of a varying velocity in the flowing fracture.
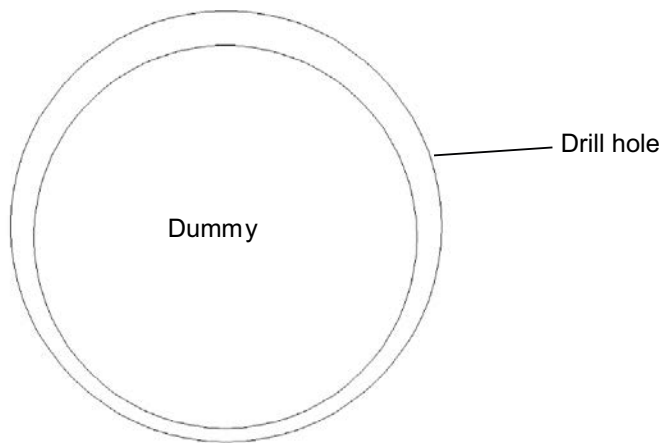
Figure B-9. Illustration of a possible deviation from ideal conditions; the aperture is varying along the circumference.
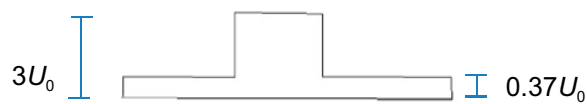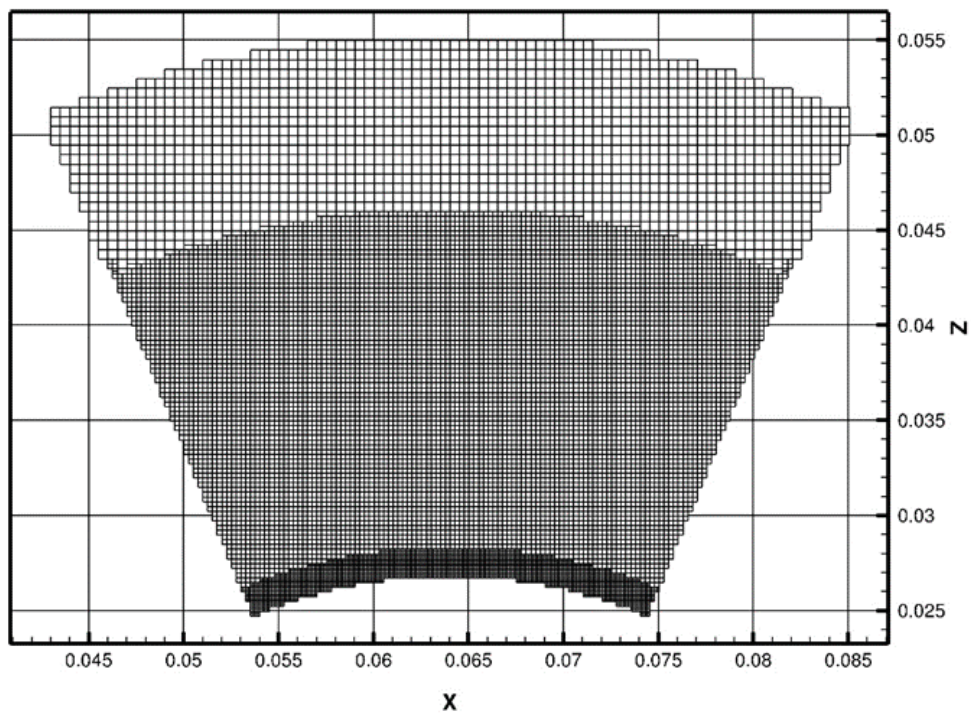

Figure B-10. Computational grid (top) and the assumed velocity profile in the flowing fracture. The grid has three parts; the finest grid is in the black part covering the flowing fracture and some distance into the matrix. The high velocity part is between x-coordinates 0.061 and 0.066 m.
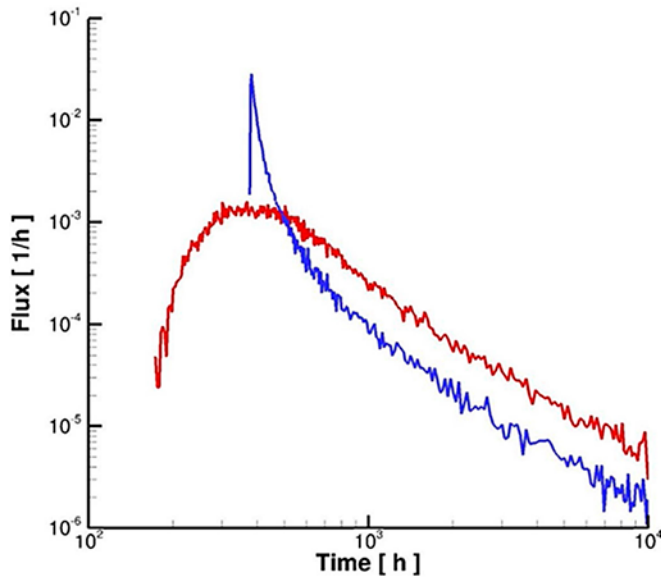
Figure B-11. *BTC for the case given in the main report (blue) and for the case with a non-uniform flow (red).*
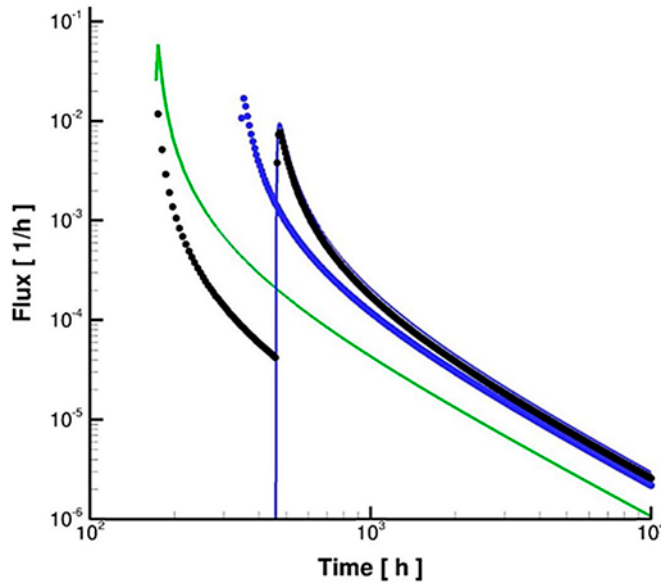
Figure B-12. *BTCs from the analytical solution for: $2U_0$ (green line), $0.75\ U_0$ (blue line), uniform U_0 (blue dots) and the weighted curve between the green and blue lines (black dots).*

B4 Discussion, conclusions and recommendations

In the TD it is stated that modellers should use readily available tools for Task 9A (hence no new developments). This recommendation has been followed, although the matrix model is a tool that is not yet established in any way. To mention one aspect; sorbing tracers have not been considered so far and the BTC:s presented in this report may hence be totally unrealistic. On the other hand, one can expect that Task 9 generally will put the model to test, which of course is of great value.

Task 9A can probably be well predicted with a simpler approach than the one shown in this report. However, it is hoped that the chosen approach will be of interest and value in coming tasks, in particular if so called non-Fickian effects are of importance.

Another central motivation for the approach is due to the interfacing with codes dealing with chemical reactions (like PFLOTRAN). This has been tested in Task 9A and will be further explored in future tasks. It is then of interest to understand transport in the intergranular parts and also keep track of different grain types. Hence, one expected development is the introduction of grains with distributions and sizes from measurements. In Figure B-13 the traces of fractures larger than 4 mm are shown together with a photo of a muscovite granite. The white parts in the map of the fracture traces are candidates for being grains. It is however hoped that more realistic figures can be generated in the near future.
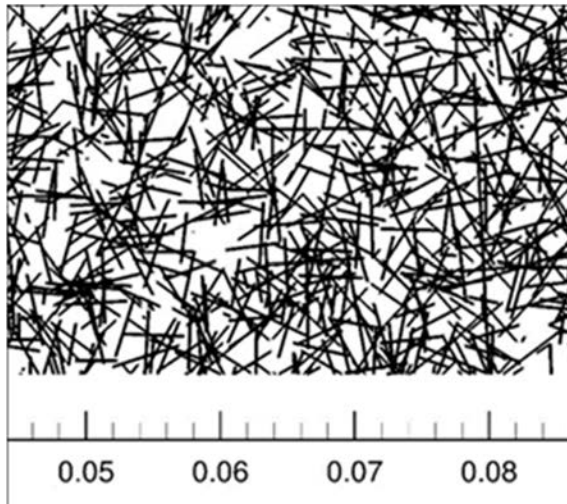
Fracture traces
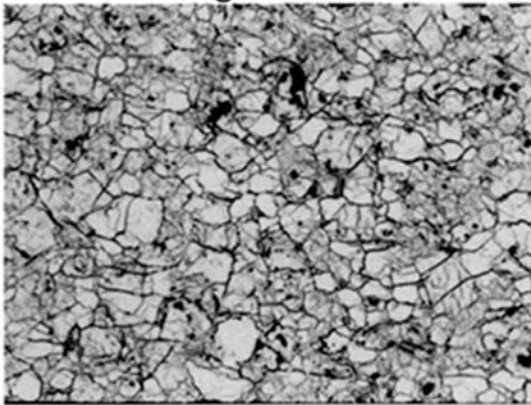
From Maikki Siitari-Kauppi. TF #32

Figure B-13. *Generated fracture traces (top) and a photo of a Muscovite granite.*

AMPHOS 21 Consulting S.L., Barcelona, Spain

Paolo Trinchero[1], Aitor Iraola[1], Hedieh Ebrahimi[1],

Jorge Molinero[1], Urban Svensson[2], Patrik Vidstrandt[3],

Guido Deissmann[4]

[1] AMPHOS 21 Consulting S.L., Barcelona, Spain

[2] Computer-aided Fluid Engineering AB, Lyckeby, Sweden

[3] Swedish Nuclear Fuel and Waste Management Company, Stockholm, Sweden

[4] Institute for Energy and Climate Research: Nuclear Waste Management and Reactor Safety (IEK-6) and JARA-HPC, Forschungszentrum Jülich GmbH, Jülich, Germany

C1 Introduction

C1.1 Background

AMPHOS 21 (hereafter, Amphos) has over twenty years of experience in radionuclide transport modelling applied to safety evaluations of deep geological repositories for nuclear waste. This experience is summarised by a number of technical reports (e.g. Piqué et al. 2010, 2013b, Trinchero et al. 2014a) and scientific publications (e.g. Piqué et al. 2013a, Trinchero et al. 2014b, 2016).

In recent years, Amphos has developed a numerical tool, denoted as iDP (interface between PFLOTRAN and DarcyTools, Molinero et al. 2016), which provides a novel innovative numerical framework for High Performance Computing (HPC) reactive transport modelling.

iDP has been tested against an exhaustive suite of benchmark examples and used to carry out micro-continuum simulations of cesium sorption in a synthetically generated heterogeneous fracture-matrix system (Trinchero et al. 2017). The participation in Task Force 9A, offered a unique opportunity to apply, for the first time, iDP to the interpretation of a "real" experimental problem.

All the modelling activities summarised in this section have been carried out in close cooperation with Urban Svensson (CFE) and Patrik Vidstrandt (SKB).

C1.2 Objectives

As stated in the Task Description, the overall goal of Task 9 is "*to develop models that in a more realistic way represent solute transport and retardation in the natural rock matrix.*". In the same document, is it said that "*this [more realistic representation] may be done by more realistically representing the rock heterogeneity and microstructural features*".

With this overall objective in mind, Amphos' contribution to Task 9A has focused on assessing the influence that the textural and mineralogical heterogeneity of the rock matrix has on radionuclide diffusion and retention.

A secondary but not less important objective of this modelling work is related to the possibility of applying iDP to a real experimental problem. In fact, the outcome of these modelling activities is expected to provide a further validation of iDP, which has never been tested before against "real world applications".

C1.3 Scope and limitations

Two different set of calculations have been carried out using two alternative models: (I) *model for production runs* and (II) *model for process understanding*.

In the *model for production runs* (from now on, *2D model*), a minimum level of complexity is used. These calculations, which are carried out using PFLOTRAN (Lichtner et al. 2013, Hammond et al. 2014) as standalone code, assume a homogeneous rock matrix that is described using a 2D axisymmetric domain.

In the *model for process understanding* (from now on, *3D model*), iDP and a highly refined three dimensional domain are used to describe matrix heterogeneity at the micron scale.

The reason for keeping the two models separate lies in the high computational requirements of the *3D model* along with the large number of calculations required to provide central and upper/lower predictions of the two experiments. Thus, the 2D model is here used to carry out the whole range of calculations required by the data delivery specifications (see Task Description) whereas the 3D model is used to assess specific features such as the tailing of the radionuclide breakthrough curves and its dependence on matrix heterogeneity.

Both models focus on radionuclide transport in the slot and surrounding rock while the influence of PEEK tubings is neglected.

C2   Methodology and model

C2.1   Conceptual model

An exhaustive description of the features, events and processes of the experiments is provided in the Task Description. Starting for this detailed information, we have formulated a simplified representation of the experiment, which is what we call "conceptual model".

The geometry of the conceptual model is shown in Figure C-1. An artificial fracture, also called "slot", is obtained by placing a dummy inside the drillhole. In our conceptual model, the dummy is assumed to be coaxial with the drillhole (the influence of the dummy being not coaxial is discussed in the next sub-sections of the document). The fracture aperture is 1.25 mm and the length of the considered section (i.e. outlet-inlet) is 1.9 m. The matrix is heterogeneous.

A tracer cocktail is injected along the inlet boundary. The injection is short compared to the total duration of the experiment. A "parcel" of radionuclide mass that enters the domain can follow two alternative pathways: (I) move along the flowing fraction until reaching the outlet boundary or (II) move along the fracture, diffuse into the rock matrix and then out-diffuse into the fracture once the chemical gradient is reversed. Anion exclusion, which is likely to affect one of the tracers included in the cocktail, is taken into account using lower accessible porosity values (see Section C3.1)

The main transport drivers are advection and mechanical dispersion in the fracture and molecular diffusion in the matrix. Some of the tracer mass that diffuses into the matrix might eventually be sorbed onto the available pool of sorption sites. Taylor dispersion in the slot is neglected. Solute transport is simulated using the Advection-Dispersion Equation (ADE) whereas linear sorption (i.e. K_d based sorption) is assumed.

C2.2   Model setup

Model for production runs (2D model)

To implement the 2D model, a further assumption is made, namely that matrix is homogeneous (i.e. constant porosity in the matrix). Under this assumption, the geometry can be simplified using axial symmetry (Figure C-2) and the domain reduces to 2D axisymmetric. Compared to the three dimensional model (see below), the 2D model offers the great advantage of providing the same degree of accuracy (i.e. same degree of refinement) with a much lower number of elements (i.e. grid cells) and this reduces dramatically the computational burden of the calculations.
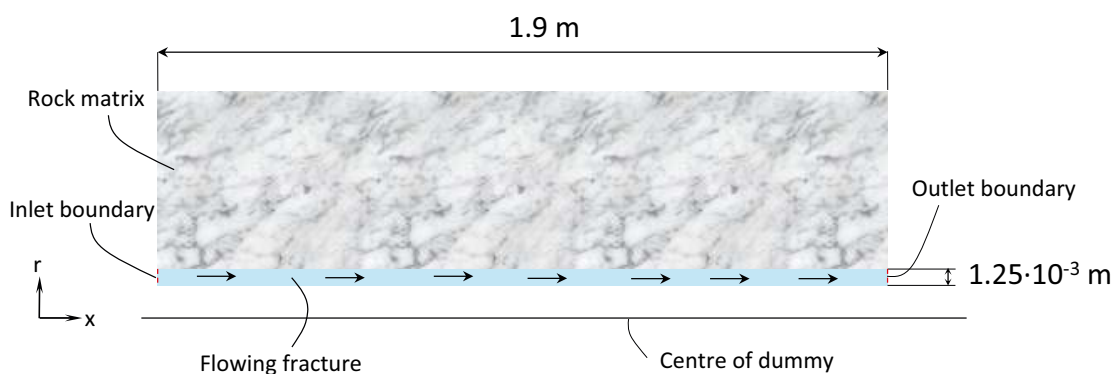

Figure C-1. *Illustrative sketch of the model domain.*
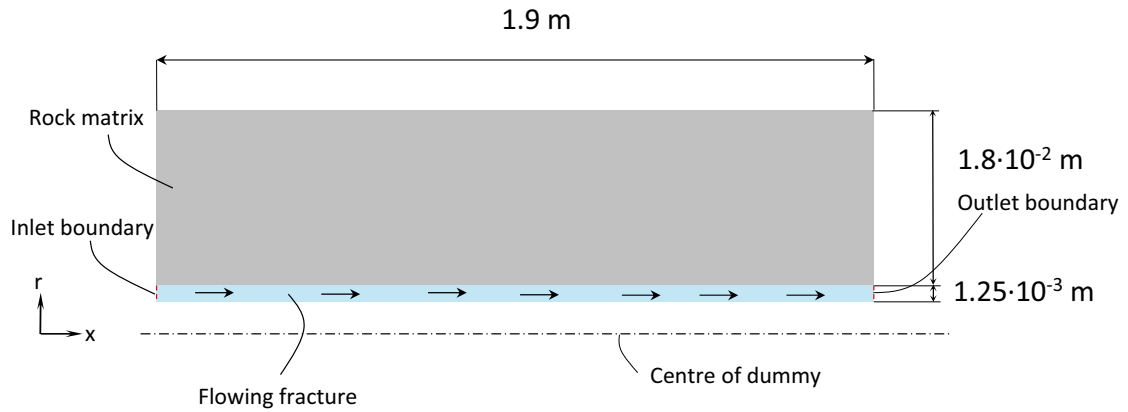
Figure C-2. *Domain of the 2D model.*

To reduce numerical dispersion and avoid spurious numerical effects, the numerical calculations are carried out over an extremely refined grid. The flow direction is discretized with 1 905 equally spaced grid cells ($\Delta = 1 \times 10^{-4}$ m), whereas 520 grid cells are used in the radial direction (480 cells with $\Delta = 6.25 \times 10^{-6}$ m and 40 outermost cells with $\Delta = 4.0 \times 10^{-4}$ m). Thus, the computational grid is made up of a total of 990,600 rectangular elements.

It is worthwhile noting that the extension of the matrix (1.8×10^{-2} m) is rather limited. As discussed in Section C3.1, this has some impact in the tailing of the radionuclide breakthrough curves, particularly for non-sorbing tracers.

Model for process understanding (3D model)

The 3D model is implemented using iDP. The dimension of the domain (Figure C-3) is the same used in the DarcyTools calculations (contribution by U. Svensson in this report). A semi-structured mesh, consisting of around 46 million triangular prisms (Figure C-4), is used in the PFLOTRAN calculations.
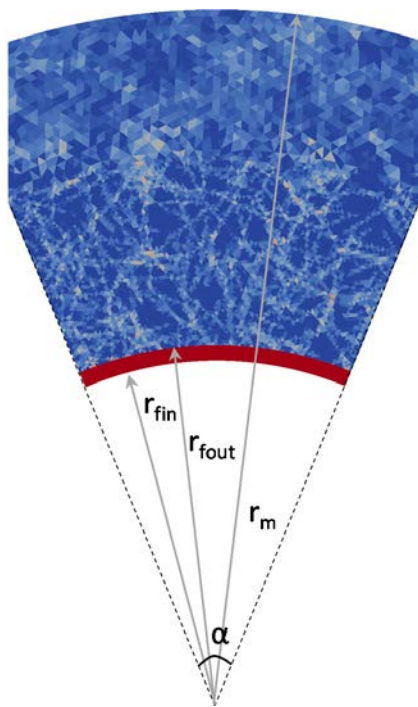

Figure C-3. *Sector of the cross-sectional area considered in the 3D model. $r_{fin} = 2.7 \times 10^{-2}$ m, $r_{fout} = 2.825 \times 10^{-2}$ m, $r_m = 5.5 \times 10^{-2}$ m and $\alpha = 45$ |°*
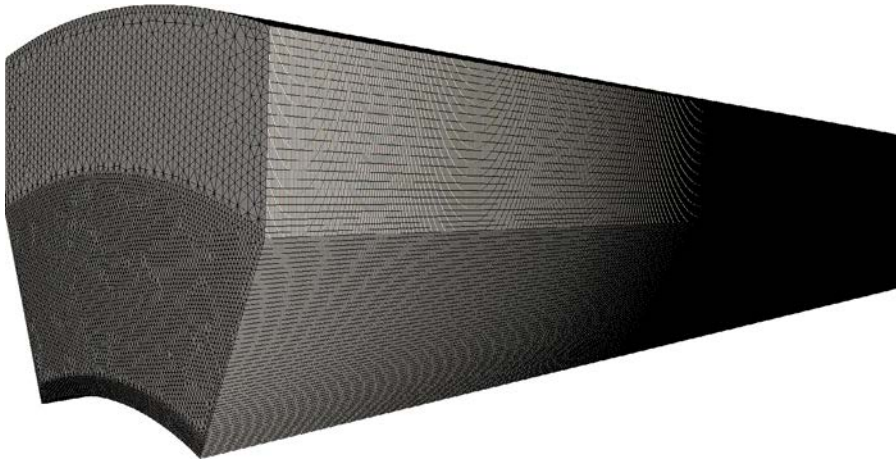
Figure C-4. *View of the numerical grid used in the 3D model.*

C2.3 Input data

Detail account of all the experimental input data is provided in the Task Description. Here, we highlight only those data that are used as direct input in the calculations.

Two successive experiments are considered: WPDE-1 and WPDE-2 (the acronym WPDE stands for Water Phase Diffusion Experiment). The flow rate used in these two experiments is 20.1 μL/min for WPDE-1 and 10.0 μL/min for WPDE-2.

In WPDE-1, five tracers were injected, namely HTO, Na-22, Cl-36, and I-125.The cocktail used in WPDE-2 was slightly different and contained HTO, Na-22, Cl-36, I-125, Sr-85 and Ba-133. All the tracers, except I-125, are included in the calculations.

The duration of the injection (flow through the injection loop) was 3 h for WPDE-1 and 25 h for WPDE-2. However, in the models a slightly longer duration of the injection is considered for WPDE-1 (i.e. 6 h). The injected activity for the two experiments is listed in Table C-1. Decay corrected activities are considered.

Table C-1. Injected activity for the two experiments.

Tracer	Injected activity WPDE-1 (Bq)	Injected activity WPDE-2 (Bq)
HTO	17.1×10^6	31.1×10^6
Na-22	1.38×10^6	2.04×10^6
Cl-36	1.25×10^6	5.09×10^6
Sr-85	–	4.12×10^6
Ba-133	–	2.46×10^6

Sorption parameters are taken from the values reported in the Task Description for veined gneiss. These values are summarised in Table C-2.

Table C-2. Sorption partitioning coefficients used in the calculations. These values have been obtained from experimental studies carried out by the Helsinki University (unpublished data).

Radionuclide	Sorption partitioning coefficients (m³/kg)
Na-22	0.0013
Sr-85	0.0011
Ba-133	0.06

According to the Task Description, during the experiment very controlled flow conditioned are achieved in the slot, which means that velocity in the fracture is expected to be almost constant. As thoroughly discussed in a recent paper (Molz 2015) "[…] *in any fluid flow, including groundwater flow, there is only advection and diffusion. So if we could reproduce the true velocity […], all we would need in order to model solute transport would be molecular diffusion*". For this fundamental reason, in all the calculations, except the sensitivity analysis presented in Section C3.1, mechanical dispersion is minimised using a very low value of dispersivity ($\alpha = 1 \times 10^{-3}$ m).

All the other input parameters (e.g. diffusion coefficient, matrix porosity, etc) are specified in each corresponding modelling sub-section.

C2.4   Sources of uncertainty

The Water Phase Diffusion Experiment is affected by different sources of epistemic uncertainty, which, loosely speaking, can be categorised into two groups:

1. Sources of uncertainty related to the heterogeneous structure of the rock matrix

2. Sources of uncertainty related to the actual flow conditions in the slot

Different experimental studies (e.g. Voutilainen et al. 2013, Molins et al. 2014) have pointed out that diffusion processes and chemical reactions are strongly affected by pore-scale heterogeneity. Recent advances in microscopic characterization methods (e.g. Voutilainen et al. 2013, Blunt et al. 2013, Steefel et al. 2015b) have allowed pore-scale heterogeneity to be fully resolved. However, the application of these methods is still limited to very small rock samples (typically a few cm^3). Thus, when investigating diffusion and sorption properties at the meter scale, modellers have still to rely on equivalent (homogeneous) parameters. The effect and implications of this homogenisation is here investigated by means of a synthetic realisation of the heterogeneous rock matrix. Moreover, a number of sensitivity calculations have been carried out, where values of diffusivity and matrix porosity have been varied within the plausible ranges provided by the Task Description.

Concerning the second source of uncertainty, it has already been discussed that the experiment has been designed so that flow conditions within the slot are controlled. However, given the very small aperture of the slot, it is expected that possible features such as roughness of the drillhole wall or the dummy being not-coaxial, could have important impact on the results. This is here investigated in a rather simplistic way by increasing mechanical dispersion in the slot.

Uncertainties related to sorption parameters and their scale dependency (e.g. Malmström et al. 2000) are not considered in this study.

C3   Results and discussion

C3.1   2D model (production runs)

In this sub-section, we present the results of the 2D model (Section C2.2). According to the Task Description, "*at minimum each modelling group should deliver two alternative breakthrough curves for each tracer of the WPDE-1 and WPDE-2 experiments […] which complement the central predictions*". In this work, a rather simplistic sensitivity analysis is carried out by varying pore diffusivity and matrix porosity around a central value. Thus, a central case and an upper and lower case are defined as specified in Table C-3. The corresponding results are presented below.

Table C-3. Pore diffusion coefficient (D_p [m^2/s]), matrix porosity (ϕ [-]) and effective diffusivity (D_e [m^2/s]) used in the central, lower and upper predictions.

List cases	Radionuclides	D_p (m^2/s)	ϕ	D_e (m^2/s)
Central case	HTO, Na-22 (Sr-85), Ba-133	2.5×10^{-11}	1.0×10^{-2}	2.5×10^{-13}
	Cl-36		2.0×10^{-4}	5.0×10^{-15}
Lower case	HTO, Na-22 (Sr-85), Ba-133	1.0×10^{-11}	1.0×10^{-2}	1.0×10^{-13}
	Cl-36		1.0×10^{-4}	1.0×10^{-15}
Upper case	HTO, Na-22 (Sr-85), Ba-133	1.5×10^{-11}	2.0×10^{-2}	3.0×10^{-13}
	Cl-36		7.0×10^{-4}	7.7×10^{-15}

It is worthwhile noting that anion exclusion, which affects Cl-36, is taken into account using lower accessible matrix porosity values (Table C-3). This had to be done using independent calculations, which increased the total number of simulation runs by a factor of 2 (i.e. 12 simulation runs; 6 for each experiment).

The simulation time frame is 1 y for WPDE-1 and 2 y for WPDE-2. All the calculations were carried out on a powerful workstation and the total wall-clock time for each calculation was approximately 25 h for WPDE-1 and 50 h for WPDE-2, meaning that a total of around 450 h of computational time were used.

The central prediction (central case)

The breakthrough curves computed with the central case are shown in Figure C-5 (WPDE-1) and Figure C-6 (WPDE-2). To facilitate result comparison among the different modelling groups, in the Task Description it is suggested that a number of performance measures are computed. These performance measures, which are records of the time when each tracer reaches specified concentrations as well as values of tracer peak concentration, are provided in Table C-4 and C-5 for WPDE-1 and Table C-6 and C-7 for WPDE-2.

From the two set of breakthrough curves (Figures C-5 and C-6), one can see that:

*   Breakthrough curves for non-sorbing tracers (i.e. HTO and Cl-36) are affected by boundary effects. These boundary effects, which are further discussed below, are related to the limited extension of the matrix included in the model and affect the tailing of the breakthrough curves, which deviate from the theoretical slope observed for an infinite matrix.

*   As a result of anion exclusion, late time normalized mass fluxes are lower for Cl-36 than for HTO.

*   The slope (in log-log scale) of the tailings of Na-22 and Sr-85 breakthrough curves is in agreement with the 1.5 value typically observed in fractured media (Hadermann and Heer 1996, Haggerty et al. 2000, Willmann et al. 2008).

*   As a result of sorption processes in the matrix, which are modelled using the K_d values listed in Table C-2, Na-22 and Sr-85 are retarded and their peak concentration values are shifted by a factor of 1.14 (i.e. time of peak concentration for the sorbing tracer divided by time of peak concentration for one of the non-sorbing tracers). Note that same partitioning coefficient is used for both Na-22 and Sr-85.

*   Ba-133 is strongly retarded and its peak concentration is shifted in time by a factor of 11.6, approximately.
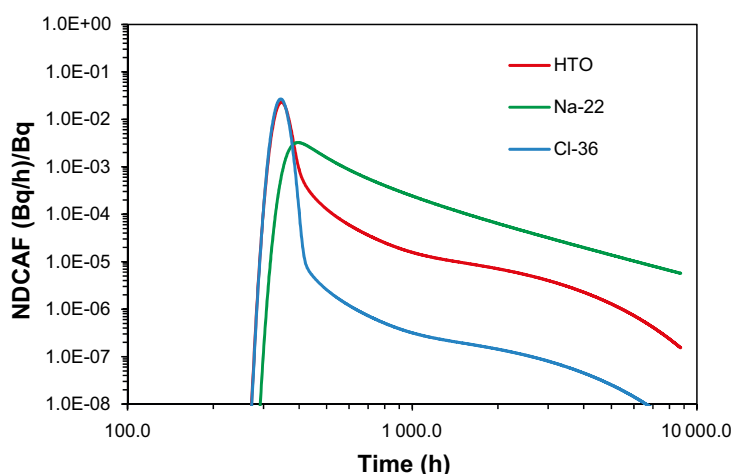

Figure C-5. Central Case 2D model: breakthrough curve for WPDE-1. Results are provided as normalised decay corrected activity flow ((Bq/h)/Bq).
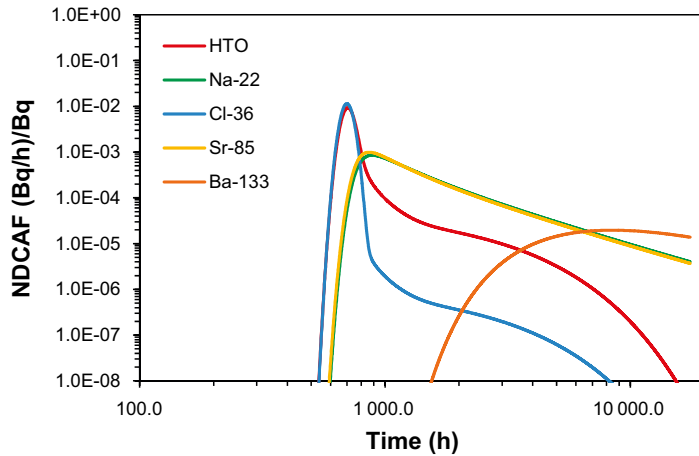
Figure C-6. *Central Case 2D model: breakthrough curve for WPDE-2. Results are provided as normalised decay corrected activity flow ((Bq/h)/Bq).*

Table C-4. Performance measures of central prediction of WPDE-1: time when event occurs.

	HTO time (h)	Na-22 time (h)	Cl-36 time (h)
Leading edge, 10 % of tracer peak concentration	315	340	314.5
Leading edge, 50 % of tracer peak concentration	329	361	328
Tracer peak concentration	346	396	345
Tail, 10 % of tracer peak concentration	387	877	379.5
Tail, 1 % of tracer peak concentration	452	2 969	395.5
Tail, 0.1 % of tracer peak concentration	832	> 8 760	410

Table C-5. Performance measures of central prediction of WPDE-1: tracer peak concentration.

Tracer	Concentration (Bq/g)
HTO	3.26E+05
Na-22	3.72E+03
Cl-36	2.79E+04

Table C-6. Performance measures of central prediction of WPDE-2 : time when event occurs.

	HTO time (h)	Na-22 time (h)	Cl-36 time (h)	Sr-85 time (h)	Ba-133 time (h)
Leading edge, 10 % of tracer peak concentration	629.5	710	628	710	2 622
Leading edge, 50 % of tracer peak concentration	662.5	768.5	659	768.5	4 024
Tracer peak concentration	703	878	697	878	8 179
Tail, 10 % of tracer peak concentration	802	2 737	778	2 737	> 17 520
Tail, 1 % of tracer peak concentration	1 006	10 749	815	10 749	> 17 520
Tail, 0.1 % of tracer peak concentration	3 092	> 17 520	850	> 17 520	> 17 520

Table C-7. Performance measures of central prediction of WPDE-2: tracer peak concentration.

Tracer	Concentration (Bq/g)
HTO	4.82E+05
Na-22	2.90E+03
Cl-36	9.67E+04
Sr-85	6.81E+03
Ba-133	8.06E+01

The upper and lower predictions (upper and lower case)

Fick's law establishes a linear dependence between diffusive mass fluxes and the effective diffusion coefficient (i.e. pore diffusion coefficient times porosity). The higher the mass fluxes the stronger is the retention capacity of the matrix, and vice versa. This theoretical evidence is confirmed by the results of WPDE-1 (Figure C-7 and Table C-8 and 3-9), particularly when one compares the performance measures among the different modelling cases. For instance, for a non-sorbing tracer like tritium, the tailing (i.e. 1 % of tracer peak concentration) is observed at time 452 h for the central prediction ($De = 2.5 \times 10^{-13}$ m^2/s) in WPDE-1. When the effective diffusion coefficient is slightly increased ($De = 3.0 \times 10^{-13}$ m^2/s, upper case), the tailing is slightly shifted (491 h); whereas when the effective diffusion coefficient is decreased ($De = 1.0 \times 10^{-13}$ m^2/s, lower case), the tailing is observed at earlier times (425 h). Same qualitative results are observed for the mildly sorbing tracers (i.e. Na-22a and Sr-85). Cl-36 appears to be much less sensitivity to the effective diffusion coefficient, probably because of the very low porosity values used in the calculations.

Results of WPDE-2 (Figure C-8 and Table C-10 and C-11) are qualitatively similar to those of WPDE-1. Given the strong retardation of barium, no much can be said about its sensitivity to the investigated parameters, as its tailing is far beyond the time frame of the calculations.
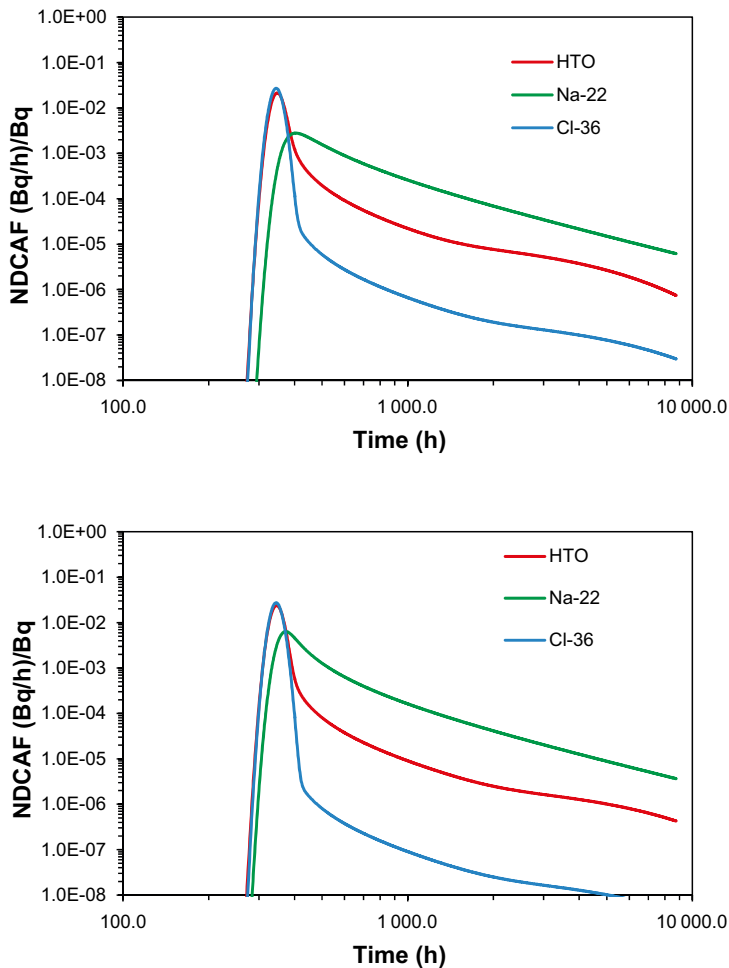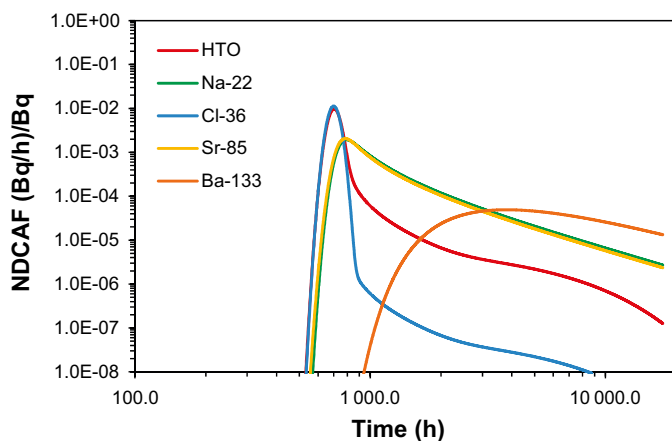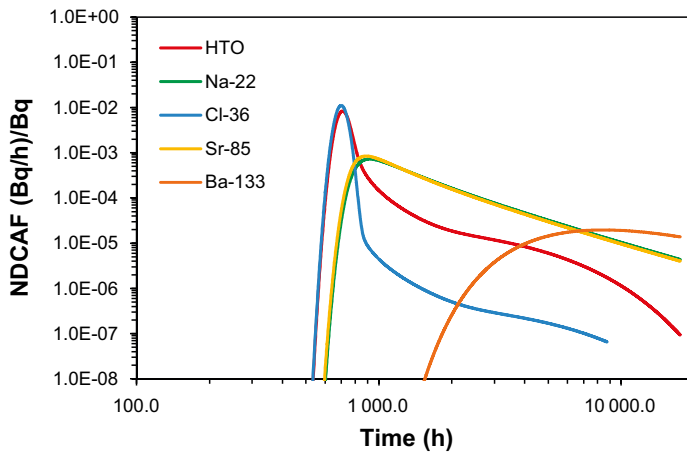

Figure C-7. *Breakthrough curve for WPDE-1: upper prediction (top) and lower prediction (bottom). Results are provided as normalised decay corrected activity flow ((Bq/h)/Bq).*

Table C-8. Performance measures of upper and lower prediction of WPDE-1 (results for lower prediction are in parentheses): time when event occurs.

	HTO time (h)		Na-22 time (h)		Cl-36 time (h)	
Leading edge, 10 % of tracer peak concentration	316	(314.5)	343	(329.5)	315	(315)
Leading edge, 50 % of tracer peak concentration	330	(328.5)	365	(346.5)	328.5	(362.5)
Tracer peak concentration	348	(346)	401	(372)	345	(346)
Tail, 10 % of tracer peak concentration	390.5	(384)	965	(601)	378.5	(378.5)
Tail, 1 % of tracer peak concentration	491	(425)	3414	(1586)	395	(394)
Tail, 0.1 % of tracer peak concentration	1014	(689)	> 8760	(6174)	414.5	(407)

Table C-9. Performance measures of upper prediction and lower prediction (in parentheses) of WPDE-1: tracer peak concentration.

Tracer	Concentration (Bq/g)
HTO	3.06E+05 (3.40E+05)
Na-22	3.21E+03 (7.28E+03)
Cl-36	2.85E+04 (2.85E+04)

Figure C-8. *Breakthrough curve for WPDE-2: upper prediction (top) and lower prediction (bottom). Results are provided as normalised decay corrected activity flow ((Bq/h)/Bq).*

Table C-10. Performance measures of upper and lower prediction of WPDE-2 (results for lower prediction are in parentheses): time when event occurs.

	HTO time (h)		Na-22 time (h)		Cl-36 time (h)		Sr-85 time (h)		Ba-133 time (h)	
Leading edge, 10 % of tracer peak concentration	630.5	(627)	719	(674)	627	(627)	719	(674)	2 623	(1 446)
Leading edge, 50 % of tracer peak concentration	664.5	(660)	783	(719)	658.5	(658)	783	(719)	3 994	(2 024)
Tracer peak concentration	705	(702)	904	(789)	697	(696)	904	(789)	8 619	(3 725)
Tail, 10 % of tracer peak concentration	819	(794)	3 106	(1 610)	780	(779)	3 106	(1 610)	> 17 520	(> 17 520)
Tail, 1 % of tracer peak concentration	1 132	(923)	12 571	(5 168)	819	(815)	12 571	(5 168)	> 17 520	(> 17 520)
Tail, 0.1 % of tracer peak concentration	4 014	(1 692)	> 17 520	(> 17 520)	877	(845)	> 17 520	(> 17 520)	> 17 520	(> 17 520)

Table C-11. Performance measures of upper prediction and lower prediction (in parentheses) of WPDE-2: tracer peak concentration.

Tracer	Concentration (Bq/g)
HTO	4.34E+05 (5.06E+05)
Na-22	2.46E+03 (6.62E+03)
Cl-36	9.41E+04 (9.59E+04)
Sr-85	5.80E+03 (6.63E+03)
Ba-133	8.1E+01 (2.02E+02)

Sensitivity analysis to variability of velocity in the slot

As discussed in Sections C2.3 and 3.2.4, although the experiment is designed so that water velocity is constant in the slot, there are possible sources of uncertainties that could have influence on possible spatial variations in the groundwater velocity patterns in the slot. Potential causes of inhomogeneity in these groundwater profiles are e.g. the dummy being not coaxial, with locally reduced/enlarged fracture apertures, or possible roughness of the drillhole wall.

Here, we conceptualise flow in the slot as an ensemble of non-interactive flow channels (streamtubes). Each "parcel" of radionuclide mass is transported by advection along one of these channels, and transverse dispersion, which tends to smear out transverse gradients of concentration, is neglected. The breakthrough curve at the outlet of the slot is computed as the ensemble of individual contributions (i.e. from each single streamtube). It is also assumed that streamtube travel times are normally distributed with mean travel time, $\bar{\tau}$, equal to 687 h (this analysis has focused on WPDE-2) and standard deviation, σ_τ, equal to 100 h. This is equivalent to assume that the dummy is not co-axial with the drillhole and that in some parts of the section the slot aperture is reduced by 30 % (i.e. $\Delta = 8.8 \times 10^{-4}$ m, being Δ the slot aperture) and in some other parts the aperture is increased by 45 % ($\Delta = 1.8 \times 10^{-3}$ m). It is worthwhile noting that this is a highly idealised simulation. The fact that the sum of the minimum and maximum fracture aperture (2.69 mm) is larger than the double of the constant aperture (2.5 mm) however can be seen as the effect of possible asperities in the fracture wall. A sketch of this conceptual model is shown in Figure C-9.

By analogy between the cumulative distribution function (CDF) of the standard normal distribution of travel times and the analytical solution for the 1D advective-dispersive equation (Ogata 1970), the following relationship can be established:

$$\alpha_L = \frac{(\sigma_\tau \cdot \bar{v})^2}{2L} \approx 2 \cdot 10^{-2} m \qquad (C\text{-}1)$$

where α_L (m) is the longitudinal dispersivity of the equivalent 1D ADE, $\bar{v}$ is the average groundwater velocity (m/h) and L (m) is the distance between the inlet and the outlet.
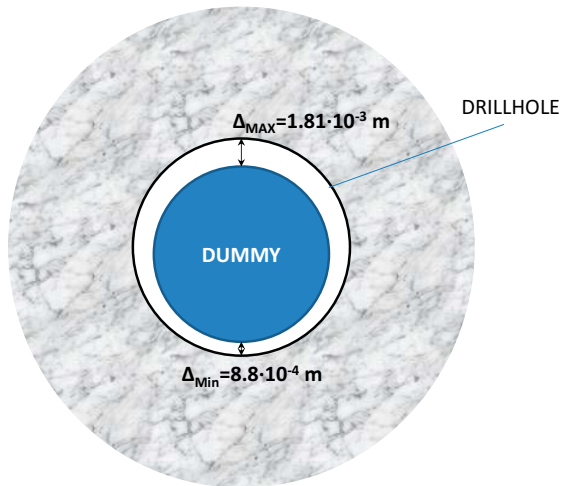
Figure C-9. *Sketch showing the dummy being not co-axial with the drillhole.*

The numerical calculation has been carried by modifying the model used for the central case prediction of WPDE-2, which is here run with the value of dispersivity specified in Equation C-1. A comparison between the results of the "original" model and the model with increased dispersivity is shown in Figure C-10 for HTO and Figure C-11 for Na-22. The overall effect of increasing mechanical dispersion is to enhance spreading with related earlier tracer first-arrival times and a strong decrease of peak concentration.
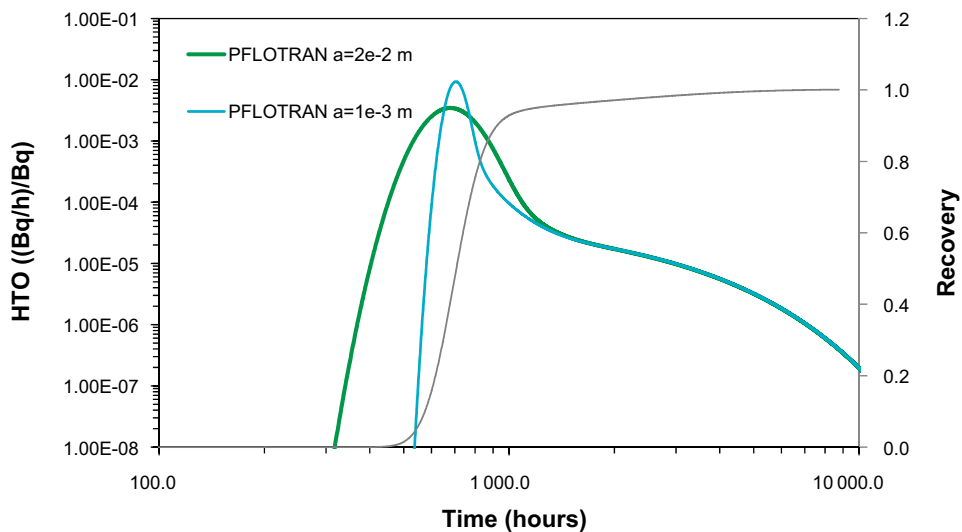
Figure C-10. *HTO breakthrough curves for WPDE-2. The results of the central case prediction (thin blue line) are compared with the related calculation with increased value of dispersivity (thick green line). Mass recovery for the calculation with increased dispersivity is shown in the secondary y-axis (grey line).*
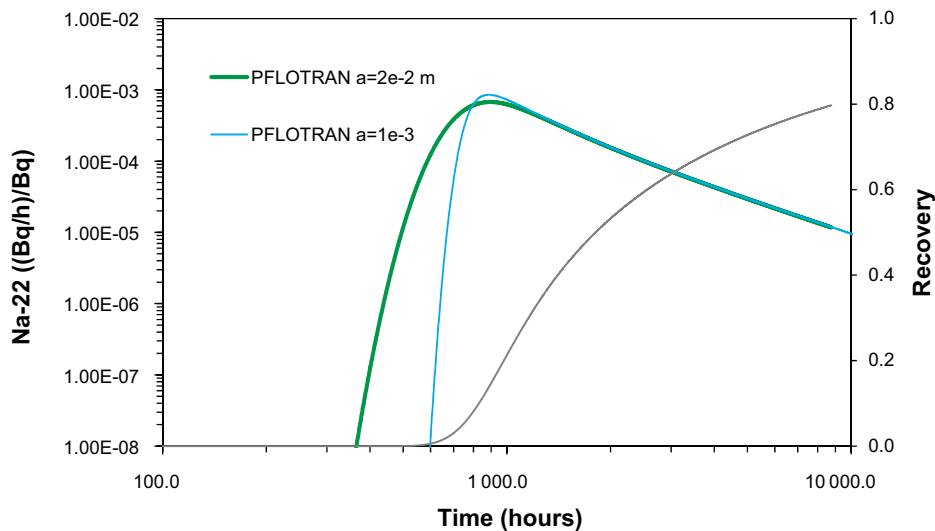
Figure C-11. *Na-22 breakthrough curves for WPDE-2. The results of the central case prediction (thin blue line) are compared with the related calculation with increased value of dispersivity (thick green line). Mass recovery for the calculation with increased dispersivity is shown in the secondary y-axis (grey line).*

Model verification

When the ADE is solved using an Eulerian scheme (e.g. the numerical approach used by PFLOTRAN), results are affected by numerical dispersion. This spurious effect is further amplified in presence of strong contrasts of hydraulic and transport properties, such as the case of the dual-porosity fracture-matrix system considered in these calculations. The minimisation of these artificial effects requires a very fine spatial and temporal discretisation as well as the use of very tight tolerances. Moreover, a careful cross-check of the results is always needed.

To ensure that the models presented in this section are properly parameterised and that results are robust and reliable, here the lower predictions of WPDE-1 and the central case of WPDE-2, namely breakthrough curves of HTO and Na-22, are compared against the following three independent solutions:

1. **Tang's solution** (Tang et al. 1981). It is an analytical solution that considers a single fracture with infinite matrix. The solution is provided in Laplace space. Although an explicit analytical inversion is provided by the authors, in these calculations the analytical solution is computed in Laplace space and numerically inverted using the MATLAB routine invlap.m (Hollenbeck 1998)

2. **MARFA** (Painter et al. 2008). It is a time-domain particle tracking code. As all the particle-based methods, it is free of numerical dispersion. In the calculations presented hereafter, MARFA is used with the retention model denoted as MD (unlimited matrix diffusion), which means that it is assumed that the extension of the accessible matrix is infinite.

3. **Sudicky's solution** (Sudicky and Frind 1982). It is an extension and generalisation of Tang's solution, which accounts for the limited extension of accessible matrix. As for Tang's solution, this calculation is here carried out in Laplace space and back-transformed using invlap.m. In these calculations, the exact extension of the matrix (i.e. 1.8 cm) is used as input.

Figure C-12 shows the comparison between the PFLOTRAN calculation and the independent solutions, which are here used to produce the HTO breakthrough curves for WPDE-1. The agreement between the different solutions is very good for the rising limb of the curve and the "early tailing". Starting from time 2 000 h, the PFLOTRAN solution starts to diverge from Tang's analytical solution and from the MARFA result. This is indeed a boundary effect caused by the very limited extension of the matrix included in the model. This boundary effect is well captured by Sudicky's solution, which accounts for the limited matrix thickness.

For Na-22 (WPDE-1; Figure C-13), the PFLOTRAN calculation agrees well with both Tang's solution and MARFA. This agreement is also good for the late tailing. In fact, being Na-22 mildly sorbed in the matrix, the extension of its penetration front is much more limited compared to HTO and thus, for this tracer the matrix included in the PFLOTRAN model can be considered as infinite.

Similar qualitative conclusion can be drawn for WPDE-2 (Figure C-14 for HTO and Figure C-15 for Na-22). However, for this second experiment, a slight divergence can be observed between the HTO tailing computed by PFLOTRAN and the results of Sudicky's solution.
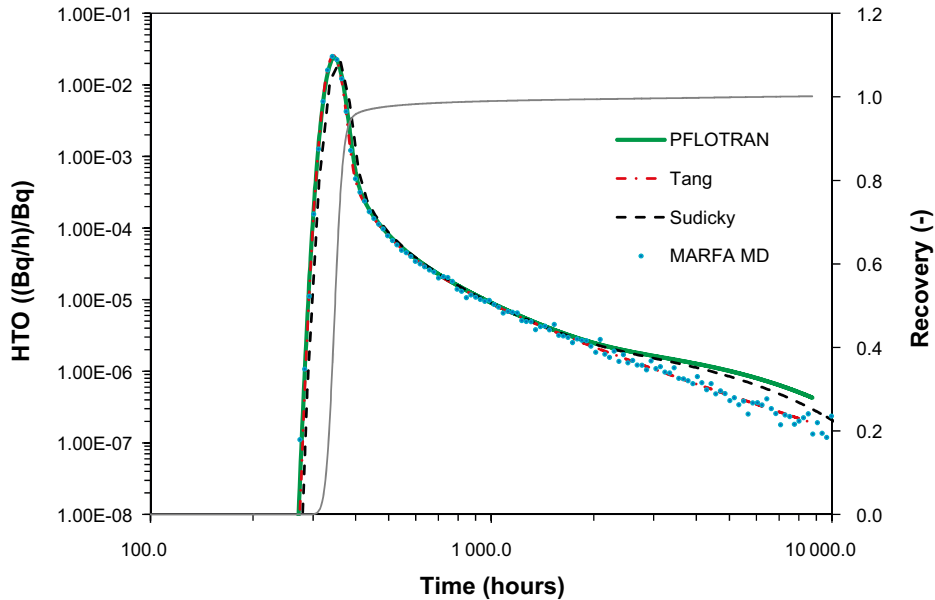
Figure C-12. *HTO breakthrough curves for the lower prediction of WPDE-1. The results of PFLOTRAN are compared with Tang's and Sudicky's analytical solutions and with MARFA with unlimited diffusion. Mass recovery for the calculation with increased dispersivity is shown in the secondary y-axis (grey line).*
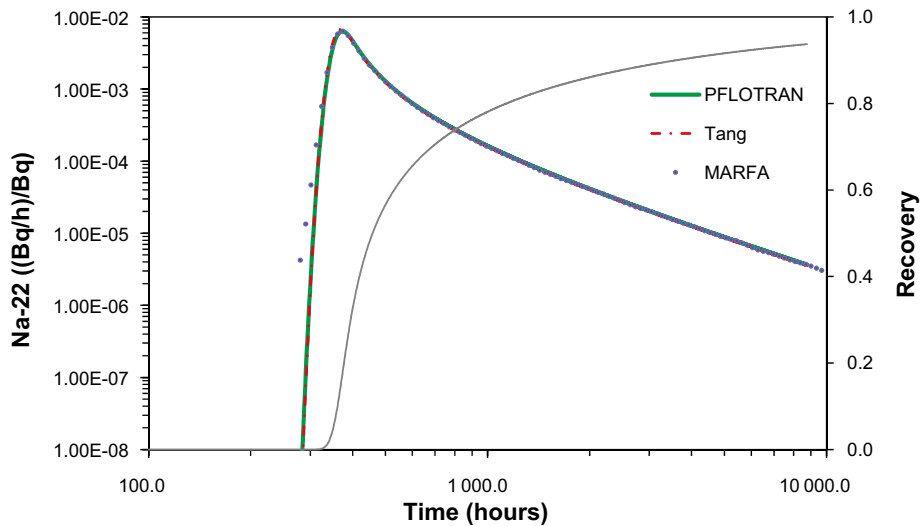
Figure C-13. *Na-22 breakthrough curves for the lower prediction of WPDE-1. The results of PFLOTRAN are compared with Tang's analytical solutions and with MARFA with unlimited diffusion. Mass recovery for the calculation with increased dispersivity is shown in the secondary y-axis (grey line).*
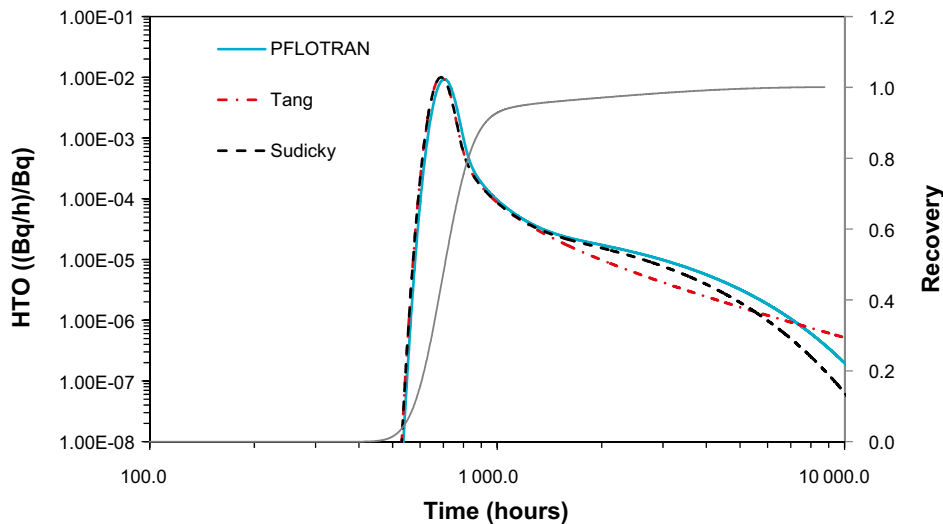
Figure C-14. *HTO breakthrough curves for the centra case of WPDE-2. The results of PFLOTRAN are compared with Tang's and Sudicky's analytical solutions. Mass recovery for the calculation with increased dispersivity is shown in the secondary y-axis (grey line).*
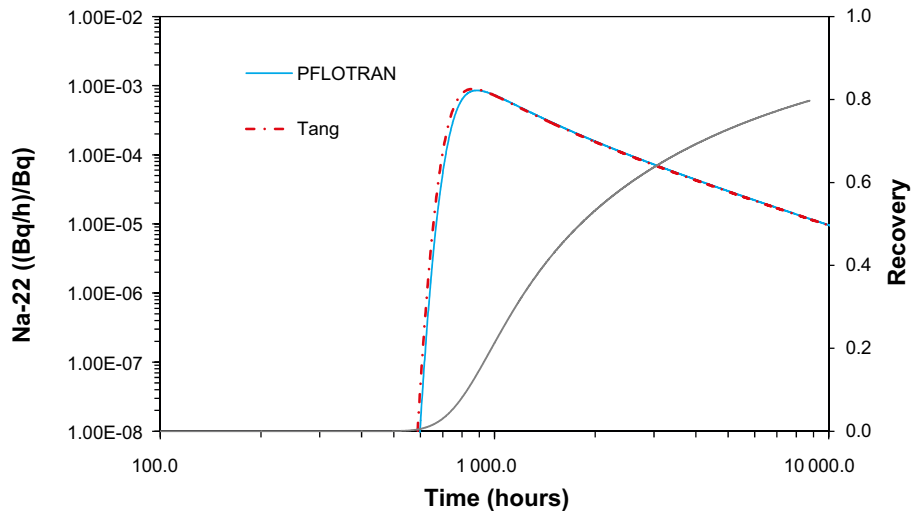

Figure C-15. *Na-22 breakthrough curves for the centra case of WPDE-2. The results of PFLOTRAN are compared with Tang's analytical solutions. Mass recovery for the calculation with increased dispersivity is shown in the secondary y-axis (grey line).*

C3.2   3D model (process understanding)

In the 3D model, the heterogeneous distribution of porosity in the matrix is generated using a micro DFN, with two set of fracture groups:

• A "traditional" Discrete Fracture Network (DFN) model is assumed for fractures down to a length scale of 5 mm.

• A grain size DFN (DFNgs), with the length scale interval 4–5 mm, will represent the high porosity regions between grains.

The DFN is then used to "map" an underlying micro-continuum model, using the procedure and formulation provided by Svensson (2001a, b). This resulting micro-continuum model (i.e. porosity at the centroids of an unstructured Cartesian grid) is imported into PFLOTRAN (Figure C-16). More details about the micro-continuum DFN are provided in a previous section (see contribution by U. Svensson).
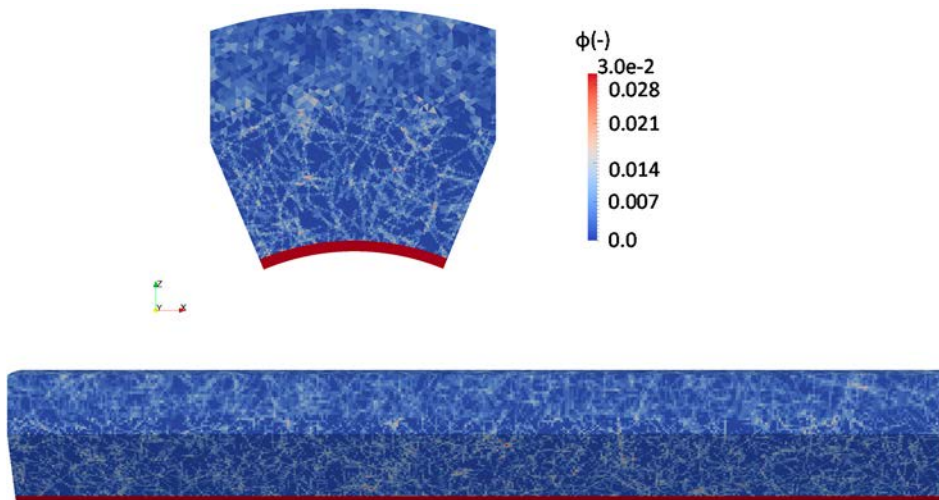
Figure C-16. *Distribution of porosity used in the 3D calculations.*

The complex network of higher-porosity inter-granular regions is evident from a visual inspection of Figure C-16. In these regions is where the highest diffusive fluxes are expected.

The model has been run using the parameters of the central case of WPDE-1 (Table C-3), except for matrix porosity, which, as explained in the previous paragraph, has been taken from the DarcyTools micro-continuum model. Only HTO and Na-22 are considered in these calculations. Na-22 sorption properties in the matrix are considered constant (Table C-2). In future calculations we plan to include "scattered" distributions of sorption sites to mimic sorption taking place only onto the surface of mineral grains that is actually exposed to the inter-granular regions. The simulation runs are carried out on the supercomputer JUQUEEN at the Jülich Supercomputing Centre (Stephan and Docter 2015). The time frame of the simulation is 1 300 h. A total of 12 000 computational hours have been spent for the calculation.

Snapshots of Na-22 concentration at two different times are shown in Figure C-17. From the figure one can notice that (1) sodium is strongly sorbed and its penetration into the matrix is very modest and (2) the shape of the penetration front is uneven. When heterogeneous sorption properties will be included into the matrix, it is expected that this uneven shape of the penetration front will be further amplified, with fingers along inter-granular regions and a more pronounced matrix penetration. Similar qualitative findings have been recently found by Trinchero et al. (2017), who assessed cesium transport in a synthetically generated heterogeneous fracture-matrix system.
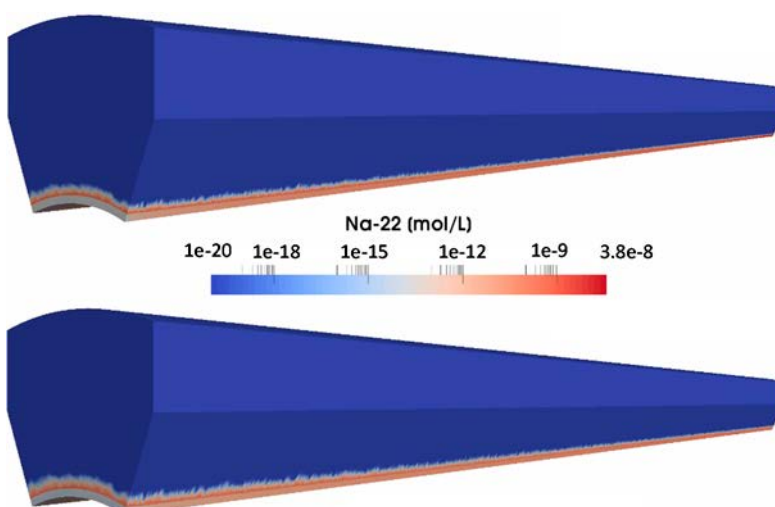

Figure C-17. *Na-22 concentration (in mol/L) at (top) 320 h and (bottom) 720 h from the beginning of the injection.*

The breakthough curves of HTO and Na-22 are shown in Figures C-18 and C-19. The results of the PFLOTRAN calculation are compared with Thang's analytical solution (see Section C3.1). Here, the arithmetic mean of the porosity distribution ($\bar{\varphi} = 4 \times 10^{-3}$) is used as input for the analytical solution. The agreement between Tang's solution and the PFLOTRAN calculation is very good for the tracer but evident differences exist for Na-22. More specifically, fracture heterogeneity seems to affect the peak and the intermediate part of the tailing. The peak is in fact displaced to earlier times while an anomalously smooth slope (i.e. tailing of the slope smaller than the typically expected $-3/2$ value) is observed. This conclusion need to be further validated during the future modelling activities, which will extend the scope of the calculations by including heterogeneous distributions of sorption sites.
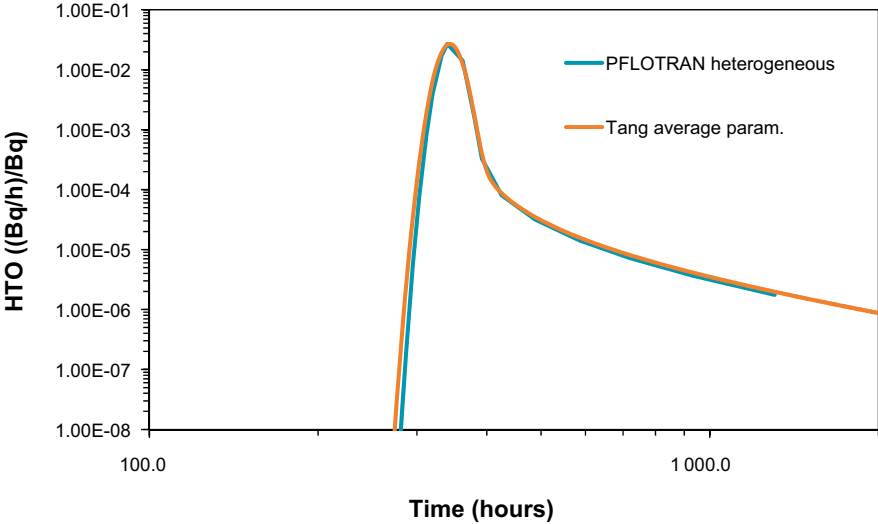
Figure C-18. *HTO breaktrough curve: 3D PFLOTRAN model vs. Tang's analytical solution.*
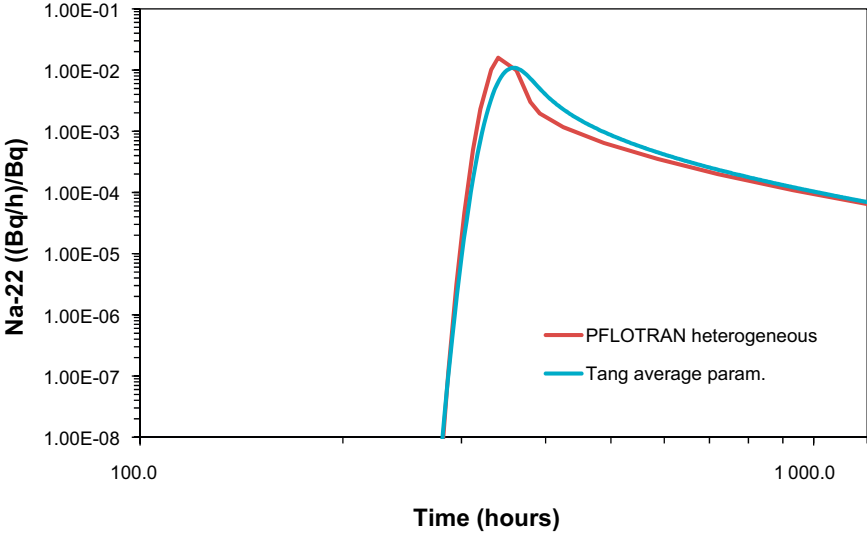

Figure C-19. *Na-22 breaktrough curve: 3D PFLOTRAN model vs. Tang's analytical solution.*

SKB R-17-10

C4 Summary, conclusions and future work

The interface between PFLOTRAN and DarcyTools (iDP) has been used to perform blind predictions of WPDE-1&2.

Two different models have been used in this study: a simplified 2D axisymmetric model has been used to carry out a large number of "production runs", whereas a 3D heterogeneous model has been used for "process understanding".

The analysis of the 2D model leads to the following conclusions:

- Results (i.e. breakthrough curves computed at the outlet of the slot) are sensistive to the value of effective diffusivity used in the calculations. As expected, the large is the effective diffusivity, the stronger is the retention capacity of the matrix.

- Due to the limited extension of the matrix, the breakthrough tailings for non-sorbing tracers are affected by boundary effects

- Cl-36 is affected by anion exclusion, and this is particular evident at late-times, where much lower diffusive fluxes are observed

- Na-22 and Sr-85 are mildly retained whereas Ba-133 is strongly retarded and its tailing falls out of the time frame of the analysis

- Results are strongly dependent on the velocity profile within the slot. A modest variability of the slot aperture has strong impact on the shape of the breakthrough curve, which turns out to be more dispersive, with earlier first arrival times.

- The numerical calculations have been successfully validated by comparing the results with analytical solutions and independent Lagrangian simulations

The three-dimensional model has been used to analyse the influence that matrix heterogeneity has on radionuclide transport. This preliminary analysis has pointed out that matrix heterogeneity seems to affect the peak and the intermediate part of the tailing. The peak is in fact displaced to earlier times while an anomalously smooth slope (i.e. tailing of the slope smaller than the typically expected $-3/2$ value) is observed.

As a future improvement of this analysis, it is planned to modify the 3D model by including also heterogeneous sorption properties. The goal of this future study is to analyse the effect of sorption taking place only at the exposed surface of minerals grains.

Technical University of Liberec, Czech Republic

Jakub Říha, Milan Hokr

D1   Introduction

This document deals with description of simulation process of WPDE experiments. For the simulation, we used Flow123d software which is being developed on Technical University of Liberec.

D1.1   Background

In the Technical University of Liberec, we are involved in multiple activities that include mathematical modelling of flow and transport in fractured rock. One of our focuses is modelling of radionuclide transport in the repository far-field. For this purpose we are developing our own simulation software (Flow123d). Flow123d is a simulator of underground water flow, solute and heat transport in fractured porous media. Novelty of this software is support of computations on complex meshes consisting of simplicial elements of different dimensions. Therefore, we can combine continuum models and discrete fracture network models.

D1.2   Objectives

The main objective of Task9a simulations is to provide a blind prediction of the experiment results. For us, this means that we are going to be able to compare the results of our modelling software with the results of others. This comparison should be interesting for us because all the modelling groups should use the same input data.

D1.3   Scope and limitations

Our main limitation is the high computational demands which cause the simulation time to be quite long.

D2   Methodology and model

We used Flow123d software (TUL 2015) for the simulation of WPDE experiments. Flow123d is a simulator of underground water flow, solute and heat transport in fractured porous media. Novelty of this software is support of computations on complex meshes consisting of simplicial elements of different dimensions. Therefore, we can combine continuum models and discrete fracture network models.

Current version includes mixed-hybrid solver for steady and unsteady Darcy flow, finite volume model and discontinuous Galerkin model for solute transport of several substances and heat transfer model. Using operator splitting, we support models for various local processes including dual porosity, diffusion, sorption, decays and simple reactions.

Computations can be run in parallel using MPI with scalability up to hundreds of processors. The input interface based on JSON file format allows specification of general space-time dependent data for any physical parameter that does not compromise performance. Program supports output into GMSH and VTK formats.

The developers website is http://flow123d.github.io/. The simulations have been done with the version 1.8.3.

In the following paragraphs I will briefly describe the most important parts of the model (relevant to the simulation of the experiment).

The computation of the steady or unsteady flow in porous and fractured medium is given by the Darcy equation and the continuity equation. Currently, three basic types (Dirichlet, Neuman and Robin) of boundary conditions are supported in order to obtain unique solution. The principal unknowns of the system are the pressure head and the flux.

The motion of substances dissolved in water is governed by the advection and the hydrodynamic dispersion. The following system of mass balance equations is considered:

$$\partial_t\big(\delta\vartheta c^i\big) + div\big(\boldsymbol{q}c^i\big) - div\big(\vartheta\delta\boldsymbol{D}^i\nabla c^i\big) = F_S^i + F_C^c + F_R(c^1, \ldots, c^s).$$

The principal unknown is concentration c^i [kgm^{-3}] of a substance $i \in \{1, \ldots, s\}$, which means the weight of the substance in the unit volume of water. Other quantities are:

- The porosity ϑ [-], i.e. the fraction of space occupied by water and the total volume.

- The hydrodynamic disperzivity tensor $\boldsymbol{D}^i$ [m^{2}s^{-1}] has the form

$$\boldsymbol{D}^i = D_m^i\tau\boldsymbol{I} + |\boldsymbol{v}|\left(\alpha_T^i\boldsymbol{I} + \big(\alpha_L^i - \alpha_T^i\big)\frac{\boldsymbol{v}\otimes\boldsymbol{v}}{|\boldsymbol{v}|^2}\right),$$

which represents (isotropic) molecular diffusion and mechanical dispersion in longitudal and transversal direction to the flow. Here D_m^i [m^{2}s^{-1}] is the molecular diffusion coefficient of the i-th substance, $\tau = \vartheta^{1/3}$ is the tortuosity, α_L^i [m] and α_T^i [m] is the longitudal dispersivity and transverse disperzivity respectively. Finally, $\boldsymbol{v}$ [ms^{-1}] is the microscopic water velocity related to the Darcy flux $\boldsymbol{q}$ by the relation $q = \vartheta\delta v$, where δ_d [m^{3-d}] is the cross section coefficient (thickness of a fracture or cross section of a channel). The molecular diffusion coefficient which is used as a model input is obtained from effective diffusivity D_e as follows:

$$D_m = \frac{D_e}{\vartheta \cdot \tau}.$$

- F_S^i [kgm^{-d}s^{-1}] represents the density of concentration sources in the porous medium.

- F_C^c [kgm^{-d}s^{-1}] is the density of concentration sources due to Exchange between regions with different dimensions.

- $F_R(\ldots)$ [kgm^{-d}s^{-1}] is the reaction term (dual porosity, sorption, radioactive decay).

Within the above presented model, Flow123d presents two possible approaches to solute transport:

- For modelling pure advection ($\boldsymbol{D} = 0$) one can choose Transport operator splitting method, which represents an explicit in time finite volume solver. The solution for one time step is faster but the maximal time step is restricted. The resulting concentration is piecewise constant on mesh elements. This solver supports reaction term (involving simple chemical reactions, dual porosity and sorption).

- The full model including dispersion is solved by an implicit in time discontinuous Galerkin solver. It has no restriction of the computational time step and the space approximation is piece-wise polynomial, currently up to order 3. Reaction term is implemented only for the case of linear sorption:

$$F_R^i = -\partial_t\left((1 - \vartheta)\delta M^i\rho_s c_s^i\right), \qquad c_s^i = \frac{k_l^i}{\rho_l}c,$$

where c_s^i [mol kg^{-1}] is the concentration of sorbed substance, k_l^i [mol kg^{-1}] is the sorption coefficient, ρ_s and ρ_l [kgm^{-3}] is the density of the solid (rock) and of the liquid (solvent) respectively. M^i [kg mol^{-1}] denotes the molar mass of the i-th substance. The initial concentration in solid is assumed to be in equilibrium with the concentration in liquid. The sorption coefficient k_l [mol kg^{-1}] which is used as a model input is obtained from sorption coefficient K_D [m^3 kg^{-1}] as follows:

$$K_l = K_D\rho_l/M$$

For further information on the mathematical model used by Flow123d please refer to the developers website mentioned above.

D2.1 Model setup

In the section the model setup and its inputs are described. In the first part the model geometry and computational mesh are described. We follow with the description of the flow model and conclude with the transport model.

Geometry and mesh

The geometry consists of a 2D fracture and a 3D rock (divided into three parts). The geometry is shown in Figure D-1.

The 3D part is divided into three volumes to differentiate the rock types: VGN1 (0–0.35 m in the direction of x axis), PGR (0.35–0.5 m) and VGN2 (0.5–1.905 m). The radius of the dummy is 28.25 mm, the aperture of the fracture is 1.25 mm and the thickness of rock is 0.1 m.

The discretisation of the geometry is shown in Figures D-2 and D-3. The mesh has 720 2D elements (representing the fracture) and 12 096 3D elements (representing the rock). There are two thin layers of elements surrounding the fracture. Their presence helped to improve the simulation results of sorbing species.
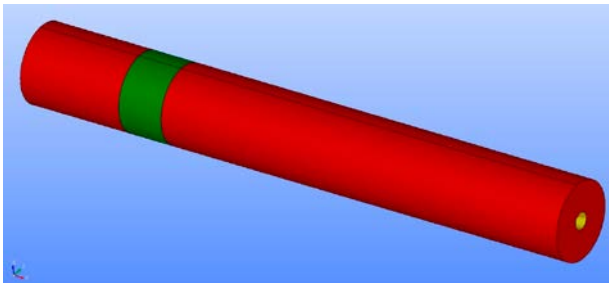
Figure D-1. *The model geometry. The red part represents veined gneiss (VGN) and the green part represents pegmatitic granite (PGR).*
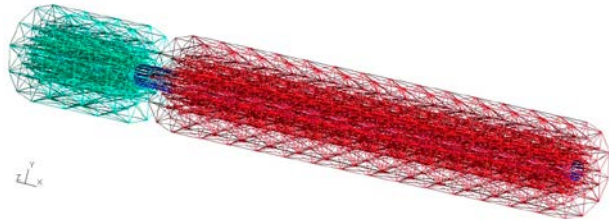
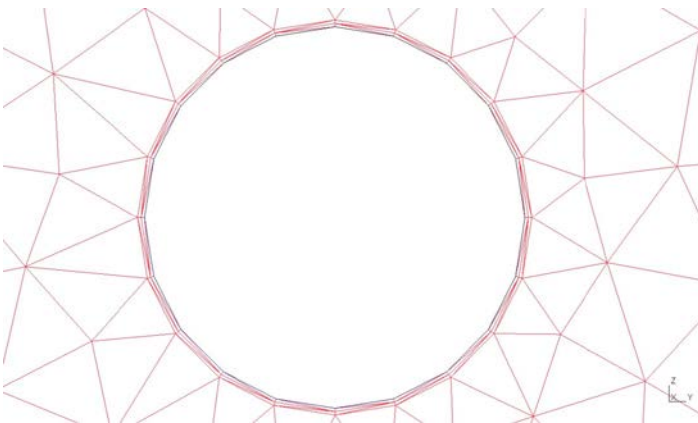***Figure D-2.*** *The model mesh (with hidden PGR part to show a discretisation of fracture).*

Figure D-3. *The model mesh – two thin layers surrounding the fracture.*

Flow model

The flow model was set up so that it reproduces the target flow rates of WPDE-1 and WPDE-2 experiments. Its parameters are shown in Table D-1.

Table D-1. Parameters of the flow model.

	WPDE-1	WPDE-2
Hydraulic conductivity of fracture	1.28 m/s	1.28 m/s
Hydraulic conductivity of rock	9.81E−13 m/s	9.81E−13 m/s
Boundary condition left	Dirichlet Φ = 0 m	Dirichlet Φ = 0 m
Boundary condition right	Neumann q = −1.536E−6 m/s	Neumann q = −0.768E−6 m/s
Boundary condition rest	Homogeneous Neumann (no flow)	Homogeneous Neumann (no flow)
Water balance	3.35E−10 m³/s ~ 20 µl/min	1.68E−10 m³/s ~ 10 µl/min

Hydraulic conductivity of fracture was computed from its aperture using the cubic law.

Hydraulic conductivity of rock was computed based on the estimated permeability of $1E−19$ m².

Boundary conditions were prescribed on both ends of the fracture. On the outflow end, there is a Dirichlet boundary condition and on the inflow end there is a Neumann boundary condition. Its value was computed as the ratio of the expected flow and the area of the fracture cross section. On the rest of the boundary there is a homogeneous Neumann condition (no flow).

The computed velocity field is shown in Figure D-4 (for WPDE-1). In this case, we assume the velocity to be equal to the Darcy flux. It is apparent that there is non-zero velocity in the rock matrix but it is many orders smaller than the velocity in the fracture.

Transport model

In this section, a setup of the transport model will be described.

Boundary conditions for transport were prescribed only on the inflow end of the fracture. Their values were calibrated so that the injected amounts of tracers are equal to the amounts described in the experiment documentation. In Flow123d the transported quantity is mass (not activity) hence the injected activities were converted to mass (divided by specific activity).

The duration of the injection was computed from the known quantities (total volume of injection solution and flow rate).

The starting point of the simulation period is when the valve to the tracer injection loop is switched on. To account for the travel time in the PEEK tube between the injection loop and the experimental section the boundary condition was delayed. This delay was computed based on the known quantities (length of PEEK inlet tube, its inner diameter and flow rate).
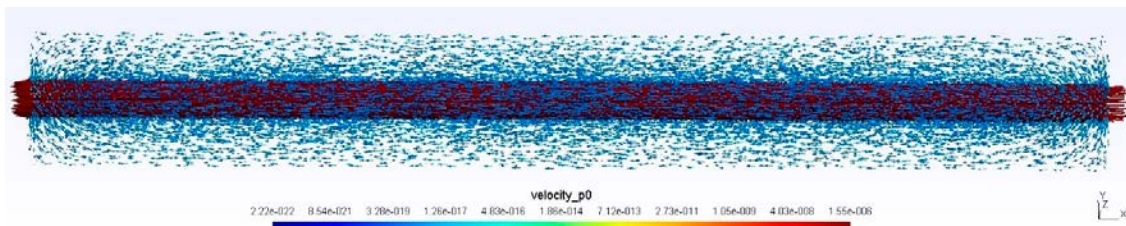

Figure D-4. *Velocity field. Result of WPDE-1 simulation.*

Similarly, the outflow delay was computed and used to account for the PEEK outlet tube.

The time constants of the simulations are shown in Table D-2.

Table D-2. Time constants of the transport model.

	WPDE-1	WPDE-2
Simulation period	8760 h (1 year)	17 520 h (2 years)
Boundary condition/outflow delay	16 h/17 h	32 h/34 h
Injection duration	50 min	5 h

The porosities used in the simulations are shown in Table D-3. Their values were derived from Table 2-8 in Task Description as an arithmetic mean for each rock type. The values for Cl-36 were derived from Table 2-9 (rock capacity factor).

Table D-3. Porosities used in the model.

Porosity [-]	
Fracture	1
VGN	8.2E−3
PGR	5E−3
Cl-36 VGN	1.75E−4
Cl-36 PGR	1.3E−2

Mechanical dispersion is computed only in the fracture. The longitudal dispersivity is approximately 10 % of the characteristic length ($\alpha_L = 0.19$ m), the transverse dispersivity $\alpha_T = 0.019$ m.

Effective diffusivities for both rock types are shown in Table D-4. Their values were partially obtained from Table 2-9 in Task Description. Values for Na-22, Sr-85 and Ba-133 were not stated in the documentation. Their source is hence mentioned in the table.

Table D-4. Effective diffusivities (*Vanýsek 2009).

	Effective diffusivity D_e [m^2/s]		Free water diffusivity [m^2/s]
	VGN	PGR	Fracture
HTO	1.83E−13	5.7E−13	2.3E−9*
Cl-36	0.05E−13	5E−13	1.33E−9*
Na-22	4.65E−13 (Kaukonen et al. 1997)		2.03E−9*
Sr-85	3.3E−13 (Skagius et al. 1999)		7.91E−10*
Ba-133	1.47E−13 (Widestrand et al. 2007)		5.41E−10*

The linear sorption partitioning coefficients used in the simulations are shown in Table D-5. Their values were obtained from Table 2-11 in Task Description. There is no sorption in the fracture.

In this section, the simulation results are presented. Sensitivity analysis was performed for WPDE-2 and will be discussed in Section D3.2.

Table D-5. The linear sorption partitioning coefficients.

Linear sorption partitioning coefficient [m³/kg]

	VGN	PGR
HTO	0	
Cl-36	0	
Na-22	0.0013	0.0008
Sr-85	0.0011	
Ba-133	0.06	0.08

D3 Results and discussion

D3.1 The central prediction

WPDE-1

The results of WPDE-1 simulation are shown in Figures D-5 and D-6. The outflow is normalized according to the instructions (except for the units of mass in place of activity).

In Table D-6 there are fractions of injected tracers that flew out of the simulation area.

Table D-6. Fractions of total output and total input (recovery) for WPDE-1.

HTO	99.33 %
Na-22	90.1 %
Cl-36	99.89 %
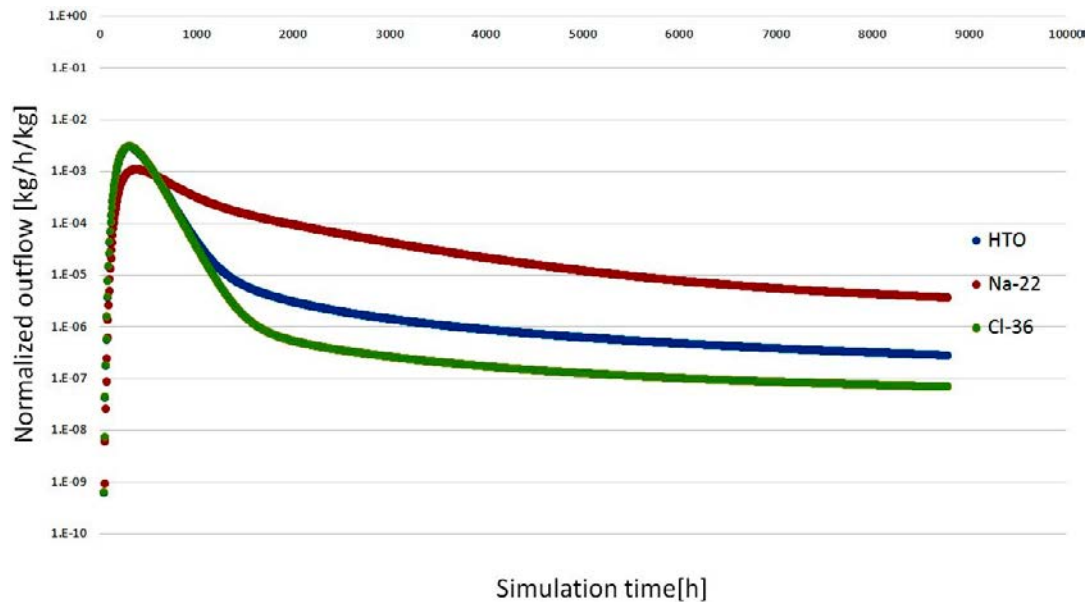
Figure D-5. *Results of WPDE-1 simulation.*
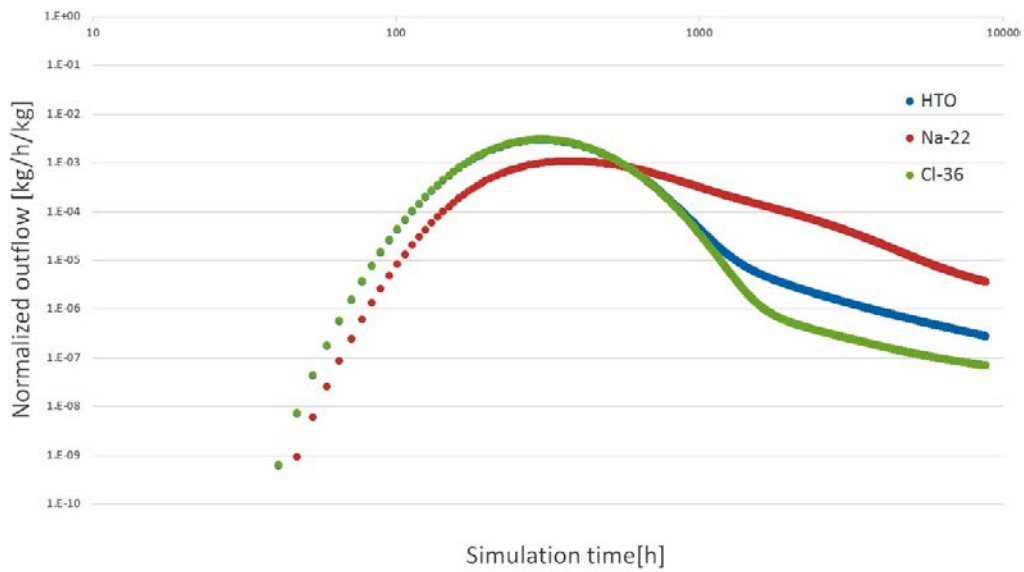
Figure D-6. *Results of WPDE-1 simulation, logarithmic time scale.*

WPDE-2

The results of WPDE-2 simulation are shown in Figures D-7 and D-8. The outflow is normalized according to the instructions (except for the units of mass in place of activity).

In Table D-7 there are fractions of injected tracers that flew out of the simulation area.

Table D-7. Fractions of total output and total input (recovery) for WPDE-2.

HTO	100 %
Na-22	88.95 %
Cl-36	100 %
Sr-85	92.73 %
Ba-133	44.8 %
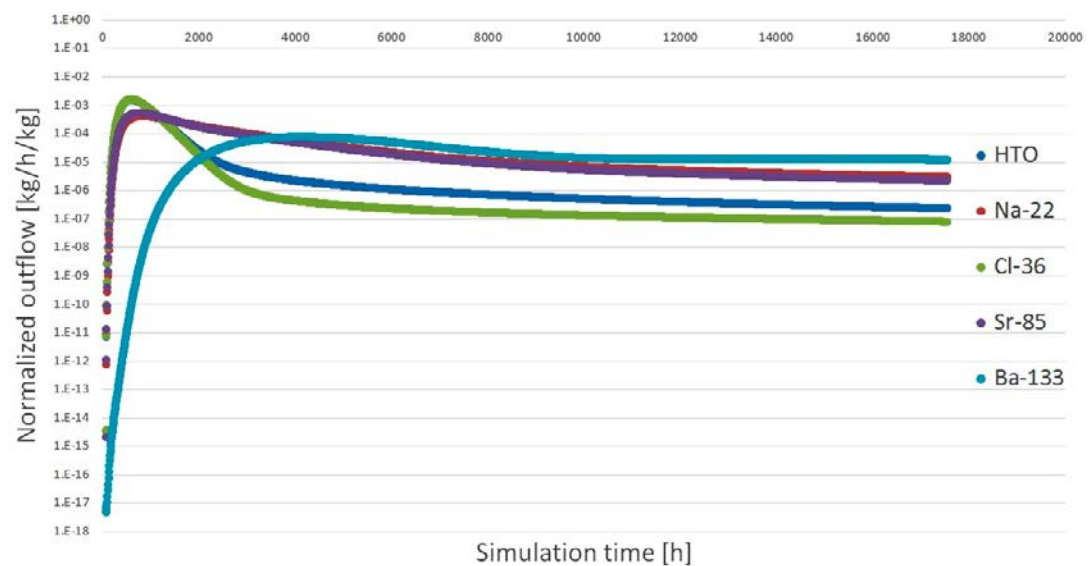
Figure D-7. *Results of WPDE-2 simulation.*
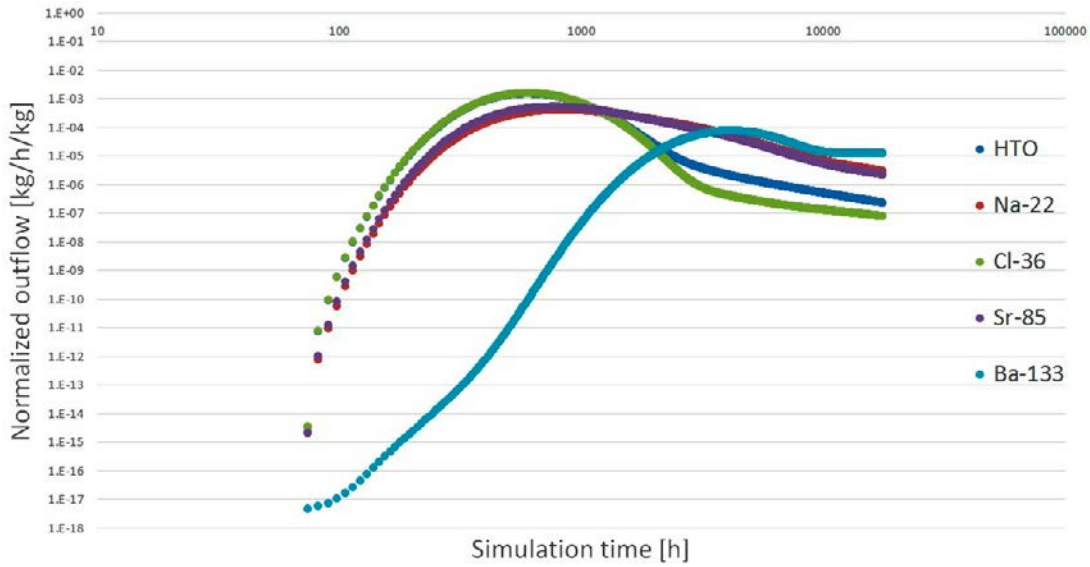
Figure D-8. *Results of WPDE-2 simulation, logarithmic time scale.*

Results of the sorbing tracers proved to be strongly dependent on discretisation in the vicinity of the fracture. In Section D2.1, two thin layers of elements around the fracture are shown. This dramatically improved the results for sorbing tracers in comparison with previous results. The results for Ba-133 (the most sorbing tracer) are still doubtful (e.g. tail deviating from a slope of −1.5 in Figure D-8) which could be solved by further tinkering of the discretisation. This is very hard to do since this is supposed to be a blind prediction hence there are no results we could be fitting. We know the Ba-133 results of ours are a little off only by comparing them to the results of others. This dependence of results on thickness of thin layers around the fracture is shown in Figure D-9.
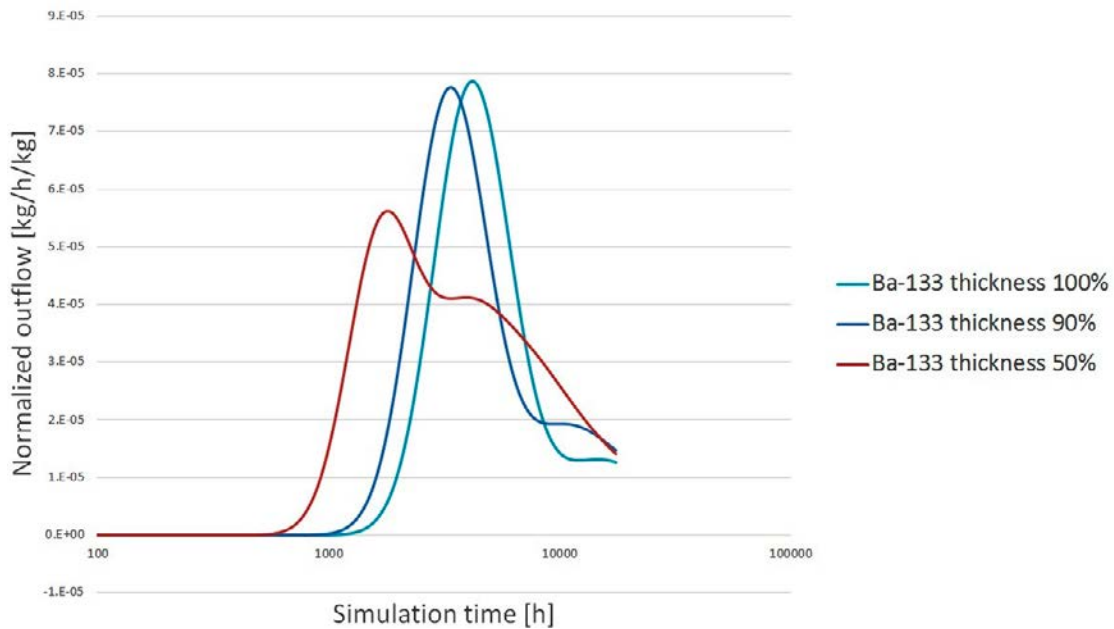
Figure D-9. *WPDE-2 simulation – dependence of Ba-133 results on space discretisation.*

D3.2   Other alternative models, sensitivity cases and results

In this section, the sensitivity analysis for WPDE-2 will be described and evaluated. The sensitivity analysis was performed for each of the parameters in Table D-8. Ranges of parameters were taken mostly from the Task Description. The results (qualitative comparison) are shown in Figure D-10 to Figure D-14.

Table D-8. Sensitivity analysis parameter ranges.

| Parameter	Default	Minimum	Maximum
Longitudal disperzivity [m]	0.19	0.1	0.28
Porosity VGN [-]	0.0082	0.0011	0.03
Porosity PGR [-]	0.005	0.0026	0.0077
Porosity VGN [-] Cl-36	0.000175	0.0001	0.0006
Porosity PGR [-] Cl-36	0.013	0.011	0.015
Kd Na-22 VGN [m³/kg]	0.0013	0.001	0.0016
Kd Na-22 PGR [m³/kg]	0.0008	0.0005	0.0011
Kd Sr-85 VGN [m³/kg]	0.0011	0.0008	0.0014
Kd Sr-85 PGR [m³/kg]	0.0011	0.0008	0.0014
Kd Ba-133 VGN [m³/kg]	0.06	0.04	0.08
Kd Ba-133 PGR [m³/kg]	0.08	0.06	0.1
De HTO VGN [m²/s]	1.83E−13	1.2E−13	2.8E−13
De HTO PGR [m²/s]	5.7E−13	5.1E−13	6.3E−13
De Na-22 VGN [m²/s]	4.65E−13	3.7E−13	5.6E−13
De Na-22 PGR [m²/s]	4.65E−13	3.7E−13	5.6E−13
De Cl-36 VGN [m²/s]	5E−15	2E−15	8E−15
De Cl-36 PGR [m²/s]	5E−13	4E−13	6E−13
De Sr-85 VGN [m²/s]	3.3E−13	2.5E−13	4.1E−13
De Sr-85 PGR [m²/s]	3.3E−13	2.5E−13	4.1E−13
De Ba-133 VGN [m²/s]	1.47E−13	1.17E−13	1.77E−13
De Ba-133 PGR [m²/s]	1.47E−13	1.17E−13	1.77E−13
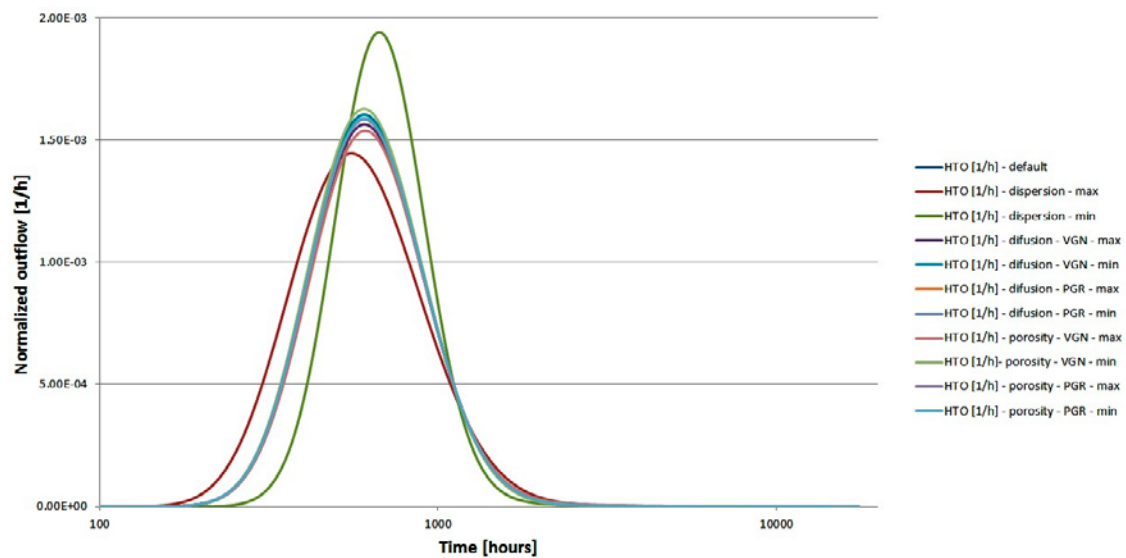
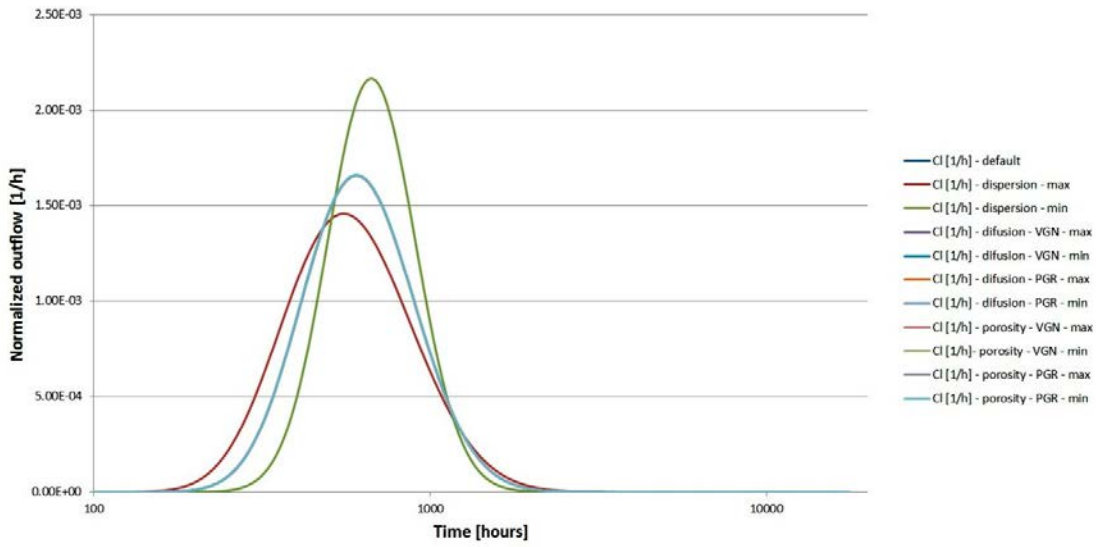***Figure D-10.*** *WPDE-2 sensitivity analysis – HTO.*

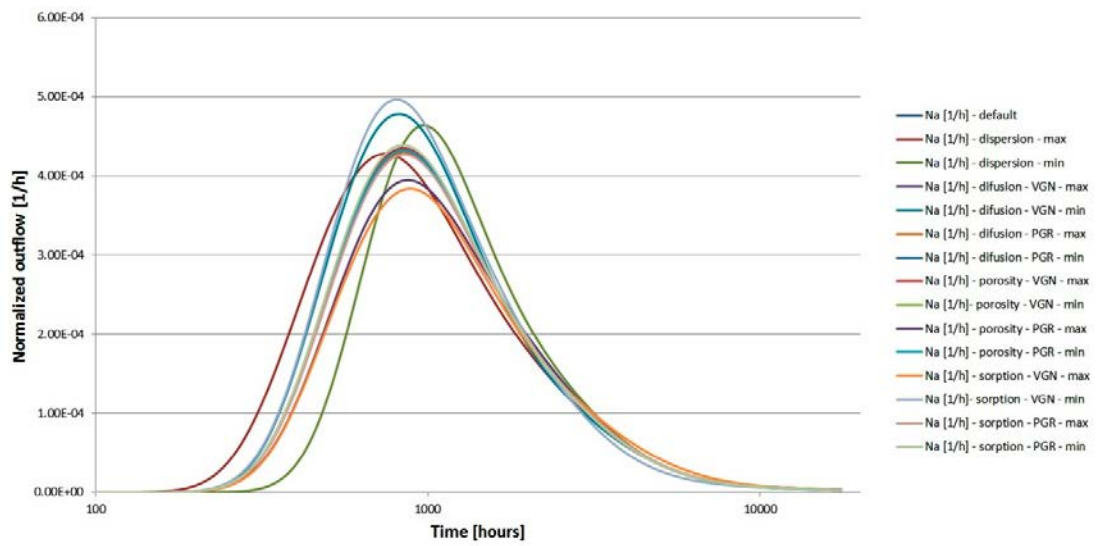***Figure D-11.*** *WPDE-2 sensitivity analysis – Cl-36.*

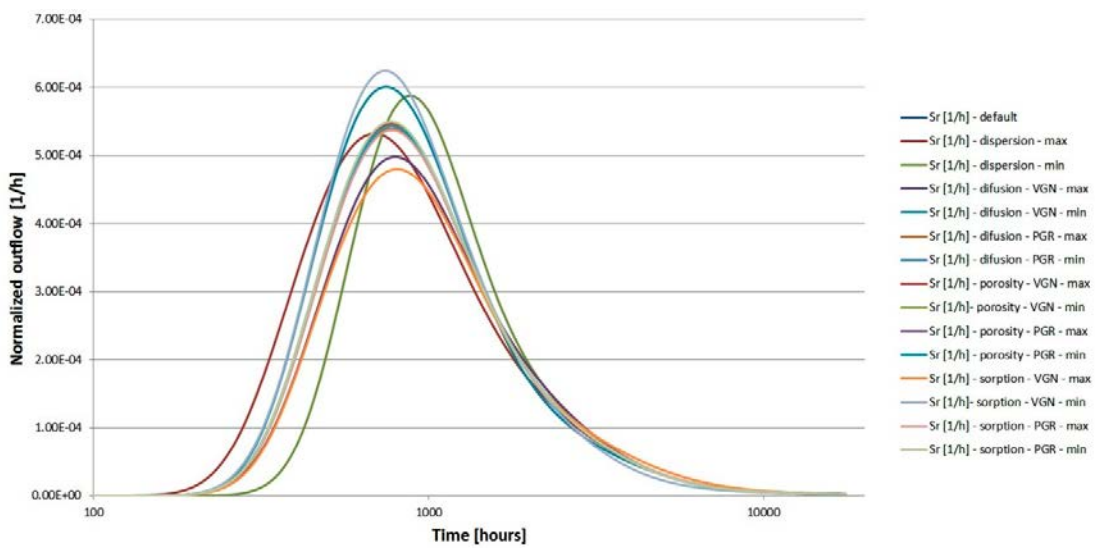***Figure D-12.*** *WPDE-2 sensitivity analysis – Na-22.*

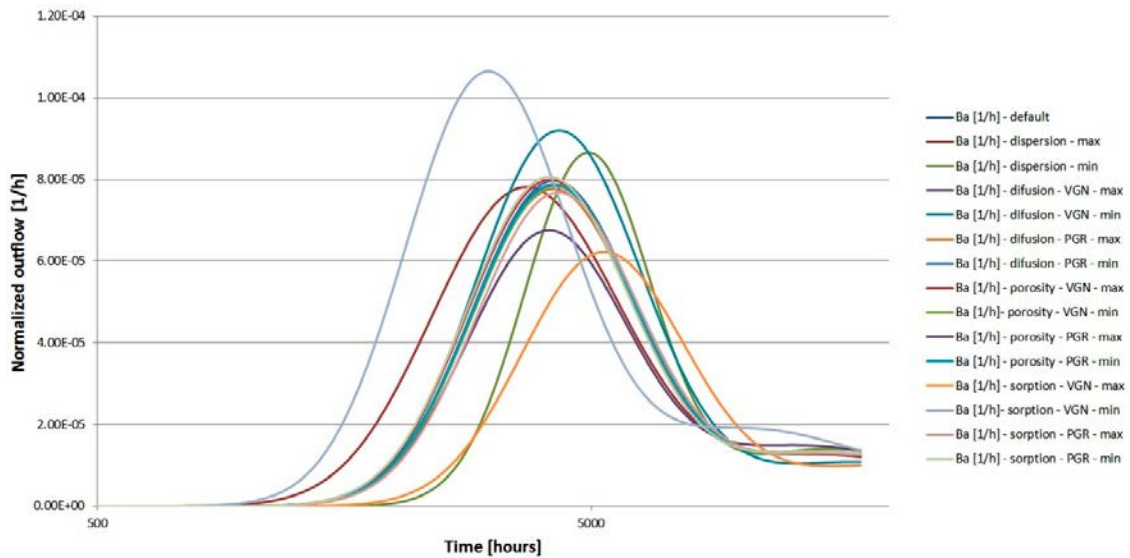***Figure D-13.*** *WPDE-2 sensitivity analysis – Sr-85.*

Figure D-14. *WPDE-2 sensitivity analysis – Ba-133.*

In addition to the qualitative comparison the quantitative evaluation of sensitivity was proposed and computed using the following formula:

$$s = \frac{\left(1 - \left(\frac{y_2}{y_1}\right)\right)}{\left(1 - \left(\frac{b_2}{b_1}\right)\right)},$$

where y_1 is the default output (using default parameter value b_1) and y_2 is the altered output (using altered parameter value b_2). It is basically a ratio of relative change of output and relative change of input.

Three quantities were chosen to be evaluated:

- Position of breakthrough curve peak [hours].
- Peak value [kg/h/kg].
- Peak width as a time from 50 % of peak value (leading edge) to 50 % of peak value (trailing edge) [hours].

The results of quantitative sensitivity analyses are shown in Table D-9. Zero sensitivities are caused by the simulation output step which was 8 hours in case of WPDE-2 (the resolution isn't fine enough to capture a change of evaluated quantity). Nonzero sensitivities might be slightly inaccurate for the very same reason.

Four main conclusions resulted from both qualitative and quantitative evaluation of sensitivity:

- Non-sorbing tracers are practically only sensitive to disperzivity.
- Sorbing tracers are sensitive to disperzivity, diffusion and sorption.
- Sensitivity to porosity is negligible.
- Sensitivity to PGR parameters is much lower than sensitivity to VGN parameters. This does not come as a surprise since VGN is the dominant rock type.

Table D-9. WPDE-2 sensitivity analysis – quantitative.

	HTO			Na-22			Cl-36			Sr-85			Ba-133		
	Position	Width	Value	Position	Width	Value	Position	Width	Value	Position	Width	Value	Position	Width	Value
Disperzivity max	−1.7E−01	1.8E−01	−1.9E−01	−2.4E−01	−2.5E−02	−2.1E−02	−1.7E−01	1.8E−01	−2.6E−01	−2.4E−01	1.5E−02	−4.2E−02	−2.6E−01	4.6E−02	−1.5E−02
Disperzivity min	−2.5E−01	2.9E−01	−4.7E−01	−3.2E−01	1.2E−01	−1.5E−01	−2.2E−01	3.3E−01	−6.4E−01	−2.8E−01	1.5E−01	−1.7E−01	−3.7E−01	2.2E−01	−2.1E−01
Porosity VGN max	5.0E−03	5.2E−03	−1.1E−02	0.0E+00	−2.2E−03	2.3E−03	0.0E+00	0.0E+00	−2.9E−04	−3.9E−03	−2.7E−03	2.2E−03	−6.4E−03	−6.7E−03	5.8E−03
Porosity VGN min	0.0E+00	0.0E+00	−3.0E−02	0.0E+00	0.0E+00	1.2E−03	0.0E+00	0.0E+00	−5.3E−04	0.0E+00	0.0E+00	−5.2E−04	−6.6E−03	−4.6E−03	4.3E−03
Porosity PGR max	0.0E+00	0.0E+00	−2.2E−03	0.0E+00	0.0E+00	1.2E−04	0.0E+00	0.0E+00	−3.1E−03	0.0E+00	0.0E+00	1.4E−04	0.0E+00	−3.7E−03	4.6E−04
Porosity PGR min	0.0E+00	0.0E+00	−3.0E−03	0.0E+00	0.0E+00	7.8E−05	0.0E+00	0.0E+00	−3.5E−03	0.0E+00	0.0E+00	1.4E−04	0.0E+00	0.0E+00	5.1E−04
Diffusion VGN max	2.5E−02	0.0E+00	−2.6E−02	1.4E−01	5.4E−01	−4.3E−01	0.0E+00	0.0E+00	−6.7E−04	8.5E−02	3.2E−01	−3.4E−01	−1.1E−01	−6.8E−02	−6.9E−01
Diffusion VGN min	0.0E+00	0.0E+00	−3.2E−02	1.4E−01	4.6E−01	−5.2E−01	0.0E+00	0.0E+00	−8.6E−04	1.7E−01	2.9E−01	−4.4E−01	−1.2E−01	−1.2E−01	−8.3E−01
Diffusion PGR max	0.0E+00	0.0E+00	−3.8E−03	4.7E−02	2.9E−02	−2.9E−02	0.0E+00	0.0E+00	−5.2E−03	0.0E+00	2.9E−02	−3.0E−02	−9.3E−03	−9.8E−03	−6.2E−02
Diffusion PGR min	0.0E+00	0.0E+00	−4.0E−03	0.0E+00	5.7E−02	−3.3E−02	0.0E+00	0.0E+00	−5.7E−03	4.2E−02	2.9E−02	−3.4E−02	−9.3E−03	−2.0E−02	−6.3E−02
Sorption VGN max	–	–	–	2.1E−01	3.8E−01	−4.9E−01	–	–	–	1.1E−01	3.4E−01	−4.3E−01	7.9E−01	7.8E−01	−6.3E−01
Sorption VGN min	–	–	–	2.1E−01	4.1E−01	−6.4E−01	–	–	–	1.9E−01	3.4E−01	−5.5E−01	7.9E−01	7.6E−01	−1E+00
Sorption PGR max	–	–	–	2.5E−02	1.6E−02	−3.4E−02	–	–	–	0.0E+00	2.6E−02	−4.0E−02	8.4E−02	1.0E−01	−9.6E−02
Sorption PGR min	–	–	–	0.0E+00	4.7E−02	−4.2E−02	–	–	–	3.8E−02	2.6E−02	−4.4E−02	8.4E−02	1.0E−01	−9.8E−02

D4 Discussion, conclusions and recommendations

Results of WPDE-1 and WPDE-2 simulations seem to be in good concordance with the expected behaviour. There is one exception from this statement which is the result for Ba-133 tracer. It is not apparently erroneous when we perform solely a blind prediction but since we have seen results of other models we know that our results are not entirely accurate. This is probably caused by discretisation of rock in the vicinity of the fracture. By fine tuning the discretisation we should be able to match the results of other modelling teams. This, of course, should not be and is not a part of our blind prediction.

The sensitivity analysis was performed which helped us to determine which model parameters influence its outputs the most. For non-sorbing tracers, the most influential parameter is the longitudal dispersivity coefficient. This is also true for the sorbing tracers but their results are additionally strongly influenced by coefficients of effective diffusivity and linear sorption. Based on the sensitivity analysis results the upper and lower predictions could be computed.

The next logical step is to try to calibrate the model so that its results match the measurements acquired from the experiment.

Department of Nuclear Chemistry (DNC), Czech Technical University in Prague (CTU), Czech Republic

Aleš Vetešník, Dušan Vopálka

E1 Introduction

E1.1 Background

Migration group of Department of Nuclear Chemistry (CTU-DNC) focuses, among others, on diffusion experiments aimed at determining values of effective (D_e) and apparent (D_a) diffusion coefficients of selected critical radionuclides in barrier materials of the final disposal of radioactive waste. In particular, CTU-DNC performs diffusion experiments in blocks of compacted bentonite. To evaluate experimental data we use also a tool developed in GoldSim software that models diffusion through layers of different characters, e.g. separating filters and the studied layer of compacted bentonite (Vopálka et al. 2006). This tool was created in cooperation with UJV ŘEŽ to represent more realistically diffusion experiments that cannot be described by any analytical solution of diffusion equation derived for simplified initial and boundary conditions.

Modelling group of CTU-DNC also developed in GoldSim software a model of near field for safety assessment of the Czech concept of final disposal of radioactive waste and performed with it some uncertainty and sensitive analyses (Vetešník et al. 2015).

The rationale to participate in 9A task force is thus to improve both, our skills in modelling solute transport with GoldSim software and our knowledge about radionuclides migration into heterogeneous crystalline rock matrix at depth.

E1.2 Objectives

Following Task Description we have considered task 9A as a "warm-up" case allowed us to familiarize with the experimental setup of the WPDE campaign and to check our capabilities to model basic processes for solute transport using GoldSim software. The main objective for us was to validate our model results within the Czech modelling group also with the aim to formulate common simplified assumptions and set values of model parameters.

E1.3 Scope and limitations

Our scope does not deviate from the general scope of Task 9A. Our modelling tool, however, imposes on us several limitations although GoldSim development environment is very useful and advanced tool for modelling solute transport. One of these limitations is a geometric restriction on the mesh of elementary volumes. GoldSim software provides a tool for automatic generation of mesh with only two 2D geometries, namely cylindrical and cubic. There is also limitation of the number of elementary volumes (ten thousand). GoldSim does not have capabilities of advanced finite element programing.

E2 Methodology and model

E2.1 Conceptual description of features, events and processes of the experiments

For the sake of simplification, we did not consider speciation of tracers within injected cocktail. We treated each tracer as one entity without considering its possible forms. Tracers migrate by advection and dispersion in inlet and outlet PEEK tubing as well as through annular slot around rock matrix. These transport processes shall determine a first part of detected breakthrough curves. While passing around rock matrix tracers migrate into it by diffusion, we excluded possibility of advection. Cations of tracers become immobilized due to the sorption on to rock matrix. Diffusion and sorption retard migration and affect the shape of detected breakthrough curves.

E2.2 Description of features, events and processes in our conceptual model

Our conceptual model is depicted in Figure E-1. Due to necessary simplifications of model approach we simplified both advection and dispersion processes (red arrows in Figure E-1) assuming that they are relevant only in one direction. This simplification is highly likely plausible for transport through PEEK tubing, but it can be erroneous for migration through the annular slot. The rock matrix was modelled as a network of finite volumes. We assumed that a rock matrix is composed from three homogenous parts connected in a series along axis of annular slot (a light and dark brown regions in Figure E-1). This simplification was introduced in order to make our results comparable within the Czech modelling group although it is highly likely that transport properties of a rock matrix along annular slot will be heterogeneous. We therefore designed our model so as to account for heterogeneities of rock matrix in our future simulations. Following Task Description we assumed the Fickian character of diffusion transport. We represented rock matrix using cylindrical geometry which allowed within Goldsim simulation framework to model diffusion in a radial (R coordinate) and a height (Z coordinate along axis of cylinder) directions. This simplification neglects rock heterogeneities on the plane perpendicular to the axis of the cylinder. We did not consider surface sorption. This simplification can lead to overestimation of distribution coefficient when fitting model to experimental data.

E2.3 Model Setup within GoldSim simulation framework

The GoldSim simulation framework offers an extension module, called the Contaminant Transport Module, which allows to model mass transport by using a number of specialized GoldSim elements. A Cell pathway and a Pipe pathway are the most important for our modelling task (GoldSim 2014). The element Cell pathway enables to model migration by means of a finite-volume method. Modelled region is divided into elemental volumes, each represented by one Cell pathway. A region is thus covered by a net of Cell pathways which can be mutually connected by transport links. The program element Pipe pathway provides a computationally efficient and accurate way to a representation of a fluid conduit (GoldSim 2014). The basic mathematical details of the Cell pathway are now presented, a more detailed description of the Pipe pathway can be found in the report prepared by ÚJV Řež.
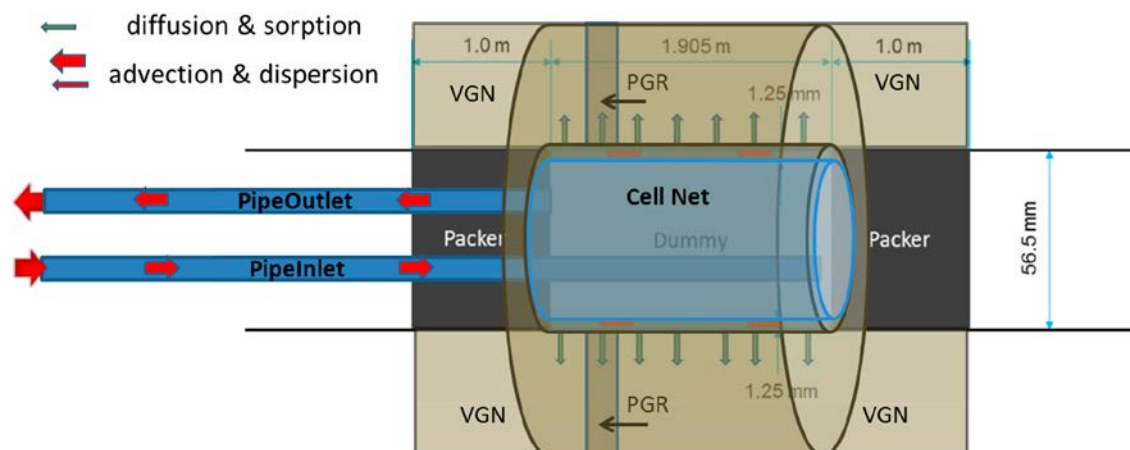

Figure E-1. *The graphical representation of the conceptual model. Inlet (**PipeInlet**) and outlet (**PipeOutlet**) PEEK tubing were modelled by two Pipe pathways. An annular slot and rock matrix were modelled by Cell pathway network (**Cell Net**) of a cylindrical geometry. **Cell Net** was composed of four zones of homogenous material; two zones represent **VGN** and one **PGR** rock matrices and a fourth zone represents an annular slot with flowing fluid. Advective mass flux links were implemented in **PipeInlet**, **PipeOutlet** and in a flowing fluid zone of **Cell Net**. Diffusive mass flux links were implemented in **VGN** and **PGR** zones of **Cell Net**.*

The basic mass balance equation of *i-th* Cell has a form (GoldSim 2014):

$$\frac{dm_k^i}{dt} = -m_k^i \lambda_k + m_p^i \lambda_p \frac{A_k}{A_p} + \sum_{c=1}^{NF^i} f_k^c,$$

where the first and the second terms on the right-hand side accounts for radioactive decay and the third term represents a mass transfer in or out of the Cell via mass flux links f_k^c [M/T]. Lower indexes k and p denote a daughter and parent radionuclides, respectively, m_k^i [M] is a mass of k-th radionuclide in Cell i, t [T] is a time, $\lambda_{k,p}$ [T^{-1}] are decay constants, $A_{k,p}$ [M/mol] are atomic weights, and NF^i is a number of mass flux links from to Cell i.

The advective mass flux link is defined as:

$$f_{i \to j}^A = q_{i \to j} c_k^i, \qquad c_k^i = \frac{m_k^i}{K_{d,k}^i M^i + V^i},$$

where $K_{d,k}^i$ [L^3/M] denotes a partition coefficient of k-th radionuclide between fluid and rock matrix of Cell i, M^i [M] is a mass of rock matrix in a Cell i, and V^i [L^3] is a volume of a fluid in a rock matrix of Cell i.

GoldSim solves a separate set of coupled differential equations for each decay family in a Cell pathway network. A set of equations can be written in the matrix form as:

m´ = [D + T]m

where **m** and **m´** are vectors, and **D** and **T** are matrices. **m** [M] denotes masses of each radionuclide in the decay family in a Cell pathway network, **m´** [M/T] denotes rates of increase of masses of each radionuclide in the decay family, **D** [1/T] is a matrix containing the decay constants $\lambda_{k,p}$, **T** [1/T] a matrix of the mass transfer coefficients.

GoldSim uses the backward Euler method (Press et al. 2007) to solve above mentioned set of differential equations. **m** is then in each time step calculated as

m($t + \Delta t$) = [**I**–**D**Δt – **T**Δt]$^{-1}$**m**(t)

where **I** is the identity matrix and $^{-1}$ denotes matrix inversion.

E2.4 Input data

We shared within the Czech modelling group common values of most of model input parameters. Common parameter values can be found in the report prepared by TUL. In particular, the porosities, $\in^i$, are introduced there in Table D-3, effective diffusivities, D_e^i, in Table D-4, partition coefficients, $K_{d,k}^i$, in Table D-5. These values were used in calculations of central prediction cases.

Similarly to TUL, and in accordance with Task Description, we used for delineation of rock matrix zones following intervals: VGN1 (0–0.35 m), PGR (0.35–0.5 m), and VGN2 (0.5–1.905 m). An aperture of the annular slot was set to 1.25 mm, the radius of the dummy was set to 28.25 mm. A thickness of rock matrix was variable depending on $K_{d,k}^i$ of tracers. But in all cases thickness was set so as to assure the boundary condition of an infinite rock matrix.

Parameters of pipe pathways representing inlet and outlet PEEK tubing are introduced in Table E-1. An injection of tracers to inlet PEEK tubing was modelled via values of an input mass rate [M/T] of PipeInlet pipe pathway. If the simulation time was from the time interval (0; 48.7) [min] for WPDE1, or (0; 300)[min] for WPDE2, an input rate was set to a proper constant. Input rate was set to zero for times of other simulations.

Table E-1. Parameters of inlet and outlet PEEK tubing.

	PipeInlet	PipeOutlet
Length [m]	24.2	25.7
Area [m²]	7.854E−7	7.854E−7
Dispersivity [m]	2.42	2.57
Flow rate [μl/min]	20/10	20/10

One directional dispersion in annular slot was implemented by increasing D_f of Cell pathways representing annular slot using equation: $D_L = D_f + \alpha_L v_L$, where α_L [L] is the dispersivity and v_L [L/T] is the fluid flow velocity along annular slot.

It turned out during validations of Cell Net geometry that it is necessary to adjust it with the aim to avoid numerical errors. This could happen especially for highly sorbing tracers. We validated model results assuming only one rock matrix zone (VGN). This simplification makes possible to compare obtained model results of Cell Net and one pipe pathway. Because GoldSim imposes a limit (99×99) on number of Cell pathway within Cell Net it was necessary to determine two grids, one, for highly sorbing Ba-133 and the other for remain tracers.

E3 Results and discussion

We calculated central predictions for WPDE-1 and WPDE-2 experiments as well as upper and lower predictions for a set of selected uncertain parameters. The results of our computations are presented in the following two sub-sections.

E3.1 The central prediction

If we neglect a dispersion in the inlet and outlet PEEK tubing, the advection in tubing causes the delay τ_{TU} which is given by a ratio of tubing length, L_{TU}, and a fluid velocity, v_L, i.e. $\tau_{TU} = \frac{L_{TU}}{v_L}$. If we neglect also a dispersion in the annular slot and assume only one directional diffusion within a rock matrix, the transfer function of annular slot, $N(t)$, can be written as (Barten 1996)

$$N(t) = \frac{\gamma}{2\sqrt{\pi}} \theta(t - \tau_S)[t - \tau_S]^{-\frac{3}{2}} exp\left(-\frac{\gamma^2}{4[t - \tau_S]}\right),$$

where $\theta(t)$ denotes the Heaviside step function, τ_s is an advection delay in annular slot. A parameter γ is proportional to rock matrix properties as

$$\gamma \approx \in [D_e R]^{1/2}$$

where R a is retardation coefficient $R = 1 + \rho_d K_d / \in$, ρ_d is a rock matrix density (bulk dry density). A dispersion will smear advective steep onset $\theta(t - \tau_s)$ and steep offset $[t - \tau_S]^{-\frac{3}{2}}$. It follows, therefore, that an onset period of detected breakthrough curves will be predominantly determined by advection and dispersions, and that offset of breakthrough curves will be mainly influenced by a diffusion and a sorption into rock matrix. Calculated results confirm this conclusion. Figure E-2 depicts in a log-log scale the simulation results of WPDE-1 experiment and Figure E-3 of WPDE-2 experiment. In spirit of analysis introduced above, the breakthrough curves of Cl-36 can be considered as a reference curves for advective and dispersive transports because Cl-36 has a low D_e and zero K_d. A higher D_e of HTO slightly changes a tail part of calculated breakthrough curves, higher diffusion and non-zero sorption of Na-22 and Sr-85, both shift an onset period and substantialy influences decay part of breakthrough curves. High K_d of Ba-133 substantially influences both, the onset and the offset parts of breakthrough curve as can be seen in Figure E-3.
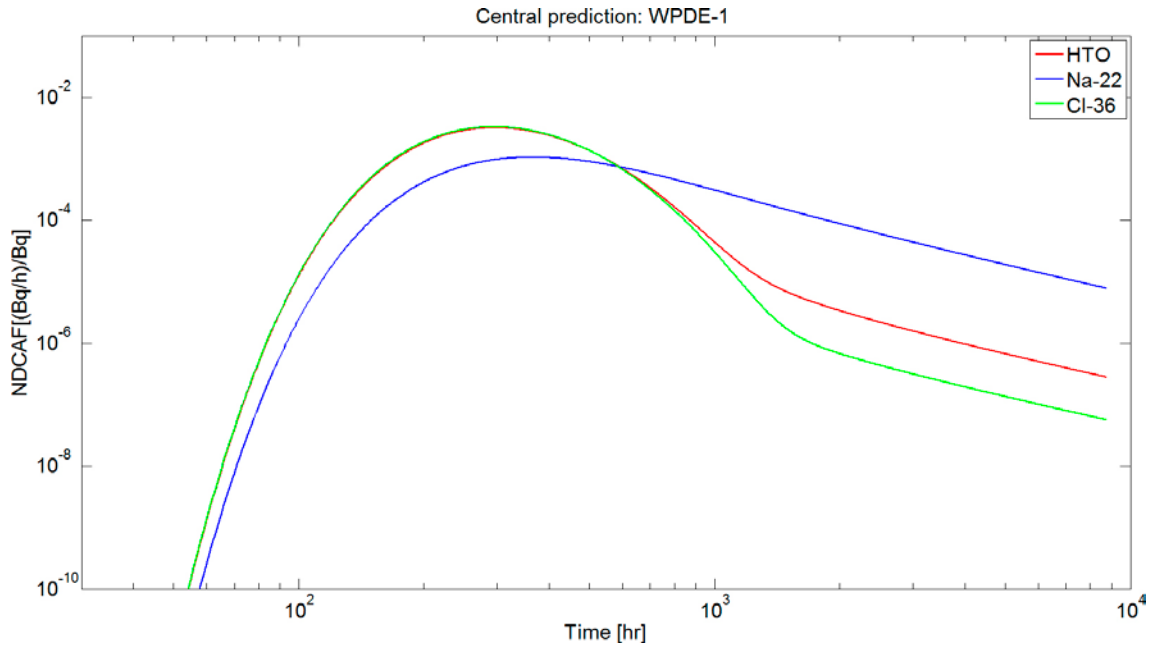
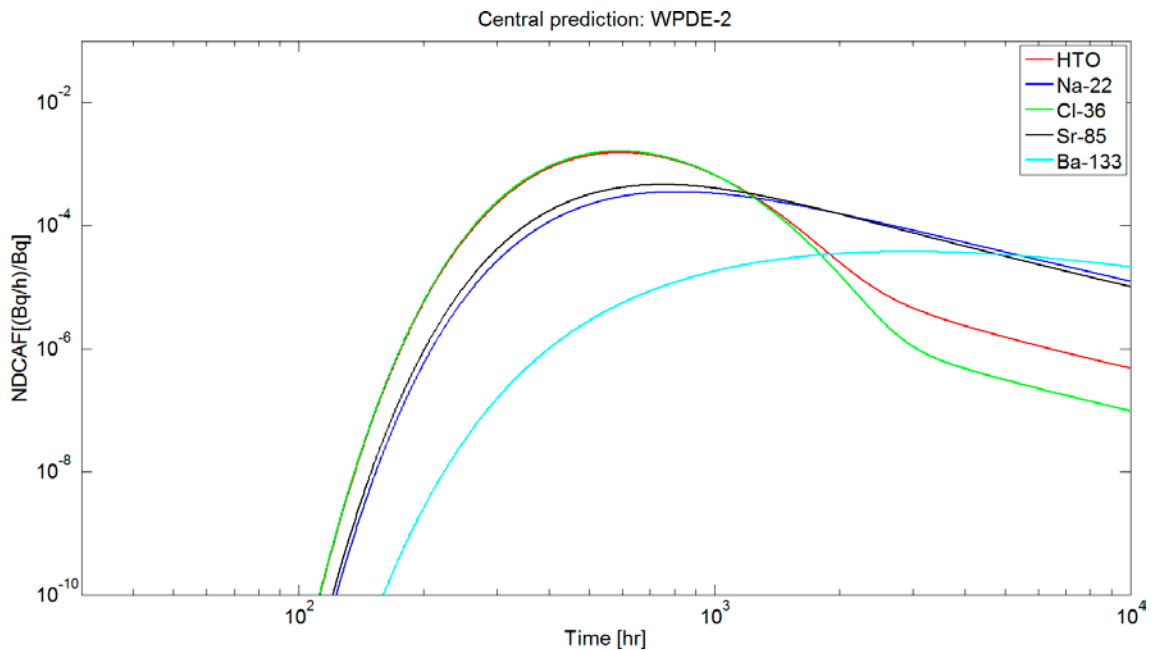***Figure E-2.*** *Central prediction of WPDE-1 experiment.*

Figure E-3. *Central prediction of WPDE-2 experiment.*

E3.2   The upper and lower predictions

We calculated the upper and lower predictions by assigning intervals of values to some of important transport parameters. The list of parameters with their min-max values can be found in Table 4-8 of the report prepared by TUL. We performed with these values the interval analysis, i.e. we calculated breakthrough curves for all combination of min-max values and then we determined the upper prediction as a maximum of all calculated breakthrough curves at given time point, and the lower predictions as minima of all calculated breakthrough curves. The upper and lower predictions can thus be not identified with an individual breakthrough curve.

Figure E-4 shows the upper and lower predictions calculated for WPDE-1 experiment and Figure E-5 shows the upper and lower predictions calculated for WPDE-2 experiment. In both cases the calculated breakthrough curves was most sensitive to changes of the dispersivity in annular slot, α_s, within assumed range. The breakthrough curves of Na-22, Sr-85, and Ba-133 were sensitive also to a rock matrix transport properties (ε, D_e, K_d) of VGN. The sensitivity to parameters was quantified by TUL using their procedure.

E4 Discussion and conclusions

We implemented within Goldsim simulation framework a model of WPDE-1,2 experiments using the network of Cell pathways of the Contaminant Transport Module. It turned out that it is necessary to adjust Cell Net geometry to avoid numerical errors. Finally, we found a proper Cell Net geometry within GoldSim limitation of 99×99 number of Cell pathways.

Model composed of the network of Cell pathways was designed to simulate heterogeneities of rock matrix properties. Nevertheless, a pipe pathway provides a computationally efficient and accurate way to calculate breakthrough curves in the approximation of homogenous rock matrix.

We will adopt model according to experimental data. The values of some of parameters will be optimized using GoldSim's optimization feature which fit automatically a model to experimental data.
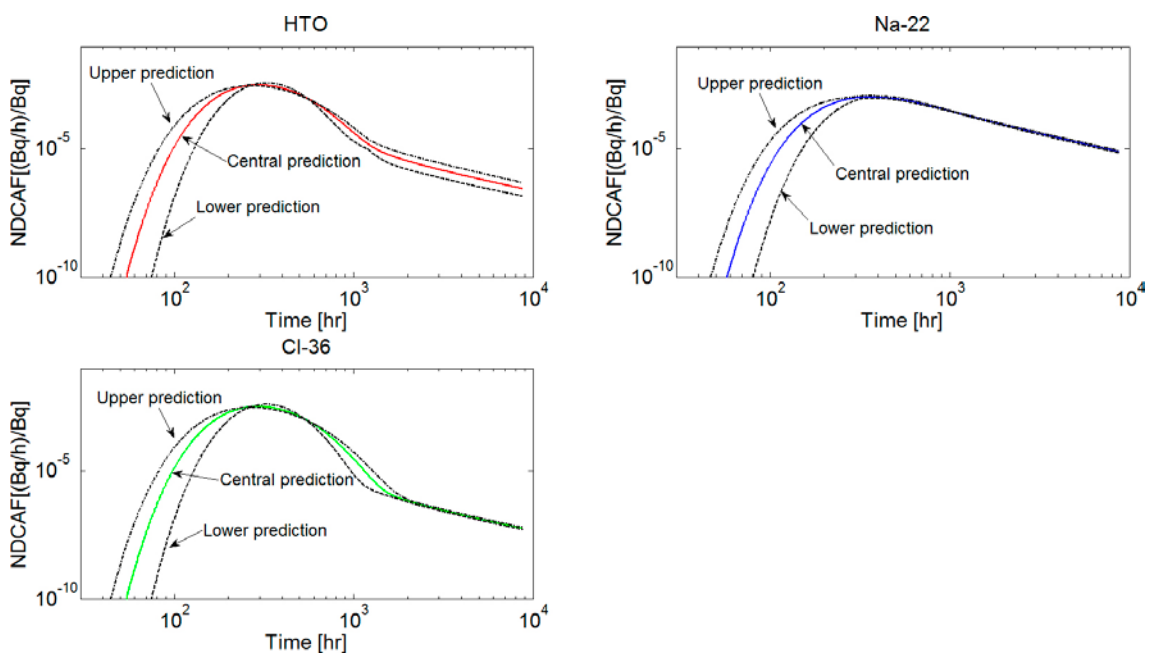
Figure E-4. *Upper and lower predictions of WPDE-1 experiment.*
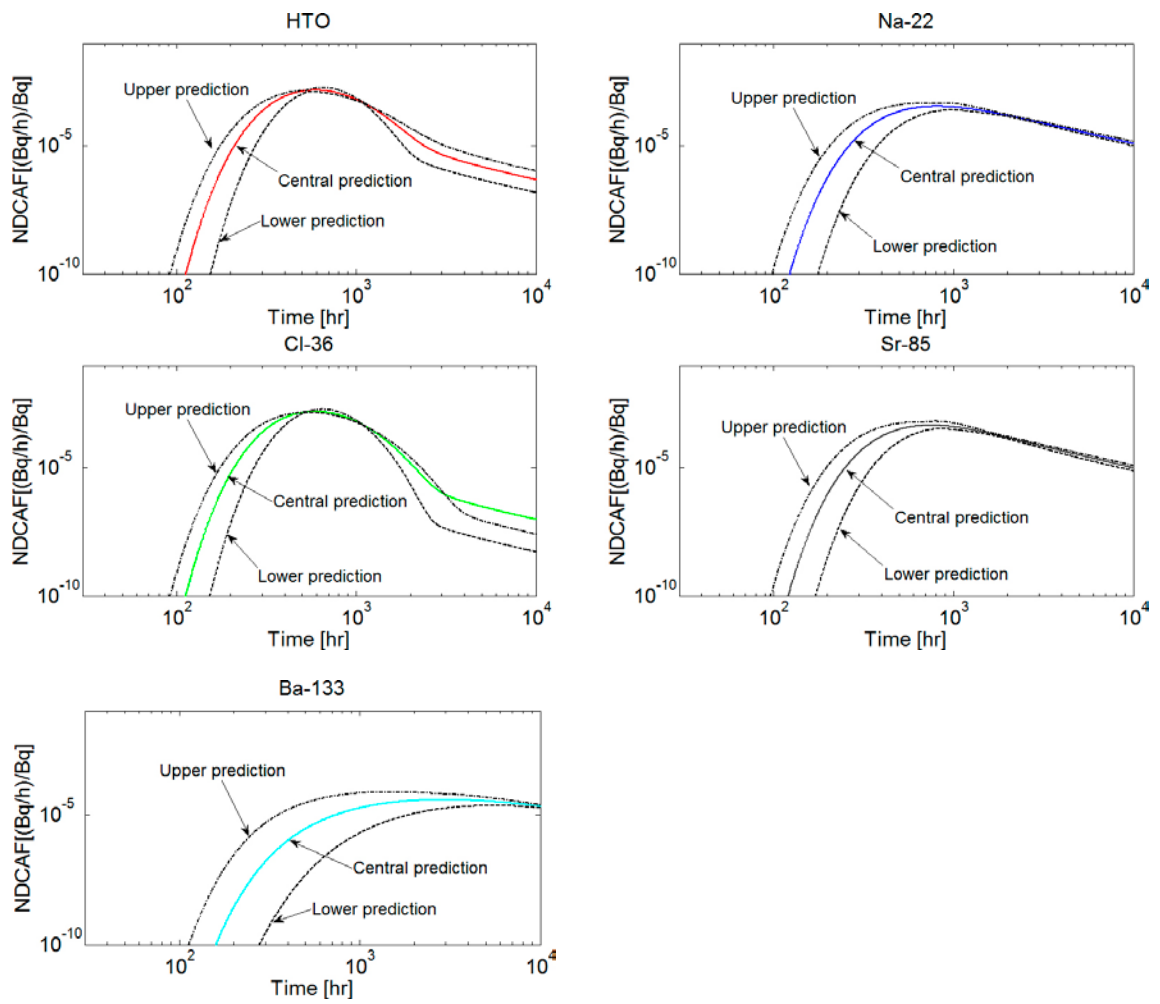
Figure E-5. *Upper and lower predictions of WPDE-2 experiment.*

PROGEO, Ltd. Czech Republic

Libor Gvoždík, Michal Polák

F1 Introduction

This document focuses on predictive modelling of the WPDE-1 in situ experiment in MT3DMS transport model.

F1.1 Background

PROGEO deals with regional and local scale groundwater flow and transport modelling in sedimentary and fractured rock hydrogeology. We are also involved in several research projects focused on modelling of advection-diffusion transport of radionuclides in low permeable rock matrix. As a member of the Czech modelling group, we are supposed to participate primarily in microscale modelling in multiple softwares based on discrete fracture network (DFN) and/or continuum porous medium (CPM) approach – NAPSAC (DFN), FEFLOW (DFN+CPM) and/or MODFLOW/MT3DMS (CPM).

F1.2 Objectives

Main objective of our participation in predictive Task9a task is to verify capabilities of MT3DMS transport model to simulate a problem (with combined transport in fracture and matrix) that is completely different from the usual usage of the model in contaminated groundwater systems.

F1.3 Scope and limitations

PROGEO have modelled only the WPDE-1 experiment and only tracers HTO, Cl-36 and Na-22. Primarily we have simulated central prediction with the same input data used within Czech modelling group. For HTO and Na-22 we have modelled also some sensitivity cases for dispersivity. And moreover we made special case with zero dispersion in the artificial fracture with variable gap.

F2 Methodology and model

F2.1 Description of features, events and processes in our conceptual model

Only the experimental section with the artificial fracture, where the tracer solution is in contact with the rock matrix is simulated in MT3DMS. The delay of 32 hours (calculated travel time in the inflow and outflow PEEK tubes in the WPDE-1 experiment) is included in the output results. Advection is supposed to be dominant process in the artificial fracture. The velocity field in the fracture could be influenced by the non-uniform width of the gap between the drillhole wall and the dummy. So the flow channelling and/or dispersion can affect the experimental and modelling results. Processes of diffusion and sorption are supposed to be dominant in the rock matrix. Fickian diffusion and local equilibrium assumption (LEA) with linear sorption isotherm is invoked.

F2.2 Model setup

The WPDE-1 experiment is simulated as 2D axisymmetric problem on rectangular grid. In the x-direction, parallel to the borehole axis, 190 columns with regular cell length of 10 mm is used. In the y-direction, perpendicular to the borehole axis, the first uppermost row of cells with the width of 1.25 mm represents the artificial fracture. Next 42 rows with the total width of 200 mm represent the rock matrix. For more precious solution non-regular cell width is used, width varies from 1 mm (close to the fracture) to 20 mm (furthermost cells). Rock matrix is divided into three volumes to differentiate the rock types: VGN1, PGR and VGN2 (VGN1 and VGN2 could be referred as VGN type with the same model parameters). To preserve the rock mass volume, the thickness (z dimension) of each cell is equal to the circumference at the radial distance from the borehole axis to the cell center. The discretisation of the 2D model geometry is shown in Figure F-1.

Figure F-1. *The 2D model geometry and discretisation.*

Flow boundary conditions are in accordance with conditions prescribed in Flow123d model (Table 4.1 in contribution by Říha and Hokr). A Dirichlet boundary condition (zero constant hydraulic head) is prescribed on the outflow fracture end, a Neumann boundary condition on the inflow end (constant flux) and a homogeneous Neumann condition (no flow) on the rest of the boundary. A Neumann transport boundary condition is prescribed on the inflow end of the artificial fracture. This condition is active only during the tracer injection (for 50 minutes in WPDE-1)

The simulation runs in two steps. First, steady state flow in MODFLOW2000 (Harbaugh et al. 2000) is simulated and the velocity field (fluxes between cells) is calculated. Second, MT3DMS (Zheng 2010) is used for simulation of transient transport with constant time step of 100 s.

F2.3 Input data

Input values of all hydraulic and transport parameters – hydraulic conductivities of fracture and rock matrix, dispersivity, diffusion coefficients, effective porosities, sorption coefficients, rock density – are prescribed in accordance with Flow123d model (Table 4.3, 4.4 and 4.5 in contribution by Říha and Hokr). In MODFLOW2000 and MT3DMS all parameters have to be defined in each model cell.

F2.4 Alternative models and sensitivity cases

The list of simulated model cases in MT3DMS is summarized in Table F-1. Except the central cases for HTO, Cl-36 and Na-22 tracers, several predictions of variable dispersivity were simulated for conservative HTO and sorptive Na-22 tracer.

For sorptive tracers, the big difference between dispersion-diffusion parameters at the fracture-matrix interface can cause erroneous modelling results. In order to obtain more precious solution, it is necessary to use model with fine grid discretisation (cases with "F" suffix). For Na-22 tracer, 10 times smaller width (0.1 mm) of rock matrix cells close to the fracture have been used.

For the conservative HTO tracer an alternative model with zero dispersion, but variable fracture aperture, was calculated. The 2D model was upscaled to the 3D model, the one-layer model was divided into four layers with widths of 1.25-0.25-1.25-2.25 mm.

Table F-1. Overview of model cases with prescribed parameters.

Tracer	Model case		Dispersivity [mm]	Discretisation	Fracture aperture
HTO	Central	var0	200	Coarse	Constant
	Sensitivity	var0_DISP0	0	Coarse	Constant
	Sensitivity	var0_DISP100	100	Coarse	Constant
	Sensitivity	var0_DISP280	280	Coarse	Constant
	Alternative	varAPER_DISP0	0	Coarse	Variable
Cl-36	Central	var0	200	Coarse	Constant
Na22	Central	var0	200	Coarse	Constant
	Central	var0-F	200	Fine	Constant
	Sensitivity	var0-F_DISP100	100	Fine	Constant
	Sensitivity	var0-F_DISP280	280	Fine	Constant

F3 Results and discussion

In MT3DMS only the WPDE-1 experiment was simulated. Predictions of the breakthrough curve for the central case, sensitivity cases and the alternative model are presented.

F3.1 The central prediction

The central prediction of the WPDE-1 experiment is shown in Figure F-2. In Figure F-3, the results of the sorbing tracer Na-22 proved to be dependent on discretisation in the vicinity of the fracture.
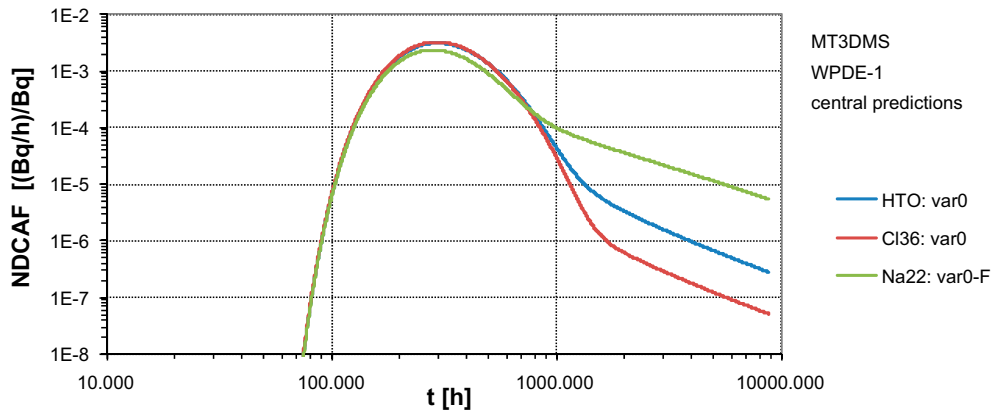
Figure F-2. Results of WPDE-1 simulations in MT3DMS – central predictions of HTO, Cl-36 and Na-22.
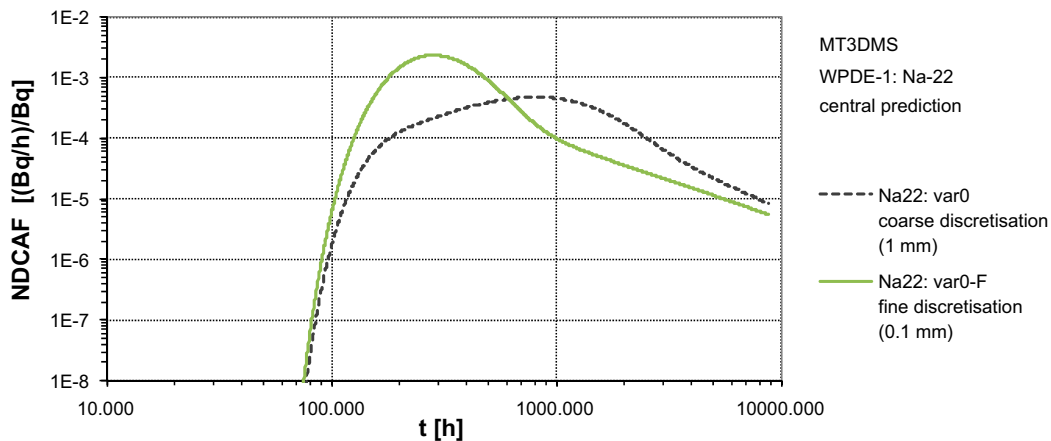
Figure F-3. Results of WPDE-1 simulations in MT3DMS – central predictions of Na-22 with coarse and fine discretisation.

F3.2 Other alternative models, sensitivity cases and results

Sensitivity cases with upper and lower dispersivity were simulated for HTO and Na-22. Predicted breakthrough curves are shown in Figures F-4 and F-5. HTO breakthrough curve for the alternative 3D model with variable aperture is shown in Figure F-6, in comparison with the results for central case and zero dispersion case.
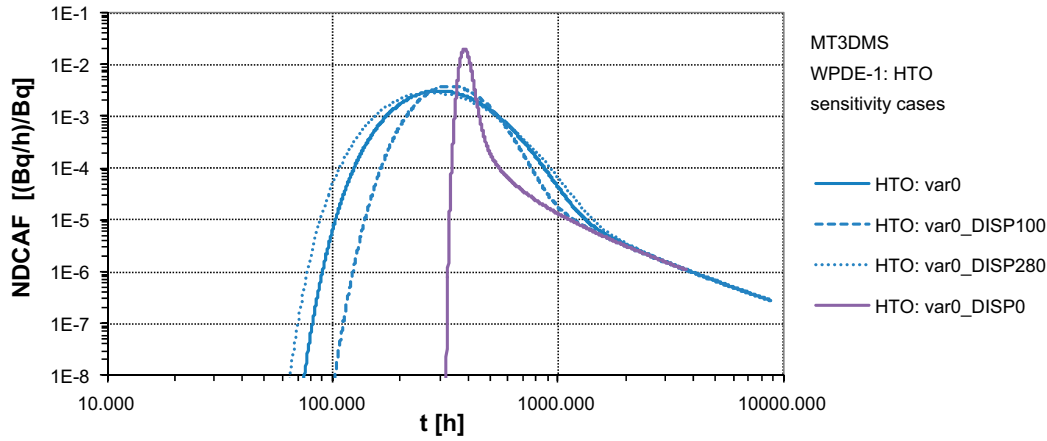

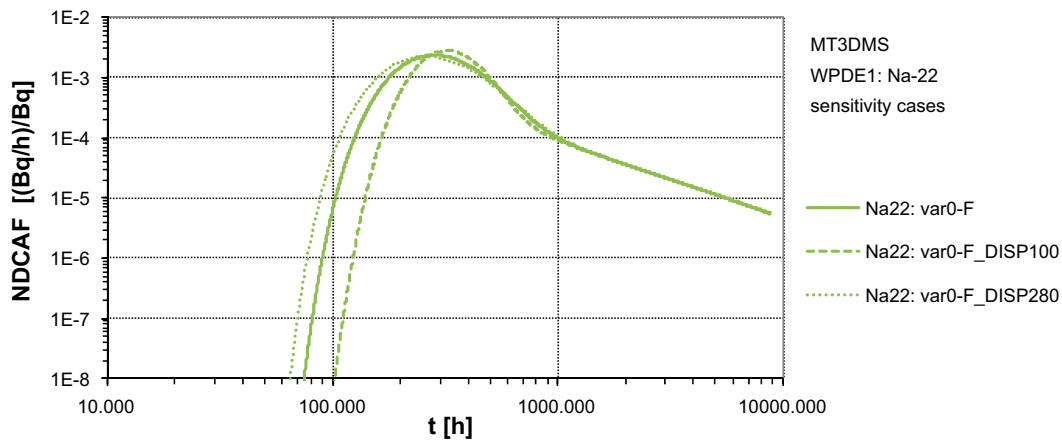***Figure F-4.*** *Results of WPDE-1 simulations in MT3DMS – sensitivity cases with lower and upper dispersivity of HTO.*

Figure F-5. *Results of WPDE-1 simulations in MT3DMS – sensitivity cases with lower and upper dispersivity of Na-22.*
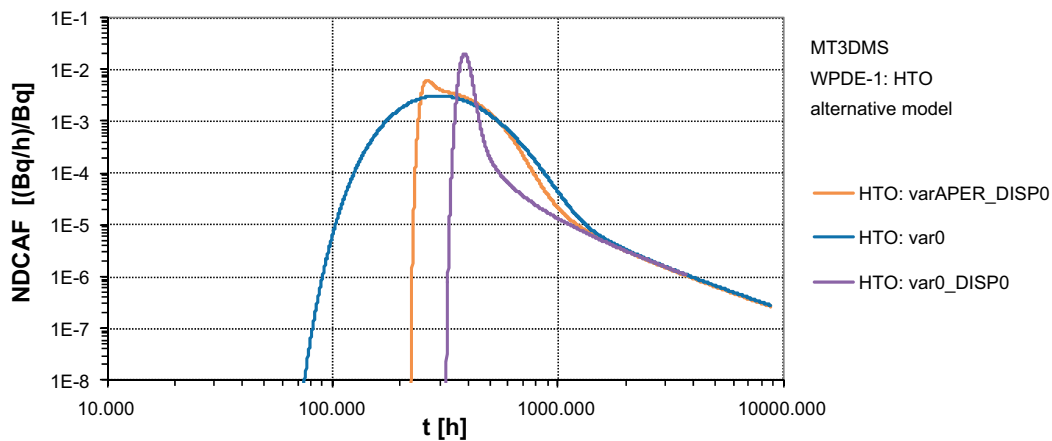
Figure F-6. *Results of WPDE-1 simulations in MT3DMS – alternative model with variable aperture of the artificial fracture.*

F4   Discussion, conclusions and recommendations

Simulated breakthrough curves consist of two stages. First the advection-dominated "parabolic" stage for time until about 1 000 hours, when the tracer is transported by the flowing fluid through the experimental section (PEEK tubes, fracture, etc.). The peak height and width depends on prescribed dispersivity parameters. The lower dispersion causes higher maximum activity and narrower shape of the curve. In the central predictions the amplitudes for all simulated tracers are very similar due to the same flow field and dispersion. The lower peak of Na-22 is related to the higher sorption into the rock matrix.

Second part of the curves show "asymptotic" stage that is caused by matrix diffusion and sorption. The location of the asymptotic lines depends on prescribed diffusion and sorption parameters. For the sorptive tracers simulated in MT3DMS, it is necessary to use finer discretisation (in the rock matrix subdomain) to obtain more precious solution.

Result of the alternative model with non-homogeneous fracture cross-section (variable aperture) shows steep increase of activity caused by the zero dispersion. But, in the latter stage, the breakthrough curve is very similar to the central case and the inhomogeneous flow field causes the dispersion-like effect.

ÚJV Řež, a.s., Czech Republic

Dagmar Trpkošová, Václava Havlová

G1 Introduction

This document deals with description of simulation process of WPDE experiments. For the simulation, we used GoldSim software which using component "Pipe".

G1.1 Background

ÚJV Řež, a.s. would like to exploit and share its experience from previous involvement in migration experiments; we would like to also develop a specific approach toward modeling of radionuclide migration experiments (using the GoldSim program).

ÚJV Řež, a.s. is focused namely on laboratory experimental support of DGR safety assessment, altogether with several in situ experiments; however, development of hydrogeology and radionuclide transport models represent inevitable part of Fuel Cycle Chemistry Dept. activities (LTD III. in Grimsel test site, HG and transport models in R&D support of DGR SA project etc.).

GoldSim (www.goldsim.com) is a Monte Carlo simulator that supports decision and risk analysis by simulating future development of the system.

G1.2 Objectives

Task 9 focuses on the realistic modelling of coupled matrix diffusion and sorption in heterogeneous crystalline rock matrix at depth.

According to ÚJV Řež, a.s. opinion the TASk should namely prove the degree of realism in simulation of combined processes of radionuclide retardation in heterogeneous granitic matrix.

Involvement of several modelling teams should enable to compare different approaches toward both rock-fracture-solution matrix and processes of radionuclide retardation and find appropriate solution for their simulation.

The main objective of Task9A simulations is to provide a blind prediction of the WPDE experiment results. The results of modelling teams are then compared one to each other not being over weighted with the results knowledge that many times pushed the modeller toward the intention to fit the model as best as possible, sometimes even against physical and natural laws.

G2 Methodology and model

The task 9A was solved using program GoldSim. The solution was gained using a *Pipe pathway* component in all of the observed parts of the system, which means for simulation of processes in rock mass and also for input of the tracer from its source to the part, which is defined by the dummy (inlet tube), and subsequent outflow of the tracer to the sample collection device (outlet tube). Only the sample collection device itself is simulated by a *Cell pathway* component, but this component does not have any influence on simulated processes.

The *Pipe pathway* component represents a "chromatographic column", where the fluid flows into the column at the upper part of the component mixed with the other substances (e.g. contaminants, radionuclides), it flows through the component and leaves the component on the end part. The concentration of the ith component, ${}^F C_k^i$ in the mobile zone, is defined by the relation

$$\frac{\partial {}^F C_k^i}{\partial t} = -\frac{Q_k^i}{{}^F S^i \, {}^F R_k^i \, {}^F \varepsilon_k^i} \frac{\partial {}^F C_k^i}{\partial x} + \frac{\alpha^i Q_k^i}{{}^F S^i \, {}^F R_k^i \, {}^F \varepsilon_k^i} \frac{\partial^2 {}^F C_k^i}{\partial x^2} - \lambda_k C_k^i + \frac{P^i \, {}^G D_{e,k} \, {}^G \delta \, {}^G \varepsilon}{{}^F S^i \, {}^F R_k^i \, {}^F \varepsilon_k^i} \frac{\partial {}^G C_k^i}{\partial z} ,$$

where the first member of the right side represents the advective member, the second the dispersive member, the third the radioactive decay and the fourth the sorption and the diffusion in the direction perpendicular to the flow direction (the flow direction is represented by the axis x, the perpendicular direction is represented by axis z). Q_k^i [L^3/T] stands for a volumetric flow rate in the mobile zone of the ith component, $^FS^i$ [L^2] stands for a flow area of the mobile zone of ith component, $^FR_k^i$ is a retardation factor of the kth radionuclide, α^i [L] is a dispersivity of the ith component, P^i [L] is a wetted perimeter of the ith component, $^GD_{e,k}$ [L^2/T] is an effective diffusion coefficient of the rock mass, $^G\delta$ is a tortuosity of the rock mass, $^G\varepsilon$ stands for a porosity of the rock mass and $^GC_k^i$ is a concentration kth radionuclide in the rock mass.

The change of the concentration $^GC_k^i$ is defined by relation

$$\frac{\partial\, ^GC_k^i}{\partial t} = \frac{^GD_{e,k}^i \; ^G\delta}{^GR_k^i}\frac{\partial^2\, ^GC_k^i}{\partial z^2} + \frac{^GD_{e,k}\; ^G\delta}{^GS^i\; ^GR_k^i}\frac{\partial\, ^GS^i}{\partial z}\frac{\partial\, ^GC_k^i}{\partial z} - \lambda_k C_k^i,$$

where the first two members represent diffusion and sorption members and the third describes the radioactive decay. $^GS^i$ [L] is a diffusion area per unit length.

$^GR_k^i$ is the retardation factor, defined by the relation

$$^GR_k^i = 1 + \frac{^G\rho\; ^GK_{d,k}}{^G\varepsilon},$$

where $^G\rho$ [M/L^3] is a dry bulk density of the considered rock and $^GK_{d,k}$ [L^3/M] is a distributive coefficient of the kth radionuclide in the rock mass. The *Pipe pathway* component uses the Laplace transform to solve the transport, where the advection dominates.

Inside the *Pipe pathway* component may occur following processes:

* 1D advective flow.
* Longitudinal dispersion.
* Longitudinal diffusion.
* Retardation.
* Radionuclide decay.
* Exchange between mobile and immobile zone (the diffusion to the rock mass).

The component is defined by following parameters:

* Length.
* Flow area.
* Wetted perimeter.
* Dispersion.
* Presence of the filling material.
* Presence of the seal layer.
* Presence of the layer, where the diffusion to the rock mass takes place.
* Flow on the entry and on the end of the component.

G2.1 Conceptual description of features, events and processes of the experiments

Advection flow was considered as the main transport process in all parts of the transport path, considering also a dispersion process. Diffusion into the rock matrix and sorption were also considered as the addition processes in sections consisting of rock matrix (Table G-1).

The process of dispersion in the inlet and outlet tubes was included after a discussion with the members of the Czech modelling team. The radionuclides are transported by advection and dispersion in the inlet tube and their transport in the specified part of the dummy has been considered by advection and dispersion and also by molecular diffusion and sorption.

Due to the dispersion the concentration of the radionuclides spreads in the flow direction. Due to the process of molecular diffusion radionuclides diffuses into the rock matrix to be retained, altogether due to the sorption process. Then those can be subsequently released back to the fluid flow field in the joint between the borehole "wall" and the dummy (Figures G-1 and G-2). The major driving power is the concentration gradient. The radionuclides flow out through the outlet tube to the tube leading to the sample collection device. Moreover, the considered processes in these tubes are the advection and dispersion. The longitudinal dispersion was considered as a 1/10 of the task scale, which means 10 %, also the thickness of the diffusion zone 1 m was prescribed.

Table G-1. The transport processes considered in the individual parts of the transport path.

Inlet_tube	VGN2	PGR1	VGN1	Outlet tube to detector	Tube to sample collection	Sample collection
Advection	Advection	Advection	Advection	Advection	Advection	Mixing of concentration
Dispersion	Dispersion	Dispersion	Dispersion	Dispersion	Dispersion	
	Matrix diffusion	Matrix diffusion	Matrix diffusion			
	Sorption	Sorption	Sorption			

G2.2   GoldSim model Setup

The transport path of the tracer was divided into the several parts that differ in the considered transport processes (Figure G-2, Table G-1):

- Inlet tube.
- Rock mass consisting of the rock type VGN (divided into two parts).
- Rock mass consisting of the rock type PGR.
- Outlet tube to the detector.
- Tube to the sample collection device.

The geometry of the individual parts of the transport path is shown in Table G-2.
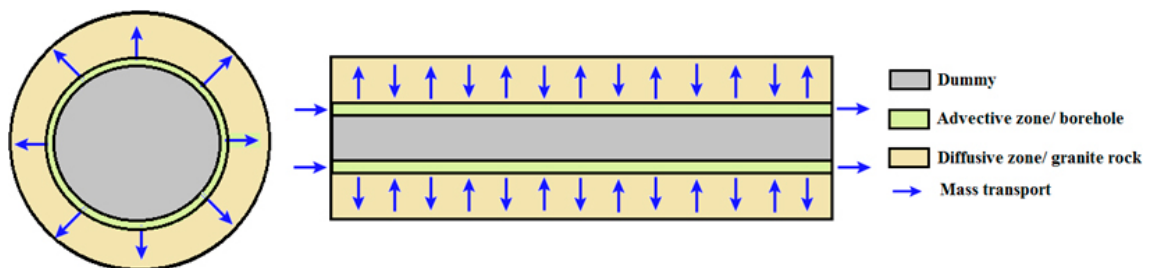

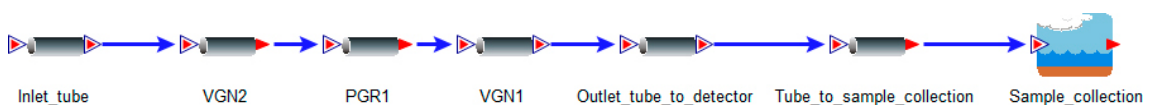*Figure G-1.* *The simplified scheme of the radionuclide transport.*

Figure G-2. *The scheme of the transport path divided into the individual intervals according to their geometry and processes that are considered in them (GoldSim code).*

Table G-2. The geometry of the individual parts of the transport path.

	Inlet tube	VGN2	PGR1	VGN1	Outlet tube to detector	Tube to sample collection
Length [m]	2.42E+01	1.41E+00	1.50E−01	3.50E−01	2.57E+01	4.60E+00
Flow area [m²]	7.85E−07	2.17E−04	2.17E−04	2.17E−04	7.85E−07	7.85E−07

As the flow rate in the inlet tube and the activity of the observed radionuclides were prescribed as the boundary conditions. The values varied due to the simulated experiment. The flow rate in the experiment WPDE_1 was 20×10^{-6} l/min and the flow rate in the experiment WPDE_2 was 10×10^{-6} l/min. The injected activity is described in Table G-3. The time step of the experiment was 2 minutes, the reporting step was 1 hour.

Table G-3. The injected activity of radionuclides in the experiments WPDE_1 and WPDE_2.

Radionuclide	Activity WPDE_1 [Bq]	Activity WPDE_2 [Bq]
H3	1.71E+07	3.11E+07
Na22	1.38E+06	2.04E+06
Cl36	1.25E+06	5.09E+06
Sr85		4.12E+06
Ba133		2.46E+06

G2.3 Input data

In the mathematical model following parameters were considered:

- K_d as a sorption parameter, was considered in the form of a linear sorption isotherm.

- D_e and D_w as the parameters of diffusion, are fundamental for the calculation of the porosity fraction, which means the porosity that truly participates in the radionuclide transport.

- The porosity as a parameter which is necessary for the calculation of the porosity fraction and the tortuosity.

- Rock bulk density.

- Radioactive half-life.

The porosity fraction is given by the relation

$$f_{m,s} = \frac{D_{f,m,s}}{n_m \cdot t_m \cdot d_f \cdot d_{f,s}} = \frac{D_{f,m,s}}{n_m \cdot t_m \cdot d_f \cdot \dfrac{D_{f,s}}{d_f}} = \frac{D_{f,m,s}}{n_m \cdot t_m \cdot D_{f,s}}$$
(Eq G-1)

where:

d_f reference diffusivity for the reference fluid f, $[L^2 \times T^{-1}]$

$D_{f,m,s}$ effective diffusivity of species s in the mobile zone (De)

$D_{f,s}$ diffusivity of species s in the reference fluid f at infinite dilution, (Dw), $[L^2 \times T^{-1}]$

$d_{f,s}$ relative diffusivity of species s in the reference fluid f at infinite dilution, [-]

$f_{m,s}$ fraction of porosity of medium m available to species s [-]

n_m porosity of porous medium m [-]

t_m tortuosity of porous medium m [-] , $t_m \in (0,1]$

A sensitivity analysis was performed also for the experiment WPDE_2, the experiment WPDE_1 was simulated only with basic (default) parameters. The values of the parameters for the basic setting are shown in the contribution by Říha and Hokr (Table 4.3, 4.4, 4.5, 4.8). The dispersivity for the rock mass area in basic setting was considered 0.19 m.

G2.4 Alternative models and sensitivity cases

Minimal and maximal parameter values are shown in the contribution by Říha and Hokr (Table 4.8). The minimal resp. maximal dispersivity in the rock mass area was considered 0.1 m resp. 0.28 m.

Only one parameter for all studied radionuclides was changed in minimum/maximum value version. Other parameters remained identical in comparison with parameters, used in the basic version. For example: during studying the effect of the sensitivity impact on the porosity parameters, the porosity parameters were changed firstly for VGN, while the parameters for PGR remained the same as in the basic version. Later on the VGN porosity values were turned back to the basic version and the PGN porosity parameters were varied. We did not consider the case were minimum/maximum values of all parameters (K_d, D_e,…) were used simultaneously.

G3 Results and discussion

The development of the radionuclide activities was observed in both experiments on the outflow from the outlet tube prior to the inflow into the tube, which leads to the sample collection device (Figure G-3). The results of the activity development of the individual radionuclides from the experiment WPDE_1 are shown in Figure G-4 to Figure G-6. The results of sensitivity impact on the porosity parameters from the experiment WPDE_2 are shown in Figure G-7 to Figure G-11. The results of the impact on the K_d values are shown in Figure G-12 to Figure G-16. The results of the impact on the D_e values are shown in Figure G-17 to Figure G-21. The results of the impact on the dispersion are shown in Figure G-22 to Figure G-26. The comparison of the activity development for all the radionuclides in the experiment WPDE_2 is shown in Figure G-27 to Figure G-29. The comparison of the development of all the monitored radionuclides in the experiment WPDE_1 is shown in Table G-4 and for the case of the experiment WPDE_2 in Table G-5.

Table G-4.The results of WPDE_1 experiment.

| Performace meassures central prediction WPDE-1			
Time when event occurs	HTO, time (h)	Na-22, time (h)	Cl-36, time (h)
Leading edge, 10 % of tracer peak concentration	139	149	139
Leading edge, 50 % of tracer peak concentration	191	212	189
Tracer peak concentration	291	360	291
Tail, 10 % of tracer peak concentration	701	1797	698
Tail, 1 % of tracer peak concentration	1013	7256	998
Tail, 0.1 % of tracer peak concentration	1398	NaN	1307
Decay corrected activity per mass unit of solution at outlet, at	HTO, activity (Bq/g)	Na-22, activity (Bq/g)	Cl-36, activity (Bq/g)
Tracer peak concentration	3.2034E−03	1.0443E−03	3.2285E−03
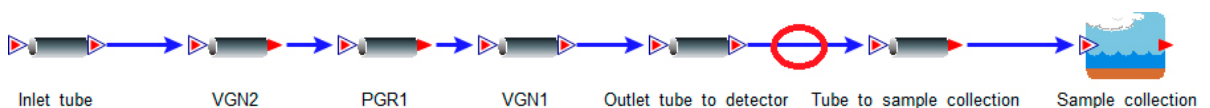
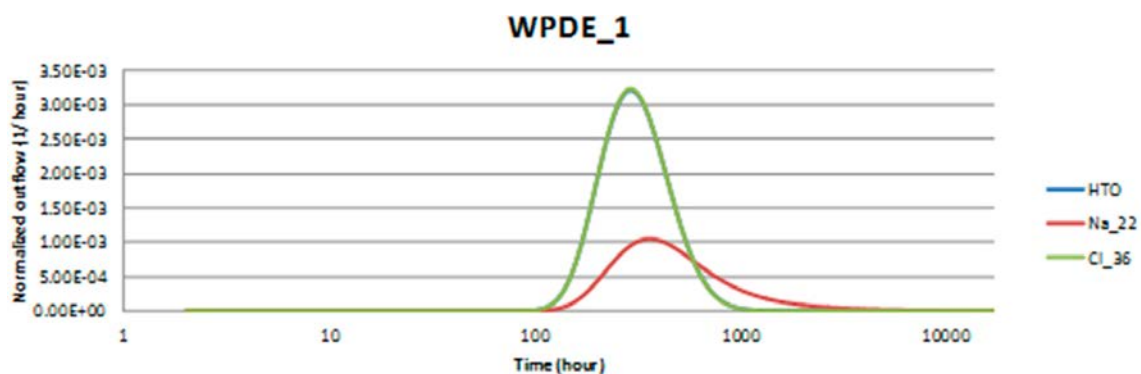*Figure G-3.* *The position of the radionuclides activity development observation point.*

Figure G-4. *The comparison of the activity development for all of the observed radionuclides in the experiment WPDE_1 (log-normal scale).*
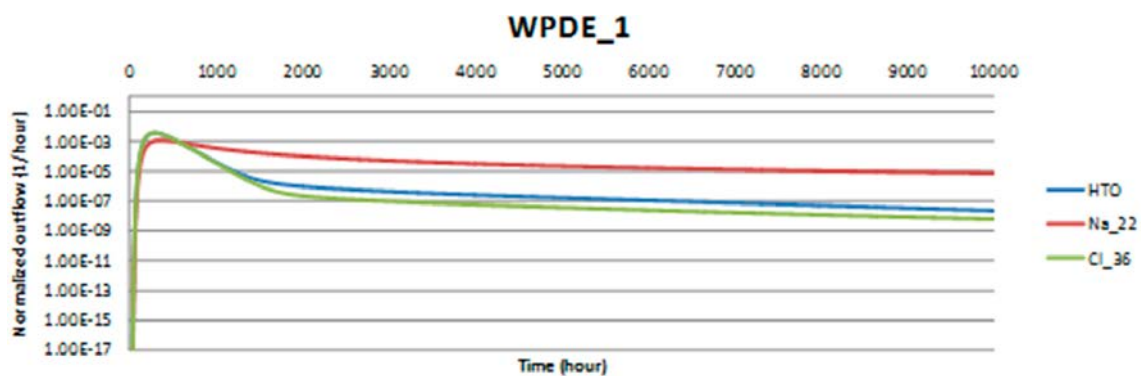

Figure G-5. *The comparison of the activity development for all of the observed radionuclides in the experiment WPDE_1 normal-log-scale).*
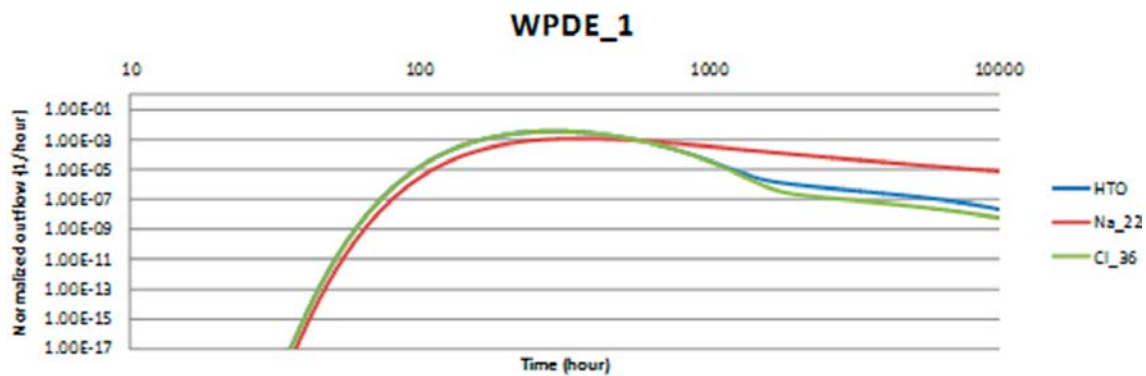

Figure G-6. *The comparison of the activity development for all of the observed radionuclides in the experiment WPDE_1 (log-log scale).*
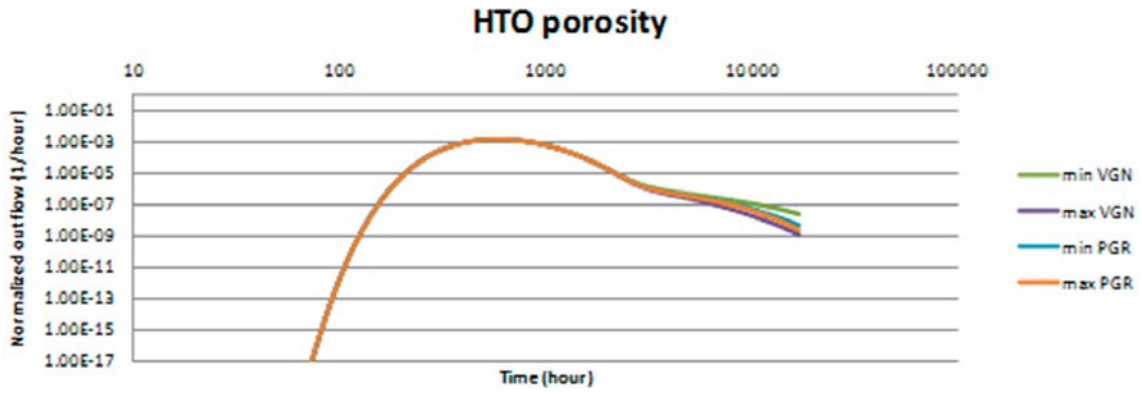
Figure G-7. *The comparison of the HTO activity development in the experiment WPDE_2 depending on the change of the porosity parameters.*
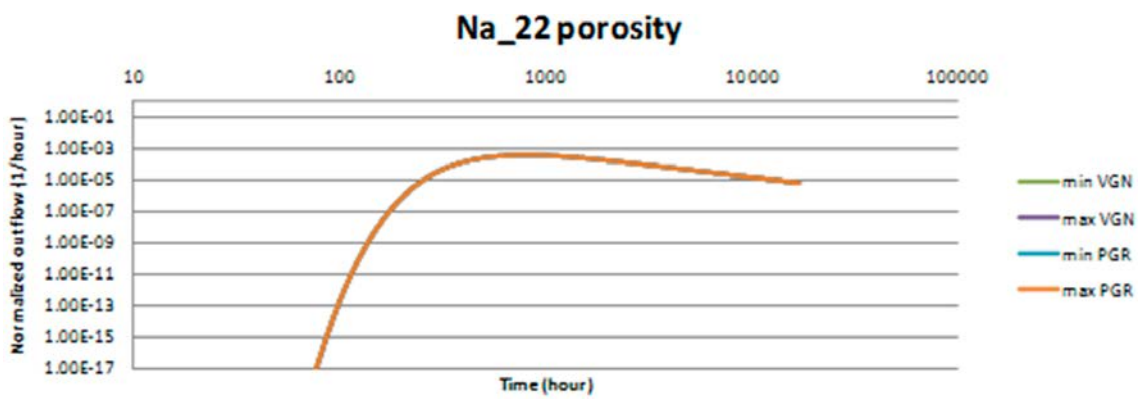
Figure G-8. *The comparison of the Na_22 activity development in the experiment WPDE_2 depending on the change of the porosity parameters.*
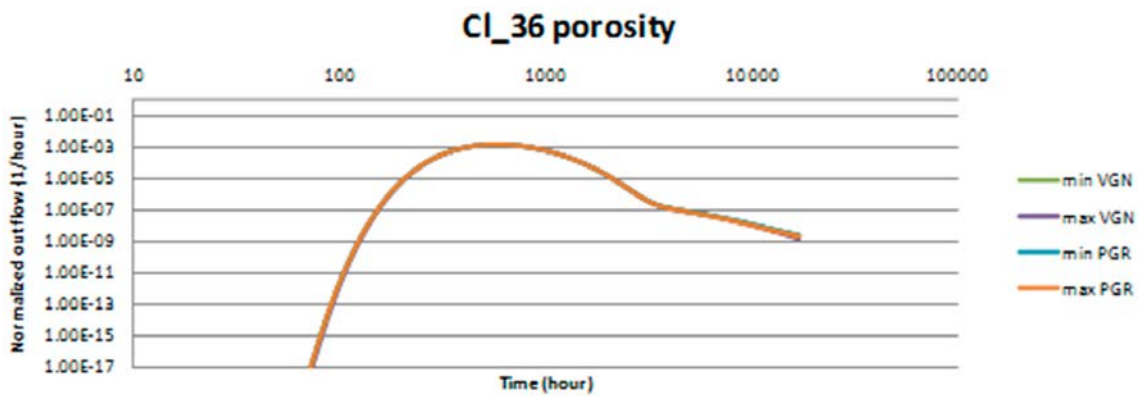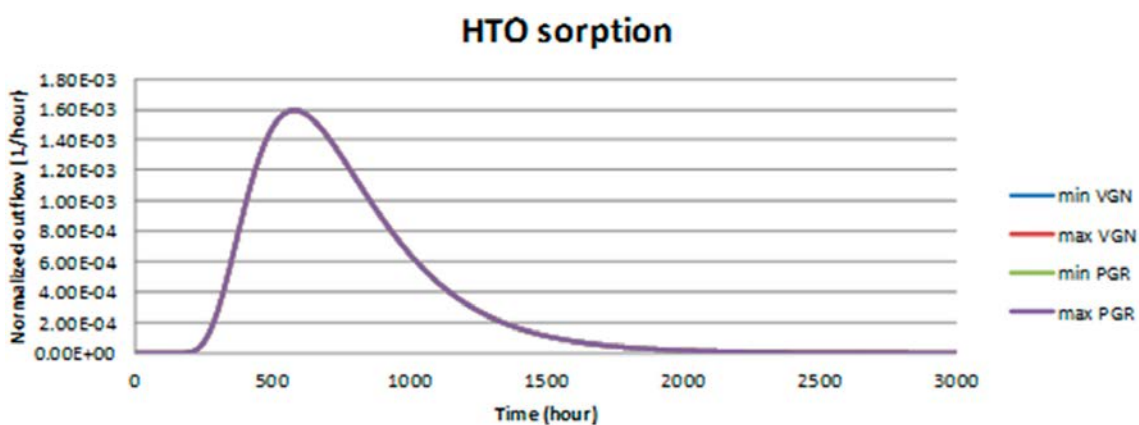

Figure G-9. *The comparison of the Cl_36 activity development in the experiment WPDE_2 depending on the change of the porosity parameters.*
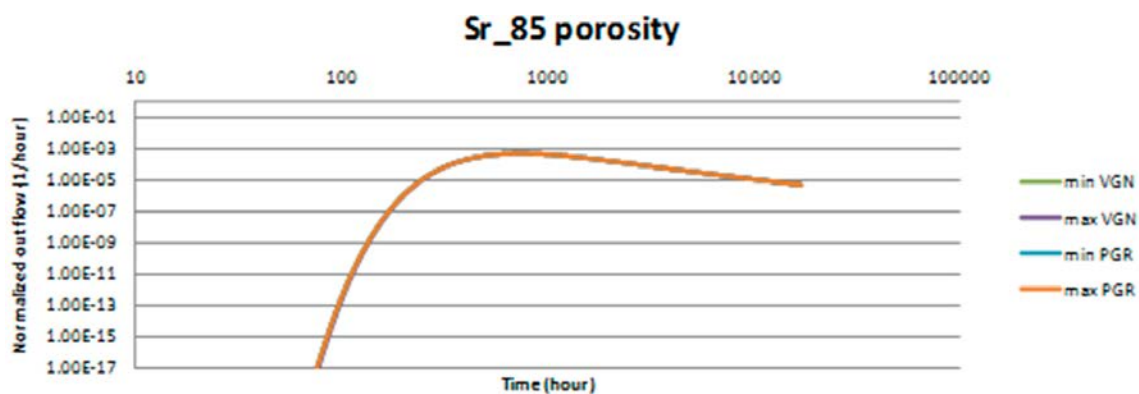
Figure G-10. *The comparison of the Sr_85 activity development in the experiment WPDE_2 – dependence on the change of the porosity parameters.*
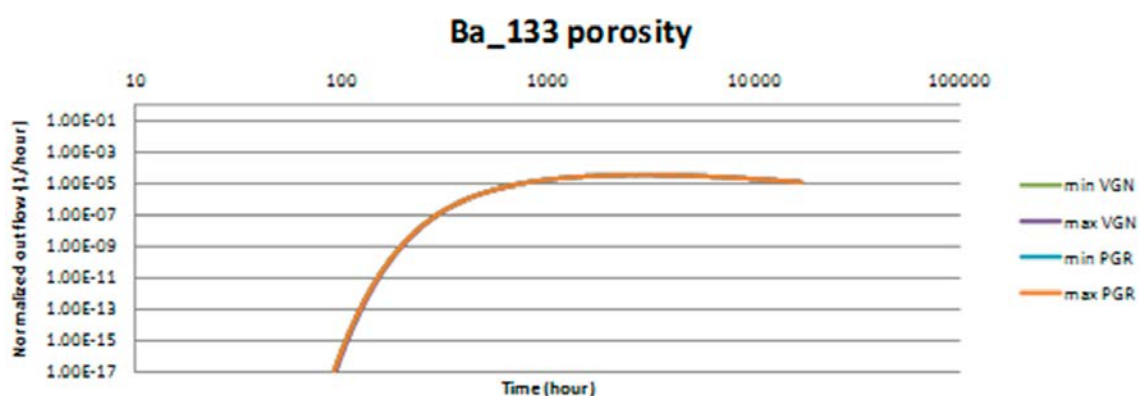
Figure G-11. *The comparison of the Ba_133 activity development in the experiment WPDE_2 – dependence on the change of the porosity parameters.*

Figure G-12. *The comparison of the HTO activity development in the experiment WPDE_2 – dependence on the change of the K_d parameters.*
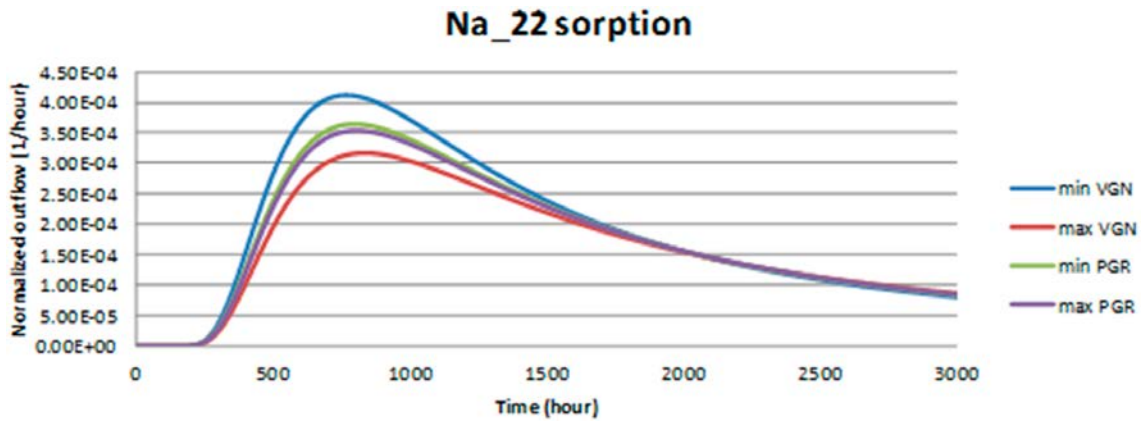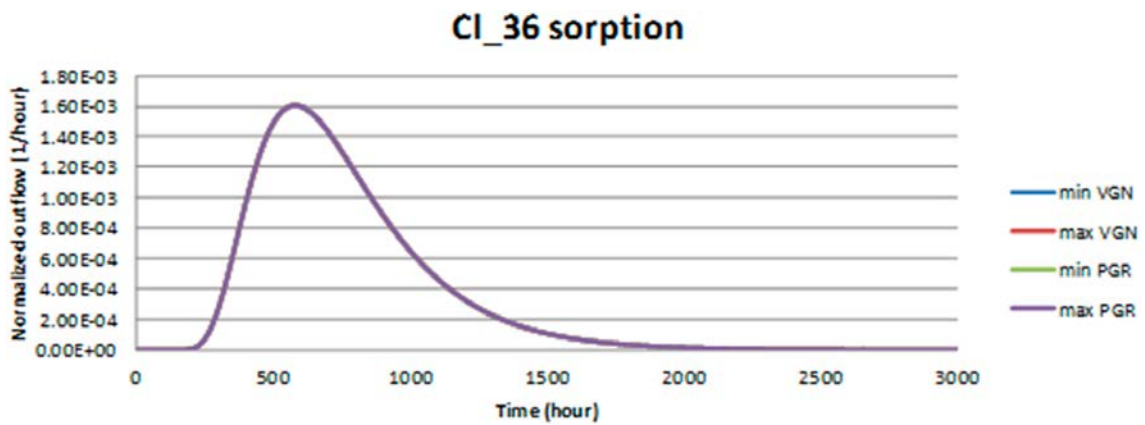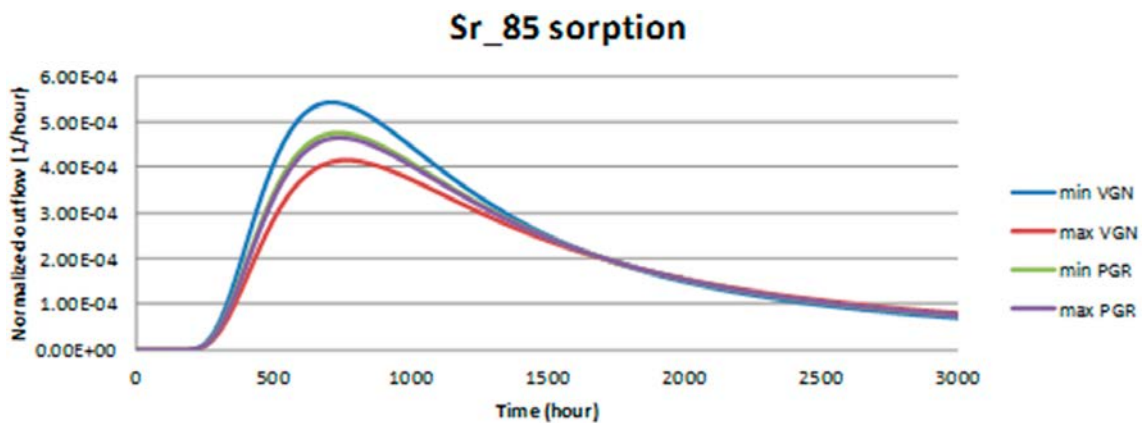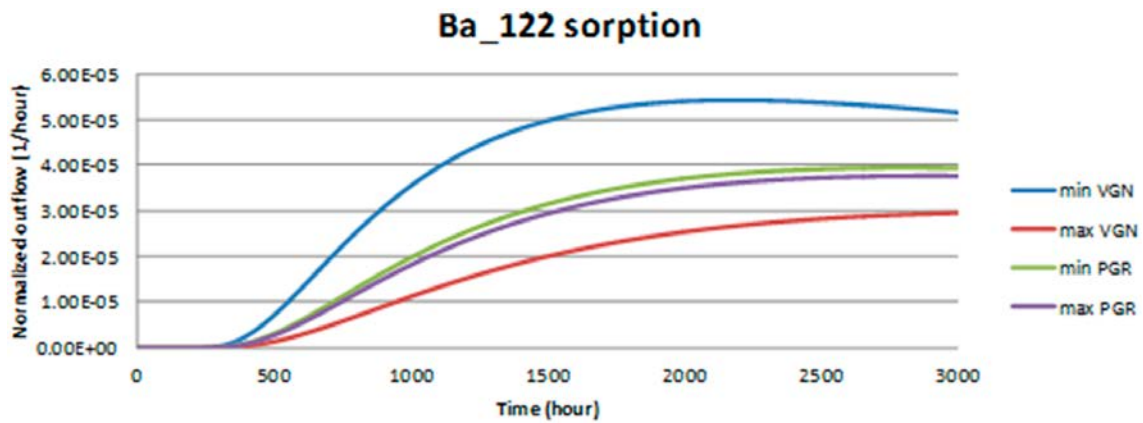
Figure G-13. *The comparison of the Na_22 activity development in the experiment WPDE_2 – dependence on the change of the Kd parameters.*

Figure G-14. *The comparison of the Cl_36 activity development in the experiment WPDE_2 – dependence on the change of the K_d parameters.*

Figure G-15. *The comparison of the Sr_85 activity development in the experiment WPDE_2 – dependence on the change of the K_d parameters.*

Figure G-16. *The comparison of the Ba_122 activity development in the experiment WPDE_2 – dependence on the change of the K_d parameters.*
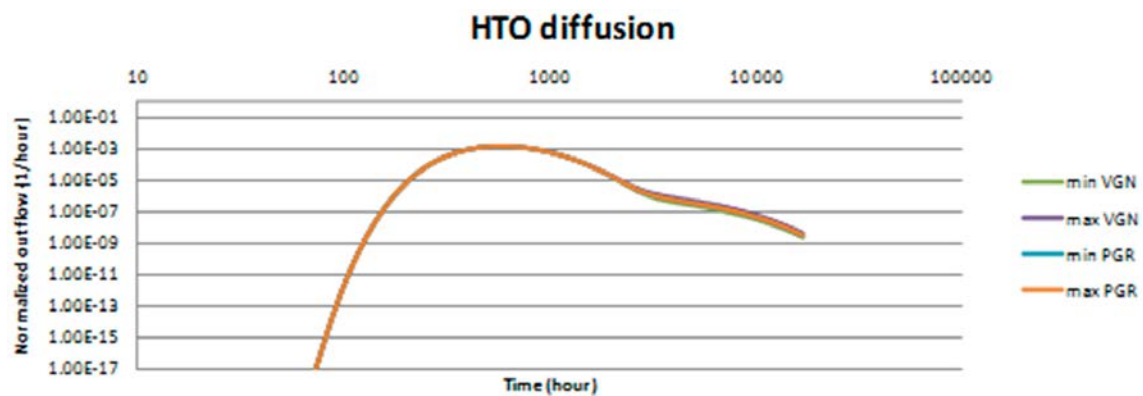

Figure G-17. *The comparison of the HTO activity development in the experiment WPDE_2 – dependence on the change of the D_e parameters.*
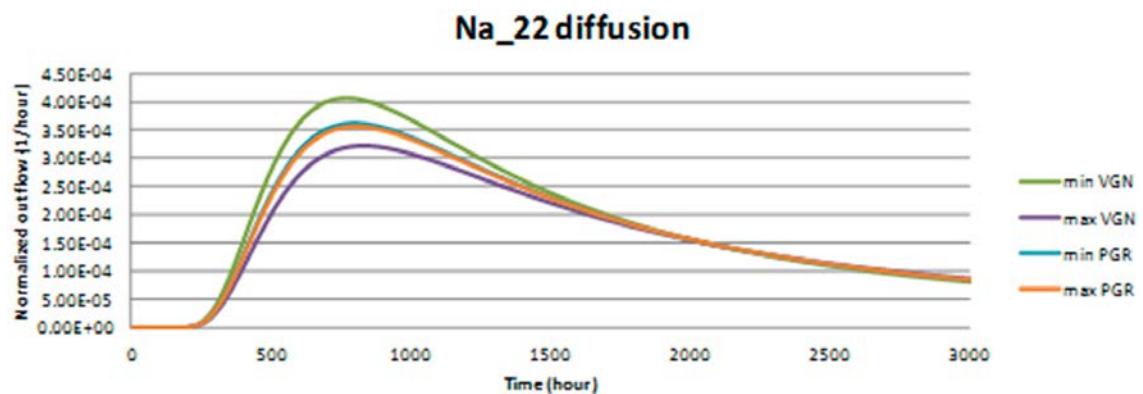

Figure G-18. *The comparison of the Na_22 activity development in the experiment WPDE_2 – dependence on the change of the D_e parameters.*
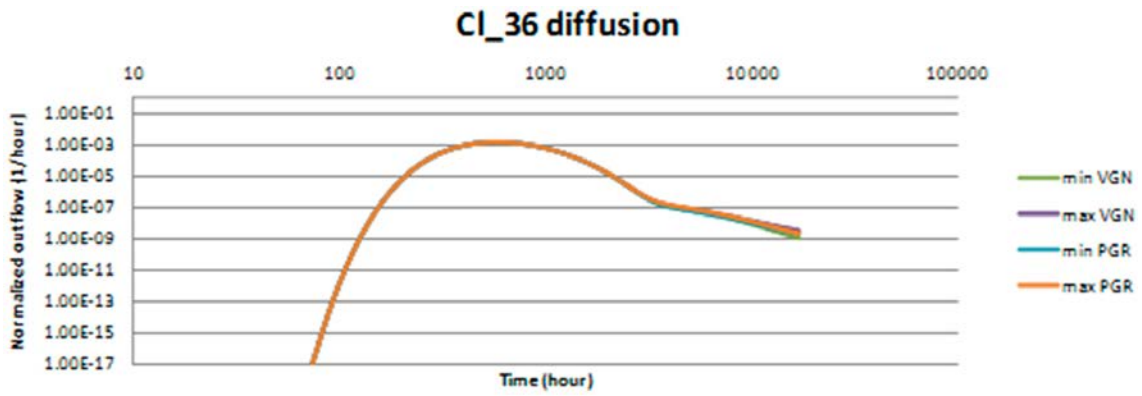
Figure G-19. *The comparison of the Cl_36 activity development in the experiment WPDE_2 – dependence on the change of the D_e parameters.*
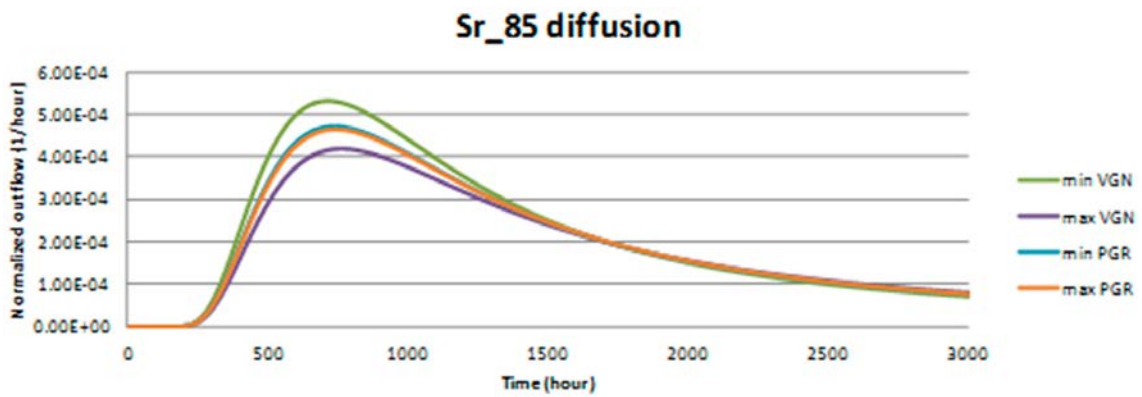

Figure G-20. *The comparison of the Sr_85 activity development in the experiment WPDE_2 – dependence on the change of the D_e parameters.*
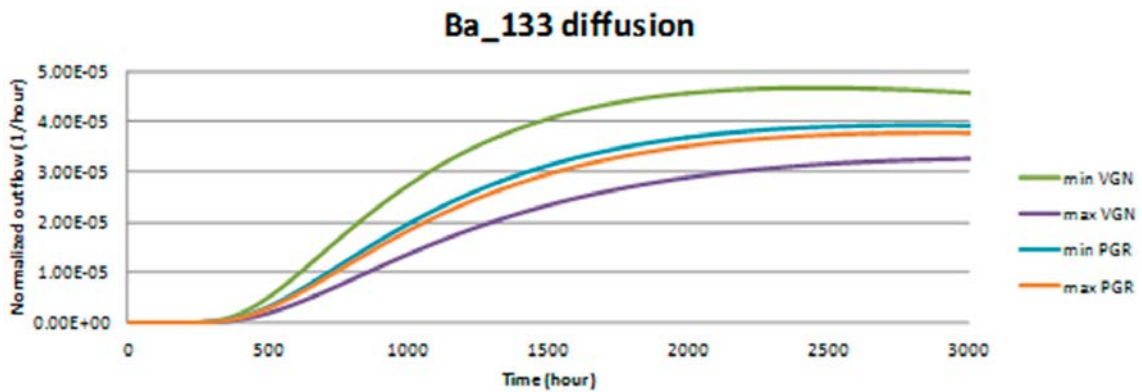

Figure G-21. *The comparison of the Ba_133 activity development in the experiment WPDE_2 – dependence on the change of the D_e parameters.*

Figure G-22. *The comparison of the HTO activity development in the experiment WPDE_2 – dependence on the dispersivity change.*

Figure G-23. *The comparison of the Na_22 activity development in the experiment WPDE_2 – dependence on the dispersivity change.*

Figure G-24. *The comparison of the Cl_36 activity development in the experiment WPDE_2 – dependence on the dispersivity change.*
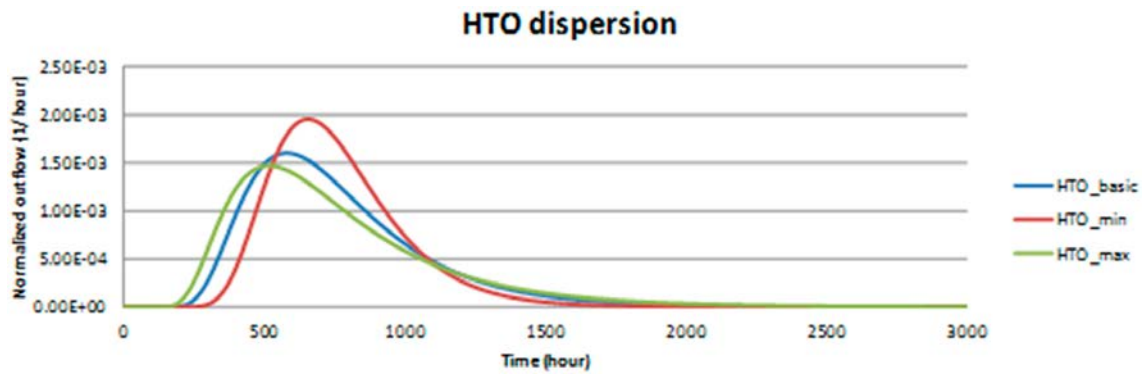
Figure G-25. *The comparison of the Sr_85 activity development in the experiment WPDE_2 – dependence on the dispersivity change.*

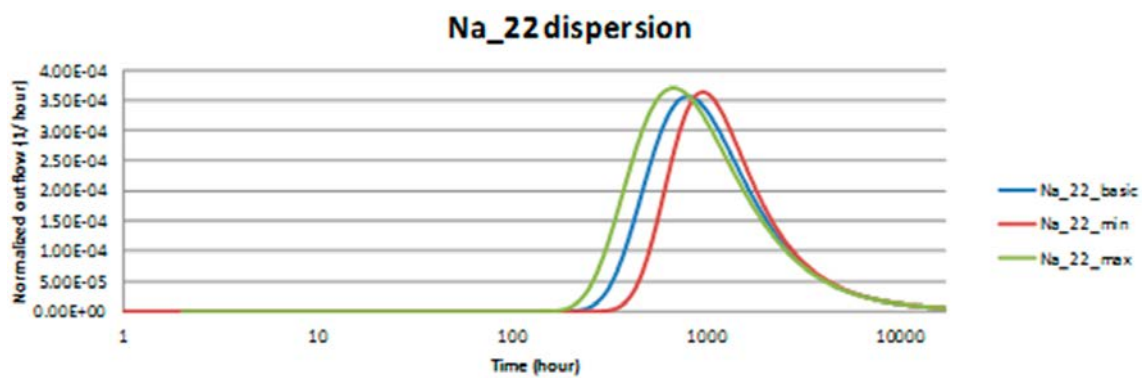**Figure G-26.** *The comparison of the Ba_133 activity development in the experiment WPDE_2 – dependence on the dispersivity change.*
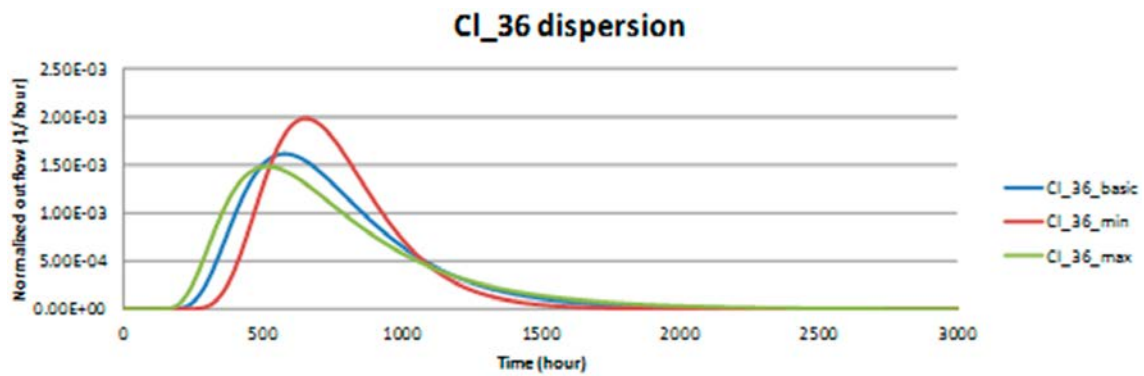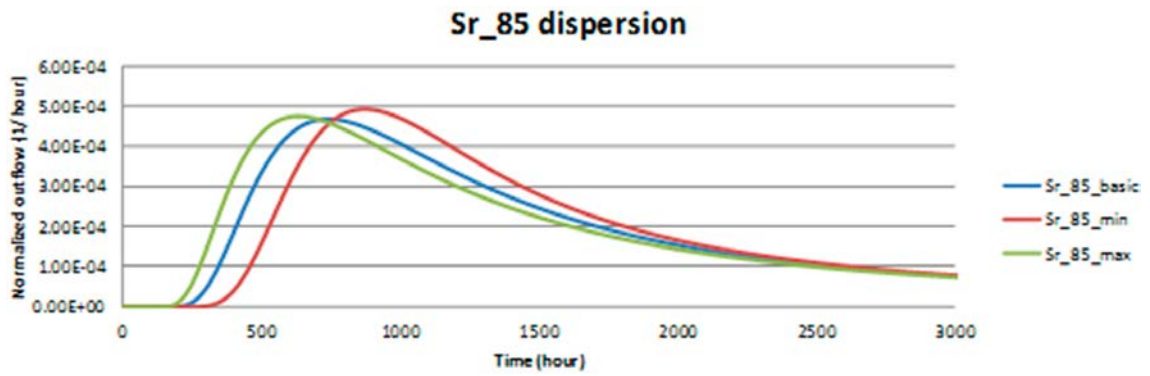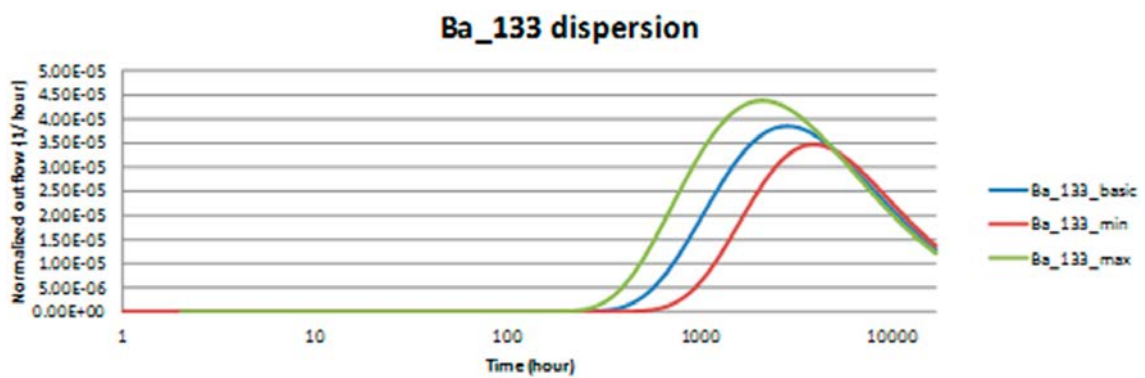

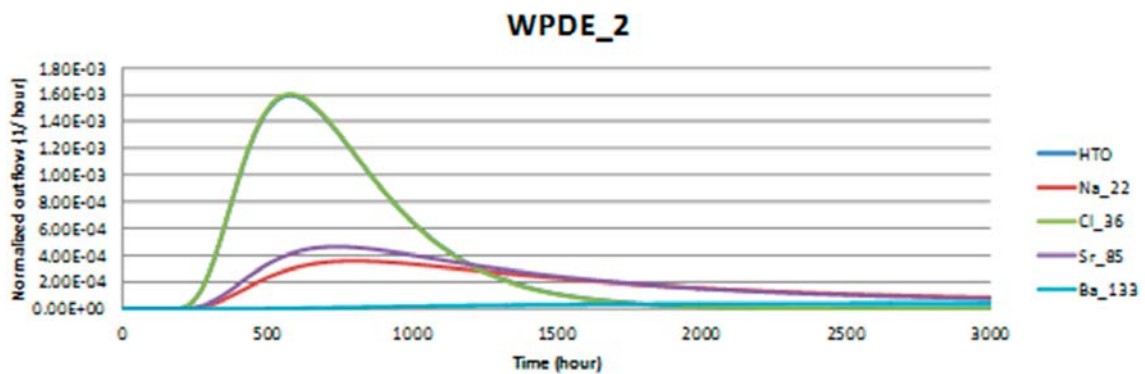**Figure G-27.** *The comparison of the activity development for all of the radionuclides in the experiment WPDE_2 (normal scale).*
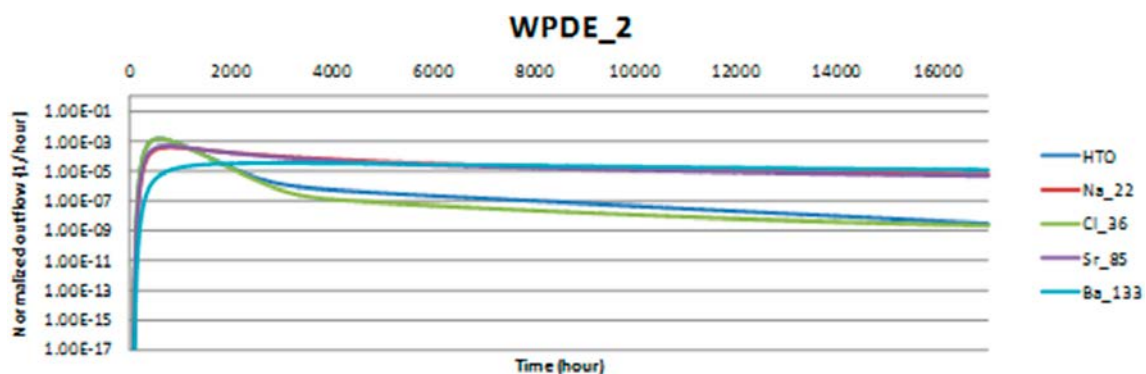
Figure G-28. *The comparison of the activity development for all of the radionuclides in the experiment WPDE_2 (normal-log scale).*
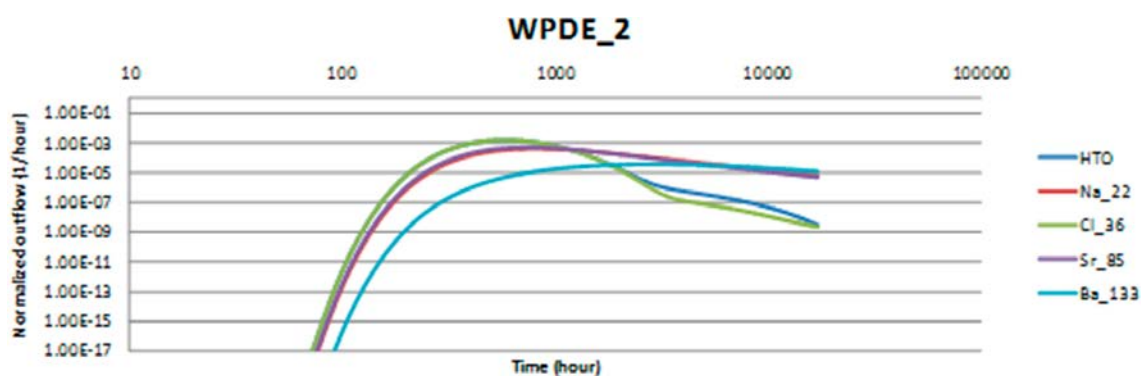
Figure G-29. *The comparison of the activity development for all of the radionuclides in the experiment WPDE_2 (log-log scale).*

Table G-5. The results of WPDE_2 experiment.

Performace meassures central prediction WPDE-2

Time when event occurs	HTO, time (h)	Na-22, time (h)	Cl-36 time (h)	Sr-85, time (h)	Ba-133, time (h)
Leading edge, 10 % of tracer peak concentration	276	309	277	301	535
Leading edge, 50 % of tracer peak concentration	377	448	377	430	1012
Tracer peak concentration	581	802	580	741	2859
Tail, 10 % of tracer peak concentration	1408	5176	1398	3994	NaN
Tail, 1 % of tracer peak concentration	2050	NaN	2004	16634	NaN
Tail, 0.1 % of tracer peak concentration	2928	NaN	2641	NaN	NaN
Decay corrected activity per mass unit of solution at outlet, at	**HTO, activity (Bq/g)**	**Na-22, activity (Bq/g)**	**Cl-36, activity (Bq/g)**	**Sr-85, activity (Bq/g)**	**Ba-133, activity (Bq/g)**
Tracer peak concentration	1.5926E−03	3.5791E−04	1.6099E−03	4.6797E−04	3.8423E−05

Korea Atomic Energy Research Institute, Daejeon, Republic of Korea

Dong-Kyu Park, Sung-Hoon Ji

H1 Introduction

For the first step of Task 9 for realistic modelling of coupled matrix diffusion and sorption in hetero-geneous rock matrix, the semi-predictive modelling was accomplished under various diffusion and sorption conditions based on the in situ WPDE experiments in REPRO project at the ONKALO underground rock characterisation facility, Finland.

H1.1 Background

Korea Atomic Energy Research Institute (KAERI) participated in Task 9 (1) to understand the mechanisms of matrix diffusion and sorption affecting the fate and transport of radionuclides in fractured rock; (2) to develop a numerical analysis model for interpretation of a tracer test and a diffusion test; and (3) to apply the developed model to the conducted tracer tests and diffusion tests.

As a modelling tool for this task, COMSOL Multiphysics, which is a finite element model program developed to solve partial differential equations for a wide range of scientific and engineering prob-lem, phenomena and applications (Li et al. 2009, Perko et al. 2009), was used. It enables to couple more than one type of physics, so-called multiphysics, simultaneously in a complicated geometry of model domain. It has been used recently in the modelling studies on the radionuclide transport in the fractured rock for the radioactive waste disposal with engineering and geological barriers (Olin et al. 2008, Pulkkanen 2009, Sentís et al. 2009, Itälä et al. 2010, Perko et al. 2011, Kajanto 2013, Lee et al.2014, Seetharam et al. 2014). Pulkkanen (2009) and Pulkkanen and Nordman (2011) examined the effects of the geometry including fracture on the radionuclide transport near a vertical deposition hole for radioactive waste disposal. Kajanto (2013) assessed the effect of fracture geometry, such as aperture size and tortuosity, on radionuclide transport. Perko et al. (2011) and Seetharam et al. (2014) have simulated radionuclide transport in the fractured rock by implicitly dealing with fractures using COMSOL.

H1.2 Objectives

For the successful radioactive waste disposal in the crystalline fractured rock, it is essential to understand nature and processes for the fate and transport of radionuclides occurred in the fracture and rock matrix. Among several transport processes, sorption and diffusion into the rock matrix, which are main topics in Task 9, are relevant to retention of radionuclide migration from a geological repository for radioactive waste. Particularly, role and effect of microstructures such as microfracture and mineral grains in rock matrix on the diffusion and sorption are one of our ulti-mate concerns in Task 9. Task 9A is the preliminary step for understanding the effects of diffusion and sorption in the rock matrix on the transport of non-sorbing and sorbing radionuclides through numerical modelling, based on the WPDE-1 and WPDE-2 experiments. This study was to evaluate the applicability of the modelling code, COMSOL Multiphysics, by simulating these experiments under the condition provided in the WPDE campaign, to find the influential factors on the results of the experiments, and to consider the uncertainty in measurement data. It was also to make familiar ourselves with the experimental setup of WPDE campaigns for the later subtasks.

H1.3 Scope and limitations

In this subtask, as a preliminary study for Task 9, traditional solute transport was modelled by reflecting the given experimental conditions as simple as possible. Particularly, the assumption of a homogeneous and isotropic rock matrix enables to reduce model domain to 1/8 scale, while a full-scale domain will be required for realistically simulating the transport of radionuclides in heterogeneous rock matrix having significant microstructures. This study would be used as a result of reference case in the later tasks relevant to the WPDE experiments. In this subtask, therefore, it focused on evaluation of the relevance of the modelling code COMSOL in simulating the WPDE

experiments rather than assessment of effects of diffusion and sorption due to heterogeneity of rock matrix. As well, this study discussed about mesh dependency for the reliable prediction of transport of sorbing tracers. The uncertainty of properties such as diffusion coefficient (D_e) and partitioning coefficient (K_d) measured in the experiments was examined through the sensitivity analysis.

H2 Methodology and model

H2.1 Conceptual description of features, events and processes of the experiments

The tracer cocktails passing through input tube from REPRO niche were injected to the drillhole ONK-PP323. It would migrate along the controlled water flow in the slot between the drillhole wall (rock) and the dummy. Variations in velocity profile in the water flow could lead to the dispersion of tracers in the slot. The migration of tracers would be retarded and their concentration could decrease gradually because they could absorb to the mineral grain or diffuse to the rock matrix. As well, tracers absorbed at the rock matrix might diffuse out of the slot due to the reversed concentration gradient. The tracers would sorb and diffuse differentially into the rock matrix depending on the type of or structures in the rock in the drillhole, which consists of migmatitic metamorphic gneiss (VGN) and coarse-gained pegmatitic granite. The banded foliation of VGN might lead to diffuse the tracers into rock matrix more than the massive PGR. Or, open and connected microfractures or mineral grains in rock matrix might enhance their diffusion and sorption. Mechanical damages or chemical changes in rock matrix near the drillhole wall possibly occurred by the core drilling could affect the transport processes interacting between slot and rock matrix during the experiments. It is inherently uncertain whether diffusion and sorption properties obtained from the laboratory experiments on some rock samples could be the representative of the rock in the drill core.

H2.2 Description of features, events and processes in our conceptual model

In the conceptual model for WPDE experiments, in this study, traditional solute transport in fracture and rock matrix was modelled; general advection-dispersion in the slot between the drillhole and the dummy; Fickian diffusion and equilibrium sorption with linear isotherm in the rock matrix. The laminar flow condition in the slot and homogeneous and isotropic rock matrix were assumed. Decay of tracers in the experiments was not considered. We guess that the microstructure in the rock matrix could be one of the most significant factors for the experimental results obtained in WPDE campaigns. However, these microstructures in the rock matrix are highly heterogeneous and complicated and their features such as shape, size, connectivity, and distribution are too difficult to be characterized. Throughout Task 9, the ultimate objective of our study will be to reasonably characterize microstructures and predict their effects on the diffusion and sorption of radionuclide in the heterogeneous rock matrix.

H2.3 Model setup

The flow field of water in the slot was modelled with Navier-Stokes equation for laminar flow using the 'Creeping flow interface' in COMSOL. Flow given in the respective WPDE experiments was assumed under steady state. Because a thin aperture of slot can create too fine mesh to solve the problem due to limited computational sources, the slot was formulated with one layer and thus a uniform flow field was created in the slot. The 'transport of diluted species interface' module in COMSOL for solving general advection-diffusion equation were applied to simulate the transport of tracers in the slot and rock matrix and the advection in the rock matrix was neglected. The setting of model including domain geometry was as simple as possible. The homogeneous and isotropic model domain considered was reduced to 1/8 scale due to the geometric symmetry along the axis parallel to the slot. In this study, the inlet and outlet tubes were considered by calculating the time taken to pass through the tubes with their lengths and the flow velocity in each experiment. With the inlet and outlet tubes, the arrivals of tracers would be delayed about 32.66 h for the WPDE-1 and 65.32 h for the WPDE-2, respectively.

These simplified assumptions and settings in the conceptual model give easy and comprehensive understanding for the modelling process and its results as a reference case. However, any possible effects of the heterogeneous natures of rock matrix including rock type (VGN and PGR) distinguished clearly in the drill core as well as diffusion and sorption originating from microstructures, which is the primary interest of our study, could not be dealt with in this task.

At the right boundary corresponding to the slot inlet, a slightly smoothened step function of concentration was assigned for pulse types of injection of tracer cocktails in the WPDE campaigns. It has often been recommended to reduce numerical errors originating from the initial and boundary conditions with a steep gradient of parameter differences (Pulkkanen 2009). The pressure at the right boundary for inlet was zero and constant flow rates (20 µL/min for WPDE-1 and 10 µL/min for WPDE-2) at the left boundary for outlet was applied so that the tracer and water flows from the right to the left. The left boundary as the outlet of water and tracers was assigned to have free advective flux (Pulkkanen and Nordman 2011), which the diffusive flux is zero, so that the tracer can exit the model freely by advection.

The model domain was discretized with hexahedral elements. With the 1.25 mm thick of annular slot, the thickness of rock matrix was set to 71.5 mm, covering from 28.25 mm to 100 mm from the center of drill hole (Figure H-1). The rock matrix was discretized to 50 layers along the axis perpendicular to the slot, as a default mesh, while finer or coarser meshes were used for the convergence study. Increasing the element ratio can refine the mesh located at the interface between the slot and the rock matrix. With this ratio, the mesh in the rock matrix became refined as approaching the boundary between slot and rock matrix (or drillhole wall). The element size of first layer in the rock matrix (the nearest one at the boundary between slot and rock matrix) was 20 times smaller than that of end layer for all the used tracers except for Ba-133, in other words their element ratio were 20 (for example, if this value is 1, the first and the last elements have the same size).
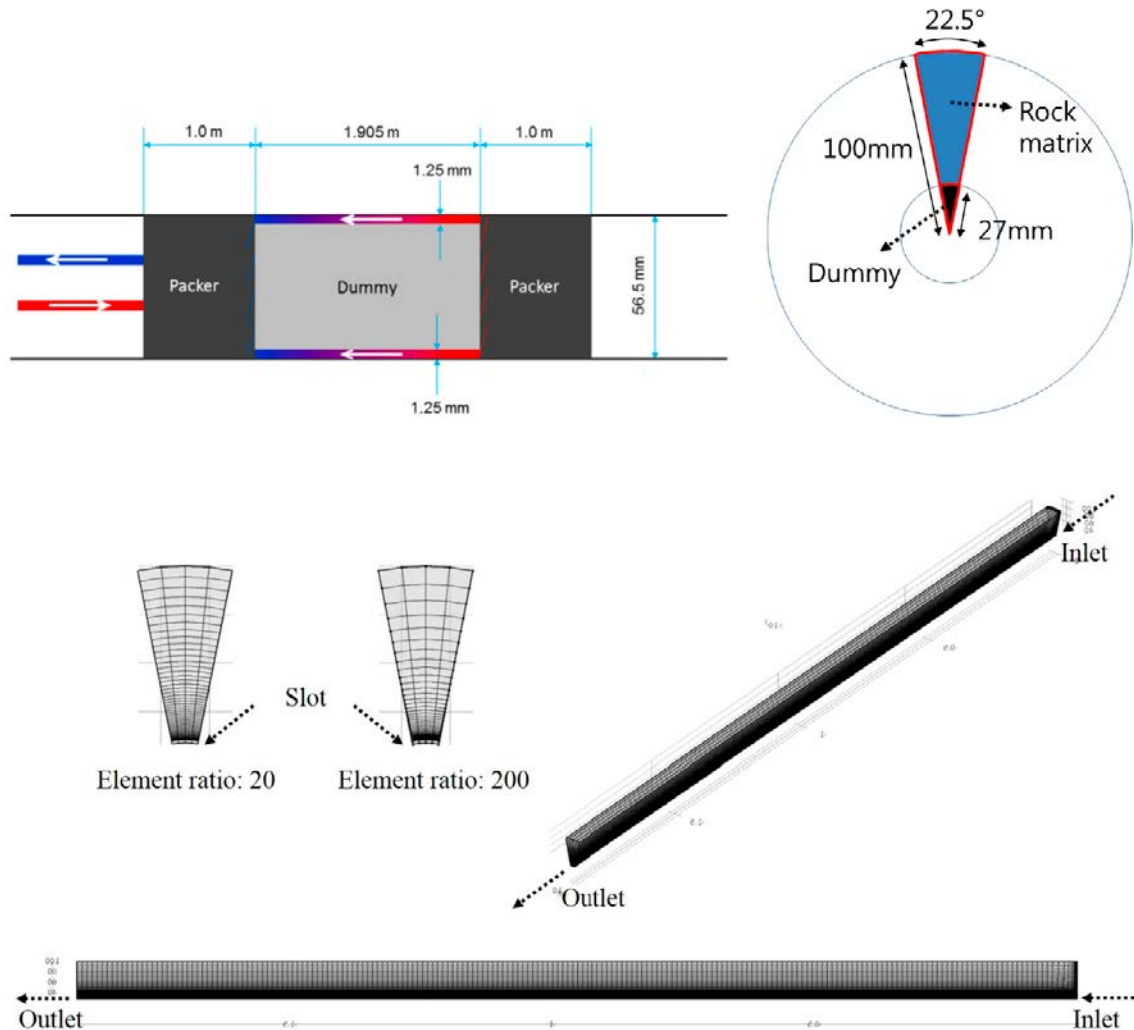

Figure H-1. Experimental setup of the WPDE campaigns (upper left), the 1/8 scale of model domain (vertical section; upper right), and the mesh (lower) considered in this study.

For Ba-133, however, the element ratio of rock matrix mesh was set to 200 so that the mesh at the interface of the rock matrix and the slot would become finer than those for the other tracers. Also, the model domain was uniformly discretized to 200 elements along the axis parallel to the slot and then was refined more on only the boundary near the inlet. For this mesh used in the default modelling, the total numbers of elements was 42,432.

Because of assuming the general solute transport in the homogeneous and isotropic rock matrix, the uncertainty originating from inherent heterogeneity of a rock including rock type, microstructure, and mineral grains as well as their possible effects on the diffusion and sorption was not involved in the modelling for Task 9A. Modelling with the one layer of slot might be not enough to thoroughly quantify hydrodynamic dispersion due to the variation in flow velocity in the slot.

H2.4 Input data

Most of data in Task Description of Task 9A (Table 2-9 and Table 2-11) were used as inputs of D_e and K_d for tracers and rock type in the modelling as they were provided (Table H-1). However, D_e for HTO was chosen to the value measured in the interval of 18.59 ~ 18.94 m in the drillhole and D_es for Na-22, Sr-85, and Ba-133 were 4.65×10^{-13} m^2/s (POSIVA-97-07), 3.3×10^{-13} m^2/s (SKB R-99-13), and 1.47×10^{-13} m^2/s (Widestrand et al. 2007), respectively. K_ds for Na-22 and Ba-133 were 1.26×10^{-3} m^3/kg and 6.16×10^{-2} m^3/kg, respectively, which were interpolated with the values given in Task Description of Task 9A and the length corresponding to the rock type (VGN and PGR) in the drill core. Rock matrix porosity was chosen to be 0.63 % which is the average porosity of VGN provided n the Task Description of Task 9A (Table 2-8) and bulk density were assumed to be 2.7×10^3 kg/m^3. The longitudinal dispersivity for hydrodynamic dispersion in the slot was assigned to 10 % of the drillhole length in the default simulations.

Table H-1. Diffusion and partitioning coefficients used in this modelling.

Tracers	D_e (×10^{-13} m^2/s)	K_d (10^{-2} m^3/kg)
HTO	2.5 ± 0.3*	–
Na-22	4.65	0.126 ± 0.03*
Cl-36	0.05 ± 0.03*	–
Sr-85	3.3	0.11 ± 0.03*
Ba-133	1.47	6.16 ± 2.0*

* In the next section, sensitivity analysis was carried out for these diffusion and sorption coefficients (+: for the upper prediction; –: for the lower prediction).

H2.5 Alternative models and sensitivity cases

In this study, sensitivity analysis for assessing the uncertainty in D_e and K_d obtained experimentally was conducted based on only the data given in the Task Description of Task 9A (Table 2-9 and Table 2-11). The upper and lower predictions for K_ds of Na-22 and Ba-133 were also obtained with their respective interpolated values used in the central predictions and the uncertainty estimates suggested in Task Description of Task 9A (Table 2-11). The D_e and K_d values used in this sensitivity analysis were summarized in the Table H-1. As well, sensitivity to the dispersivity was also analyzed.

Additional study on the reliability of results obtained in the modelling was carried out with mesh dependency of the prediction of Ba-133, as well as Cl-36 and Na-22, for WPDE-2 experiment: (1) the element ratio in the rock matrix, (2) the number of layers in the rock matrix, and (3) the numbers of elements along the axis parallel to slot.

H3 Results and discussion

H3.1 The central prediction

WPDE-1: As shown the comparison between the two non-sorbing tracers, the effect of diffusion on the breakthrough curves seems to be insignificant (Figure H-2). Even though HTO has about two orders of D_e greater than Cl-36, the shapes of both breakthrough curves were nearly identical to each

other, including peak arrival time and width of curve, while the breakthrough curve of HTO had a lower peak concentration and a very slightly lengthened tailing in the later time compared with that of Cl-36 (Table H-2). Figure H-2 also demonstrate that the effect of sorption on the WPDE-1 experiment result would be greater than that of diffusion. The breakthrough curve for the sorbing tracer Na-22 shows low peak concentration, retarded peak arrival, large width of curve, and long tailing compared to those of non-sorbing tracers. The recovery ratio for each tracer calculated for WPDE-1 experiment was summarized in Table H-3.
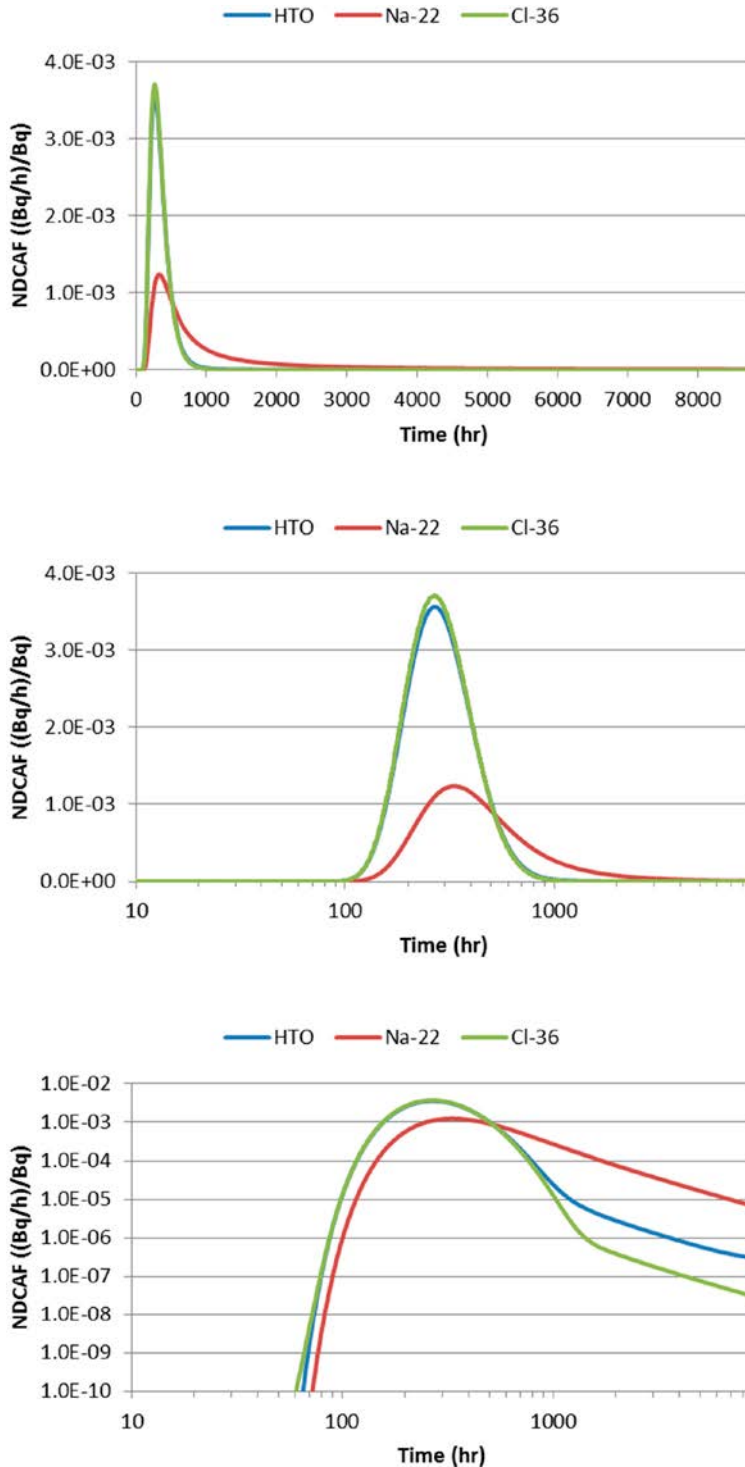

Figure H-2. *The prediction results for the WPDE-1 experiment: normal-normal (upper), log-normal (center), and log-log (lower) scales.*

Table H-2. The performance measures of prediction (central) for the WPDE-1 experiment.

Performance measures central prediction WPDE-1

Time when event occurs	HTO, time (h)	Na-22, time (h)	Cl-36, time (h)
Leading edge, 10 % of tracer peak concentration	134	149	134
Leading edge, 50 % of tracer peak concentration	178	204	178
Tracer peak concentration	268	332	267
Tail, 10 % of tracer peak concentration	630	1 518	617
Tail, 1 % of tracer peak concentration	936	6 010	876
Tail, 0.1 % of tracer peak concentration	1 764	NA	1 161
Decay corrected activity per mass unit of solution at outlet, at	**HTO, activity (Bq/g)**	**Na-22, activity (Bq/g)**	**Cl-36, activity (Bq/g)**
Tracer peak concentration	50 768.64	1 421.84	3 857.79

Table H-3. The recovery ratio calculated in the prediction (central) for the WPDE-1 experiment.

Performance measures central prediction WPDE-1

	HTO	Na-22	Cl-36
Recovery (%)	98.19	63.04	99.81

WPDE-2: The overall results in this experiment were consistent with those of WPDE-1 (Figure H-3). In particular, the breakthrough curve for Ba-133, which has the lowest D_e but the highest K_d among the sorbing tracers used in this experiment, definitely highlighted an effects of sorption on the behaviour of tracers in the WPDE experiments. The migration of Ba-133 was retarded significantly and thus its peak arrival time was 2 544 h (Table H-4). The peak concentration of this tracer was low considerably compared to those of the others and its concentration in the end of this experiment did not decrease below 29 % of the peak concentration with the elongated tailing. The recovery ratio for each tracer calculated for WPDE-2 experiment was summarized in Table H-5.

Table H-4. The performance measures of prediction (central) for the WPDE-2 experiment.

Performance measures central prediction WPDE-2

Time when event occurs	HTO, time (h)	Na-22, time (h)	Cl-36 time (h)	Sr-85, time (h)	Ba-133, time (h)
Leading edge, 10 % of tracer peak concentration	270	307	270	300	546
Leading edge, 50 % of tracer peak concentration	359	430	358	413	955
Tracer peak concentration	540	735	536	681	2 544
Tail, 10 % of tracer peak concentration	1 274	4 334	1 238	3 362	NA
Tail, 1 % of tracer peak concentration	1 941	NA	1 762	13 745	NA
Tail, 0.1 % of tracer peak concentration	4 320	NA	2 368	NA	NA
Decay corrected activity per mass unit of solution at outlet, at	**HTO, activity (Bq/g)**	**Na-22, activity (Bq/g)**	**Cl-36, activity (Bq/g)**	**Sr-85, activity (Bq/g)**	**Ba-133, activity (Bq/g)**
Tracer peak concentration	90 565.42	1 431.68	15 656.96	3 791.81	192.90

Table H-5. The recovery ratio calculated in the prediction (central) for the WPDE-2 experiment.

Performance measures central prediction WPDE-2

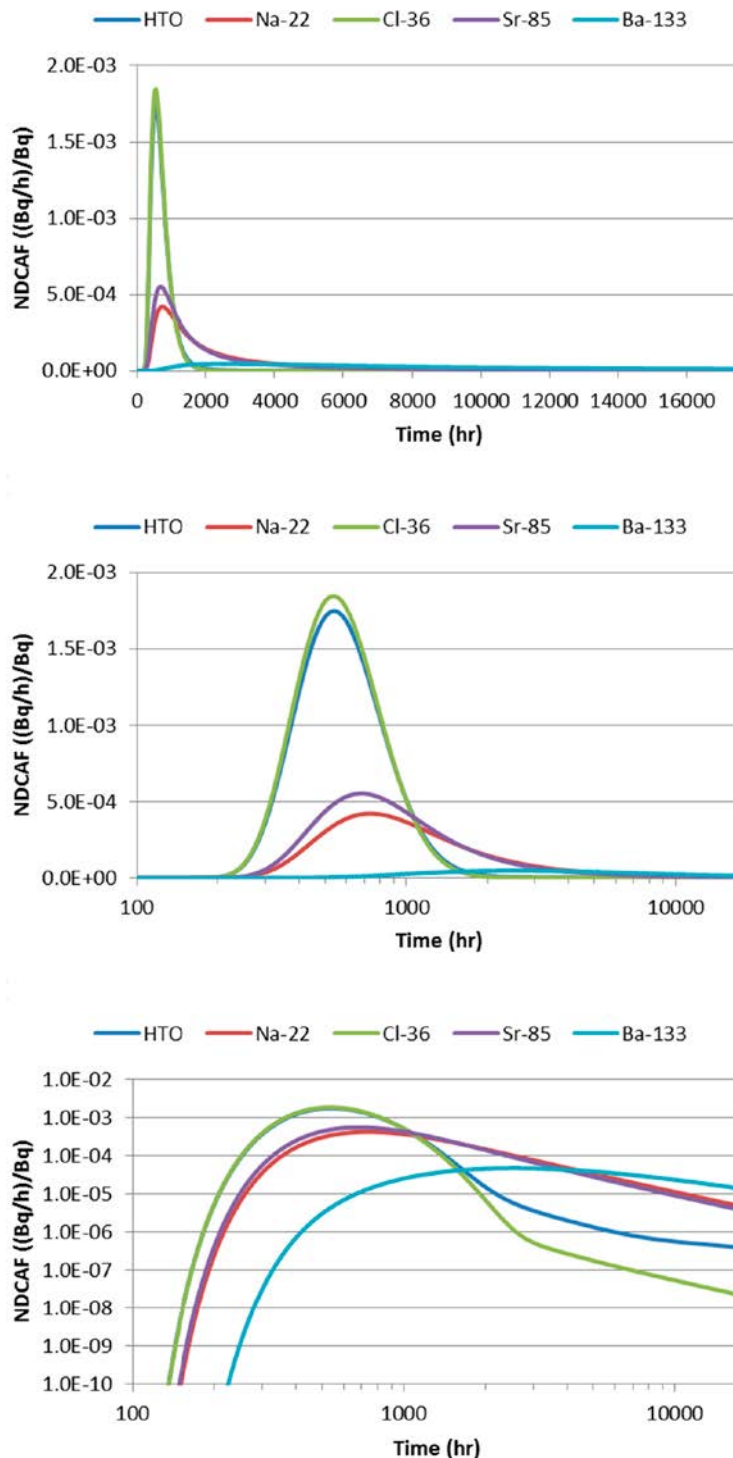|	HTO	Na-22	Cl-36	Sr-85	Ba-133
Recovery (%)	97.28	48.31	98.85	56.88	25.03

Figure H-3. *The prediction results for the WPDE-2 experiment: normal-normal (upper), log-normal (center), and log-log (lower) scales.*

H3.2   The upper and lower predictions

WPDE-1: The results demonstrates that uncertainty in the partitioning coefficient can affect the prediction of tracer behaviours more significantly than that in the diffusion coefficient under the experimental condition of this WPDE campaign (Figure H-4 and Table H-6). The predictions for the non-sorbing tracers, HTO and Cl-36, were hardly sensitive to D_e. However, Figure H-4 shows that the fate and transport of Na-22, the sorbing tracer, were predicted differently depending on K_d values. As K_d of Na-22 increased, for example, the peak concentration decreased and the peak arrivals were retarded slightly.
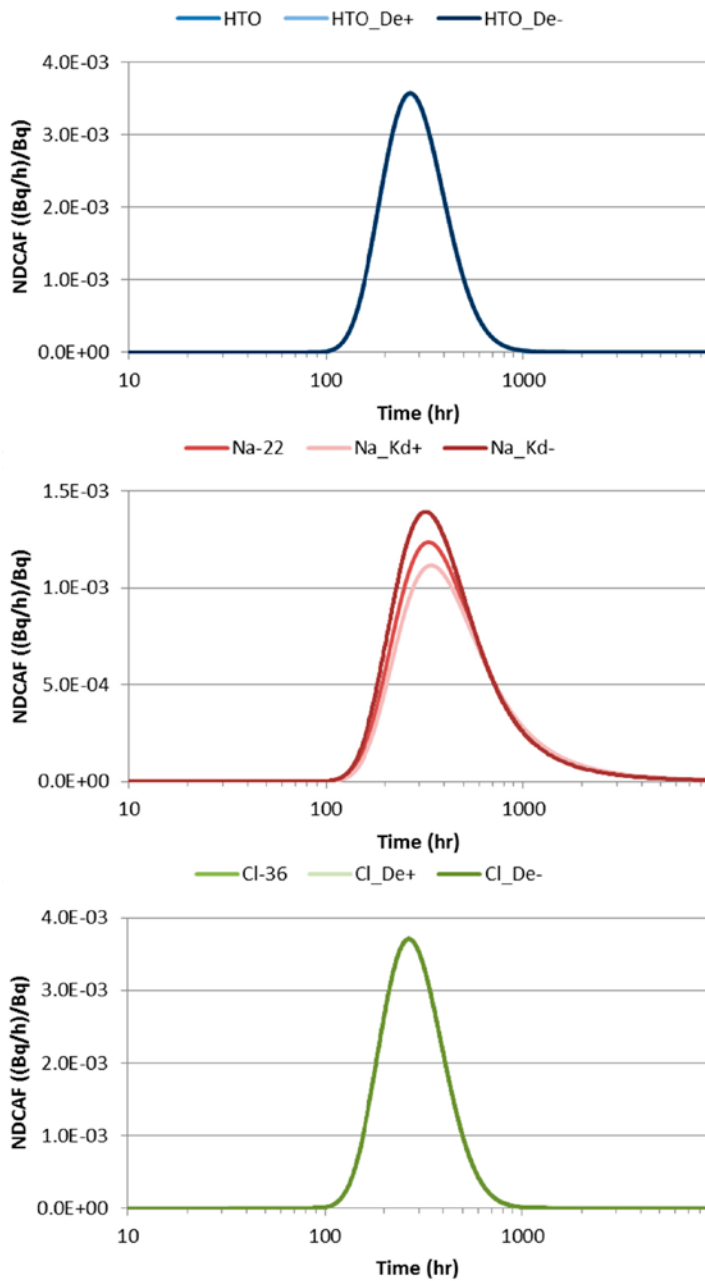
Figure H-4. *The sensitivity analysis for the measurement uncertainties in the diffusion and partitioning coefficients of tracers used in the WPDE-1 experiment: HTO (upper), Na-22 (center), and Cl-36 (lower).*

Table H-6a. Performance measures of (a) upper and (b) lower predictions for WPDE-1.

(a) Performance measures upper prediction WPDE-1

Time when event occurs	HTO, time (h)	Na-22, time (h)	Cl-36, time (h)
Leading edge, 10 % of tracer peak concentration	134	153	134
Leading edge, 50 % of tracer peak concentration	178	209	178
Tracer peak concentration	268	342	267
Tail, 10 % of tracer peak concentration	631	1672	618
Tail, 1 % of tracer peak concentration	941	6833	879
Tail, 0.1 % of tracer peak concentration	1820	NA	1175
Decay corrected activity per mass unit of solution at outlet, at	**HTO, activity (Bq/g)**	**Na-22, activity (Bq/g)**	**Cl-36, activity (Bq/g)**
Tracer peak concentration	50633.11	1283.73	3851.84

Table H-6b. Performance measures of (a) upper and (b) lower predictions for WPDE-1.

(b) Performance measures lower prediction WPDE-1

Time when event occurs	HTO, time (h)	Na-22, time (h)	Cl-36, time (h)
Leading edge, 10 % of tracer peak concentration	134	146	134
Leading edge, 50 % of tracer peak concentration	178	199	178
Tracer peak concentration	268	321	267
Tail, 10 % of tracer peak concentration	629	1 354	616
Tail, 1 % of tracer peak concentration	931	5 138	873
Tail, 0.1 % of tracer peak concentration	1 707	NA	1 143
Decay corrected activity per mass unit of solution at outlet, at	**HTO, activity (Bq/g)**	**Na-22, activity (Bq/g)**	**Cl-36, activity (Bq/g)**
Tracer peak concentration	50 911.97	1 603.02	3 866.03

WPDE-2: In this experiment, the breakthrough curves were also more sensitive to K_d of tracers (Figure H-5). In particular, for Ba-133, the measurement uncertainty of K_d might cause the differences in the predictions of peak concentration, peak arrival time, and time to begin for the injected tracer to be detected at the outlet, while the concentration shown in the tailing, in the later time (after about 12,000 h), seems to be similar to each other regardless of K_d. For example, the peak arrival time was calculated to be from 1 918 h (for lower prediction) to 3 186 h (for upper prediction) within the range of K_d (Table H-7). These results mean that it might be necessary to reduce the measurement uncertainty in sorption coefficients of tracers in order to accurately predict behaviours of sorbing tracers in the rock matrix.

Table H-7a. Performance measures of (a) upper and (b) lower predictions forWPDE-2.

(a) Performance measures upper prediction WPDE-2

Time when event occurs	HTO, time (h)	Na-22, time (h)	Cl-36 time (h)	Sr-85, time (h)	Ba-133, time (h)
Leading edge, 10 % of tracer peak concentration	270	315	270	307	680
Leading edge, 50 % of tracer peak concentration	359	442	358	424	1 169
Tracer peak concentration	540	768	536	708	3 186
Tail, 10 % of tracer peak concentration	1 277	4 916	1 240	3 794	NA
Tail, 1 % of tracer peak concentration	1 955	NA	1 770	16 038	NA
Tail, 0.1 % of tracer peak concentration	4 481	NA	2 412	NA	NA
Decay corrected activity per mass unit of solution at outlet, at	**HTO, activity (Bq/g)**	**Na-22, activity (Bq/g)**	**Cl-36, activity (Bq/g)**	**Sr-85, activity (Bq/g)**	**Ba-133, activity (Bq/g)**
Tracer peak concentration	90 206.95	1 256.49	15 622.46	3 341.07	148.93

Table H-7b. Performance measures of (a) upper and (b) lower predictions forWPDE-2.

(b) Performance measures lower prediction WPDE-2

| Time when event occurs	HTO, time (h)	Na-22, time (h)	Cl-36 time (h)	Sr-85, time (h)	Ba-133, time (h)
Leading edge, 10 % of tracer peak concentration	270	300	270	293	487
Leading edge, 50 % of tracer peak concentration	359	417	358	401	792
Tracer peak concentration	539	700	536	653	1 918
Tail, 10 % of tracer peak concentration	1 272	3 737	1 236	2 910	NA
Tail, 1 % of tracer peak concentration	1 926	15 727	1 754	11 344	NA
Tail, 0.1 % of tracer peak concentration	4 147	NA	2 314	NA	NA
Decay corrected activity per mass unit of solution at outlet, at	**HTO, activity (Bq/g)**	**Na-22, activity (Bq/g)**	**Cl-36, activity (Bq/g)**	**Sr-85, activity (Bq/g)**	**Ba-133, activity (Bq/g)**
Tracer peak concentration	90 944.60	1 671.01	15 704.53	4 415.72	278.23
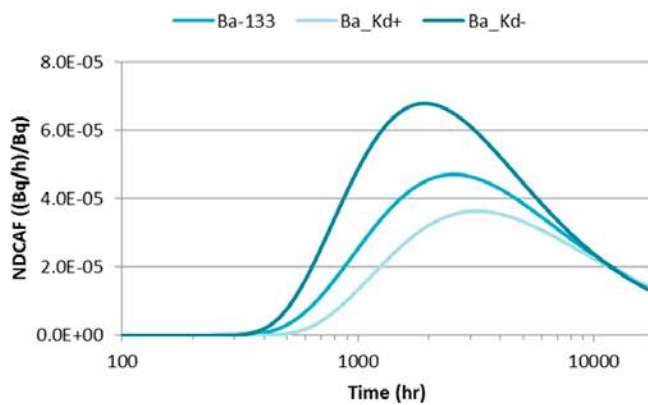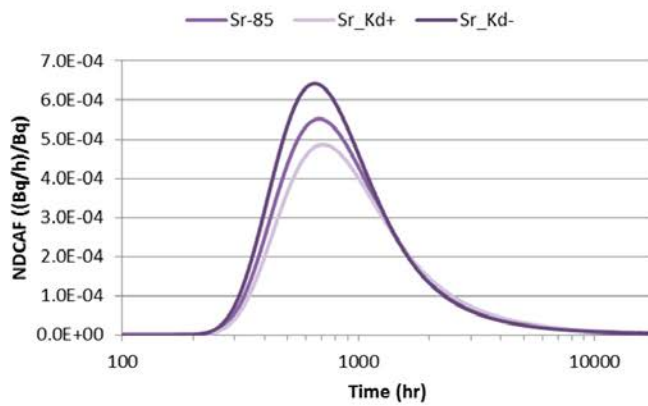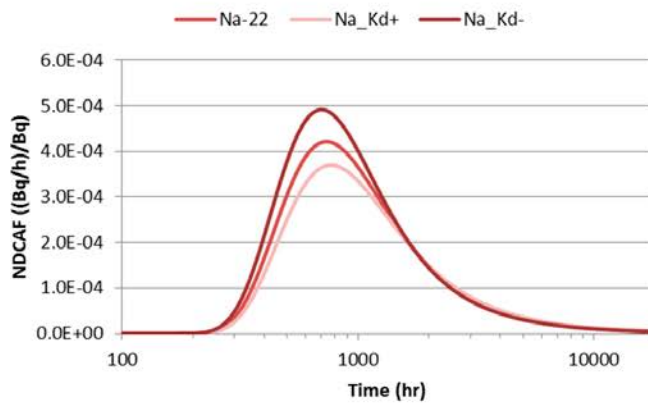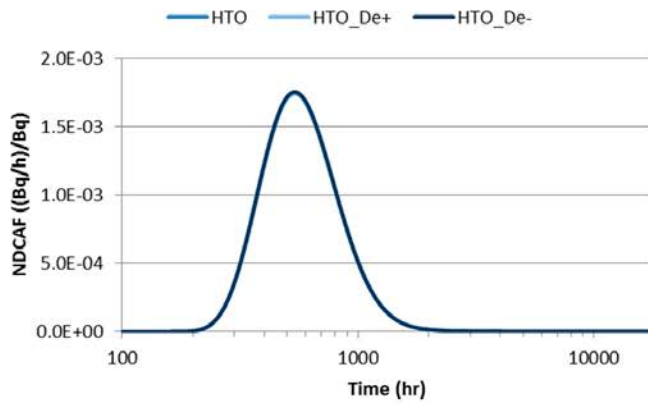
Figure H-5. *The sensitivity analysis for the measurement uncertainties in the diffusion and partitioning coefficients of tracers used in the WPDE-2 experiment: HTO, Na-22, Sr-85, and Ba-133 in sequence.*

H3.3   Other alternative models, sensitivity cases and results

Sensitivity to dispersivity: One of the distinctive features in the results obtained in this study may be the relatively rapid peak arrivals of tracers. As one of its reasons, the hydrodynamic dispersion in the slot assumed in this study was suspected. In the traditional solute transport modelling, the dispersivity was generally one of the most influential factors on the behaviours of tracers migrating along a fluid flow. The sensitivity analysis for the WDPE-1 experiment demonstrates that the dispersivity could be critical to shape of breakthrough curve including peak arrival time and peak concentration (Figure H-6), which might be dominant on the prediction rather than the diffusion and sorption processes that were of particular interest in the Task 9. Particularly, more rapid peak arrivals were obtained as the dispersivity increased. As shown in Table H-2, the peak arrival time of HTO for the WPDE-1 experiment was predicted to 268 h when the default dispersivity was used in the modelling, which is 1/10 of the drillhole length ($\alpha = 0.1905$ m). However, the dispersivity of the 1/1 000 of drillhole length (0.01α), which the dispersion effects are negligible, resulted in a sharp shape of breakthrough curve with 375 h of peak arrival time (Figure H-6 and Table H-8). The hydrodynamic dispersion and its uncertainty in slot need to be understood and characterized more in the future study in order to accurately evaluate the effects of diffusion and sorption in the rock matrix on the behaviours of tracers in the WPDE campaigns.
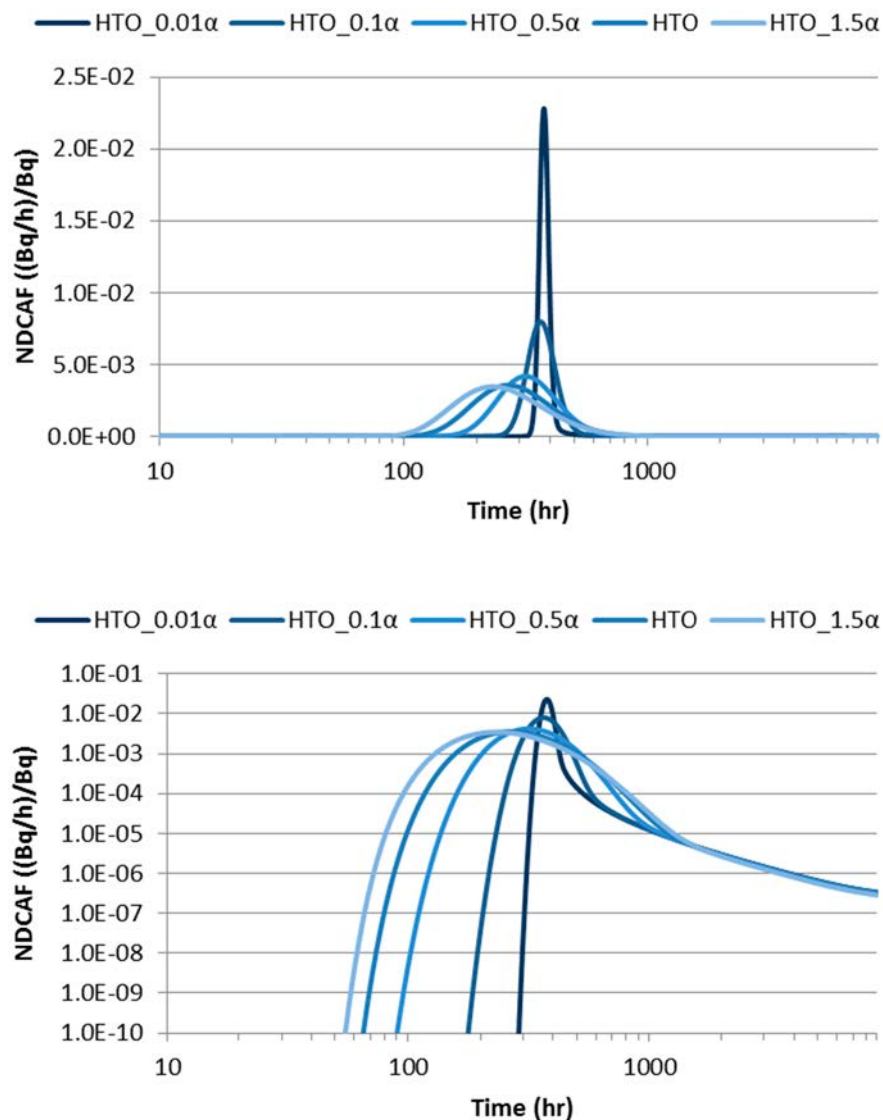

Figure H-6. *The sensitivity analysis for the uncertainty in dispersivity of HTO for the WPDE-1 experiment: log-normal (upper) and log-log (lower) scales. The "HTO" curves using the default dispersivity were also provided in Figure H-2.*

Table H-8. The performance measures of sensitivity analysis for the uncertainty in dispersivity of HTO for the WPDE-1 experiment.

Performance measures prediction WPDE-1 for dispersivity

Time when event occurs	HTO_0.01α, time (h)	HTO_0.1α, time (h)	HTO_0.5α, time (h)	HTO_1.5α, time (h)
Leading edge, 10 % of tracer peak concentration	342	277	182	109
Leading edge, 50 % of tracer peak concentration	357	313	230	147
Tracer peak concentration	375	364	316	232
Tail, 10 % of tracer peak concentration	414	488	593	631
Tail, 1 % of tracer peak concentration	467	588	810	987
Tail, 0.1 % of tracer peak concentration	787	1 211	1 649	1 766
Decay corrected activity per mass unit of solution at outlet, at	**HTO_0.01α, activity (Bq/g)**	**HTO_0.1α, activity (Bq/g)**	**HTO_0.5α, activity (Bq/g)**	**HTO_1.5α, activity (Bq/g)**
Tracer peak concentration	325 073.19	113 666.83	59 669.69	49 329.39

* The results for HTO with the default dispersivity (shown as "HTO" in Figure H-6) were provided in the Table H-2.

Convergence study: The convergence study was carried out for the mesh discretization in the rock matrix interfacing with the slot for the WPDE-2 experiment. For the non-sorbing tracer Cl-36, mesh dependency was hardly found in their results because the breakthrough curves seem to be identical to each other (Figure H-7). However, the predictions for the sorbing tracers were dependent to the mesh refinement in the interface of slot and rock matrix. The predictions for Na-22 became converged when the rock matrix was discretized to 20 layers or more (Figure H-8). With these mesh having 10 layers for the rock matrix, the peak arrival time was predicted to be about 150 h longer than those predicted with the others (Table H-9). However, the prediction for the sorbing tracer Na-22 was less sensitive to the element ratio of rock matrix layers. With 50 layers for the rock matrix domain, the difference in the peak concentrations between the meshes having the element ratios of 200 (finer at the interface) and 20 (default one) was only 2.74×10^{-6} ((Bq/h)/Bq), which was about 0.6 % discrepancy compared to the peak NDCAFs, but the peak concentration of the former was 5 h earlier than that of the latter.

Table H-9. The performance measures of convergence study on mesh discretization (number of layers and element ratio in rock matrix) of Na-22 for the WPDE-2 experiment.

Performance measures prediction WPDE-2 for mesh dependent

Time when event occurs	Na-22_ L50_ER200, time (h)	Na-22_ L40, time (h)	Na-22_ L30, time (h)	Na-22_ L20, time (h)	Na-22_ L10, time (h)
Leading edge, 10 % of tracer peak concentration	299	312	321	343	425
Leading edge, 50 % of tracer peak concentration	423	434	443	467	576
Tracer peak concentration	730	738	744	760	886
Tail, 10 % of tracer peak concentration	4 353	4 326	4 307	4 256	4 085
Tail, 1 % of tracer peak concentration	NA	NA	NA	NA	NA
Tail, 0.1 % of tracer peak concentration	NA	NA	NA	NA	NA
Decay corrected activity per mass unit of solution at outlet, at	**Na-22_L50_ ER200, activity (Bq/g)**	**Na-22_L40, activity (Bq/g)**	**Na-22_L30, activity (Bq/g)**	**Na-22_L20, activity (Bq/g)**	**Na-22_L10, activity (Bq/g)**
Tracer peak concentration	1 422.37	1 436.42	1 446.45	1 474.73	1 579.31

* The results for Na-22 with the default mesh (shown as "L50" in Figure H-8) were provided in Table H-4 (shown as "Na-22").
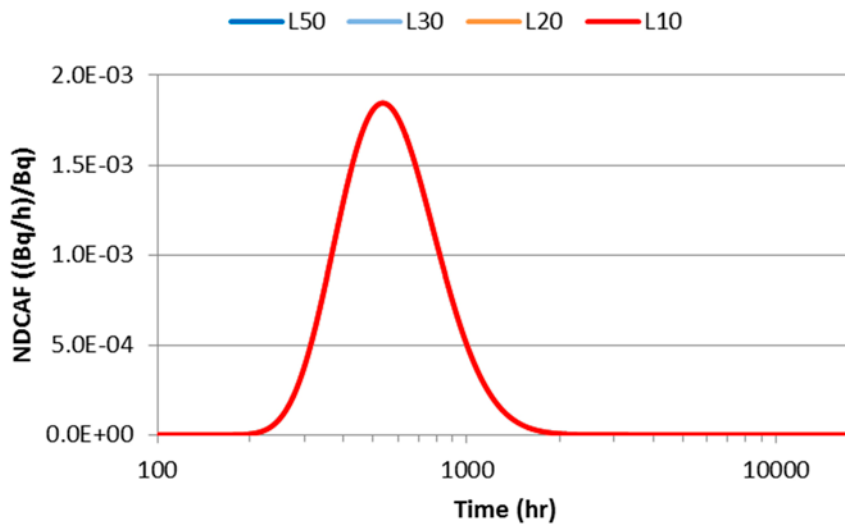
Figure H-7. *The mesh dependency of Cl-36 predictions for the WPDE-2 experiment. The legend shows the number of layers in rock matrix, which was discretized along the axis perpendicular to the slot.*
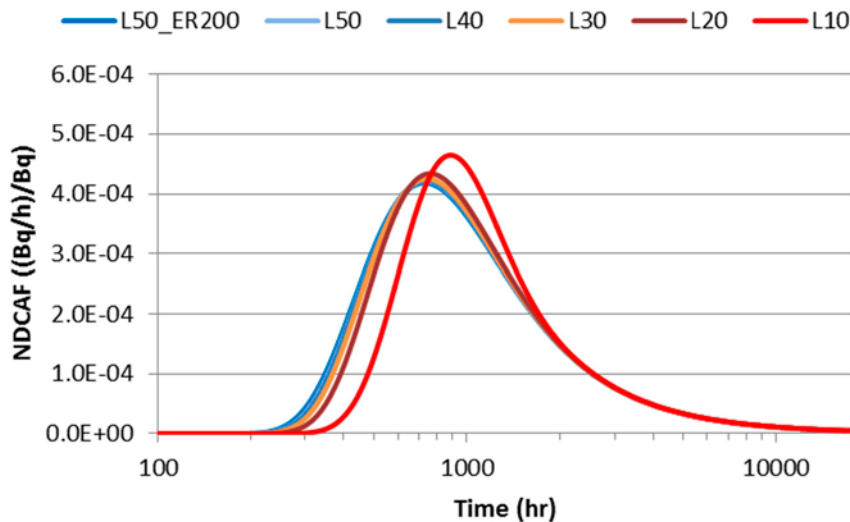

Figure H-8. *The mesh dependency of Na-22 predictions for the WPDE-2 experiment. The legend shows the number of layers (L10~L50) in rock matrix, which was discretized along the axis perpendicular to the slot. In the legend, "ER200" indicates that the element ratio was set to 200, while it was 20 for the others.*

The prediction results for Ba-133 that was the most strongly sorbing tracer in the WPDE experiments were highly dependent on the mesh refinement such as the number of layer and the element ratio for the rock matrix. For the mesh with 50 layers in the rock matrix, the effects of element ratio on the prediction were examined within its range of 20 to 300. When the ratio was more than 200, the breakthrough curve seems to be nearly converged (Figure H-9). The lower element ratio of meshes produced totally different shapes of breakthrough curves including the peak arrival time, the peak concentration, and the time taken to arrive at the outlet. For example, with the element ratio of 20, the peak arrival was predicted to be about 1 700 h later than those of the converged ones and the discrepancy in peak concentration between them was about 27 % (Table H-10). It means that the default element ratio, which had been suitable for non- or weakly sorbing tracers, must be inappropriate to the prediction for this strongly sorbing tracer.
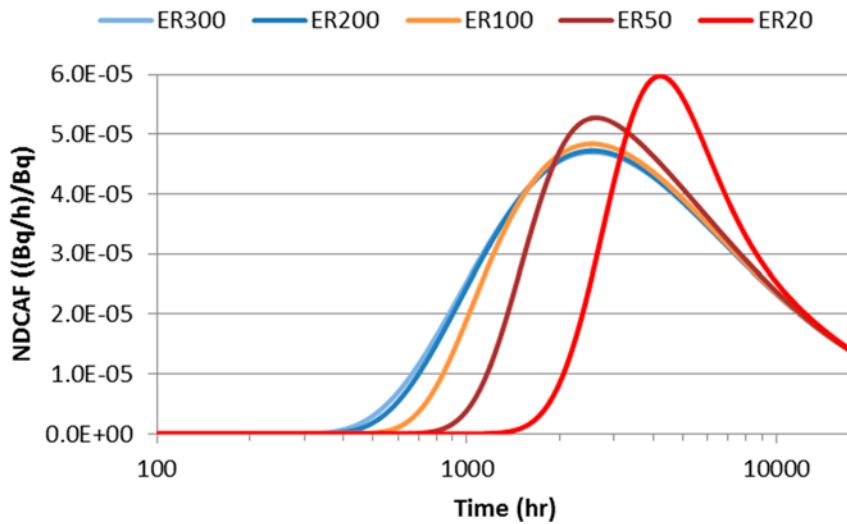
Figure H-9. The mesh dependency of Ba-133 prediction on the element ratio assigned in the rock matrix (assuming the 50 layers in the rock matrix).
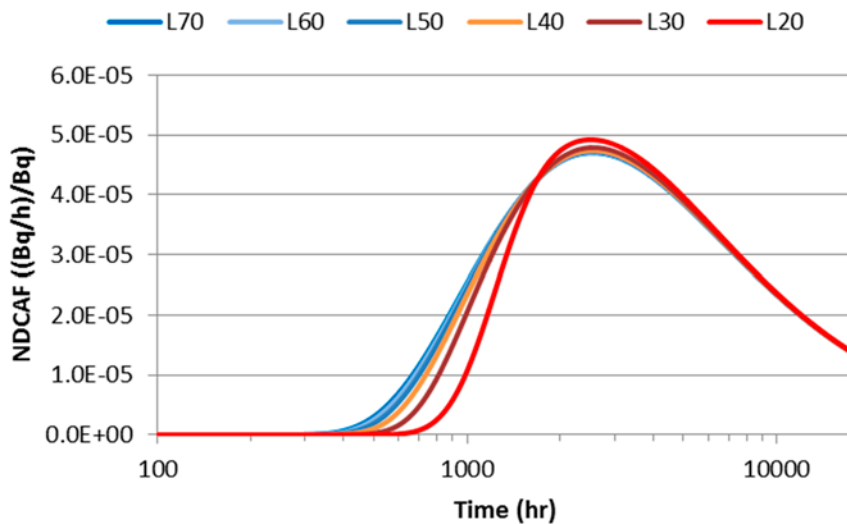

Figure H-10. The mesh dependency of Ba-133 prediction on the number of layers in the rock matrix, which was discretized along the axis perpendicular to the slot (assuming the element ratio of 200).

Figure H-10 illustrates that when the element ratio was 200, the prediction with the mesh having 20 layers in the rock matrix seems to be somewhat converged with similar peak concentration and arrival time but different time taken to arrive at the outlet. Strictly, as well as the element ratio of 200, more than 50 layers were necessary to obtain a reliable prediction for Ba-133 in a reasonable computational time (Figure H-10 and Table H-11). These results imply that the more sorbing tracer is, the finer mesh is required at the interface between the slot and the rock matrix for accurate prediction. From these results, the result for Ba-133 provided in Figure H-3 and Table H-4 in Section H3.1 was obtained with the most refined mesh at the interface between the slot and the rock matrix among ones tested in this model for achieving the accurate prediction for this tracer, including the element ratio in the rock matrix of 200, the number of rock matrix layers of 70. However, the mesh discretization along the axis parallel to the slot was insignificant in the convergence of prediction (Figure H-11).

Table H-10. The performance measures of convergence study on mesh discretization (element ratio in the rock matrix) of Ba-133 for the WPDE-2 experiment.

Performance measures prediction WPDE-2 for mesh dependent

Time when event occurs	Ba-133_ ER300, time (h)	Ba-133_ ER200, time (h)	Ba-133_ ER100, time (h)	Ba-133_ ER50, time (h)	Ba-133_ ER20, time (h)
Leading edge, 10 % of tracer peak concentration	545	583	729	1045	1887
Leading edge, 50 % of tracer peak concentration	956	980	1096	1470	2637
Tracer peak concentration	2548	2548	2542	2618	4219
Tail, 10 % of tracer peak concentration	NA	NA	NA	NA	NA
Tail, 1 % of tracer peak concentration	NA	NA	NA	NA	NA
Tail, 0.1 % of tracer peak concentration	NA	NA	NA	NA	NA
Decay corrected activity per mass unit of solution at outlet, at	**Ba-133_ ER300, activity (Bq/g)**	**Ba-133_ ER200, activity (Bq/g)**	**Ba-133_ ER100, activity (Bq/g)**	**Ba-133_ ER50, activity (Bq/g)**	**Ba-133_ ER20, activity (Bq/g)**
Tracer peak concentration	192.76	193.70	198.32	216.25	244.90

Table H-11. The performance measures of convergence study on mesh discretization (number of layers in the rock matrix) of Ba-133 for the WPDE-2 experiment.

Performance measures prediction WPDE-2 for mesh dependent

Time when event occurs	Ba-133_L60, time (h)	Ba-133_L40, time (h)	Ba-133_L30, time (h)	Ba-133_L20, time (h)
Leading edge, 10 % of tracer peak concentration	560	623	701	874
Leading edge, 50 % of tracer peak concentration	965	1008	1067	1241
Tracer peak concentration	2546	2552	2557	2507
Tail, 10 % of tracer peak concentration	NA	NA	NA	NA
Tail, 1 % of tracer peak concentration	NA	NA	NA	NA
Tail, 0.1 % of tracer peak concentration	NA	NA	NA	NA
Decay corrected activity per mass unit of solution at outlet, at	**Ba-133_ L60, activity (Bq/g)**	**Ba-133_ L40, activity (Bq/g)**	**Ba-133_ L30, activity (Bq/g)**	**Ba-133_ L20, activity (Bq/g)**
Tracer peak concentration	193.21	194.59	196.43	201.83

* The results for Ba-133 with the layer numbers of 70 and 50 (shown as "L70" and "L50" in Figure H-10) were provided in Table H-4 (shown as "Ba-133") and Table H-10 (shown as "Ba-133_ER200"), respectively.
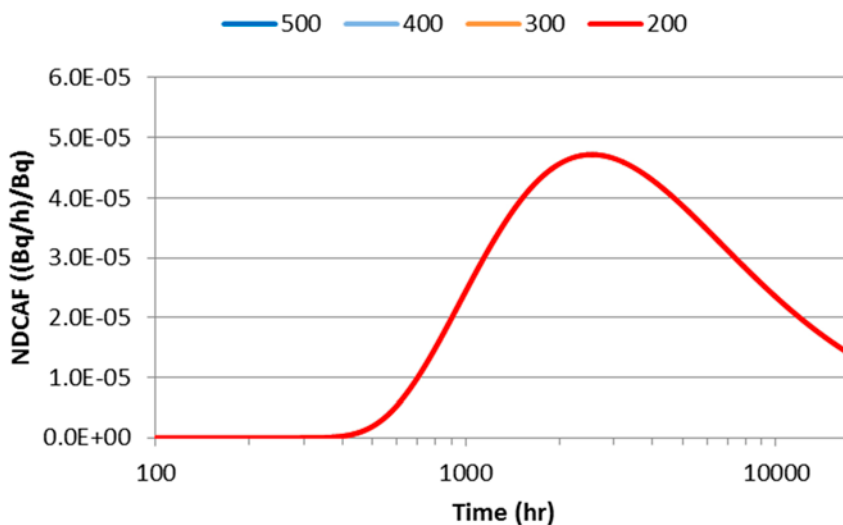

Figure H-11. *The dependency of the Ba-133 predictions on the mesh discretization along the axis parallel to the slot. The legend shows the numbers of elements.*

H4 Discussion, conclusions and recommendations

For Task 9A as the 'Warmup' case, we conducted semi-predictive numerical modelling for the WPDE campaigns with the traditional solute transport by assuming simple and ideal experimental conditions. These results are expected to be considered as the reference case in the later subtasks related to these experiments. The results demonstrated that under the experimental conditions given in WPDE campaigns, sorption and its measurement uncertainty were more influential on the behaviours of tracers in the drillhole and rock matrix than diffusion. Breakthrough curves, including peak concentration, peak arrival time, width of curve, and time taken to arrive at the outlet, were dependent on the sorption parameter, or partitioning coefficient, of tracers for the type of rock in the drillhole.

The sorption did not affect only the behaviours of tracers in the experiments but also the accuracy of prediction obtained in this modelling work. Particularly, the breakthrough curve of Ba-133, which was the most strongly sorbing tracer among the ones injected in the experiment, was highly sensitive to the mesh discretization of model domain corresponding to the rock matrix, strictly the interface between the slot and rock matrix. It means that for the accurate and reliable prediction of sorbing radionuclides the mesh discretization suitable to their transport properties should be involved in the modelling. It again highlights that the numerical solution for the behaviours of respective tracers having different properties needs to be validated in the modelling procedure for ensuring a satisfactory level of accuracy.

The sensitivity analysis to dispersivity showed that the hydrodynamic dispersion could be one of the factors dominant to the fate and transport of tracers in the WPDE experiments. In particular, it was shown that the relatively rapid peak arrivals and dispersed shape of curve could be predicted with large dispersivity. If the hydrodynamic dispersion in the slot was dominant on the behaviours of tracers in the experiments, it must be necessary to characterize the effects of hydrodynamic dispersion in these experiments definitely before examining the diffusion and sorption into the rock matrix. We will carry out additional numerical experiments for the hydrodynamic dispersion for the later subtasks associated with Task 9A.

We think that the highly heterogeneous microstructures such microfractures and mineral grains in the rock matrix would have large and small, or significant, influences on the behaviours of tracers including sorption and diffusion in fractured rocks, including WPDE experiments. However, the assessment of the effects of microstructures must be a highly complicated task because this process needs to characterize geometry, distribution, and property of numerous microstructures in rock matrix and then to describe them numerically into the model. Maybe, it might need to sort out more significant microstructures in transport of tracers such as open and connected microfractures or chemically sorption-affinitive mineral grains among all the microstructures and the uncertainty analysis for their properties should also be involved. Many small mineral grains and thin microfractures in the model domain would result in an enormous computational demand owing to the fine discretization to describe them. Therefore, it will be necessary to find a computationally effective way to represent microstructures without any significant loss in accuracy of prediction. Through solving these various problems, we will consider the effects of microstructures in the rock matrix in the later subtasks for the more realistic modelling.

Japan Atomic Energy Agency, Tokai, Japan

Yukio Tachi, Tsuyoshi Ito

I1 Introduction

I1.1 Background

The Japanese approach for development of HLW disposal concept has targeted neither a particular type of rock nor a particular area. The H12 report (JNC 1999) was published based on two decades of R&D activities and showed that disposal of HLW in Japan is feasible and can be practically implemented at sites which meet certain geological stability requirements. The Final Disposal Act which came into force in 2000 specifies deep geological disposal of HLW at depths greater than 300 metres, together with a stepwise site selection process in three stages. Nuclear Waste Management Organization of Japan (NUMO) was established in 2000 as an implementing body authorized by the Final Disposal Act. NUMO initiated the siting process with open solicitation of volunteer host municipalities for exploring the feasibility of constructing a final repository. This open solicitation approach was started in 2002. However, no municipalities have applied as volunteer areas. The Japanese Government has reviewed the siting process and has restarted by new approach.

Crystalline rocks such as granitic rocks are one of potential host rocks for the geological disposal of radioactive waste in Japan. The H12 report (JNC 1999) and recent safety report (NUMO 2013, JAEA 2015) has focused on the crystalline rocks as reference host rocks. JAEA has constructed the purpose-built generic underground research facility (URL) at Mizunami in Gifu, central Japan. The Mizunami URL Project is a comprehensive geoscientific research project investigating the deep underground environment within crystalline rock. However, the migration studies using radioactive tracers cannot be conducted.

To obtain reliable migration data under in situ conditions and to develop and validate radionuclide migration models for the in situ migration tests, JAEA has joined some international projects such as the Grimsel Test Site (GTS) project in Switzerland. The Long-term diffusion (LTD) project at the GTS is one of key projects to develop the migration model and related dataset for the performance assessments in Japan. Task 9 of SKB Task Force on Modelling of Groundwater Flow and Transport of Solutes can give us the chance to apply the modelling approaches developed in the LTD project for different types of granitic rocks and in situ migration concepts.

I1.2 Objectives

The transport of radionuclides in fractured crystalline rocks can be conceptualized by a dual-porosity model where radionuclides are transported by advective water flow through the fracture and diffusion into the surrounding rock matrix (Neretnieks 1980). Radionuclides can diffuse into the pore network of the rock matrix from the fracture surfaces and sorb onto the pore walls. Diffusion and sorption of radionuclides in rock matrix are therefore key processes controlling the safety of the geological disposal. In order to develop a reliable model and obtain parameters for the long-term safety assessment, it is necessary to understand and quantify the diffusion and sorption processes in rock matrix. The key issues for radionuclide migration in crystalline rocks have been identified such as heterogeneity in fracture and matrix including mineral and pore distribution, fracture fillings and foliation, cation excess diffusion and anion exclusion, transfer of sorption data from crushed rock to intact rock, etc. (SKB 2004, NEA 2012).

In order to solve the above-mentioned issues and develop a method for providing realistic migration parameter values, the link between laboratory and in situ experiments are critically important (e.g. Missana et al. 2006, Tachi et al. 2015). Laboratory experiments can provide reliable data and mechanistic understanding under a wide range and well-defined boundary conditions. On the other hand, in situ experiments can play important roles providing site-specific data under real conditions. Diffusion and sorption parameters are typically derived from laboratory experimental results using drilled or crushed rock samples, which have different properties in porosity, pore-connectivity and reactive surface area in comparison with in situ conditions. The laboratory measurements

can therefore lead to overestimation of matrix diffusion and sorption properties. To set reliable parameter values of matrix diffusion and sorption relevant to performance assessment, it is necessary to understand in detail the processes of diffusion and sorption both in the laboratory and in situ experiments, and to develop a way to extrapolate from the laboratory to in situ conditions.

These issues have been investigated by coupling laboratory and in situ experiments as part of the LTD project at the GTS, Switzerland (Soler et al. 2015, Tachi et al. 2015). From the comparative experimental and modelling studies between laboratory and in situ conditions we conclude that the following mechanisms are important for predicting radionuclide migration in the Grimsel granodiorite. The cation excess diffusion is a key mechanism in the Grimsel granodiorite, whereas the anion exclusion effect seems to be relatively minor. The high sorption at the disturbed surface in cored samples for laboratory experiments is critically important to evaluate radionuclide transport in both laboratory and in situ tests. The difference in porosity between laboratory and in situ conditions is also a key factor to scale laboratory data to in situ conditions.

Further studies are needed to test the applicability of the proposed extrapolating approach from laboratory to in situ conditions for a wider range of radionuclides, and for the different type of crystalline rocks. The Task 9 of SKB taskforce focusing on the modelling of different types of in situ tracer tests; WPDE-1 and WPDE-2 (Water Phase Diffusion Experiment) and TDE (Through-Diffusion Experiment) at ONKALO, LTDE-SD (Long Term Sorption Diffusion Experiment) at Äspö are good dataset for testing the approach developed for the Grimsel LTD project. For these objectives, predictive modelling of the in situ tracer experiments WPDE-1 and WPDE-2, performed within the REPRO (rock matrix Retention Properties) project, is performed based on the modelling approach developed in the Grimsel LTD project and the rock properties of the REPRO site at ONKALO.

I1.3   Scope and limitations

As mentioned above, the JAEA's approach for predictive modelling of WPDE-1 and WPDE-2 is based on the combination of the scaling approach from laboratory to in situ condition developed for Grimsel LTD project (Tachi et al. 2015, Soler et al. 2015) and key features of rock properties at REPRO site. Final goals of the modelling for WPDE-1 and WPDE-2 is to represent solute transport and retardation in ONKALO rocks by applying the scaling approach and considering key features and processes in WPDE in situ experiment. Focus and limitations of our preliminary modelling in Task 9A are;

Task 9A is first warm-up case for Task 9 for targeting the more realistic model representing solute transport and retardation in the matrix and fracture in natural crystalline rocks. First scope is to familiarize with the experimental setup of the WPDE campaign, in terms of geometries; flows; boundary conditions; supporting laboratory data; etc.

One of key features of our modelling approaches in the Grimsel LTD project is the parameter scaling from laboratory data to in situ conditions. This approach will be applied preliminarily for WPDE setup considering key features of rock properties at REPRO site.

Based on the preliminary modelling in Task 9A including sensitivity analysis and alternative models, key assumptions and uncertainties in model and related parameters will be identified by investigating which factors will have major or minor impact on the breakthrough curves. In addition, the first consideration of both parameter uncertainty and conceptual model uncertainty will be provided.

One of key features of our modelling approaches developed in the Grimsel LTD project is the parameter scaling from laboratory data to in situ conditions. However, the relatively limited supporting laboratory program reported in Task Description may not have captured the ideal parameter estimation. The limitations and challenges in the preliminary modelling will be also discussed.

I2   Methodology and model

I2.1   Conceptual description of features, events and processes of the experiments

The Water Phase Diffusion Experiment (WPDE) features advection-diffusion-sorption experiments which are carried out in a drillhole ONK-PP323, about 18 to 20 m away from the niche wall. A 1.9 m long section has been packed off, and in this section a dummy rod that is coaxial with the drillhole

has been placed, leaving a 1.25 mm gap between the drillhole wall and the dummy rod. This gap is regarded as an artificial fracture of relatively well-defined geometry. In this gap a very low steady state water flow has been applied, directed towards the niche. This is achieved by injecting the water at the far end of the packed-off section. Two experiments have been performed at different flow rates; WPDE-1 (20.1 μL/min) and WPDE-2 (10.0 μL/min), using different tracers; WPDE-1 (HTO, Na-22, Cl-36 and I-125) and WPDE-2 (HTO, Na-22, Cl-36, Sr-85 and Ba-133) (Task Description, Section 1.3.1).

The experimental section (17.95–19.85 m) in WPDE drillhole is predominantly surrounded by the rock type VGN (veined gneiss). However, a fraction of the drill core, such as the section from about 18.30–18.45 m, is predominantly of the rock type PGR (pegmatitic granite). It has been roughly estimated that little over 90 % of the experimental section is surrounded by veined gneiss, while a little less than 10 % is surrounded by pegmatitic granite (Task Description, Section 2.4.1). By detailed investigation of the drill core, it was estimated that the maximum foliation angle ranges from 60° to 90°relative to the axis of the drill core. The main direction of the foliation is almost perpendicular to the drill core axis in the veined gneiss, however, the pegmatitic granite of the section can be considered to be non-foliated. An average mineralogy of the veined gneiss and the pegmatitic granite of the drill section was reported in Task Description, Section 2.4.1. The veined gneiss has high contents (~30 %) of micas, mainly biotite.

The key assumption of the modelling in the WPDE is whether the rock matrix is either homogenous or heterogeneous. One example of simple heterogeneous model is the heterogeneity of rock types along the experimental sections. This may be considered by dividing the rock matrix along the experimental sections into a few different rock types. Second example is heterogeneous mineral and pore distributions in the rock matrix. The above-mentioned foliation effect may be related to the second example.

In addition to these heterogeneous effects, the effects of the borehole disturbed zone (BDZ) may be important in the WPDE setup. The process of drilling in the in situ condition and subsequent sample treatment for laboratory testing results in newly created cracks and microcracks through stress release and disturbance (e.g. Skagius and Neretnieks 1986, Autio et al. 1998, Tullborg and Larson 2006). The effects of the BDZ have been investigated in the in situ LTD experiment conducted at the GTS (Soler et al. 2015, Tachi et al. 2015). These results indicated that the BDZ effect caused high porosity, diffusivity and sorption capacities in near-surface disturbed zones. The BDZ effects may be modelled by considering a layered rock matrix representation featuring cylindrical layers that are coaxial with the drillhole.

Traditional advection and dispersion must be considered as the key processes in the water filled annular slot between the drillhole wall and the dummy rod in the experimental setup of WPDE. Single and constant flow rate through the experimental section was set, the measured flow rates were 20.1 ± 0.6 μL/min and 10.0 ± 0.4 μL/min for WPDE-1 and -2, respectively. No detailed information on channelized flow such as the flow distribution or potential channelling pattern in the experimental section is provided. However, channelized flow may occur in the annular slot due to surface roughness of the drillhole wall and injection method of tracer solution to the annular slot. In fact, heterogeneous channelized flow was observed in the laboratory experiment using same setup with WPDE performed in Helsinki Univ. (presented at Taskforce workshop held in Sept. 2014).

Matrix diffusion can be usually modelled by assuming Fickian diffusion in the homogeneous porous medium of the granitic rock matrix. Diffusion processes in granitic rock matrix become much more complicated due to the heterogeneous distribution of pore space and reactive mineral surfaces. Granitic rock matrices are generally composed of quartz, feldspars and micas with typical grain sizes of the order of mm to cm. The domain pore spaces between these mineral grains and intragranular secondary pores form water-filled and heterogeneous networks with varying geometric factors such as tortuosity and constrictivity (e.g. EUR 2005, Sardini et al. 2006). A number of experimental and modelling studies have been conducted in order to understand and predict these complex diffusion processes (e.g. Sardini et al. 2007, Cvetkovic and Cheng 2008, Voutilainen et al. 2013).

Laboratory measurements of matrix diffusion have been performed using small, thin rock samples by through-diffusion (TD) and/or in-diffusion (ID) tests. Rock samples used for laboratory experiments are typically centimeter scale and are generally taken from drillcores. The process of drilling and

subsequent sample shaping for laboratory experiments results in newly created cracks and micro-cracks through stress release and disturbance (e.g. Skagius and Neretnieks 1986, Autio et al. 1998, Tullborg and Larson 2006). Increased porosity values in laboratory samples at artificially disturbed conditions compared to in situ conditions have been reported (e.g. Ota et al. 2003, Tullborg and Larson 2006, Jokelainen et al. 2013). These differences in porosity may be considered in parameter setting by scaling from laboratory data to in situ conditions.

In addition to the scaling of porosity, the possible contribution of cation excess diffusion and anion exclusion to matrix diffusion may be needed to model in the granitic rocks (e.g. Skagius 1986, Ohlsson and Neretnieks 1998, SKB 2004). These effects have often been found to have a big impact on the effective diffusivities, and to be strongly dependent on porewater salinity in compacted bentonites (e.g. Muurinen 1994, Kato et al. 1995, Eriksen and Jansson 1996, Glaus et al. 2007, Van Loon et al. 2007, Tachi et al. 2014, Tachi and Yotsuji 2014) and argillaceous rocks (e.g. Van Loon et al. 2004, Tachi et al. 2011). Although these phenomena are not yet well recognized in crystalline rocks (e.g. SKB 2004), cation excess diffusion can be identified as a key mechanism both laboratory scale and in situ conditions in the Grimsel granodiorite (Tachi et al. 2015). These effects and their dependencies on mineralogy and heterogeneity including foliation may be considered in the model-ling of WPDE.

Reversible instantaneous sorption with a linear isotherm, meaning that the traditional K_d concept may be assumed in the granitic rock matrix (e.g. JNC 1999). Possible importance of sorption kinet-ics, irreversibility and the saturation of sorption sites may be concerned, however these processes are not usually considered in the calculations for the performance assessment (SKB 2004). In addition, there are significant difficulties in the definition of sorption parameter values for actual in situ rock matrix. The major difficulty lies in the estimation of sorption data from crushed rock to intact rock. Most sorption data has been measured by the batch method using crushed rock samples with a typical grain size in the range of microns to sub-millimeters. The crushing process creates new surfaces that significantly increase the specific surface area and the reactive sites that give larger sorption capacities (e.g. Missana et al. 2006, André et al. 2009b). The relationship between K_d values and particle size or specific surface area have been widely investigated by batch sorption tests (e.g. Byegård et al. 1998, Crawford et al. 2006). The K_d values have been seen to increase as the particle size decreases, and a strong correlation between sorption capacity and specific surface area has been observed over a range of particle sizes (Byegård et al. 1998). Recent K_d setting for performance assessments (Crawford 2010, Hakanen et al. 2014) used a correction factor which takes into account the differences in surface areas of crushed rocks used in laboratory sorption measurements and intact rock (in situ conditions). Although qualitative estimation is still an open question, in situ K_d values for granite matrix could be estimated from batch measurement using appropriate particle sizes by comparing the K_d values obtained for laboratory and in situ experiments (Tachi et al. 2015).

I2.2   Description of features, events and processes in the conceptual model

Based on the conceptual description of the features, events and processes (FEPs) mentioned above, the conceptual model for radionuclide transport in the WPDE setup was developed for a simplified and pragmatic representation. The radionuclide transport in the experimental drillhole section was modelled taking into account advection and dispersion in the water-filled annular slot between the drillhole wall and the dummy rod, and diffusion and sorption in the surrounded rock matrix. The key assumption of the modelling in the WPDE setup is that the rock matrix is simplified and homogenous.

We assumed homogeneous properties of VGN (veined gneiss) by ignoring around 10 % PGR (peg-matitic granite) distributed in a banded zone. On the other hand, the borehole disturbed zone (BDZ) has big impacts on both diffusion and sorption processes, then the BDZ effect can be modelled by considering a layered rock matrix representation featuring cylindrical layers that are coaxial with the drillhole.

Traditional advection and dispersion was assumed in the experimental drillhole section in the central model. Details of tracer injection methods using special equipment with a spiral globe were ignored and assumed to be homogeneous distributions of tracers at cross-section of the inlet to the experimental section. Single and constant flow rate through the experimental section was set, the

measured flow rates were directly used; 20.1 ± 0.6 μL/min and 10.0 ± 0.4 μL/min for WPDE-1 and -2, respectively. A dispersion effect in the slot caused by variations in flow velocity was investigated in an alternative modelling case.

Detailed information on the flow distribution or potential channelling pattern in the experimental section is not provided. However, we assumed a simplified channelling model based on observations using a colored tracer as an alternative case.

Traditional diffusion and sorption model was assumed in all modelling. Fickian matrix diffusion was assumed as the transport mechanisms in rock matrix. However, cation excess and anion exclusion effects were assumed based on the observations in Grimsel LTD project (Tachi et al. 2015) and supporting laboratory experiments using WPDE rock samples (presentation by Voutilainen at 2015 Task 9A workshop).

Traditional K_d model assuming instantaneous and reversible sorption was considered. The kinetics, irreversible, and isotherm effects may have to be considered, but we ignored these effects in this modelling. Based on the experience in Grimsel LTD project, the BDZ effect is critically important for deriving sorption and diffusion parameters at near-surface matrix. The K_d values derived for the disturbed near-surface part were significantly larger than the undisturbed matrix. Then we assumed a two-layer matrix consisting of the BDZ with 1 mm thickness and the undisturbed matrix with heterogeneous properties. At the disturbed surface, we assumed "High porosity, D_e and K_d, and their gradual change with linear slope to matrix".

Foliation effect may have strong impact on the effective diffusivity in the rock matrix. Considering the mineralogy with high contents of mica and strong foliation in the rock at REPRO site (presentation by Voutilainen at 2015 Task 9A workshop), these effects may be important in the modelling of WPDE.

These model concepts including key assumptions were modelled step-wisely in the following case setting shown in Figure I-1. As first case-1, the simplest concept considering homogeneous flow and matrix without the BDZ was modelled. In second case, the BDZ effect was considered. The third case defined as central case assumed the foliation effects on the effective diffusivity in the rock matrix (both BDZ and undisturbed matrix).
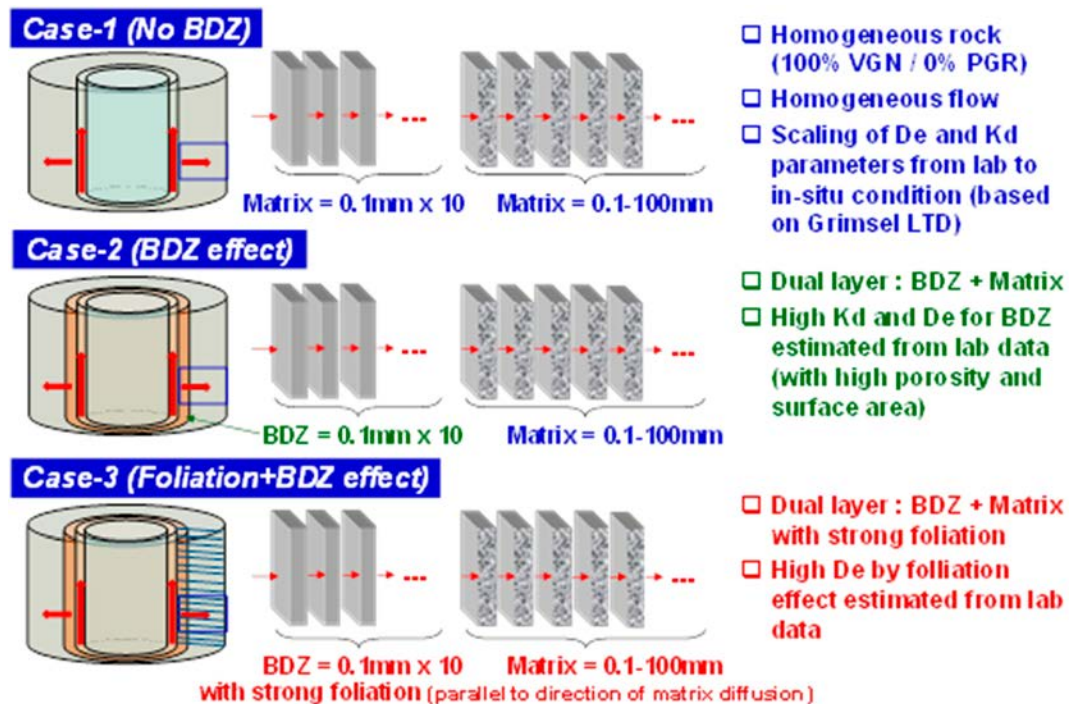

Figure I-1. *Case setting for variation in model concepts and related input parameters.*

I2.3   Model setup

Based on the conceptual model described above, the simplified model setup for radionuclide transport in the WPDE setup was developed as shown in Figure I-2. The radionuclide transport in the experimental drillhole section was modelled taking into account advection and dispersion in the water-filled annular slot between the drillhole wall and the dummy rod, and diffusion and sorption in the surrounded rock matrix.

Advection and dispersion in the artificial fracture (the water-filled annular slot between the drillhole wall and the dummy rod) was accounted as one-dimensional homogeneous flow. The initial conditions in the fracture and matrix are assumed to be zero concentration for all tracers. The boundary conditions for tracer pulse injection were treated to give the homogeneous tracer concentration as a discontinuous function in time (0.83 hours for WPDE-1, 4.94 hours for WPDE-2). In addition, the very low steady state water flows were assumed to be 20.1 µL/min for WPDE-1 and 10 µL/min for WPDE-2. The dispersion effect in the slot caused by variations in flow velocity is expressed by a dispersion coefficient.

Matrix diffusion and sorption was also modelled assuming homogeneous property of the matrix, however, the variation of diffusion and sorption properties in the BDZ was considered. Matrix diffusion was expressed by Fickian diffusion model in simplified and homogeneous matrix. Sorption of radionuclides on fracture surface is ignored and sorption on matrix pore surfaces is assumed to be reversible instantaneous sorption with a linear isotherm.

Goldsim software (ver. 10.1; GoldSim 2010) was used as the framework for model implementation. Figure I-3 shows the Goldsim model structure of the WPDE model, and the model components for radionuclide transport in a direction perpendicular to the axis of the borehole, from the inner surface in borehole to the BDZ and the surrounding rock matrix. In Goldsim software, we can create a cylindrical network of Cell pathways with advective and/or diffusive connections. Although such a network can be created manually, if it contains a large number of Cells doing so can become cumbersome and time-consuming. Therefore, GoldSim provides a special element to automate the creation of such Cell networks. The CellNet Generator discretizes a cylindrical region of space and creates a two-dimensional array of Cell elements, including any necessary advective or diffusive mass flux links between them. By using this function, we made the cylindrical cell network including fracture, BDZ and matrix parts. The BDZ was set to be total length of 1 mm and the mesh size was 0.025 mm. The matrix depth was set to be 20 cm with stepwise geometric propagation.
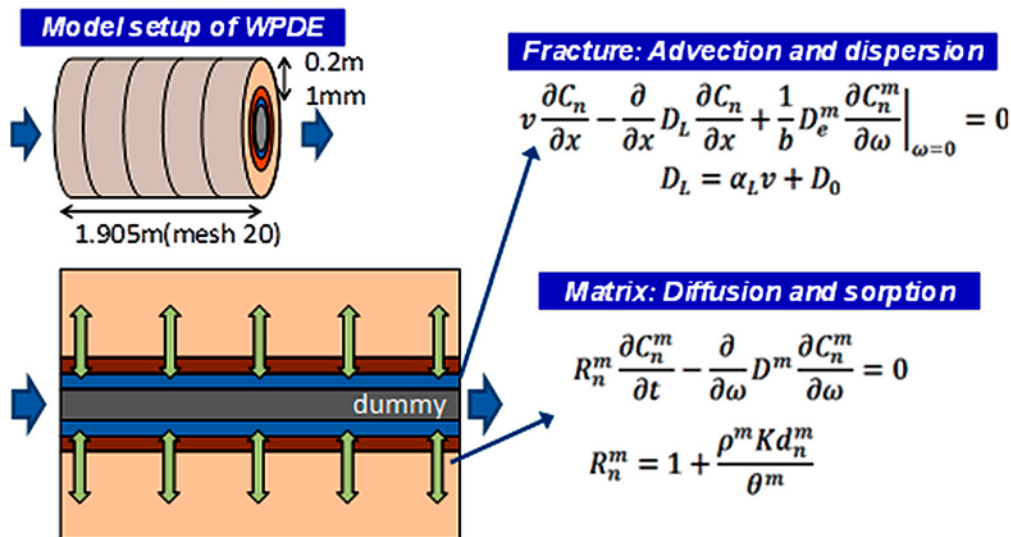

Figure I-2. *Conceptual model and governing equations for our simulation for WPDE (v; flow velocity, C_n and C_n^m ; concentration in fracture and matrix, D_L ; dispersion coefficient in fracture, α_L; dispersion length, D_0; diffusion coefficient in free water, b; half of fracture aperture, D_e^m ; effective diffusion coefficient in matrix, R_n^m ; retardation coefficient in matrix, D^m ; diffusion coefficient in matrix pores, ρ^m ; dry density, Kd_n^m ; distribution coefficient, θ^m ; porosity).*
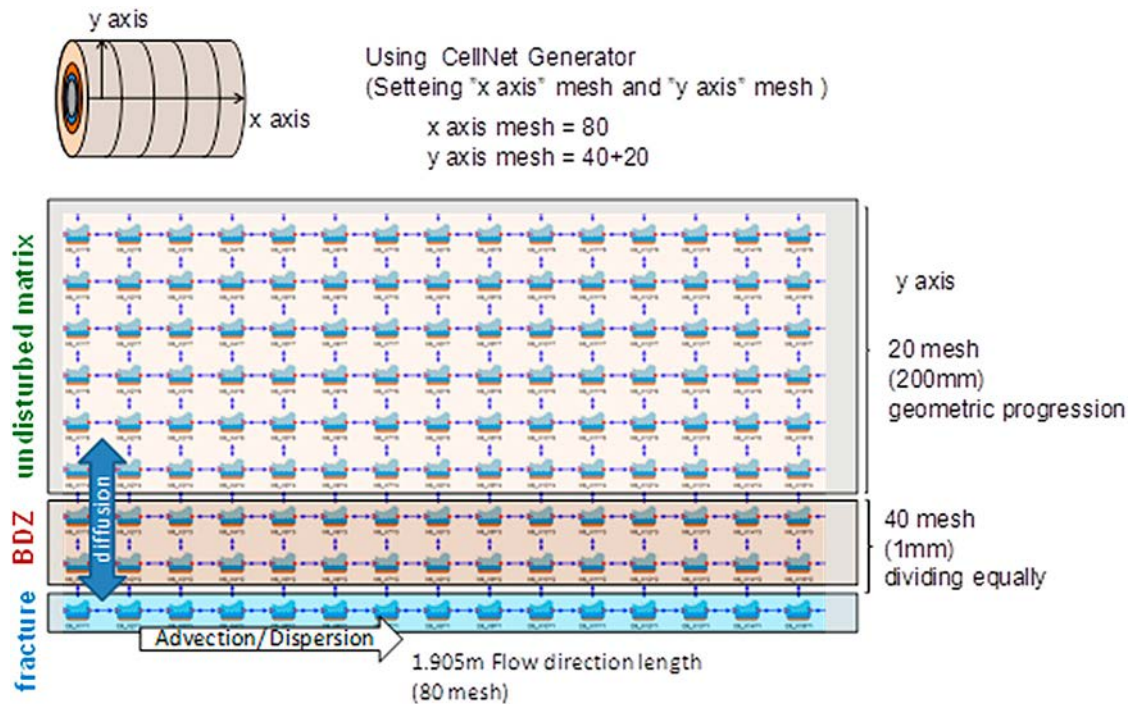
Figure I-3. *Goldsim model structure of the WPDE, made by the cylindrical cell network including fracture, BDZ and matrix.*

I2.4   Input data

Our modelling approach focused on predictive modelling based on transport parameter setting by scaling from laboratory measurements to in situ conditions. The scaling method from laboratory data to in situ condition developed for the GTS was applied and tested for the WPDE at ONKALO. Transport parameters for above-mentioned three cases were set by considering model variations and their impact on transport parameters including porosity (ε), effective diffusivity (D_e) and distribution coefficient (K_d). The transport parameters were scaled from laboratory data to in situ conditions, assuming their relationship to rock properties.

Traditional advection and dispersion must be considered as a key process in the water filled annular slot between the drillhole wall and the dummy rod in the experimental setup of WPDE. Flow rate and dispersion length are key input parameters to be determined, although these are independent on the above-mentioned model concepts.

Single and constant flow rates through the experimental section were set directly based on the measured flow rates; 20.1 ± 0.6 μL/min and 10.0 ± 0.4 μL/min for WPDE-1 and -2, respectively. Dispersion length was set in the accordance with H12 report (JNC 1999). Gelhar et al. (1992) argue that the dependence on distance of the longitudinal dispersion length arises not only due to variations in permeability, but also due to the inaccuracy of the measurements themselves. They reviewed the measurements data for 59 sites, and derived the relationship between the longitudinal dispersion length and evaluation distance. In addition, Neuman (1995) has concluded from field and laboratory measurements that, irrespective of whether the medium is fractured or porous, the longitudinal dispersion length can be expressed by the regression line ($\alpha_L = 0.017L^{1.5}$) when the evaluation distance is between 10cm and 3.5km. The longitudinal dispersion length derived from this equation was therefore used in the central case. In addition, the values of 0 and 1/10 m are compared in the sensitivity case.

The transport parameters including effective diffusivity (D_e) and distribution coefficient (K_d) were determined based on the dataset derived from laboratory diffusion and sorption experiments and their scaling to in situ conditions. No corrections for geochemical conditions are needed because the in situ geochemical conditions are consistent between laboratory and in situ experiments. All uncertainties related to laboratory-measured dataset (D_e, K_d, porosity) and their scaling were considered in consistent way for deriving the in situ dataset.

The effective diffusivity (D_e) were determined based on porosity and diffusion dataset derived from laboratory diffusion experiments. The extrapolating method from the laboratory to the in situ condition taking into account the difference in porosity between laboratory and in situ conditions. There have been many attempts to relate the effective diffusivity or the formation factor to the porosity. The most common empirical relationship is a power-law correlation, the so-called Archie's law (Archie 1942, Boving and Grathwohl 2001, Autio et al. 2003, Witthüser et al. 2006). The D_e parameters for all tracers were scaled from laboratory data to in situ conditions, assuming the exponent in the Archie's law as 1.58, derived using dataset obtained for Äspö diorite described in Ohlsson (2000) (Figure I-4).

First dataset can be derived from the D_e data for tritiated water (HTO) and Cl measured for the VGN samples at ONKALO reported in the Task Description (Table 2-9). These data seems to be measured data for the direction perpendicular to foliation. However, there are no data of D_e for cations (Na$^+$, Sr^{2+}, Ba^{2+}) measured for the REPRO rocks. Then we referred the D_e dataset measured for diorite samples at Äspö (which is similar high biotite content), reported in Byegård et al. (1998). As shown in Table I-1 [a1], D_e data are consistent between the two rocks, VGN at ONKALO and diorite at Äspö. These datasets were scaled to in situ conditions by considering the difference in porosity (0.97 % for laboratory and 0.63 % for in situ) and Archie's law (Figure I-4), as shown in Table I-1 [a2]. In case-1 and case-2, these datasets [a1 and a2] were used for the BDZ and undisturbed matrix, respectively. For the BDZ, the D_e parameters were taken directly from the laboratory through-diffusion dataset.

On the other hand, another dataset of D_e values was derived from the dataset measured for the same VGN sample but for the direction parallel to foliation. These dataset were reported in the presentation material by Voutilainen at 2015 Task 9A workshop (Figure I-5). There are large gaps in D_e values between two directions (perpendicular and parallel to foliation) as shown in Table I-1 [b1]. As in the case for the perpendicular direction, there are no data for cations. Then, D_e values were estimated by scaling from D_e of HTO considering factors for cation excess diffusion (1.2 for monovalent cation, Na$^+$), and 1.4 for divalent cations, Sr^{2+}, Ba^{2+}). These datasets were scaled to in situ conditions by considering the difference in porosity and the Archie's law, as shown in Table I-1 [b2]. In central case (case-3), these datasets [b1 and b2] were used for the BDZ and undisturbed matrix, respectively.
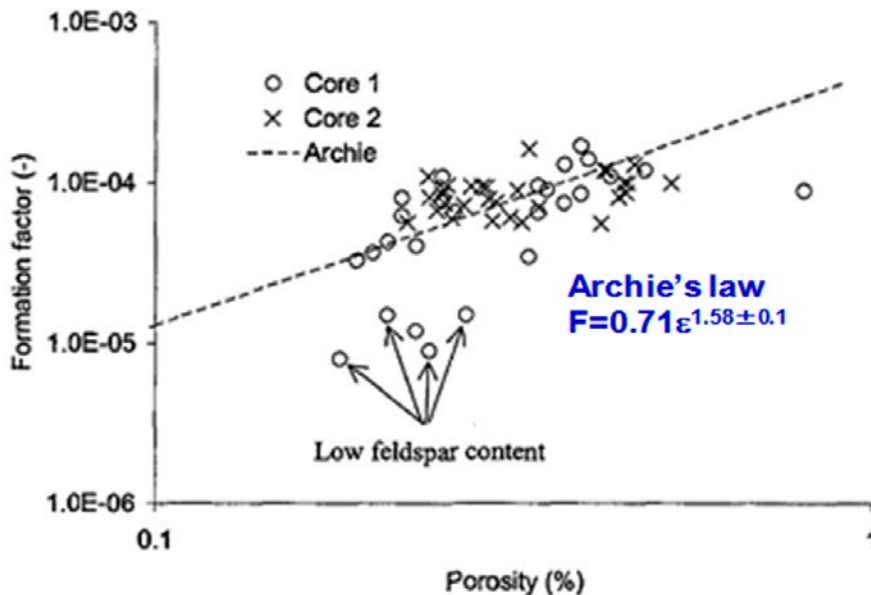

Figure I-4. *Relationship between formation factor and porosity, and curve fit according to Archie's law (Ohlsson 2000).*
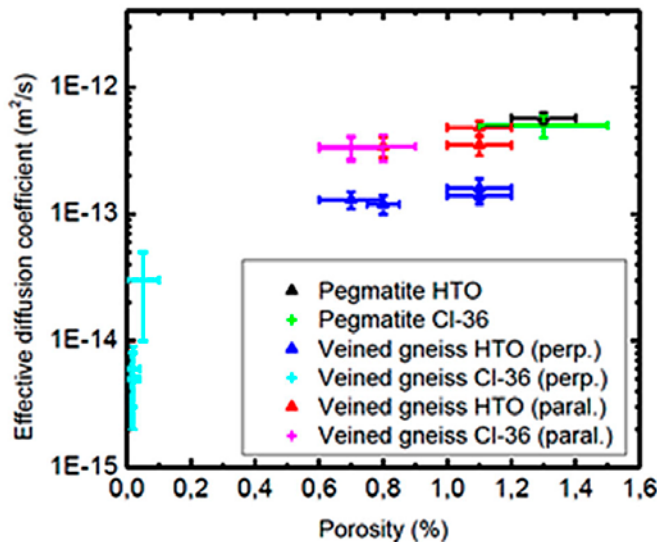
Figure I-5. *Relationship between effective diffusion coefficient and porosity derived by through-diffusion experiment for REPRO rocks (Voutilainen at 2015 Task 9A workshop).*

Table I-1. Diffusion parameters and their uncertainties of radionuclides (RNs) used to simulate the results of WPDE, which are based on laboratory diffusion data derived from the through-diffusion (TD) experiments and their scaling to in situ porosity.

(a) Perpendicular for foliation

Values derived for Laboratory (TD) [Dataset : a1]				Values for in situ scaled from laboratory [a2]		
RNs	D_e (m²/s)	error	reference	RNs	D_e (m²/s)	error
HTO	1.8E-13	2.7E-14	averaged value from Table 2-9. in Task	HTO	9.3E-14	3.5E-14
Cl-36	5.0E-15	3.0E-15	Description (9A)	Cl-36	2.5E-15	2.3E-15
Na-22	7.8E-14	1.0E-15	taken from Byegård et al. (1998) (value	Na-22	3.9E-14	1.0E-14
Sr-85/Ba-133	6.3E-14	1.0E-14	for Aspo diorite with thickness of 1 mm)	Sr-85/Ba-133	3.1E-14	1.4E-14
(HTO)	1.9E-13	3.0E-15				

(b) Parallel for foliation

Values derived for Laboratory (TD) [Dataset : b1]				Values for in situ scaled from laboratory [b2]		
RNs	D_e (m²/s)	error	reference	RNs	D_e (m²/s)	error
HTO	4.3E-13	6.4E-14	averaged value from Voutilainen's	HTO	1.8E-13	7.1E-14
Cl-36	3.5E-13	2.1E-13	presentation at 2015 Workshop	Cl-36	1.5E-13	1.4E-13
Na-22	5.2E-13	6.6E-15	scaled for De of HTO considering	Na-22	2.1E-13	5.0E-14
Sr-85/Ba-133	6.0E-13	9.6E-14	factors for cation excess diffusion (1.2 for Na and 1.4 for Sr/Ba)	Sr-85/Ba-133	2.5E-13	1.0E-13

The distribution coefficients (K_d) values of Na^+, Sr^{2+} and Ba^{2+} for the REPRO rocks were reported in the Task Description (Löfgren and Nilsson 2019, Table 2-11). These data were derived by batch sorption experiments using crushed samples with smaller particle sizes (< 0.3 mm). The major difficulty lies in the transfer of sorption data from crushed rock to intact rock. The crushing process creates new surfaces that significantly increase the specific surface area and the reactive sites that give larger sorption capacities (e.g. Missana et al. 2006, André et al. 2009, Tachi et al. 2015). The relationship between K_d values and particle size or specific surface area have been widely investigated by batch sorption tests (e.g. Byegård et al. 1998, Crawford, 2010). The K_d values seem to increase as the particle size decreases, and a strong correlation between sorption capacity and specific surface area was observed over a range of particle sizes (Byegård et al. 1998). Recent K_d setting for performance assessments (Crawford 2010, Hakanen et al. 2014) used a correction factor which takes into account the differences in surface areas of crushed rocks used in laboratory sorption measurements and intact rock (in situ conditions). In the Grimsel LTD project, sorption of cations was compared among laboratory batch sorption and through-diffusion experiments and in situ diffusion experiment, and was confirmed to be strongly dependent on disturbance due to sample preparation (Tachi et al. 2015). The K_d values for undisturbed granodiorite matrix and disturbed surfaces at the BDZ can be estimated from batch measurement using larger particle sizes (> 1 mm) and smaller particle size (< 0.1 mm), respectively. Although qualitative estimation is still an open question, the K_d values were determined and scaled as follows. The batch-derived K_d values derived for the REPRO rock with small particle size (< 0.3 mm) shown in Table I-2 [a] were applied directly for the values for the disturbed surface at BDZ, and were decreased linearly into undisturbed matrix, in case-2 and case-3. On the other hand, the K_d values for

undisturbed matrix were derived by assuming the K_d dependence on the particle size. For this purpose, the K_d values measured at particle size (0.3 mm) were scaled to larger particle size with 2 mm by using the relationship between K_d values and particle size (Figure I-6), measured for Äspö diorite in Byegård et al. (1998), as shown in TableI-2 [b]. In case-1 to case 3, these dataset [b] was used for the undisturbed matrix.

Table I-2. Sorption parameter values (K_d) and their uncertainties of radionuclides (RNs) used to simulate the results of WPDE, which are based on laboratory sorption data derived from the batch experiments and their scaling to in situ condition.

Rock	RNs	K_d for disturbed surface at BDZ - batch-derived for < 0.3 mm particle - taken from Task Description		K_d for undisturbed matrix - scaled for 2 mm using the relationship between Kd and particle size (Byegård et al., 1998)	
		K_d (m^3/kg)	error	K_d (m^3/kg)	error
VGN	Na-22	1.3E-03	3.0E-04	1.1E-03	3.0E-04
	Sr-85	1.1E-03	3.0E-04	5.9E-04	2.6E-04
	Ba-133	6.0E-02	2.0E-02	2.5E-02	1.5E-02

I2.5   Alternative models and sensitivity cases

As above-mentioned in 9.2.2, the case-3 considering the effect of BDZ and foliation was defined as the central case. Some sensitivity cases and alternative models were conducted in order to investigate the conceptual and input data uncertainties.

As sensitivity cases, the following case settings were investigated;

1) First sensitivity analysis was focused on variation of the longitudinal dispersion length as model input data. As discussed in 9.2.4, the longitudinal dispersion length was evaluated by the linear regression line ($\alpha_L = 0.017L^{1.5}$) in the central case. In the sensitivity analysis, the simulations were performed with different dispersion length, zero and 0.1.

2) Second sensitivity analysis was focused on the different models and input parameters related to the effects of the borehole damaged zone (BDZ) and the foliation. As shown in Figure I-14, simplest concept considering homogeneous flow and matrix without the BDZ (case-1) and the BDZ model without the foliation effect (case-2) were compared with the central case (case-3) assuming both BDZ and foliation effects.

As described in Task Description, no detailed information on channelized flow such as the flow distribution or potential channelling pattern in the experimental section is provided, however, channelized flow may occur in the annular slot due to surface roughness of the drillhole wall and injection method of tracer solution to the annular slot. In fact, heterogeneous channelized flow was observed in the laboratory experiment using same setup with WPDE performed in Helsinki Univ. (presented at Taskforce workshop held in Sept. 2014) as shown in Figure I-7(a). Although there is no detailed information, we assumed the simplified two pathway model considering heterogeneous flow; three times faster flow in 10 % of fracture and slower flow in 90 %, as shown in Figure I-7(b). The breakthrough curves simulated separately for two different flow were simply summed up.
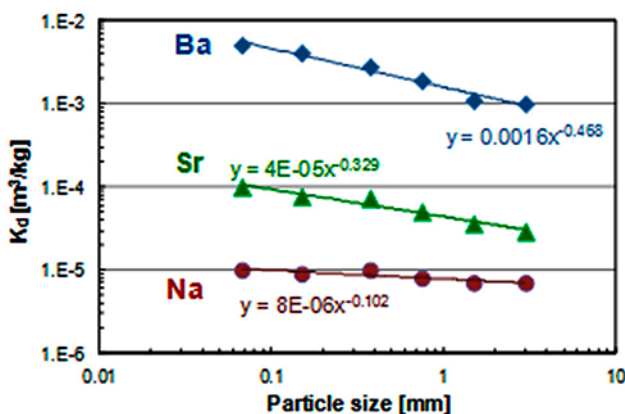

Figure I-6. *Relationship between distribution coefficient and particle size derived by batch sorption experiment for Äspö diorite.*
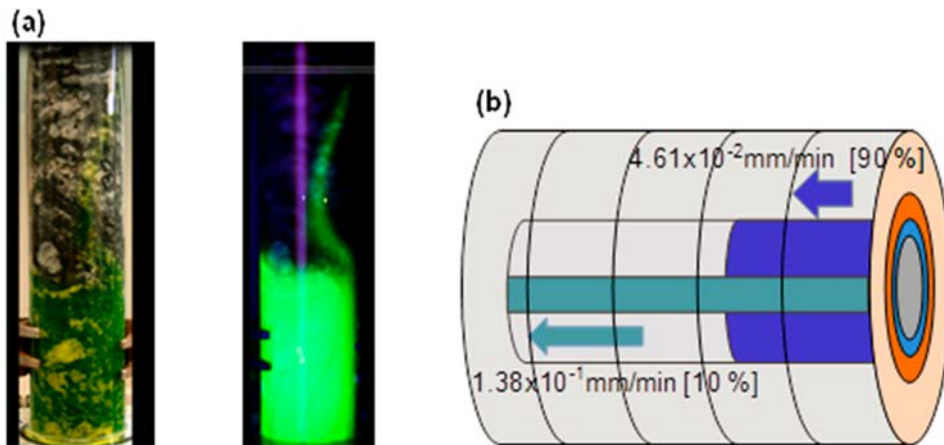
Figure I-7. *(a)Heterogeneous channelized flow observed in the laboratory column experiment using same setup with WPDE performed in Helsinki Univ. (presented at Taskforce workshop held in Sept. 2014), and (b) Conceptual image for alternative dual flow model.*

I3 Results and discussion

In this chapter we present our preliminary modelling results for WPDE-1 and WPDE-2 according to the Task Description. The results will be shown to allow comparable predictions of the breakthrough curve and performance measures. All breakthrough curves are represent the normalised decay corrected activity flow ((Bq/h)/Bq), in $\log_{10}$ scale in the y-axis.

I3.1 The central prediction

As shown in the Section I2.3, the central prediction in our modelling is based on the simplified model assuming homogeneous medium as follows;

- Homogeneous distribution of veined gneiss by ignoring around 10 % pegmatitic granite.
- Homogeneous and constant flow rate through the experimental section.
- The borehole damaged zone (BDZ) and their impacts on sorption and diffusion properties.
- The foliation effects on the effective diffusivity in the rock matrix.

The breakthrough curves of the central case in our predictive models are shown in Figures I-8 and I-9; (a) WPDE-1 and (b) WPDE-2, respectively.

As described in papers related to similar tracer tests (e.g. Heer 1997), peak position of early main peak is to a large extent determined by advection in the water filled fracture, indicating the average water flow rate. Height and width of the main peak are largely determined by dispersion. The tail of the breakthrough curve is attributed to the effect of matrix diffusion and sorption.

As shown in Figure I-8 for WPDE-1, breakthrough curves for non-sorbing traces, HTO and Cl are very similar shape. The breakthrough curve for weak-sorbing Na is different shape indicating lower height of the main peak and larger tail due to higher matrix diffusivity and sorption coefficients.

The breakthrough curves in WPDE-2 in Figure I-9 show delayed, lower and wider peaks due to lower flow rate in comparison with those in WPDE-1 shown in Figure I-8. In WPDE-2 we can find reasonable trends for different sorbing tracers, Na, Sr, Ba. The curves for Na and Sr are similar, but slight differences in height and tail can be explained by their difference in sorption and diffusion properties. The curve for Ba is significantly delayed and reduced because of high sorption. The diffusion parameter is the same for Sr and Ba, and then the difference between Sr and Ba is caused by only sorption.
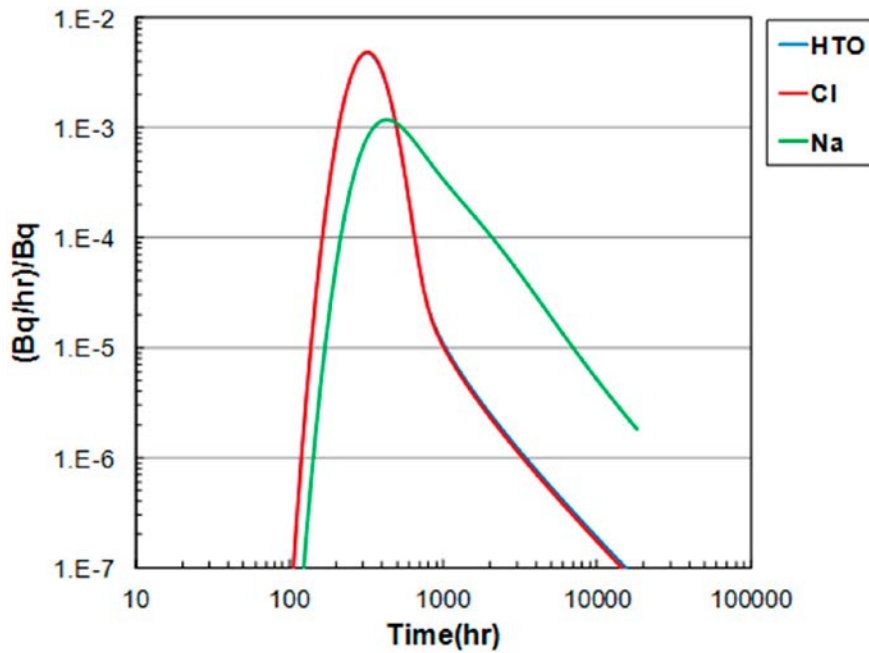
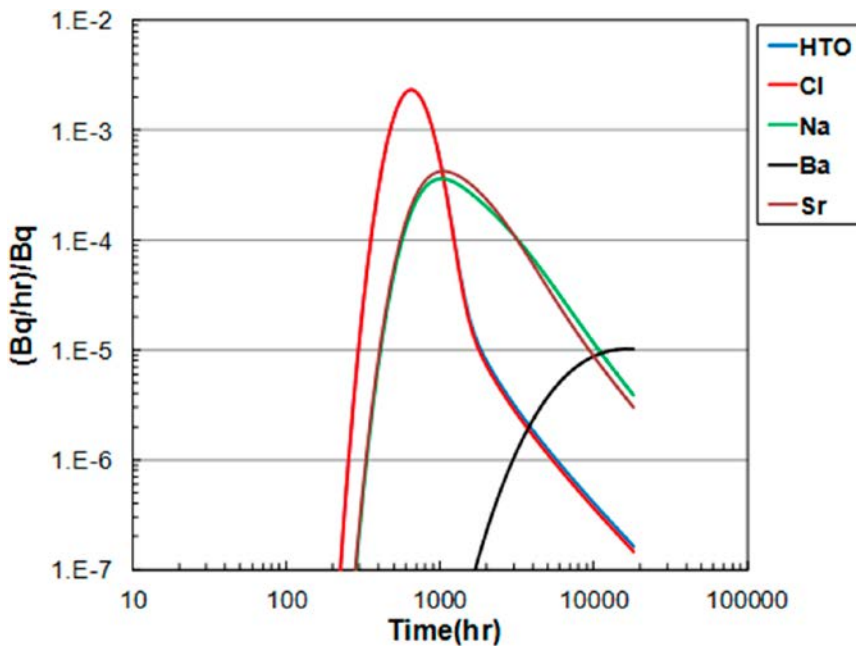**Figure I-8.** *Simulated results for WPDE-1 : central case (case 3).*

Figure I-9. *Simulated results for WPDE-2 : central case (case 3).*

I3.2 The upper and lower predictions

The simulated results of our central prediction are shown as solid lines in Figures I-10 and I-11; (a) WPDE-1 and (b) WPDE-2, respectively, and the uncertainty ranges caused by the parameter uncertainties are shown as dashed lines. The parameter uncertainties considered in these upper and lower predictions are for diffusion and sorption parameters in the BDZ and matrix, as shown in Table I-1 and I-2. All uncertainties related to laboratory-measured dataset were considered in consistent way for deriving the in situ dataset. The uncertainty ranges of Cl and Ba are relatively larger as shown in Figures I-10 and I-11, due to the larger uncertainties of D_e of Cl and Ba, and those of Cs, Sr, Ba. This uncertainty analysis focuses only diffusion and sorption parameters, however, the uncertainties related to flow and dispersion such as flow rates, gaps of annular slot, and dispersion lengths need to be further considered.
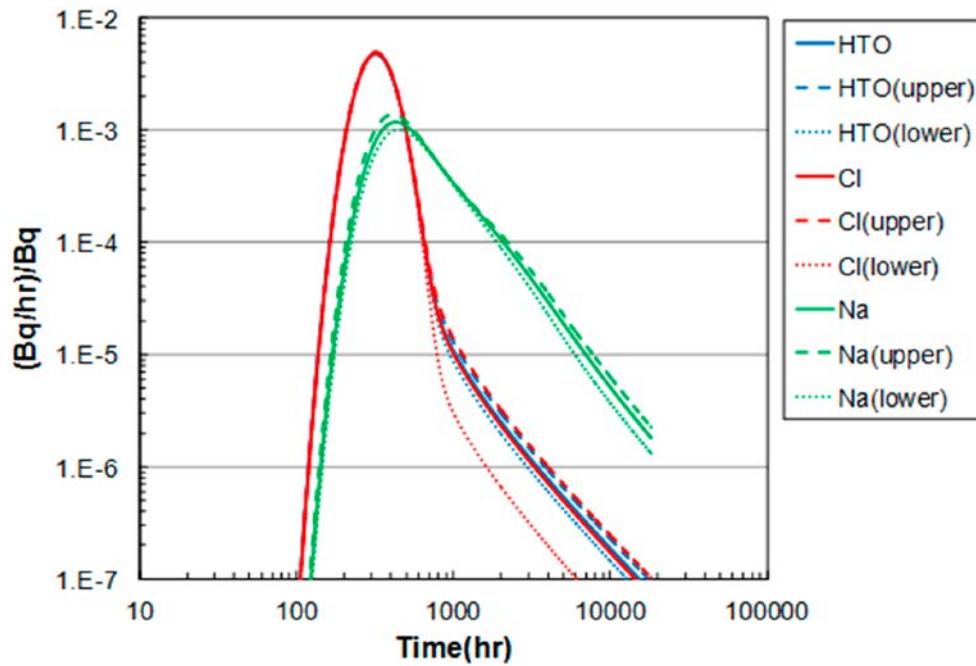
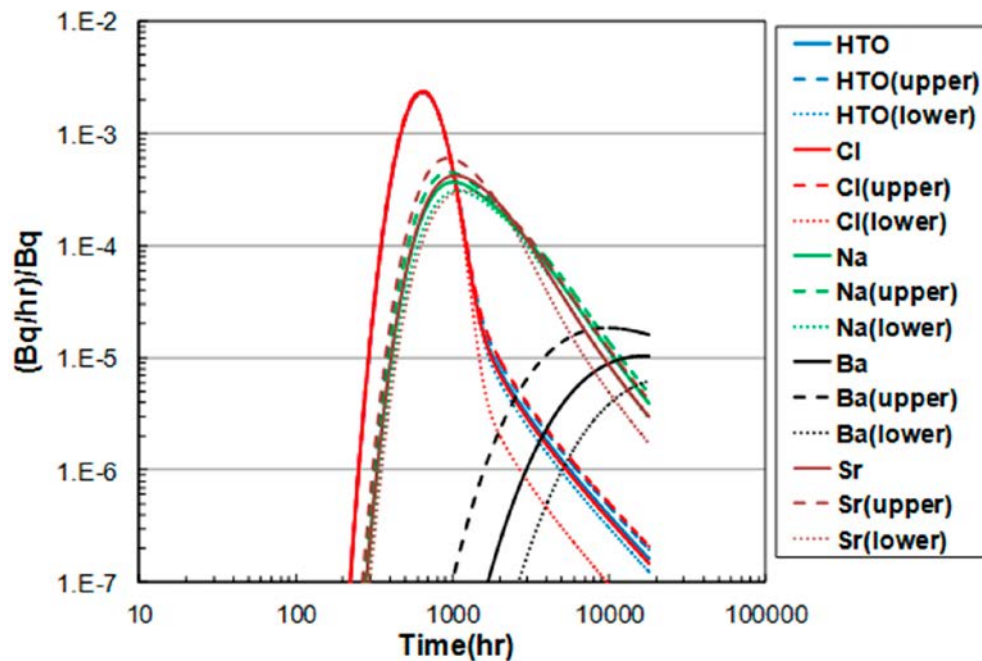***Figure I-10.*** *Simulated results for WPDE-1 : central case with upper and lower predictions.*

Figure I-11. *Simulated results for WPDE-2 : central case with upper and lower predictions.*

I3.3   Other alternative models, sensitivity cases and results

First sensitivity analysis focuses on variation of the longitudinal dispersion length as model input data. In the central case, the longitudinal dispersion length was evaluated by the linear regression line ($\alpha_L = 0.017L^{1.5}$). In the sensitivity analysis, two different dispersion lengths, zero and 0.1 m were assumed. As shown in Figure I-12 for WPDE-2, the main effect of dispersion is spreading the main peak. The increasing of dispersion length widens the main peak and decreases the height of main peak. This dispersion effect has larger impact in the case of non-sorbing tracers (HTO and Cl).
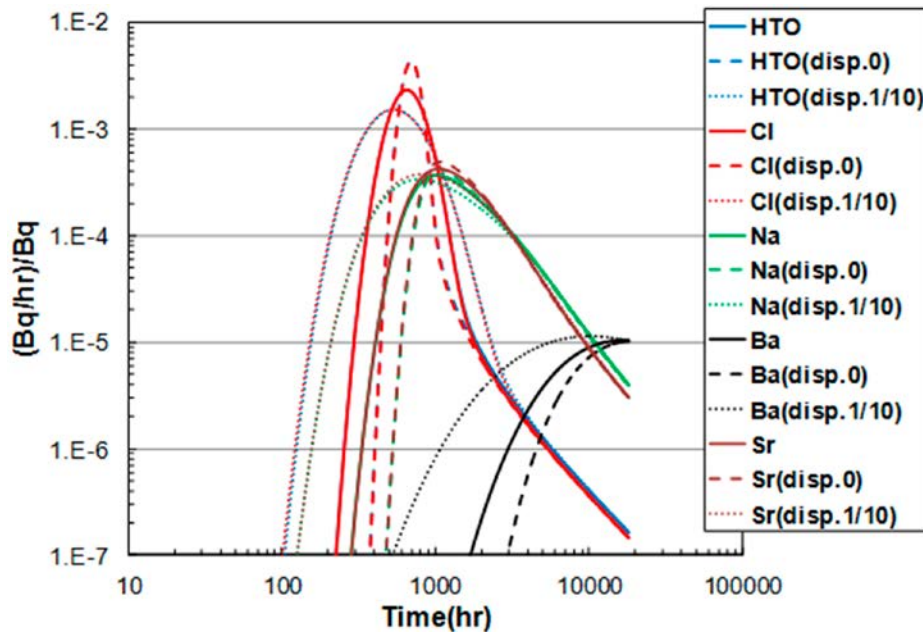
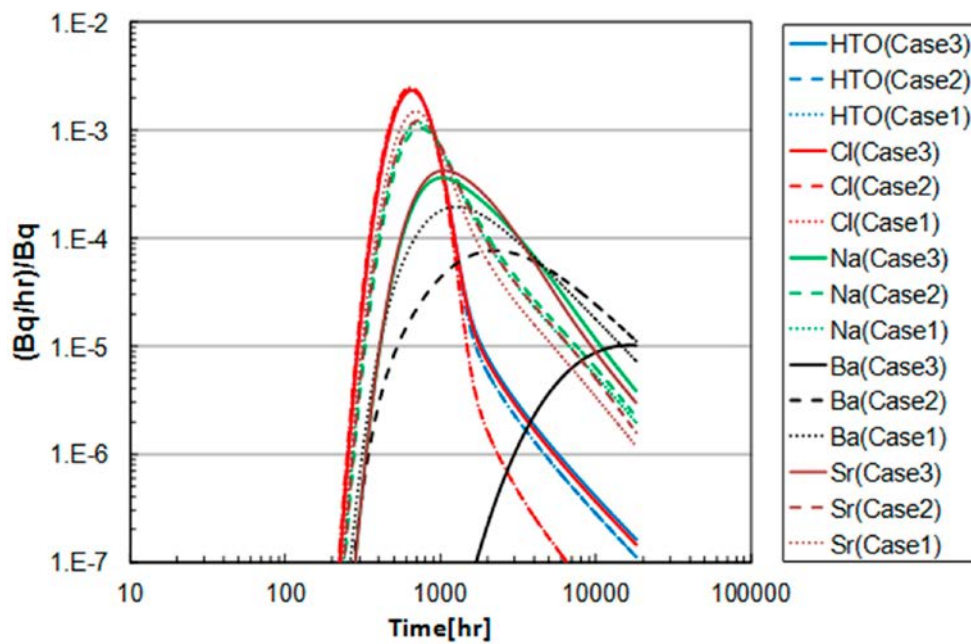*Figure I-12. Simulated results for WPDE-2 : sensitivity analysis for dispersion effect.*

Figure I-13. Simulated results for WPDE-2 : comparison between case-1, 2, 3.

Second sensitivity analysis was focused on the different models and input parameters related to the effects of the BDZ and the foliation. Both BDZ and foliation effects were assumed in the central case (case-3) shown in Figures I-8 and I-9 (results for central case), however, simpler concept considering matrix without the BDZ (case-1) and the BDZ model without the foliation effect (case-2) were simulated. The simulated breakthrough curves are shown and compared with the central case (case-3) in Figure I-13. As described in 9.2.2, compared to the simplest case-1 without the BDZ, case-2 assumed the BDZ with high K_d and D_e. In addition to the BDZ effect, case-3 assumed the high D_e for both BDZ and undisturbed matrix. As shown in Figure I-13, the BDZ effect (difference between case-1 and case-2) was insignificant in the case of non-sorbing tracer (HTO and Cl), however, the foliation effect was more pronounced in the tailing of the breakthrough curves. On the other hand, the simulated results for sorbing tracers (Na, Sr, Ba) indicated that both BDZ and foliation effects were significant.

As an alternative model, we investigated the effect of the heterogeneous flow in the annular slot. Although there is no detailed information, heterogeneous channelized flow was observed in the laboratory experiment using same setup with WPDE performed in Helsinki Univ. Based on this observation shown in Figure I-7(a), we assumed the simplified two pathway model considering heterogeneous flow; three times faster flow in 10 % of fracture and slower flow in the remaining 90 %, as shown in Figure I-7(b). The breakthrough curves simulated separately for the two different flow rates and were summed up considering the fractional contributions. The simulated results for WPDE-1 and WPDE-2 are shown in Figures I-14 and I-15, respectively. The main peaks in the breakthrough curves were divided to two peaks by the two different flows. Two peaks can be clearly distinguished in the case of non-sorbing tracer, on the other hand, two broader peaks seems to be overlapped in the case of high sorbing tracers, especially for Ba.
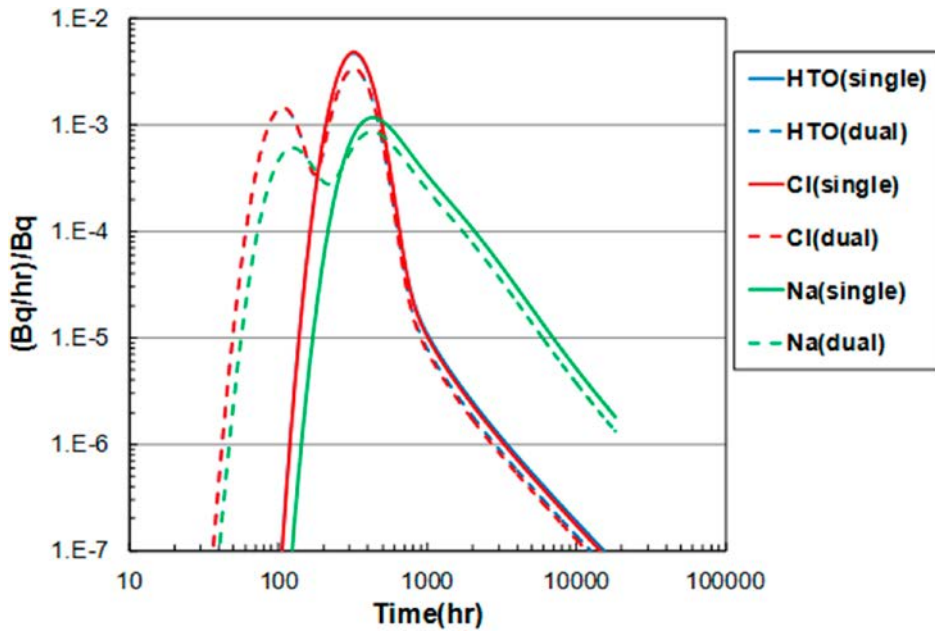

Figure I-14. *Simulated results for WPDE-1 : comparison between single and dual flow model.*
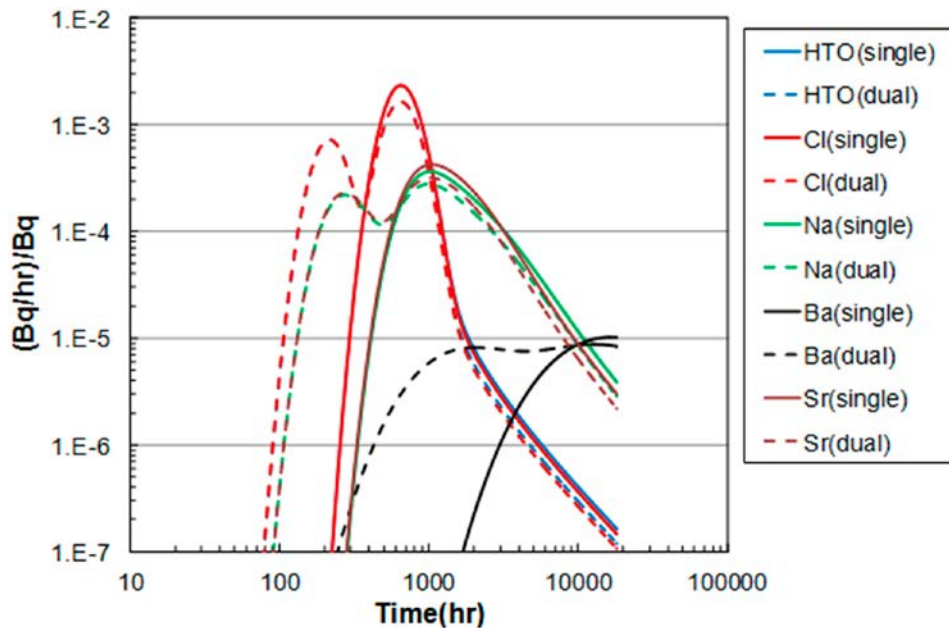

Figure I-15. *Simulated results for WPDE-2 : comparison between single and dual flow model.*

As in the central case assuming homogeneous flow, the uncertainty ranges caused by the parameter uncertainties are shown as dashed lines and compared with solid lines for reference case of dual flow model. We considered here only the parameter uncertainties related to diffusion and sorption parameters in the BDZ and matrix. The uncertainty ranges of Cl and Ba are relatively larger as shown in Figures I-16 and I-17, due to the larger uncertainties of D_e of Cl and Ba, and those of Cs, Sr, Ba. This uncertainty analysis focuses only diffusion and sorption parameters, however, the uncertainties related to heterogeneous flow need to be further considered.
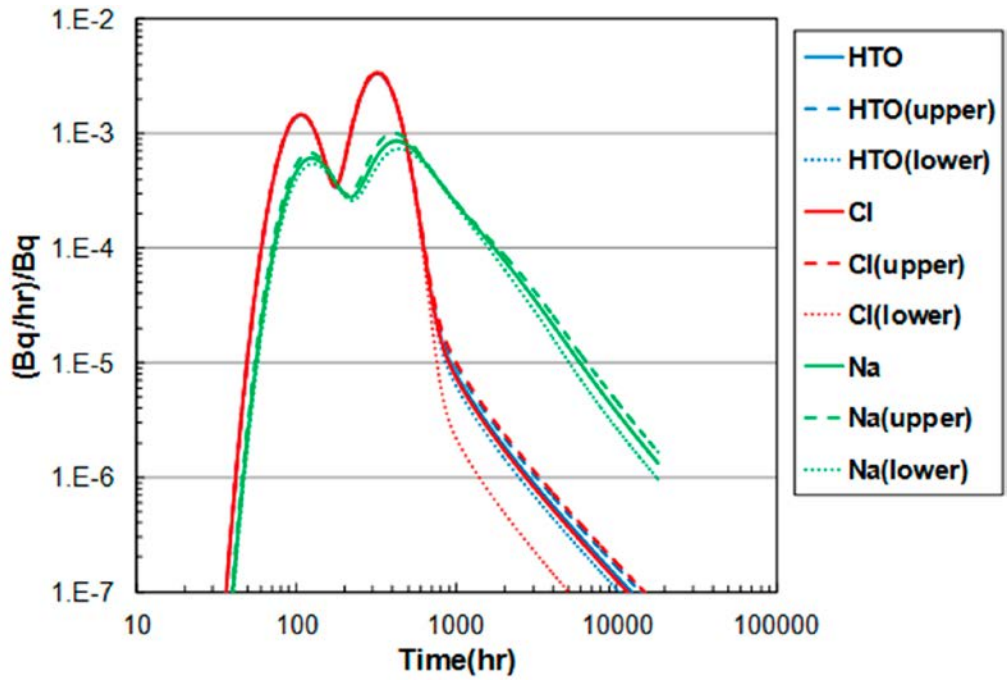

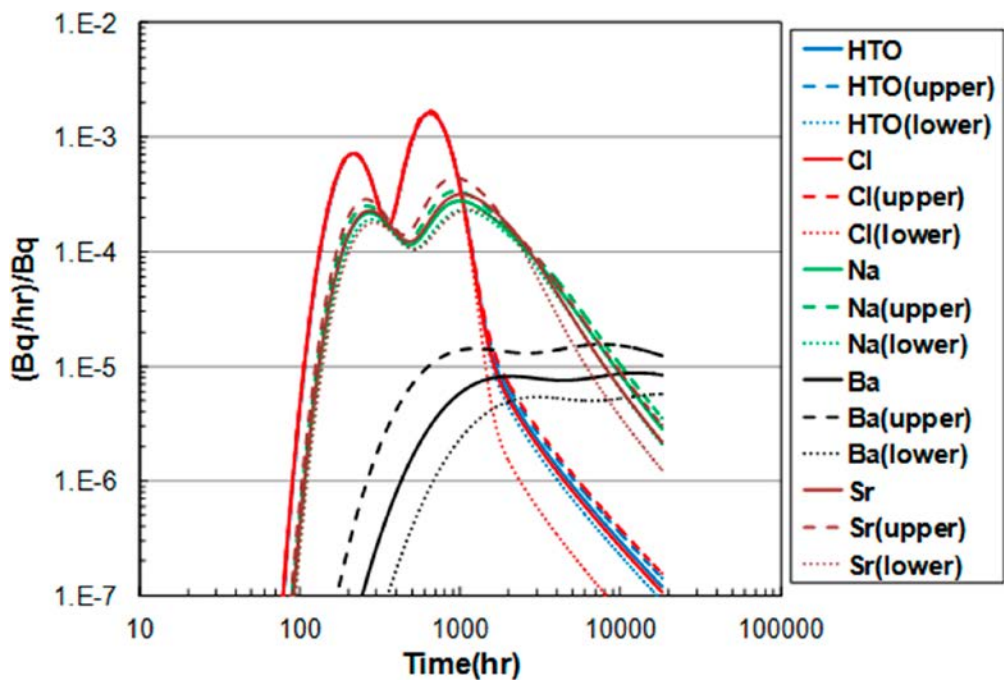**Figure I-16.** *Simulated results for WPDE-1 : dual flow model with upper and lower predictions.*

Figure I-17. *Simulated results for WPDE-2 : dual flow model with upper and lower predictions.*

I4   Discussion, conclusions and recommendations

Our approach for predictive modelling of WPDE-1and WPDE-2 of REPRO is based on the combination of the scaling approach from laboratory to in situ condition developed for Grimsel LTD project (Tachi et al. 2015, Soler et al. 2015) and key features of rock properties at the REPRO site. One of key features of our modelling approaches in the Grimsel LTD project is the parameter scaling from laboratory data to in situ conditions. Although the final goal of the modelling for WPDE-1 and WPDE-2 is to find the model concept and related parameters in order to represent solute transport and retardation in the WPDE in situ experiment, our predictive modelling in Task 9A focuses on: (1) warm-up calculation to familiarize with the experimental setup of the WPDE campaign, (2) application of the scaling method from laboratory data to in situ conditions, (3) sensitivity analysis and alternative modelling to find key assumptions and uncertainties in model and related parameters.

As preliminary warm-up calculation, we tried to familiarize with the experimental setup of the WPDE campaign, in terms of geometries, flows, boundary conditions, supporting laboratory data, etc. We identified key features at the REPRO site; dominant veined gneiss (VGN) with strong foliation, banded pegmatitic granite (PGR) distribution, and heterogeneous flow in fracture.

Based on these features and the assumed features, events and processes (FEPs), the conceptual model for radionuclide transport in the WPDE setup was developed for a simplified and pragmatic representation. Radionuclide transport was modelled taking into account advection and dispersion within an artificial fracture and diffusion and sorption within a two-layered matrix, i.e., borehole disturbed zone (BDZ) and undisturbed matrix, adjacent to the fracture. Traditional advective and dispersion was assumed in the experimental drillhole section. However, the effects of the heterogeneous flow and the dispersion were investigated sensitively.

For matrix diffusion and sorption, our modelling approach is based on the parameter estimation using the scaling approach from laboratory to in situ condition developed for the Grimsel LTD project (Tachi et al. 2015, Soler et al. 2015). This approach has been applied for the WPDE setup considering key features of rock properties at the REPRO site. The key assumption of the modelling in the WPDE setup is that the rock matrix is simplified and homogenous. The D_e parameters for all tracers were scaled from laboratory data to in situ conditions, assuming Archie's law. The effects of strong foliation on D_e values were estimated from comparison of D_e values between parallel and perpendicular directions to foliation. Batch-derived K_d values for crushed rocks from the REPRO site were assumed to be directly applicable to the BDZ, and were scaled for undisturbed matrix by considering the particle size dependence of K_d.

The features of REPRO rocks and related FEPs were stepwisely modelled using the GoldSim code. The simulated breakthrough curves showed typical shapes and trends: position and height of main peaks for both non-sorbing and sorbing tracers were to a large extent determined by advection and dispersion in the water-filled fracture. The tail of the breakthrough curve is attributed to the effect of matrix diffusion and sorption. The curves for Na and Sr are similar. However, that for Ba is significantly delayed and reduced because of high sorption. Based on the simulated results including sensitivity and alternative modelling, key assumptions and uncertainties in model and related parameters were identified which will have major impact on the breakthrough curves: heterogeneous flow and dispersion, D_e data and their relation to foliation, K_d data for cations and their relation to particle sizes, etc. These uncertainties must be further analyzed and may be reduced by additional detailed information related to in situ conditions and laboratory supporting experiments.

I5   Acknowledgments

SKB is responsible for managing spent nuclear fuel and radioactive waste produced by the Swedish nuclear power plants such that man and the environment are protected in the near and distant future.

skb.se